

DEVELOPMENT OF ANALYTICAL FLEXURAL MODELS FOR STEEL FIBRE-REINFORCED CONCRETE BEAMS WITH AND WITHOUT STEEL BARS

By

Peter Binali Kamowa Mbewe

Thesis presented in partial fulfilment of the requirements for the degree of Master of Civil
Engineering at the University of Stellenbosch



Study Leader: Prof. GPAG van Zijl

December 2011

DECLARATION

I, the undersigned, hereby declare that the work contained in this thesis is my own original work except where specifically acknowledged in the text, and that I have not previously in its entirety or in part submitted it at any university for a degree.

Signed.....

Date.....

SYNOPSIS

There is an increasing demand for the development and use of innovative materials with reduced cost of construction while offering improved structural properties. Steel fibre reinforced concrete (SFRC) can be used as a structural material to substitute the conventional reinforcing bars partially or fully. However, there is little or no codified approach on the design procedures for SFRC members in the latest guidelines outlined in the draft 2010 Model code.

It is against this background that analytical methods are derived in this study for the determination of the flexural capacity of strain-softening, deflection-hardening SFRC with and without steel reinforcing bars. Models used for the determination of the flexural capacity of SFRC rectangular sections are based on equivalent stress blocks for both compression and tensile stresses. These are derived from an elastic-perfect plastic model for compression and either an elastic-constant post-peak response or Rilem's multi-linear model for tension, in which strain compatibility and force equilibrium theories are used. By employing the equivalent stress blocks for both tensile and compressive stress states, parameters are defined by converting the actual stress-strain distribution to an equivalent stress block, depending on the ratio of yield (or cracking) strain and post-yield (post-cracking) strains. Due to the simplicity of a drop-down tensile model and a bilinear compression model, these material models are used for the subsequent derivation of the flexural models for both SFRC with and without steel reinforcing bars.

An experimental program is designed and executed for model verification. This includes material characterisation experiments for the determination of material model input parameters, and main beam flexural experiments for the determination of the beam bending capacity. An indirect tensile test is used for the characterisation of the tensile behaviour while a four-point bending test is used for beam bending behaviour.

Both flexural models for SFRC with and without reinforcing bars have been verified to fairly predict the flexural capacity of the beams. However, the flexural model for SFRC with steel bars offers some challenges as to whether the synergetic effect of using both steel bars and steel fibres should be incorporated at the low fibre volumes as used in the verification exercise. Furthermore, the use of indirect methods to characterise tensile behaviour added some uncertainties in the material model parameters and hence may have affected the predictability of the model. More research on the verification of the models is required to enable the use of a wider concrete strength spectrum for the verification and possible modification of the models. Studies on the model uncertainty may also help determine the reliable safety factor for the use of the model in predicting design strength of beam sections at a prescribed reliability index.

SINOPSIS

Daar is 'n groeiende aanvraag na die ontwikkeling en gebruik van innoverende materiale met verminderde konstruksiekoste maar verbeterde strukturele eienskappe. Staalvesel-gewapende beton (SVGB) kan gebruik word as strukturele materiaal om die konvensionele wapeningstawe gedeeltelik of ten volle te vervang. Daar is egter min of geen gekodifiseerde benaderings tot die ontwerpprosedures vir SVGB-dele in die nuutste riglyne uitgestippel in die konsepweergawe van die 2010 Modelkode nie.

Dit is teen hierdie agtergrond dat in hierdie studie analitiese metodes afgelei is vir die bepaling van die buigkapasiteit van spanning-versagtende, defleksie-verhardende SVGB met en sonder staalbewapeningstawe. Modelle wat gebruik is vir die bepaling van die buigkapasiteit van SVGB reghoekige snitte is gebaseer op ekwivalente spanningsblokke vir beide druk- en trekspannings. Hierdie is afgelei van 'n elasties-perfekte plastiese model vir druk en óf 'n elasties-konstante post-piek respons óf Rilem se multi-lineêre model vir spanning, waarin teorieë vir drukkapasiteit en krag-ewewig gebruik is. Deur die ekwivalente spanningsblokke vir beide trek- en drukspanningstoestande te implementeer, is parameters bepaal deur die werklike verspreiding van spanningsdruk om te wissel na 'n ekwivalente spanningsblok, afhangend van die verhouding van swig- (of kraak-)spanning en post-swig (post-kraak) spannings. Te wyte aan die eenvoud van 'n aftrek trekmodel en 'n bilineêre kompressiemodel, is hierdie materiaalmodelle gebruik vir die daaropvolgende afleiding van die buigingsmodelle vir beide SVGB met en sonder staalbewapeningstawe.

'n Eksperimentele program vir modelkontrolering is ontwerp en uitgevoer. Dit sluit eksperimente in vir materiaalbeskrywing, om invoerparameters van materiaalmodelle te bepaal, asook eksperimente vir hoofbalkbuigings, om balkbuigingskapasiteit te bepaal. 'n Indirekte trektoets is gebruik vir die beskrywing van die trekgedrag, terwyl 'n vierpunt-buigingsstoets gebruik is vir balkbuiggedrag.

Dit is bewys dat beide buigingsmodelle vir SVGB met en sonder staalbewapeningstawe die buigingskapasiteit van die balke redelik akkuraat kan voorspel. Nietemin, bied die buigingsmodel vir SVGB met staalbewapeningstawe sekere uitdagings: die vraag ontstaan rondom die insluiting van die sinergetiese effek van die gebruik van beide staaltawe en staalvesels met die lae veselvolumes soos gebruik in die kontroleringsoefening. Verder het die gebruik van indirekte metodes om die buigingsgedrag te bepaal, onsekerhede gevoeg by die materiaalmodelparameters en dit mag dus as sulks die voorspelbaarheid van die model beïnvloed. Meer navorsing moet uitgevoer word oor die kontrolering van die modelle sodat 'n wyer spektrum van betonsterkte gebruik kan word vir die verifikasie en moontlike aanpassing van die modelle. Navorsing oor die wisselvalligheid van die modelle mag ook help om die betroubare veiligheidsfaktor te bepaal vir die model se gebruik in die berekening van ontwerpkrag van balkdele teen 'n voorgeskrewe betroubaarheidsindeks.

ACKNOWLEDGEMENT

I would like to thank the following people:

- Prof. GPAG van Zijl, my promoter, for guidance and support
- Staff members of the Laboratory and Workshop of the Department of Civil Engineering at University of Stellenbosch for their support in the execution of my experimental program
- DAAD German Exchange program and the Department of Civil Engineering of the University of Stellenbosch, for their financial support.
- Lastly, but not least, my wife Lydia and our daughter Isabel for their love, support and patience during my studies.

NOTATIONS, DEFINITIONS AND ABBREVIATIONS

NOTATIONS

A_{cc} :	Areas of concrete acted on by the compressive stress
A_{ct} :	Areas of concrete acted on by tensile stress
A_s :	Area of steel bars
b :	Breadth of the section
b_r :	Breadth of a bearing strip
d :	Effective depth of the section
d_f :	Fibre diameter
E_c :	Young's modulus of concrete
E_{cm} :	Mean young's modulus of concrete
E_f :	Young's modulus of fibres
E_s :	Young's modulus of steel
E_{sm} :	Mean young's modulus of steel
f_c :	Maximum cylinder compressive strength
f_{cd} :	Design compressive strength of concrete
f_{ck} :	Characteristic cylinder compressive strength of concrete
f_{cu} :	Characteristic cube compressive strength of concrete
f_{cy} :	Yield compressive strength of concrete
$f_{eq,2}$:	Equivalent flexural strength at service state taken at a deflection of $\delta_L+0.65\text{mm}$
$f_{eq,3}$:	Equivalent flexural strength at ultimate state taken at a deflection of $\delta_L+2.65\text{mm}$
f_{fs} :	Flexural service stress of a beam
f_{fu} :	Maximum flexural strength of a beam
f_{Lk} :	Characteristic flexural strength of a beam
f_{Ri} :	Residual flexural strength at CMOD_i
f_{Rik} :	Characteristic residual flexural strength at CMOD_i
f_{teq} :	Equivalent post cracking tensile strength at ultimate tensile strain as defined by Drop down tensile stress distribution
f_{teqk} :	Characteristic value of the equivalent post cracking tensile strength at ultimate tensile strain as defined by Drop down tensile stress distribution
f_{teq1} :	Equivalent flexural tensile strength at tensile strain of ε_{t1} as defined by Rilem's tensile stress distribution
f_{teq1k} :	Characteristic value of the equivalent flexural tensile strength at tensile strain of ε_{t1} as defined by Rilem's tensile stress distribution
f_{teq2} :	Equivalent flexural tensile strength at ultimate state as defined by Rilem's tensile stress distribution
f_{teq2k} :	Characteristic value of the equivalent flexural tensile strength at ultimate state as defined by Rilem's tensile stress distribution
f_s :	Tensile strength of steel bar

f_{sy} :	Yield strength of tension steel bar
f'_{sy} :	Yield strength of compression steel bar
f_{t-N} :	Maximum tensile strength of SFRC derived from block shift approach
f_{t-M} :	Maximum tensile strength of SFRC derived from elastic approach by Rocco <i>et al</i> (2001)
f_{td} :	Design uniaxial tensile strength of concrete
f_{tk} :	Characteristic uniaxial tensile strength of concrete
f_{ts} :	Splitting stress
f_{tsp} :	Maximum (peak) splitting strength of concrete
f_{tu} :	Maximum uniaxial tensile strength of concrete
f_{ty} :	Cracking tensile strength of concrete
F_c :	Total compressive force provided by concrete
F_{t+s} :	Total tensile force provided by concrete and steel bars
F_t :	Total tensile force provided by concrete
F_{be} :	Bond efficiency of fibres which varies between 1.0 and 1.2 depending on fibre characteristics
f_{uc} :	Maximum cube compressive strength
G_{sp} :	Toughness derived from splitting stress-crack width relationship
G_{t-N} :	Toughness derived from direct tension (f_{t-N}) vs. crack width
G_{t-M} :	Toughness derived from direct tension (f_{t-M}) vs. crack width
h :	Overall height of the section
h_s :	The distance from the tip of the notch to the top of the beam cross section
K_f :	Dimensionless ultimate moment of resistance of concrete section ($= M / f_{cu} b d^2$)
K_n :	Fractile estimator
L :	Span length of a beam
l_f :	Fibre length
L_g :	Gauge length
m_{δ_e} :	Coefficient of variation of error term δ_e in model verification analysis
M :	Moment capacity of the section
M_a :	Applied moment
M_{cr} :	Cracking moment of the section
M_y :	Moment of the section when steel reinforcement yields
M_p :	Moment of the section at the ultimate tensile strength of steel reinforcement
M_{ut} :	Moment of the section at ultimate tensile strength of concrete
n :	Number of test specimen in a batch or sample group
P :	Applied load
P_u :	Maximum applied load recorded in an experiment
r_e :	Experimental results for model verification

- r_t : Theoretical predictions from the proposed model
- s_{Δ}^2 : Estimate of the variance of the error term in model analysis
- t : Calculated t - value in statistical analysis
- $t_{df,0.05}$: t - value for a given degree of freedom at a prescribed risk of 0.05 in statistical analysis
- T_s^f : Area under force-displacement curve for a bending test taken up to a deflection of $\delta_L+0.65\text{mm}$
- T_u^f : Area under force-displacement curve for a bending test taken up to a deflection of $\delta_L+2.65\text{mm}$
- ν : Degree of freedom in statistical analysis
- V_f : Volume fraction of fibres
- w : Crack width
- w_T : Total displacement measured from the splitting test
- x : Neutral axis depth from compression face of concrete section
- x_u : Maximum allowable neutral axis depth from compression face of concrete
- X_c : Characteristic strength parameter for a material sample
- X_m : Mean strength parameter for a material sample
- y : Distance from the neutral axis to the extreme tensile fibre stress considered in an elasto-plastic model (Di Prisco *et al*, 2009)
- Z : Lever arm between the points of application of the resultant compression and tension forces for a SFRC section
- Z_o : The lever arm between the application of the resultant tensile force of concrete and the tensile force due to reinforcement steel bars.
- Z_{eq} : Lever arm between the points of application of the resultant compression force and tensile forces from reinforcing bars
- α_1 : Coefficient representing the fraction of bond mobilized at first crack matrix cracking
- α_2 : Efficient factor of fibre orientation in the uncracked state of the composite
- β_c : Product of conversion factors, λ_c and η_c
- β_{cd} : Product of design conversion factors, λ_{cd} and η_{cd}
- β_{ceq} : Product of conversion factors, λ_c and η_c used for SFRC failure in stage Three
- β_t : Product of conversion factors, λ_t and η_t
- β_{td} : Product of design conversion factors, λ_{td} and η_{td}
- δ_c : Correction factor/ model bias in model verification analysis
- δ_e : Error term in model verification analysis
- δ_L : Maximum elastic displacement
- ε_c : Compressive strain of concrete
- ε_{ty} : Cracking tensile strain of concrete

- ε_{c2eq} : Equivalent compressive strain for SFRC failure in stage Two
- ε_{c3eq} : Equivalent compressive strain for SFRC failure in stage Three
- ε_{cp} : Post yield compressive strain of concrete
- ε_{cu} : Ultimate compressive strain of concrete
- ε_{cy} : Yield compressive strain of concrete
- ε_t : Tensile strain of concrete
- ε_{tm} : Tensile strain at maximum splitting strength during a splitting test
- ε_{tu} : Ultimate tensile strain of concrete
- $\varepsilon_{t(u)}$: Maximum tensile strain of concrete for a given stain in steel bars in R-SFRC
- ε_s : Tensile strain of steel bars
- ε_{sy} : Yield tensile strain of steel bar
- ε_{uk} : Ultimate characteristic tensile strain of steel bar
- ε_{ud} : Ultimate design tensile strain of steel bar
- ε_0 : Compressive strain of 0.00005
- ε_1 : Compressive strain at 40% compressive strength
- ξ : Factor calibrated for Mobasher and Soranakom's flexural model (2007)
- λ_c, η_c : Conversion factors for an equivalent rectangular compressive stress block
- λ_{cd}, η_{cd} : Design conversion factors for an equivalent rectangular compressive stress block
- λ_t, η_t : Conversion factors for a rectangular tensile stress block
- λ_1 : Expected pull-out length ratio (equal to $\frac{1}{4}$ from probability considerations)
- λ_2 : Efficiency factor for orientation in cracked state
- λ_3 : Group reduction factor associated with the number of fibres pulling out per unit are (or for density of fibre crossings)
- ρ : The ratio of area of steel bars to effective cross sectional area of a reinforced concrete section
- ρ_g : The ratio of area of steel bars to overall cross sectional area of a reinforced concrete section
- ϕ_p : Reduction factor for uncertainties due to use of post peak tensile strength, usually 0.7
- σ : Standard deviation of a sample
- σ_c : Compressive stress of concrete
- σ_{cc} : Cracking tensile strength of SFRC
- σ_f : Tensile stress developed at pull-out (dynamic bond stress of 2.3MPa)
- σ_{mu} : Tensile strength of concrete matrix
- σ_{pc} : Post cracking tensile strength of SFRC
- $\bar{\sigma}_{pc}$: Average tensile strength of SFRC

- σ_t : Tensile stress of concrete
- σ_{tf} : Tensile stress in fibrous concrete
- σ_0 : Compressive stress at strain of 0.00005
- σ_1 : Compressive stress equal to 40% of maximum compressive strength in an experiment
- τ : Average bond strength at the fibre matrix interface
- μ_i : The ratio of post peak tensile strength to peak tensile strength
- $\mu_{cr,fl}$: Critical ratio of post peak tensile strength to peak tensile strength that must be exceeded for deflection hardening behaviour of SFRC composites
- μ_{R1} : The ratio of the first post peak tensile strength (at 0.1% strain from yield strain) to peak tensile strength
- μ_{R2} : The ratio of the ultimate post peak (residual) tensile strength (at 25‰ strain) to peak tensile strength
- ω_{eq} : The ratio of yield to post yield equivalent compressive strain (ϵ_{c2eq} or ϵ_{c3eq})
- ω : The ratio of yield to post yield compressive strain
- ω' : The ratio of yield to post yield tensile strain for drop down tensile model.
- ω'_{13} : The ratio of yield to ultimate tensile strain for Rilem model.
- ω'_{23} : The ratio of strain at service (ϵ_{t1}) to ultimate tensile strain for Rilem model.
- γ_m : Material safety factor
- $\bar{\Delta}$: Estimate of the expected value in model verification analysis

DEFINITIONS

Block shift approach: A method used for conversion of post cracking tensile stress derived from splitting test whereby peak tensile strength is derived from code definition (i.e. use of 0.9) and subsequent post cracking stresses are derived from subtracting post cracking splitting stresses by a uniform value equivalent to the difference between direct tensile strength and splitting strength (i.e. uniform subtraction of the value $0.1f_{tps}$ from any post cracking splitting stress)

Deflection hardening: Flexural response of a material whereby multiple cracks develops in bending resulting in the material supporting more flexural load after cracking.

Direct tension-M: Direct tension derived from splitting test using method based on elastic theory as defined by Rocco *et al* (2001) (see Section 4.3.4)

Direct tension-N: Direct tension derived from splitting test using block shift

Drop down tensile stress distribution:

Elastic tensile stress-strain behaviour up to cracking strength, drop down at cracking strain followed by plastic response

Normal concrete: Concrete without fibres

Strain hardening: Tensile response of a material whereby multiple cracks develop in tension resulting in the material supporting more tensile load after cracking.

ABBREVIATIONS

CMOD:	Crack mouth opening displacement
DOF:	Degree of freedom
LOP:	Limit of proportionality
SFRC:	Steel fibre reinforced concrete
NRC:	Normal reinforced concrete
MOR:	Modulus of rupture- the maximum value of equivalent elastic bending stress corresponding to the maximum bending resistance of a beam.
R-SFRC:	Reinforced steel fibre reinforced concrete

TABLE OF CONTENTS

DECLARATION.....	i
SYNOPSIS.....	ii
SINOPSIS.....	iii
ACKNOWLEDGEMENT.....	iv
NOTATIONS, DEFINITIONS AND ABBREVIATIONS.....	v
TABLE OF CONTENT.....	xi
CHAPTER 1 INTRODUCTION.....	1
1.1 BACKGROUND.....	1
1.2 PROBLEM STATEMENT.....	2
1.3 RESEARCH OBJECTIVES.....	2
1.3.1 MAIN OBJECTIVE.....	2
1.3.2 SPECIFIC OBJECTIVES.....	2
1.4 IMPORTANCE OF THE RESEARCH.....	3
1.5 METHODOLOGY.....	3
1.5.1 DATA COLLECTION.....	4
1.5.1.1 CHARACTERISATION OF MATERIAL PROPERTIES.....	4
1.5.1.2 VERIFICATION OF ANALYTICAL MODELS.....	4
1.5.2 SAMPLING AND SAMPLE SIZE.....	4
1.5.3 DATA ANALYSIS.....	5
1.5.3.1 MATERIAL CHARACTERISATION PROCESS.....	5
1.5.3.2 VERIFICATION OF ANALYTICAL MODELS.....	5
1.6 SCOPE OF STUDY.....	5
1.7 STRUCTURE OF REPORT.....	6
1.8 CONCLUSION.....	6
CHAPTER 2. THEORETICAL FOUNDATION.....	7
2.1 INTRODUCTION.....	7
2.2 MATERIAL BEHAVIOUR AND CONSTITUTIVE MODELS FOR SFRC.....	8
2.2.1 COMPRESSIVE BEHAVIOUR.....	8
2.2.2 TENSILE BEHAVIOUR.....	9
2.2.3 BENDING BEHAVIOUR.....	13

2.3 CONSTITUTIVE MODELS FOR SFRC.....	15
2.3.1 COMPRESSION BEHAVIOUR.....	15
2.3.2 TENSILE BEHAVIOUR.....	16
2.3.3 MODEL CODE 2010 CONSTITUTIVE LAWS FOR FRC.....	16
2.4 CURRENT FLEXURAL MODELS FOR SFRC BEAM SECTIONS.....	18
2.4.1 SORANAKOM AND MOBASHER APPROACH.....	18
2.4.2 APPROACH PROPOSED BY A.E. NAAMAN.....	19
2.4.3 APPROACH BY HENAGER AND DOHERTY.....	21
2.4.4 APPROACH BY TAN <i>ET AL</i> (1995).....	22
2.5 REVIEW OF DESIGN MODELS FOR NORMAL REINFORCED CONCRETE.....	23
2.5.1 CONCRETE AND REINFORCING STEEL MATERIAL PARAMETERS.....	23
2.5.2 STRUCTURAL ANALYSIS APPROACHES.....	24
2.5.2.1 LINEAR ELASTIC ANALYSIS.....	25
2.5.2.2 NON-LINEAR ANALYSIS.....	25
2.5.2.3 ULTIMATE MOMENT OF RESISTANCE.....	26
2.6 REVIEW OF SPLITTING STRENGTH PARAMETERS.....	27
2.7 RELIABILITY BASED VERIFICATION OF MODELS.....	29
2.7.1 VERIFICATION OF ANALYSIS MODELS.....	29
2.8 CONCLUSION.....	31
CHAPTER 3 DEVELOPMENT OF ANALYTICAL MODELS.....	32
3.1 INTRODUCTION.....	32
3.2 DESIGN STRESS BLOCKS FOR SFRC.....	32
3.2.1 DESIGN COMPRESSION STRESS BLOCKS.....	32
3.2.1.1 PARABOLIC-RECTANGULAR STRESS-STRAIN MODEL.....	33
3.2.1.2 BILINEAR COMPRESSIVE STRESS-STRAIN MODEL.....	35
3.2.2 DESIGN TENSILE STRESS BLOCKS.....	37
3.2.2.1 DROP-DOWN CONSTANT MODEL.....	37
3.2.2.2 RILEM TENSILE MODEL.....	40
3.3 FLEXURAL MODELLING FOR SFRC RECTANGULAR BEAM SECTION.....	42
3.3.1 FLEXURAL MODEL FOR SFRC BEAMS USING THE DROP-DOWN TENSION AND THE BILINEAR COMPRESSION MODELS.....	42

3.3.2 FLEXURAL MODEL FOR SFRC BEAMS USING THE RILEM TENSION AND THE BILINEAR COMPRESSION MODELS.....	45
3.3.3 FLEXURAL MODELS FOR REINFORCED SFRC BEAMS.....	48
3.3.4 CONSIDERATION FOR PROVISION OF REINFORCEMENT IN SFRC BEAMS...	54
3.3.5 PROVISION OF REINFORCEMENT IN SFRC BEAMS.....	56
3.4 CONCLUSION.....	58
CHAPTER 4.0 EXPERIMENTAL DESIGN AND METHODOLOGY.....	59
4.1 INTRODUCTION.....	59
4.2 EXPERIMENTAL DESIGN.....	59
4.2.1 PHASE I: PRELIMINARY EXPERIMENTAL PHASE.....	60
4.2.2 PHASE II: EXPERIMENTAL PROGRAM FOR MODEL VERIFICATION.....	61
4.3 METHODOLOGY.....	62
4.3.1 MATERIAL MIX DESIGN, CASTING AND CURING PROCEDURES.....	62
4.3.3 TESTING METHODS.....	64
4.3.3.1 MATERIAL CHARACTERISATION TESTS.....	64
4.3.3.2 MODEL VERIFICATION-FLEXURAL TEST.....	67
4.3.4 DATA ANALYSIS.....	68
4.3.5 VERIFICATION OF ANALYSIS MODELS.....	73
4.4 CHALLENGES AND LIMITATIONS.....	74
4.5 UNCERTAINTIES WITH EXPERIMENTAL DATA ACQUISITION.....	75
4.6 CONCLUSION.....	75
CHAPTER 5.0 EXPERIMENTAL RESULTS.....	76
5.1 INTRODUCTION.....	76
5.2 MATERIAL CHARACTERISATION.....	76
5.2.1 CONCRETE COMPRESSIVE BEHAVIOUR.....	77
5.2.2 CONCRETE TENSILE BEHAVIOUR.....	78
5.2.3 CONCRETE FLEXURAL BEHAVIOUR.....	81
5.2.4 TENSILE RESPONSE OF REINFORCING BARS.....	83
5.3 MODEL VERIFICATION FLEXURAL TEST RESULTS.....	84
5.3.1 FLEXURAL RESPONSE FOR MB2-A0.0% AND MB2-F0.0%.....	84
5.3.2 FLEXURAL RESPONSE FOR MB0-C1.0% AND MB0-E1.5%.....	87

5.3.3 FLEXURAL RESPONSE FOR MB2-B1.0% AND MB2-D1.5%.....	88
5.4 CONCLUSION.....	90
CHAPTER 6. ANALYSIS OF EXPERIMENTAL RESULTS.....	92
6.1 INTRODUCTION.....	92
6.2 EVALUATION OF MATERIAL BEHAVIOUR.....	92
6.2.1 COMPRESSIVE BEHAVIOUR.....	93
6.2.2 TENSILE BEHAVIOUR.....	96
6.3 STATISTICAL ANALYSIS OF MATERIAL CHARACTERISATION DATA.....	98
6.3.1 COMPRESSION TEST RESULTS.....	99
6.3.2 SPLITTING TEST RESULTS.....	101
6.4 PARAMETERS FOR MODEL VERIFICATION PROCESS.....	103
6.5 INVERSE ANALYSIS FOR VERIFICATION OF TENSILE CONSTITUTIVE MODEL	107
6.5.1 FINITE ELEMENT MODELLING APPROACH.....	108
6.5.2 INVERSE ANALYSIS RESULTS AND EVALUATION.....	110
6.6 ANALYSIS OF MODEL VERIFICATION EXPERIMENTAL DATA.....	114
6.6.1 FLEXURAL BEHAVIOUR FOR REINFORCED CONCRETE BEAMS WITHOUT STEEL FIBRES.....	115
6.6.2 FLEXURAL BEHAVIOUR FOR STEEL REINFORCED CONCRETE BEAMS.....	116
6.6.3 FLEXURAL BEHAVIOUR FOR SFRC BEAMS WITH REINFORCING BARS.....	117
6.7 CONCLUSION.....	118
CHAPTER 7. MODEL VERIFICATION AND DISCUSSIONS.....	120
7.1 INTRODUCTION.....	120
7.2 FLEXURAL BEAM CAPACITY FOR REINFORCED CONCRETE-2Y10.....	120
7.3 FLEXURAL BEAM CAPACITY FOR SFRC.....	122
7.3.1 FLEXURAL BEAM CAPACITY FOR SFRC WITH 1.0% STEEL FIBRES-MB0- C1.0%.....	123
7.3.2 FLEXURAL BEAM CAPACITY FOR SFRC WITH 1.5% STEEL FIBRES.....	124
7.4 FLEXURAL BEAM CAPACITY FOR REINFORCED SFRC.....	125
7.4.1 FLEXURAL BEAM CAPACITY FOR R-SFRC WITH 1.0% STEEL FIBRES, 2Y10- MB2-B1.0%.....	125
7.4.2 FLEXURAL BEAM CAPACITY FOR R-SFRC WITH 1.5% STEEL FIBRES, 2Y10- MB2-D1.5%.....	128
7.5 COMPARISON OF THE MODEL PREDICTION WITH OTHER MODELS.....	132

7.5.1 DETERMINATION OF POST CRACKING TENSILE STRENGTH USING EMPIRICAL METHODS.....	133
7.5.2 COMPARISON OF THE PROPOSED SFRC FLEXURAL MODEL WITH OTHER MODELS.....	133
7.5.3 COMPARISON OF THE PROPOSED R-SFRC FLEXURAL MODEL WITH OTHER MODELS.....	134
7.6 STATISTICAL ASSESSMENT OF MODEL PREDICTIONS AND EXPERIMENTAL RESULTS.....	135
7.7 CONCLUSION.....	137
CHAPTER 8 CONCLUSIONS AND RECOMMENDATIONS.....	139
8.1 CONCLUSIONS.....	139
8.1.1 ANALYTICAL MODELS.....	139
8.1.2 MATERIAL CHARACTERISATION AND MODEL VERIFICATION DATA.....	140
8.1.3 CURRENT MODELS PREDICTIONS, VERIFICATION AND COMPARISON WITH AVAILABLE MODELS IN LITERATURE.....	141
8.2 RECOMMENDATIONS.....	142
8.2.1 ANALYTICAL MODELS	142
8.2.2 MODEL VERIFICATION DATA.....	142
REFERENCE.....	144
APPENDIX A: DERIVATIONS.....	A.1
APPENDIX B: EXPERIMENTAL RESULTS.....	A.3
APPENDIX C: ANALYSIS.....	A.15

LIST OF FIGURES

Figure 1.1: Research Plan and Objectives.....	3
Figure 2. 1: Classification of FRC based on composite mechanics (Naaman, 2003).....	7
Figure 2.2: Influence of amount of steel fibres on the compressive stress behaviour.....	8
Figure 2.3: Influence of the steel fibre aspect ratio on the compressive stress behaviour.....	9
Figure 2.4: Effects of fibre volume and strength on the tensile behaviour of SFRC.....	12
Figure 2.5: Typical load-deflection curves for bending behaviour of SFRC beams	14
Figure 2.6: Compressive stress-strain distributions adopted for SFRC.....	15
Figure 2.7: Examples of stress-strain distributions proposed in literature.....	16
Figure 2.8: Simplified constitutive laws (Di Prisco <i>et al</i> , 2009).....	17
Figure 2.9: Simplified models for determination of f_{fu} , f_{R3} and f_{fs} (Di Prisco <i>et al</i> , 2009).....	18
Figure 2.10: Typical stress-strain distribution and simplified models for bending analysis by Naaman (2003).....	21
Figure 2.11: R-SFRC section with the assumed stress and strain distribution for analysis by Henager and Doherty (1976).....	22
Figure 2. 12: R-SFRC section with the assumed stress and strain distributions for analysis by Tan et al (1995).....	22
Figure 2.13: Parabolic-rectangular compression stress-strain distribution.....	24
Figure 2.14: Bi-linear compressive stress-strain distribution.....	24
Figure 2.15: Stress-strain diagrams for typical reinforcing steel.....	24
Figure 2.16: Idealised and design stress-strain diagrams for steel reinforcement.....	24
Figure 2. 17: Moment-curvature idealisation for non-linear analysis.....	26
Figure 2.18: Specimen for splitting test.....	29
Figure 2.19: Cohesive crack and softening curves (Rocco <i>et al</i> , 2001).....	29
Figure 3.1: Definition of an equivalent rectangular stress block from the simplified parabolic-rectangular compressive stress-strain model.....	33
Figure 3.2: Values of the conversion factors and for derivation of the rectangular stress block from a parabolic-rectangular compressive stress-strain model.....	35
Figure 3.3: Definition of a rectangular stress block from the bi-linear compressive stress-strain model.....	35
Figure 3.4: Values of the conversion factors and for derivation of the rectangular stress block from a bi-linear compressive stress-strain model.....	37
Figure 3.5: Definition of a rectangular stress block from the drop-down constant tensile stress-strain model.....	38

Figure 3.6: Effects of the normalised post-peak strength, to the conversion factors λ_t , η_t and β_t	40
Figure 3.7: Definition of a rectangular stress block from the Rilem tensile stress-strain model.....	41
Figure 3.8: Stages for stress-strain states in SFRC beam.....	43
Figure 3.9: Rectangular stress distribution for design of SFRC.....	43
Figure 3.10: Possible stress-strain states at service using the Rilem's tensile model.....	46
Figure 3.11: Possible stress-strain states at ultimate condition using the Rilem's tensile model.....	46
Figure 3.12: Stress-strain state for cracking moment.....	49
Figure 3.13: Stress-strain state for the moment at yield tensile strength of steel reinforcement.....	50
Figure 3.14: Stress-strain state for the moment at ultimate tensile strength of SFRC.....	52
Figure 3.15: Stress-strain state for the moment at ultimate tensile strength of steel reinforcement..	53
Figure 3.16: Stress-strain state for the moment at ultimate compression strength of SFRC.....	54
Figure 3.17: Strain states for varying amounts of steel reinforcement in R-SFRC beam.....	55
Figure 3. 18: Effects of fibres on the neutral axis ratio; Left: Comparison with NRC at $\mu_t=0.6$; Right: Comparison for varying normalised post-peak (drop-down) tensile strength ratio.....	56
Figure 3.19: Assumed stress and strain states for the design of R-SFRC beams.....	57
Figure 4.1: Flowchart for research methodology execution.....	60
Figure 4.2: Constituents of the concrete mix used.....	63
Figure 4.3: Compression test set-up and specimen dimensions.....	65
Figure 4.4: Splitting test set-up and specimen dimensions.....	65
Figure 4.5: Four-pint bending test set-up and specimen dimensions.....	66
Figure 4.6: Three-point bending test set-up and specimen dimensions.....	67
Figure 4.7: Four-point bending test set-up and specimen dimensions for the main beams.....	68
Figure 4.8: Conversion of the post-cracking splitting stress to direct post-cracking tensile stress...	70
Figure 4.9: Force vs. deflection curves from bending test for model parameter derivation.....	72
Figure 4.10: Flowchart for statistical evaluation procedure.....	74
Figure 5.1: Stress-strain curves from compression test results for material characterisation.....	78
Figure 5.2: Splitting test results for tensile material characterisation.....	79
Figure 5.3: Tensile vs. strain derived from the splitting tests based on Rocco <i>et al</i> (2001).....	80
Figure 5.4: Typical post-cracking tensile stress vs. crack width curves superimposed on toughness (denoted G, for fracture energy) vs. crack width curves.....	80
Figure 5.5: Flexural test results.....	82
Figure 5.6: Stress vs. strain relation for Y10 steel bars used in the research.....	84

Figure 5.7: Flexural response for MB2-A0.0% and MB2-F0.0% beams.....	86
Figure 5.8: Typical cracking patterns for selected beams from MB2-A0.0% and MB2-F0.0%.....	87
Figure 5.9: Flexural response for MB0-C1.0% and MB0-E1.5% beams.....	87
Figure 5.10: Typical cracking patterns for selected beams from MB0-C1.05 and MB0-E1.5%.....	88
Figure 5.11: Flexural response for MB2-B1.0% and MB2-D1.5% beams.....	89
Figure 5.12: Typical cracking patterns for selected beams from MB2-b1.0% and MB2-D1.5%.....	90
Figure 6.1: Correlation of the Young's modulus for category I experiments with the EN 1992-1-1 analytical expression for the Young's modulus.....	94
Figure 6.2: Correlation of the Young's modulus for category II experiments with the EN1992-1-1 analytical expression for the Young's modulus.....	95
Figure 6.3: Correlation of the Young's modulus for category III experiments with the EN 1992-1-1 analytical expression for the Young's modulus.....	96
Figure 6.4: Variation of the equivalent post-peak tensile strength with crack width for MC-B1.0% (Sample no. B3).....	105
Figure 6.5: Variation of the equivalent post-peak tensile strength with crack width for MC-E1.5% (Sample no. E3).....	105
Figure 6.6: Simplified stress-strain curves for steel reinforcement for the model verification.....	107
Figure 6.7: Inverse analysis procedure for constitutive model verification.....	108
Figure 6.8: Finite element model showing meshing and layout of the beam.....	109
Figure 6.9: Boundary conditions for the finite element model.....	109
Figure 6.10: Tensile stress-strain curves from experimental data and the proposed curve for numerical analysis.....	110
Figure 6.11: The variation of flexural strength for standard beam with toughness and tensile strength.....	111
Figure 6.12: Comparison of the numerical solution with experimental data for PC1.0%.....	112
Figure 6.13: Comparison of the numerical solution with experimental data for PC1.5%.....	112
Figure 6.14: Comparison of the numerical solution (for a targeted strength) with experimental data from PC1.0% beams.....	113
Figure 6.15: Stress vs. crack width from a numerical analysis and experimental data.....	114
Figure 6.16: Typical moment-displacement curves for MB2-A0.0% and MB2-F0.0% beams.....	116
Figure 6.17: Typical moment-displacement curves for MB0-C1.0% and MB0-E1.5% beams.....	117
Figure 6.18: Typical moment-displacement curves for MB2-B1.0% and MB2-D1.5% beams.....	118
Figure 7.1: Moment-curvature curves derived from the model predictions for MB2-B1.0%.....	127
Figure 7.2: Moment-curvature curves derived from the model predictions for MB2-D1.5% using the combined characterisation parameters.....	130

Figure 7.3: Moment-curvature curves derived from the model predictions for MB2-D1.5% using characterisation parameters for batch MB2-D1.5% only.....	132
Figure 7.4: Scatter plot of experimental and model predictions for SFRC without steel bars (MB0-C1.0% and MB0-E1.5% beams)	136
Figure 7.5: Scatter plot of experimental and model predictions for R-SFRC (MB2-B1.0% and MB2-D1.5% beams).....	136

LIST OF TABLES

Table 1.1: Sampling for material characterisation tests.....	5
Table 1.2: Sampling for model verification tests	5
Table 2.1: Efficiency factor, λ_{pc} and product $\alpha_1\alpha_2$ for some fibre types (Suwannaharn, 2009).....	10
Table 2.2: Steel fibre properties in a mortar matrix.....	11
Table 2.3: Values for parameters K_1 and K_2 for different types of fibres with varying fibre percentages.....	12
Table 2.4: Neutral axis depth ratio, normalised moment and curvature for SFRC model by Soranakom and Mobasher (2007).....	19
Table 3.1: Neutral axis, curvature and lever arm formulas using the bi-linear and the drop-down models.....	43
Table 3.2: Lever arm ratios at service and ultimate states using the bi-linear and the Rilem tensile models.....	48
Table 3.3: Possible strain states combinations for determination of moments for R-SFRC beams..	48
Table 4.1: Sample groups for preliminary material characterisation tests.....	61
Table 4.2: Sample size and specimen dimensions for material characterisation tests (Phase I).....	61
Table 4.3: Sample groups of the bending test program for Phase II.....	62
Table 4.4: Sample size and specimen dimensions for Phase II tests.....	62
Table 4.5: Concrete mix proportions used in the experimental program.....	63
Table 4.6: Properties of Wiremix® ZL30/0.5.....	64
Table 4.7: Spacing for loading points and support bearing widths for the four-point bending test..	67
Table 5.1: Slump of concrete sample groups.....	77
Table 5.2: Compression strength and Young's modulus from material characterisation tests.....	78
Table 5.3: Tension strength parameters from the splitting tests.....	81
Table 5.4: Toughness and ultimate crack widths at ultimate tensile strain of 25‰ for SFRC.....	81
Table 5.5: Four-point flexural characterisation data for varying volumes of steel fibres.....	83
Table 5.6: Three-point flexural characterisation data for SFRC with 1.0% steel fibres.....	83
Table 5.7: Tensile parameters for Y10 steel reinforcement.....	83
Table 5.8: Model verification flexural tests sample groups.....	84
Table 5.9: Flexural response for MB2-A0.0% and MB2-F0.0% beams.....	86
Table 5.10: Flexural response for MB0-C1.0% and MB0-E1.5% beams.....	88
Table 5.11: Flexural response for MB2-B1.0% and MB2-D1.5% beams.....	90
Table 6.1: Compression test results summary for category I, with CoV in brackets.....	93

Table 6.2: Compression test results summary for category II, with CoV in brackets.....	94
Table 6.3: Compression test results summary for category III, with CoV in brackets.....	95
Table 6.4: Tension test results summary for Category I, with CoV in brackets.....	97
Table 6.5: Tension test results summary for Category II, with CoV in brackets.....	97
Table 6.6: Tension test results for Category III, with CoV in brackets.....	98
Table 6.7: Statistical values for the compression strength of Category I concrete.....	99
Table 6.8: Results from a t-test for the compression strength of Category I concrete.....	99
Table 6.9: Statistical values for the compression strength of Category II concrete.....	100
Table 6.10: Results from a t-test for the compression strength of Category II concrete.....	100
Table 6.11: Statistical values for the compression strength of Category III concrete.....	100
Table 6.12: Results from a t-test for the compression strength of Category III concrete.....	101
Table 6.13: Statistical values for the tensile strength of Category I concrete.....	101
Table 6.14: Results from a t-test for the tensile strength of Category I concrete.....	101
Table 6.15: Statistical values for the tensile strength of Category II concrete.....	102
Table 6.16: Results from a t-test for the tensile strength of Category II concrete.....	102
Table 6.17: Statistical values for the tensile strength of Category III concrete.....	102
Table 6.18: Results from a t-test for the tensile strength of Category III concrete.....	103
Table 6.19: Coefficients K_n for 5% characteristic value.....	103
Table 6.20: Compression parameters for the model.....	103
Table 6.21: Tension parameters for the model based on the Code definition.....	106
Table 6.22: Tension parameters for the model based the theory of elasticity by Rocco <i>et al</i> (2001).106	106
Table 6.23: Tensile parameters for Y10 steel reinforcement.....	106
Table 6.24: Program for the numerical analysis showing different cases.....	111
Table 7.1: Model input parameters for MB2-A0.0% and MB2-F0.0% beams.....	121
Table 7.2: Predicted moment capacity for MB2-A0.0% and MB2-F0.0% beams.....	122
Table 7.3: Comparison of experimental and predicted moment capacity for MB2-A0.0% and MB2-F0.0% beams.....	122
Table 7.4: Model input parameters for SFRC beams, MB0-C1.0%.....	123
Table 7.5: Comparison of experimental and predicted moment capacity for MB0-C1.0% beams...	123
Table 7.6: Model predictions using the combined characterisation parameters for MB0-E1.5% beams.....	124

Table 7.7: Model predictions for MB0-E1.5% using characterisation parameters from batch MC-E1.5% only.....	124
Table 7.8: Comparison of the experimental and predicted moment capacity for MB0-E1.5% beams.....	125
Table 7.9: Model input parameters and moment predictions for MB2-B1.0% beams.....	126
Table 7.10: Comparison of the experimental and the predicted moment capacity for MB2-B1.0% beams.....	127
Table 7.11: Model input parameters and moment predictions for MB2-D1.5% beams using the combined characterisation parameters.....	129
Table 7.12: Comparison of the experimental and the predicted moment capacity for MB2-D1.5% beams using the combined characteristic parameters.....	130
Table 7.13: Model parameters and moment predictions for MB2-D1.5% beams using characterisation parameters from MC-D1.5% only.....	131
Table 7.14: Comparison of the experimental and the predicted moment capacity for MB2-D1.5% beams using characterisation parameters from MC-D1.5% only.....	132
Table 7.15: The post-cracking tensile strength for SFRC derived from the empirical expressions...	133
Table 7.16: Comparison of the current SFRC model with the model by Soranakom and Mobasher (2009) using experimental data from literature (Soranakom & Mobasher, 2009).....	134
Table 7.17: Comparison of the current SFRC model with the model by Soranakom and Mobasher (2009) using current experimental data.....	134
Table 7.18: Comparison of the current SFRC model with the model by Naaman (2003).....	134
Table 7.19: Comparison of the current R-SFRC model with the model by Henager and Doherty (1976).....	135
Table 7.20: Correction factors and coefficient of variations of the error term for the current models.....	137

CHAPTER 1 INTRODUCTION

Steel fibre-reinforced concrete (SFRC) is a composite material characterised by an enhanced post-cracking tensile residual strength due to the fibre reinforcement mechanisms provided by fibres bridging the crack surfaces (Rossi & Chanvillard, 2000). This post peak tensile behaviour is influenced mainly by the number of fibres effectively crossing a crack and the bond and strength properties of the type of fibres used. With proper design, steel fibres can be used to substitute conventional reinforcement (Rossi & Chanvillard, 2000; and Soranakom & Mobasher, 2007, 2009).

Utilisation of steel fibres in structural systems requires thorough research on the material behaviour, development of analysis models, verification of the analysis models and ensuring adequate structural reliability (Dymond & Retief, 2010). This thesis will follow these steps in order create flexural capacity models to be used in the design of SFRC beams. Two models are devised for the determination of the flexural capacity of SFRC with and without reinforcing bars. The models developed are based on the use of equivalent rectangular stress blocks for both compression and tensile stress distributions in a beam cross-section.

When developing any design procedure for structures using common and established materials, such as reinforced normal concrete, it is standard practice to use a structural engineering theory as well as a broad experience base on the behaviour of such materials. Structural safety of these common materials is considered by means of the reliability theory, combined with proven past practice. However, in the case of new materials such as steel fibre-reinforced concrete (SFRC), the absence of past experience means that one has to either use extensive test results or make use of the reliability theory (Dymond & Retief, 2010). Therefore, an experimental program has been designed in such a way that desired data is acquired for both material characterisation and model verification processes. Due to time restrictions, only a limited amount of data is captured whereafter the reliability theory is applied in order to ensure that the models achieve the required safety levels.

In this research, standard cube specimens, as used in standard compressive testing of concrete, are used for determination of both compression and tensile (splitting) properties while standard beam specimens are used for flexural characterisation.

1.1 BACKGROUND

Fibre-reinforced concrete has received growing attention amongst international researchers, especially with the realisation that its presence in conventional concrete improves certain mechanical properties of concrete. Different combinations of fibre types and contents and matrix compositions mixed using various production methods yield a vast range of material behaviour. The mechanical behaviour of the concrete may, for a change in fibre content alone, vary between being almost as brittle as plain concrete to being close to elastic-plastic or even deformation-hardening materials. Due to this flexibility of fibre-reinforced concrete and its ability to change the mechanical behaviour for different uses, the material design becomes closely connected with the structural design and vice versa. The beneficial effects of fibre reinforcement are therefore twofold: not only are mechanical properties such as

toughness and strength improved, but there are also new possibilities for optimisation of materials for certain structures.

The most commonly used types of fibre-reinforced concrete are those with steel fibres added in low volumes (up to about 1% per volume) in normal mix proportions with coarse aggregates. When low volumes of steel fibres are used, elastic properties and strength of the composites are usually not affected. Instead, it is the improvement of toughness and the crack distributing properties that motivate the use of fibres.

Some of the applications for steel fibre reinforced concrete, SFRC, are floors, pavements and other plane structures where fibres act as crack distributing reinforcement. Another type of application is the use of SFRC in combination with reinforcement bars in structural members. The fibres may act as shear reinforcement and also improve the load carrying capacity of the reinforcing bars due to improved crack distribution.

The material characterisation, modelling and design approach for SFRC is currently being studied by many researchers (Soranakom & Mobasher, 2007, 2009; Vandewalle & Dupont, 2003; Vandewalle *et al*, 2002; ACI Committee 318, 2005; and ACI Committee 544, 1996) who aim to develop reliable guidelines for the design of structures using SFRC as a codified design approach does not exist. Flexural models based on a drop down stress distribution for tension and a bilinear stress distribution for compression have been developed by Soranakom and Mobasher (2007, 2009) where closed form equations are used, while the ACI (ACI Committee 318, 2005) outlines the possibility of using a rectangular stress block for tensile stress distributions as is the case with compression stress distributions.

In this paper, the use of equivalent stress blocks is adopted where slight modifications are made in accordance with the recommendations of ACI (ACI Committee 544, 1996) and Eurocode (European Standards, 2002). A drop down tensile stress distribution (i.e. elastic up to cracking strength, drop down at cracking strain, then plastic response) and RILEM'S tensile stress distribution (Vandewalle & Dupont, 2003) are employed.

1.2 PROBLEM STATEMENT

The utilisation of SFRC for structural applications is hindered by the absence of a codified design approach. There is therefore a need to establish and assess design models for various design aspects on the use of SFRC in various structural applications.

1.3 RESEARCH OBJECTIVES

1.3.1 MAIN OBJECTIVE

The main objective of this research is to develop analytical methods for the determination of the flexural capacity of steel fibre-reinforced concrete sections with or without reinforcing bars. The specific objectives are outlined below.

1.3.2 SPECIFIC OBJECTIVES

Specific objectives for this study are to:

- i. evaluate and characterise the material properties of SFRC, especially the post peak tensile behaviour;

- ii. develop analytical models for flexural design of SFRC with and without steel bars; and
- iii. assess and verify the analytical models based on experimental data acquired by physical laboratory testing and available data from literature.

1.4 IMPORTANCE OF THE RESEARCH

While extensive research is being conducted on this new material, the utilization of SFRC in the construction industry has been very limited due to insufficient details on the design procedures and an absence of a code allowing the use of tensile contribution in SFRC elements. This research is therefore one of numerous efforts made by researchers in understanding the material properties and developing design models in order to develop a codified approach for the utilization of SFRC. Analytical models developed in this paper are useful in providing an assessment of the potential structural benefits of using steel fibres as lone reinforcement or in combination with a reduced number of reinforcing bars. It will furthermore provide guidance to the designers and code writers for this new material on the appropriateness of using steel fibres in different situations. By following basic principles of mechanics of materials, the models offer an opportunity to evaluate the existing models and identify the critical parameters for design of SFRC members.

1.5 METHODOLOGY

A methodology for the determination and verification of the proposed flexural models for SFRC is shown in Figure 1.1. The paragraphs that follow outline the general methodology used in data collection, sampling, and analysis of experimental results.

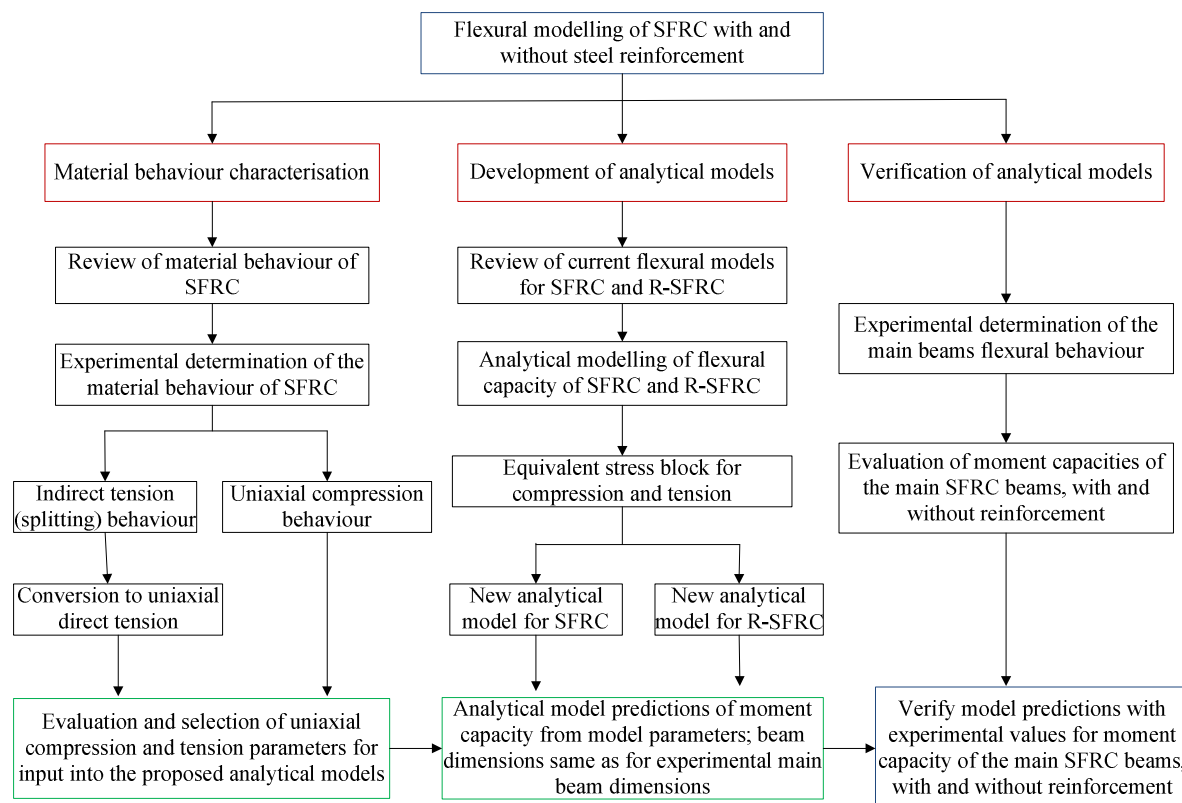


Figure 1.1: Research Plan and Objectives

1.5.1 DATA COLLECTION

The required data for the use in analytical models will be obtained through experimental testing. Both mean values and characteristic values of the material properties are used in the models. Two phases of experiments are conducted: experiments for preliminary characterisation of material behaviour and experiments for verification of analytical models.

1.5.1.1 CHARACTERISATION OF MATERIAL PROPERTIES

The splitting test is used for the determination of tensile properties. This is an indirect tensile test method used to determine the ultimate (maximum) tensile strength, strain at maximum tensile strength (cracking tensile strain), and fracture energy for post peak tensile behaviour using 100mm cubes of SFRC. A compressive test is conducted to determine the compressive response of SFRC, establishing the ultimate compressive strength, yield compressive strain and Young's Modulus using 100mm cubes of SFRC.

A four-point bending test is conducted on standard 100 x 100 x 500 mm unnotched SFRC beams to determine the flexural model parameters used in analysis when RILEM'S tensile stress distribution is used. This test ascertains the limit of proportionality, equivalent flexural stresses and residual stresses.

1.5.1.2 VERIFICATION OF ANALYTICAL MODELS

Four-point bending tests on 150 x 300 x 750 mm SFRC beams are conducted, determining the flexural response of SFRC beams used for model verification. These beams are assumed to represent the structural response of beams in a structure.

1.5.2 SAMPLING AND SAMPLE SIZE

A target cube compressive strength of 30MPa, with 1.0% and 1.5% hooked Dramix® ZP305 and Wiremix® ZL30/0.5 steel fibres by volume, thus having a dosage of 78.5kg/m³ and 117.75kg/m³ respectively, is selected. This is well above the minimum amount of fibres required for SFRC to display deflection hardening behaviour and therefore can be considered to offer structural resistance (ACI Committee 318, 2005, ACI Committe 544, 1996).

In characterisation tests, at least four (4) samples per test are used while in verification experiments at least three (3) samples are used. For experimental verification tests, three main beams of dimension 150 x 300 x 750 mm are used while 100mm cubes are used for characterisation tests.

Two level single factorial experiments are conducted for material characterisation where the amount of fibres is varied in two amounts, with the third being a control experiment as shown in Table 1.1. Verification experiments involve a two-level two-factorial experiment where the amount of steel fibres and steel reinforcements are varied as shown in the experimental matrix in Table 1.2.

Table 1.1: Sampling for material characterisation tests

Fibre %	Batch
$V_f = 0.0\%$	A, F
$V_f = 1.0\%$	C, B
$V_f = 1.5\%$	E, D

Table 1.2: Sampling for model verification tests

Fibre %	Amount of steel reinforcement	
	$\rho = 0.0\%$	$\rho = 0.4475\%$
$V_f = 0.0\%$	-	A, F
$V_f = 1.0\%$	C	B
$V_f = 1.5\%$	E	D

1.5.3 DATA ANALYSIS

The data is analysed by means of a material characterisation process and a verification of analytical models.

1.5.3.1 MATERIAL CHARACTERISATION PROCESS

In this phase both mean and characteristic values of material strength are determined. A statistical data analysis is performed in order to determine the characteristic strength properties, calculated according to EN 1990 based on the 5th percentile of the material strength. The following expression is used in establishing the characteristic strength parameters:

$$X_c = X_m - K_n \sigma \quad 1.1$$

where X_c is the characteristic strength parameter for the material;

X_m is the sample mean ;

K_n is the fractile estimator and depends on the sample size and the required level of confidence (in this case 95% is used for characteristic strength parameters); and

σ is the sample standard deviation.

1.5.3.2 VERIFICATION OF ANALYTICAL MODELS

Comparative analysis is used for verification of the analytical models with experimental results. In this case, statistical approaches are used and some refinement to the model and or process of characterisation of the material is proposed.

1.6 SCOPE OF STUDY

This paper only outlines the analytical models for the determination of flexural capacity of SFRC with strain softening deflection hardening behaviour. In this case, SFRC with and without reinforcing bars are considered. However, the models can also be applicable for material with perfect plastic post peak tensile behaviour.

1.7 STRUCTURE OF REPORT

In this chapter an introduction was supplied to the study. Chapter 2 outlines the theoretical foundations on which the analytical models are based while Chapter 3 thoroughly discusses the research problem, outlining the analytical frameworks and models developed for the determination of the flexural capacity. In Chapter 4 the research design and methodology are described, while an in depth discussion and analysis of the results are given in Chapters 5 and 6, followed by analytical model verification, conclusions and recommendations in Chapters 7 and 8 respectively.

1.8 CONCLUSION

In this study analytical models will be developed and verified for flexural strength of SFRC beams with and without reinforcing steel bars. The models are derived from simplified rectangular stress blocks for both compression and tension stresses. In order to verify the results from the analytical models, an experimental program is developed and executed to determine the material characteristics and material model parameters, as well as the flexural behaviour of SFRC beams. For comparison of experimental and analytical results, mean and characteristic experimental values are used for model parameters.

CHAPTER 2. THEORETICAL FOUNDATION

2.1 INTRODUCTION

Fibre-reinforced cement-based composites (FRCC) are known to improve concrete tensile strength and reduce brittleness. Research has shown that fibre volume, fibre aspect ratio, concrete matrix strength and interfacial properties at fibre-matrix interface influence the FRCC tensile properties (Van Zijl & Boshoff 2006). FRCC have been classified according to their post-peak response. Composites that exhibit a tensile stress-strain response characterised with strain-hardening accompanied by multiple cracking are classified as Strain-Hardening Cement-based Composites (SHCC) (Van Zijl & Wittman, 2011). All materials that display a tensile strain-hardening also exhibit deflection-hardening behaviour as shown in Figure 2.1 (Naaman, 2003). These materials include Slurry-Infiltrated Fibre Concrete (SIFCON), Fibre-Reinforced DSP (Densified Small Particles Systems), Slurry-Infiltrated Mat Concrete (SIMCON) and Compact Reinforced Concrete (CRC). However, some cement composites only exhibit multiple cracking in bending but not in tension. These composites have been classified as Ductile Fibre-Reinforced Cement-based Composites (DFRCC) (Naaman, 2003). Both SHCC and DFRCC are subclasses of High Performance Cement-based Composites (HPRCC), where HPRCC generally refers to classes of cement-based composites with high tensile or flexural strength and those with high tensile ductility.

In order to explore the benefits of SFRC, several models have been developed to predict both the tensile strength of SFRC and the flexural capacity of sections with SFRC. Since it is the objective of this paper to develop and verify flexural models, some of the models already developed for SFRC, together with common models for normal concrete will be reviewed in the following sections. A preamble of the material behaviour and characterisation methods for SFRC is given first.

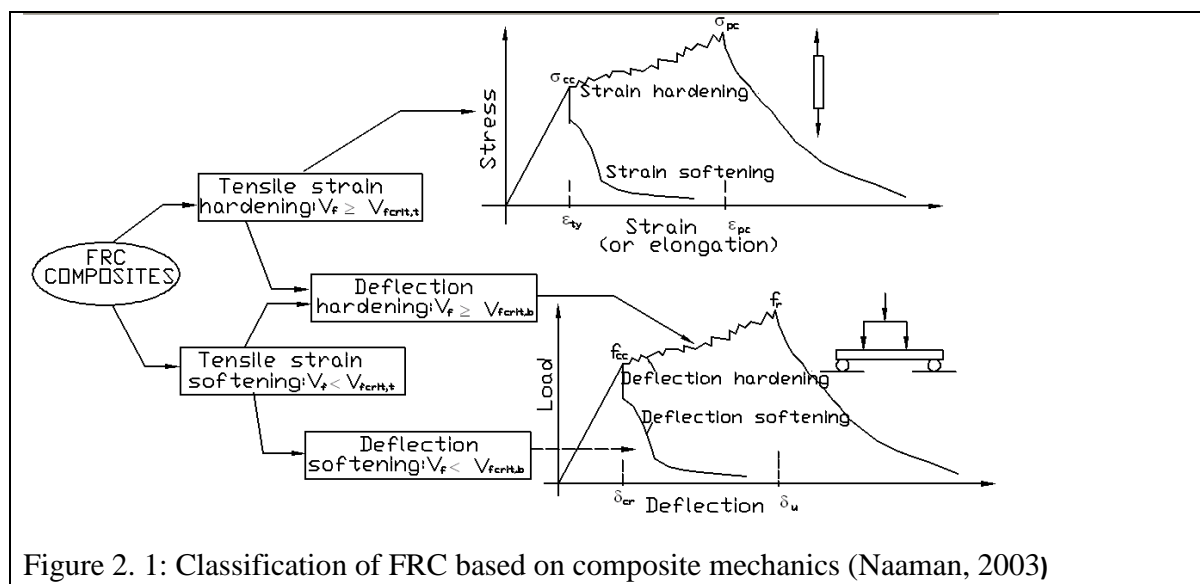
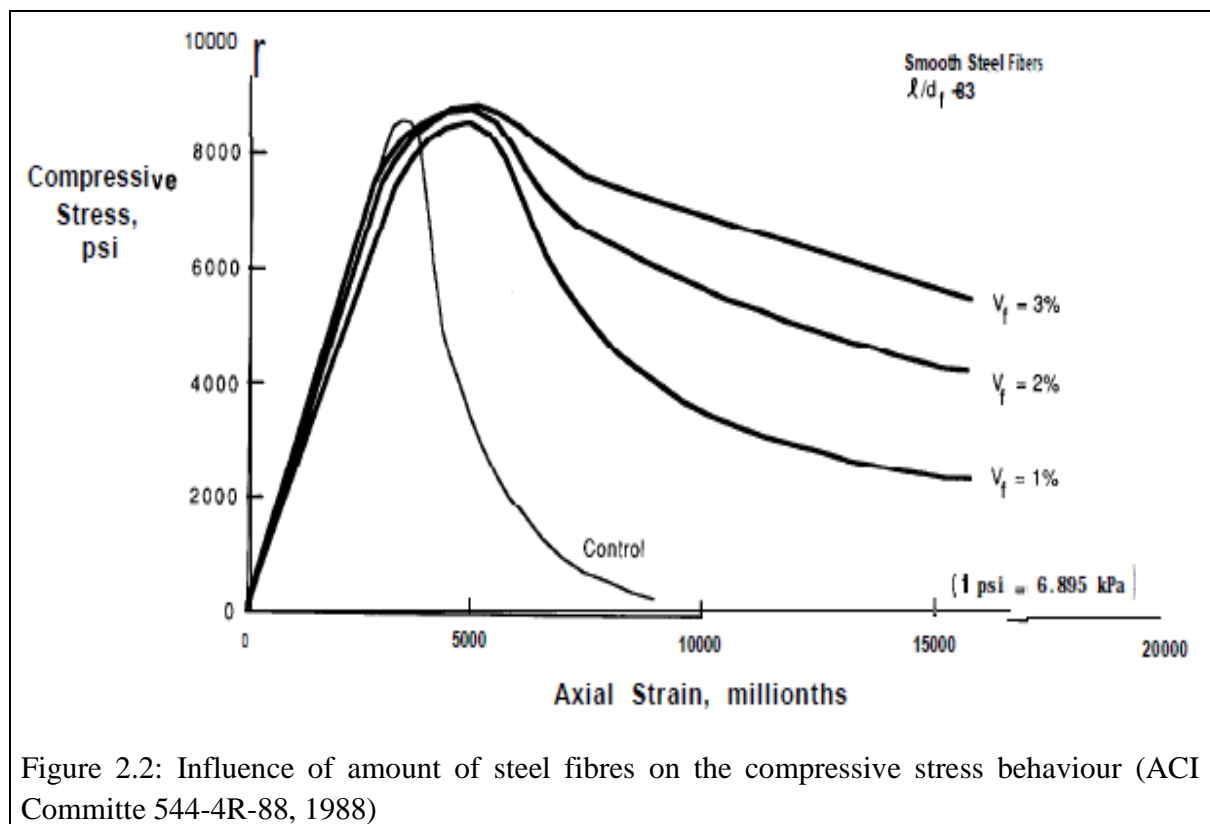


Figure 2. 1: Classification of FRC based on composite mechanics (Naaman, 2003)

2.2 MATERIAL BEHAVIOUR AND CONSTITUTIVE MODELS FOR SFRC

2.2.1 COMPRESSIVE BEHAVIOUR

The compressive behaviour of concrete is influenced by proportions and properties of its constituent materials. Concrete with a low water-to-cement ratio may display high compressive strength. Normal concrete with high compressive strength usually shows more brittle behaviour. For small amounts of steel fibres added to concrete, the compressive strength in concrete does not significantly improve (see Figure 2.2). However, post-cracking ductility of the composite may be improved with the addition of steel fibres (ACI Committee 544-4R-88, 1988). The amount of fibres and the fibre aspect ratio affect the compressive behaviour of SFRC, especially in the post-cracking region as illustrated in Figures 2.2 and 2.3, extracted from ACI544-4R-88.



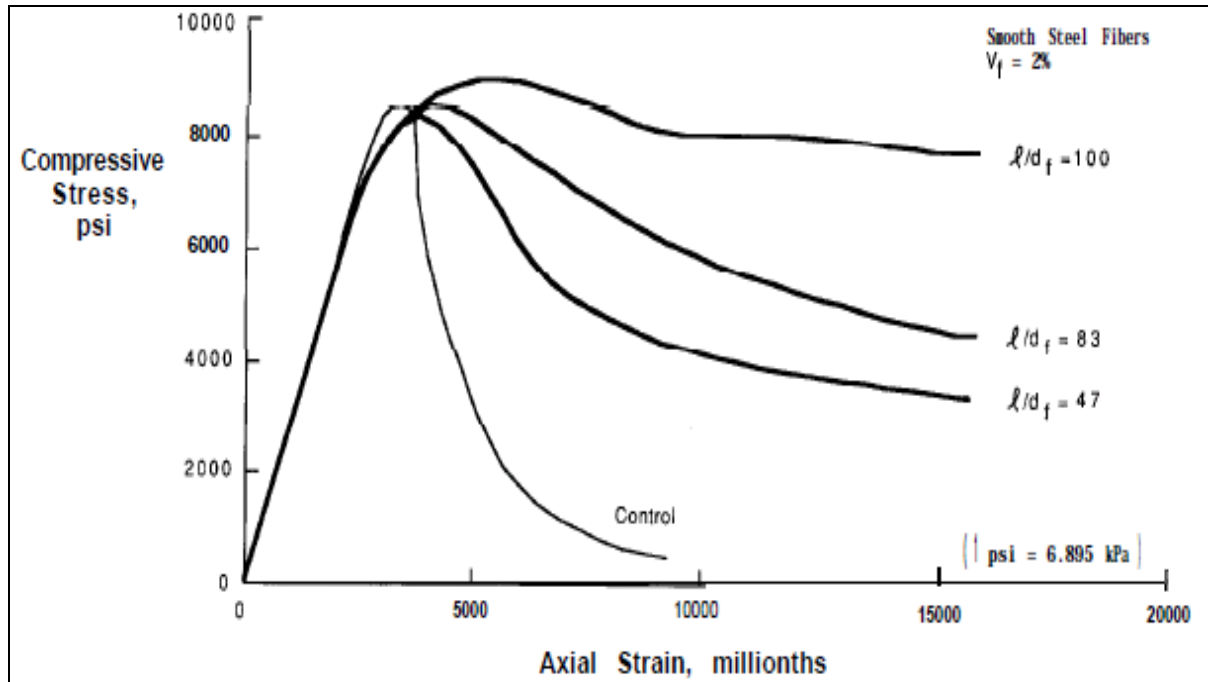


Figure 2.3: Influence of the steel fibre aspect ratio on the compressive stress behaviour (ACI Committee 544-4R-88, 1988)

2.2.2 TENSILE BEHAVIOUR

As stated earlier, SFRC may exhibit either strain-hardening or strain-softening behaviour due to the fibre content. Strain-hardening SFRC always exhibits deflection-hardening behaviour while the strain-softening material may exhibit either deflection-hardening or deflection-softening behaviour (Naaman, 2003). Certain conditions must be met in order for the material to be classified as either deflection-hardening or strain-hardening. The conditions by which FRC are classified are based on composite mechanics and fracture mechanics. Naaman developed a condition using composite mechanics (Naaman, 2003), while Li and Wu (1992), and Tjiptobroto and Hansen (1993) developed one condition each based on fracture mechanics.

Using composite mechanics, Naaman (2003) developed formulas for cracking tensile strength, σ_{cc} , and post-cracking tensile strength, σ_{pc} given in Equations 2.1 and 2.2. The post-cracking strength assumes that a critical crack exists across the entire section of the tensile member, the crack is normal to the tensile stress field and the contribution of the matrix is neglected.

$$\sigma_{cc} = \sigma_{mu} (1 - V_f) + \alpha_1 \alpha_2 \tau V_f \frac{l_f}{d_f} \quad 2.1$$

$$\sigma_{pc} = \lambda_{pc} \tau V_f \frac{l_f}{d_f} \quad 2.2$$

$$\text{and } \lambda_{pc} = \lambda_1 \lambda_2 \lambda_3$$

where

λ_1 is the expected pull-out length ratio (equal to $\frac{1}{4}$ from probability considerations);

λ_2 is the efficiency factor for orientation in cracked state;

λ_3 is the group reduction factor associated with the number of fibres pulling out per unit area (or for density of fibre crossings);

α_1 is the coefficient representing the fraction of bond mobilised at first crack matrix cracking;

α_2 is the efficient factor of fibre orientation in the uncracked state of the composite;

σ_{mu} is the tensile strength of the matrix;

τ is the average bond strength at the fibre matrix interface;

d_f is the fibre diameter;

l_f is the fibre length; and

V_f is the volume fraction of fibres.

Based on the above formulas, a critical volume fraction of fibres above which the material exhibits strain-hardening is the fibre volume at which the post-cracking tensile strength is greater than the cracking tensile strength and is given as follows:

$$V_f \geq V_{f_{crit}} = \frac{1}{1 + \frac{\tau}{\sigma_{mu}} \frac{l_f}{d_f} (\lambda_1 \lambda_2 \lambda_3 - \alpha_1 \alpha_2)} \quad 2.3$$

Suwannakarn (2009) developed empirical expressions for an efficiency factor λ_{pc} and the product of factors α_1 and α_2 for some fibre types. He found out that the efficiency factor λ_{pc} varies for different fibre types and reduces with increase in the amount of fibres. Average values for the product $\alpha_1 \alpha_2$ were used as no trend existed. Table 2.1 summaries the analytical expressions for λ_{pc} and average values of $\alpha_1 \alpha_2$ with the range of fibre volumes over which the expressions are valid.

Table 2.1: Efficiency factor, λ_{pc} and product $\alpha_1 \alpha_2$ for some fibre types (Suwannakarn, 2009)

Fibre type	Efficiency factor λ_{pc}		Product of $\alpha_1 \alpha_2$	
	Analytical expression	Range of fibre volume	Average value	Range of fibre volume
PVA fibre	$-0.707V_f + 2.093$	0.75% -2.0%	0.520	0.75% -2.0%
Torex steel fibre	$-26.6V_f + 0.97$	0.75% -2.0%	0.094	0.75% -2.0%
Spectra fibre	$-20.8V_f + 0.63$	0.75% -2.0%	0.042	1.0% -2.0%
Hooked steel fibre	$-55.6V_f + 2.58$	1.0% -2.0%	0.295	1.0% -2.0%

The post-cracking tensile strength (ultimate tensile strength) can also be determined by considering the effect of fibre pull-out at an angle (snubbing factor) as outlined by Li (Li, 1992a and Li *et al*, 1990). The following expression for post-peak tensile strength was developed:

$$\sigma_{pc} = \frac{1}{2} g \tau V_f \frac{l_f}{d_f} \quad 2.4$$

where g is the snubbing factor.

The material model parameters in Equation 2.4 for various fibre types have been determined and confirmed by various researchers (Van Zijl & Boshoff, 2006; Li *et al*, 1990; Bentur & Mindess, 1990; Li *et al*, 2002 and Kosa & Naaman, 1990). Table 2.2 supplies the properties of different types of fibres.

Suwannakarn (2009) explored the post-cracking behaviour of HPFRCC using a regular mortar having an unconfined compressive strength of 56MPa. His research findings confirmed that tensile behaviour of HPFRCC is influenced by the amount of fibres and the strength of steel fibres used. Figure 2.4 shows some of the results from direct tensile tests conducted on mortars. High strength steel fibres tend to display strain-hardening at low volumes of steel fibres as low as 0.75%. For regular steel fibres, the maximum tensile stresses were found to be 2.04MPa, 1.94MPa and 2.98MPa for fibre percentages of 1.0%, 1.5% and 2.0% respectively. In composites with high strength fibres, the maximum tensile stresses were found to be 2.71MPa, 3.69MPa, 4.19MPa and 5.78MPa for fibre percentages of 0.75%, 1.0%, 1.5% and 2.0% respectively.

Table 2.2: Steel fibre properties in a mortar matrix (Van Zijl & Boshoff, 2006)

Fibre Type	RD	E_f (kPa)	Strength (MPa)	Elongation (%)	l_f (mm)	l_f/d_f (μ m)	g	τ (MPa)
Steel	7.85	200	300-2000	2-5	15-50	100	2.0	4.0
Asbestos	2.55	164	200-1800	2-3	5-40			
Polyethylene:	0.96			3-20				
Spectra		73		4	12.7	335	1.6	0.5
Dyneema		73		4	6.7	670	1.6	0.5-1
Polyvinyl Alcohol:	1.3							
Untreated		40	1620	6	12	300		3.5
Surface treated								1
Untreated		60	1660	6	6	430		3.6
Surface treated								2
Glass:	2.7	70	600-2500	3.6	10-50			
		80			36	3000		0.3
E-glass		72.4	2400					
S-glass		88	4600					
Polypropylene	0.9	4-6	300-500	10	5-50			
		6			13	186		0.7
		3.7	295		10	556		
		3.7	295		6	333		
		3.7	295		10	233		
Carbon	1.2-2	200-345	2000-2400	<2		300	1.0	2-8

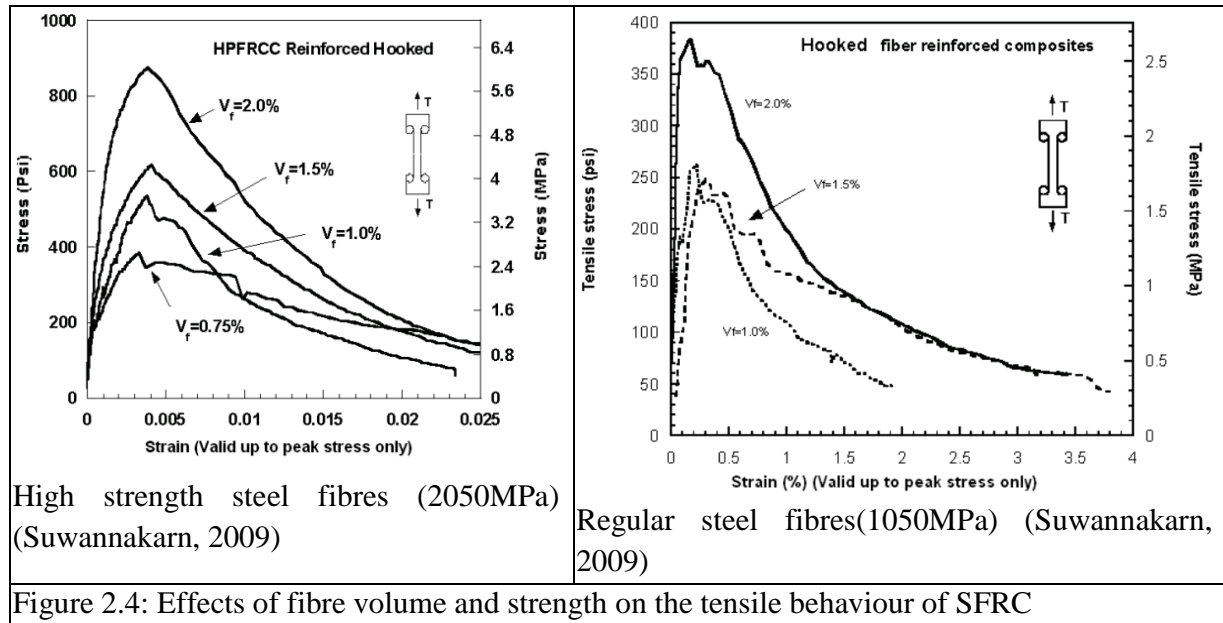


Figure 2.4: Effects of fibre volume and strength on the tensile behaviour of SFRC

Kosa and Naaman (1990) developed an expression for predicting post-cracking tensile stress vs. crack opening for a notched specimen. Fibre length together with a modifier, K_1 , was used to define the cracking behaviour (Kosa & Naaman, 1990). The modifier K_1 was used to account for any deterioration due to corrosion during pull-out. Using separate experimental data, Suwannakarn (2009) modified the expression by including a K_2 modifier to account for the change in shape of the stress-crack width curve as shown in Equation 2.5. Both K_1 and K_2 modifiers are given in Table 2.3.

$$\frac{f_t(w)}{f_{t,m}} = \left(1 - \frac{w}{0.5K_1L_f}\right)^2 e^{-K_2w} \quad 2.5$$

Table 2.3: Values for parameters K_1 and K_2 for different types of fibres with varying fibre percentages

V_f	PVA fibres		Spectra fibres		Hooked steel fibres		Torex fibres	
	K_1	K_2	K_1	K_2	K_1	K_2	K_1	K_2
0.75%	0.111	0	1	11.787	1	4.165	1	6.958
1.0%	0.085	0	1	10.354	1	2.791	1	3.413
1.5%	0.103	0	1	1.9	1	15.156	1	7.291
2.0%	0.1075	0	1	1.774	1	15.839	1	5.45

De Oliveira (2010) proposed analytical models for predicting post-cracking tensile behaviour based on fibre orientation and fibre pullout. Through a comprehensive study of the factors affecting fibre orientation, he developed models for capturing the fibre orientation. A stress vs. crack width relationship for SFRC was developed by De Oliveira (2010) on the basis of the normal concrete stress vs. crack width relationship proposed by Gopalaratman and Shah (1985).

The contribution of fibres is deduced separately and added to the stress vs. crack width relation for the normal concrete as given in Equation 2.6:

$$f_t(w) = f_{tc}(w) + f_{tf}(w)$$

$$\text{with } f_{tc}(w) = f_{tcm} e^{-kw}, \quad f_{tf}(w) = \frac{\sum P_{N,\theta_i}(w)}{A_{\text{sec}}} \quad \text{and } P_{N,\theta_i} = P_{\theta_i} \cdot N_{\theta_i} \quad 2.6$$

where

$k = 39.8/\text{mm}$;

P_{θ_i} is single fibre pullout response; and

N_{θ_i} is the number of fibres at an inclination θ_i .

Using fracture mechanics, Li (1992a) developed a formula for predicting the critical volume of fibres beyond which strain-hardening takes place:

$$V_f \geq V_{f_{\text{crit}}} = \frac{12J_c}{g\tau \frac{l_f}{d_f} w_c} \quad 2.7$$

Where

J_c is the crack tip toughness of the composite; and

w_c is the crack width of the matrix at maximum fibre pullout force and is given as follows:

$$w_c = \frac{d_f^2}{E_f d_f \left(1 + \frac{V_f E_f}{V_m E_m} \right)} \quad 2.8$$

where

E_f is the fibre elasticity modulus;

E_m is the matrix elasticity modulus; and

V_m is the volume fraction of the matrix.

2.2.3 BENDING BEHAVIOUR

As stated earlier, SFRC can exhibit either strain-hardening or strain-softening behaviour under uniaxial tension. SFRC displaying strain-softening behaviour may either present deflection-hardening or deflection-softening behaviour. The deflection-hardening behaviour in strain-softening SFRC is possible, because in bending tests the linear strain profile along the uncracked cross section favours a more stable propagation of the cracks. This may induce a significant hardening in bending even if, in uniaxial tension, the material shows a softening behaviour after cracking of the concrete matrix (Di Prisco *et al*, 2009).

Load deflection curves for typical SFRC are shown in Figure 2.5. Usually, a linear response is observed up to first cracking (Limit Of Proportionality - LOP). Beyond this point, the material can exhibit hardening or softening behaviour. Maximum load after initial cracking can be greater or less than the limit of proportionality. Research has been done on the critical parameters determining whether the material will exhibit deflection-hardening or -softening (Naaman, 2003). The cracking moment (moment calculated at the cracking stress of the section) and the modulus of rupture are determined based on linear elastic response. (Note that, in the case of deflection-hardening, MOR is a mere expression of tensile resistance, because the assumption of linear stress distribution in the section does not hold). In a rectangular beam section, the cracking moment and modulus of rupture are given by the following expressions:

$$M_{cr} = \sigma_{cc} \frac{bh^2}{6} \quad 2.9$$

$$MOR = \frac{6M}{bh^2} \quad 2.10$$

where b and h are breadth and overall height (depth) of a rectangular beam; and σ_{cc} is the cracking tensile strength and M is the moment at maximum load after cracking.

Using composite mechanics, Naaman (2003) developed a formula predicting the minimum amount of fibres in order to have deflection-hardening for FRC for cases where fibre pull-out prevails after cracking, as opposed to fibres breaking.

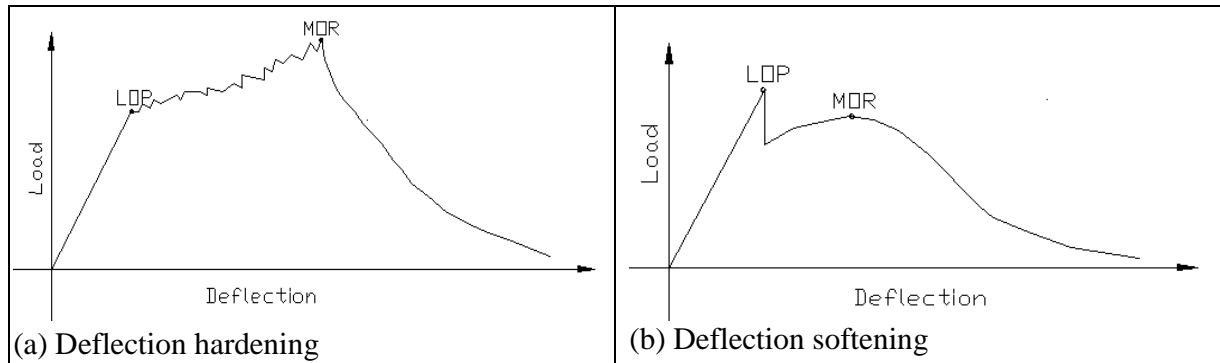


Figure 2.5: Typical load-deflection curves for bending behaviour of SFRC beams

Deflection-hardening occurs when the average post-cracking tensile strength, $\bar{\sigma}_{pc}$, satisfies the following condition:

$$\bar{\sigma}_{pc} \geq k\sigma_{cc} \quad 2.11$$

where k is a coefficient between $\frac{1}{3}$ and 1.0.

The minimum volume of fibres required in order to achieve deflection-hardening in FRC with fibre pull-out and where the fibre length is significantly larger than the crack opening was determined by Naaman (2003) as follows:

$$V_f \geq V_{fcri,b} = \frac{k}{k + \frac{\tau}{\sigma_{mu}} \frac{l_f}{d_f} (\lambda_1 \lambda_2 \lambda_3 - k \alpha_1 \alpha_2)} \quad 2.12$$

where k is a coefficient less than 1.0. Naaman (2003) suggested the use of a minimum value of $k=0.4$ in practical design consideration.

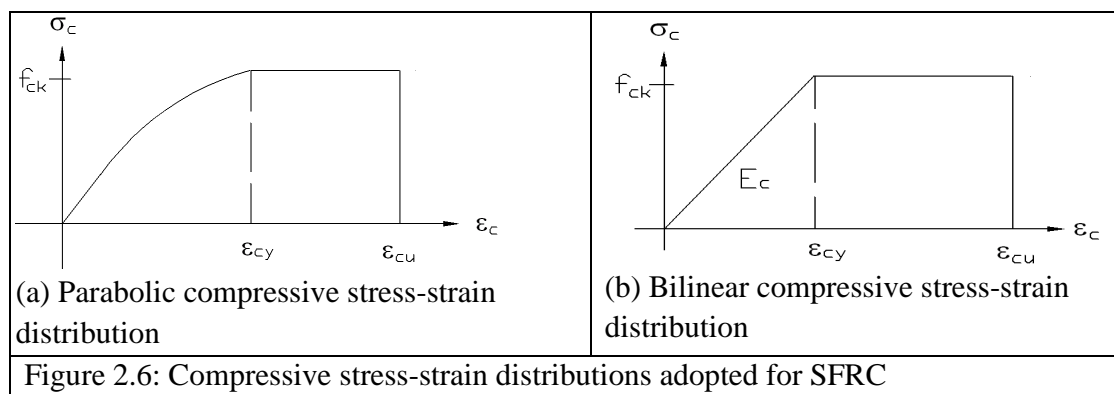
2.3 CONSTITUTIVE MODELS FOR SFRC

In this section a brief outline of material characterisation process is given together with several constitutive models for tension and compression stress distribution.

2.3.1 COMPRESSION BEHAVIOUR

Various constitutive models have been proposed to define the compressive stress-strain relationship for FRC. Some guidelines, such as RILEM (Vandewalle *et al*, 2002) and CNR-DTF (2006), have adopted the same stress-strain relation used in normal concrete for design at ultimate state. Twenty eight day compression strength is determined by uniaxial compression testing using either cubical or cylindrical specimens just as is the case with normal concrete. A parabolic or rectangular compressive stress block is used with ultimate compressive strain (ϵ_{cu}) of 0.0035 and a cracking compressive strain at the peak stress (ϵ_{ty}) of 0.002 for concrete with strength of not more than 50MPa (see Figure 2.6(a)). A simplified bilinear model has been used by Soranakom and Mobasher (2007, 2009) in developing analytical models for bending behaviour (see Figure 2.6(b)).

Various analytical models for the compression stress-strain relationship in SFRC have been proposed by Ezeldin and Balaguru (1992), Barros and Figueiras (1999) and Nataraja *et al*, (1999). Bencardino *et al*, (2007) reviewed these analytical models and concluded that most showed satisfactory agreement with the results from which they were derived, but failed to indicate the same agreement with results obtained from other experiments. They also claimed that the generally recommended ultimate compressive strain of 0.0035 is generally lower than the strain at failure of SFRC. However the ultimate compression strain of 0.0035 is considered by most to be appropriate approximation for the ultimate compression strength.



2.3.2 TENSILE BEHAVIOUR

Characterisation of tensile behaviour is performed either by direct tensile tests or indirect tensile tests. Indirect tests may include the normal splitting test, a wedge splitting test and flexural tests. Using any of these methods, constitutive models have been developed to define the material behaviour for use in design. Most of the models proposed in literature have simple and non-differentiable constitutive diagrams characterised through macroscopic properties by means of inverse analysis (De Oliveira, 2010). These models focus on either the stress-strain (σ - ϵ) or stress-crack width (σ - w) relationships.

Lim *et al* (1987a) proposed a simple drop down model for tension. In this model, tensile stress increases linearly up to cracking point after which resistance drops and is followed by a perfect plastic behaviour (see Figure 2.7(a)). Lok and Xiao (1998) developed a more complex constitutive model incorporating nonlinear behaviour of concrete before reaching ultimate strength. Two gradients for stress-strain curves are used to define the behaviour up to cracking strength. Thereafter, the tensile resistance reduces linearly up to a prescribed strain beyond which perfect plastic behaviour is ensued up to ultimate strain (see Figure 2.7(b)). Another model was proposed by Dupont and Vandewalle (2002), similar to the model proposed by Lim *et al* (1987a), but with a stepped strain-softening response as shown in Figure 2.7(c). A summary of tensile models adopted in some codes in Europe is reported by De Oliveira (2010).

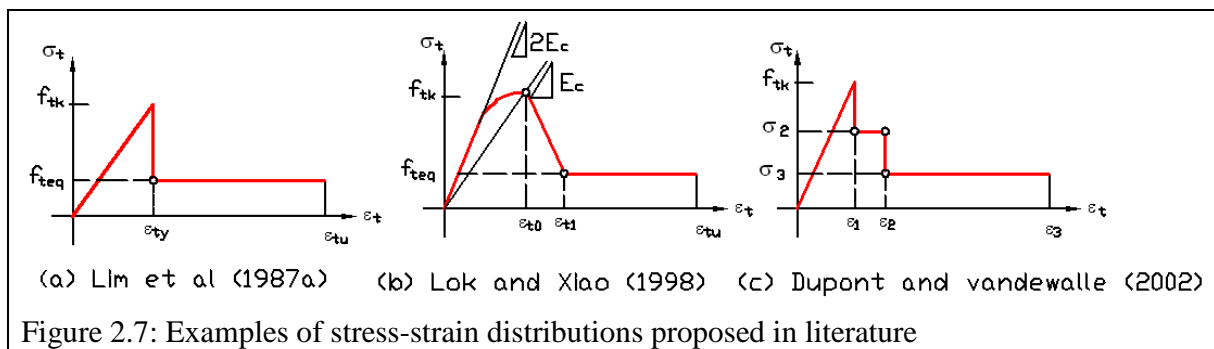


Figure 2.7: Examples of stress-strain distributions proposed in literature

2.3.3 MODEL CODE 2010 CONSTITUTIVE LAWS FOR FRC

The approach adopted in the draft Model Code 2010 uses two constitutive laws deduced from a bending test, namely rigid-plastic behaviour and linear post cracking behaviour (see Figure 2.8). These laws, as outlined by Di Prisco *et al* (2009), are modelled based on mode I crack propagation using a stress-crack opening law. When considering softening materials, the definition of a stress-strain law is based on the identification of a crack width and its corresponding structural characteristic length, l_{cs} , of the structural element as first introduced by Bazant (1983a, 1983b) and then extended and refined by other researchers (Bazant & Pijaudier-Cabot, 1988), (Bazant & Novak, 2003), (De Borst *et al*, 1992), (Fokwa & Berthaud, 1993) and (Di Prisco *et al*, 1999)). Di Prisco *et al* (2009) used this concept of structural characteristic length as a “bridge” to connect continuum mechanics governed by stress-strain constitutive relationships and fracture mechanics governed by stress-crack opening as first proposed by

Hillerborg *et al* (1976) in concrete mechanics frameworks. Using these constitutive models, ultimate tensile strength, residual bending strength and service stress can be determined as shown in Figure 2.9.

Rigid plastic model: This identifies a unique reference value, f_{fu} , based on ultimate behaviour taking into account the static equivalence as shown in Figure 2.8(a). The compressive force is assumed to be concentrated in the top fibre of the section. The following formulae are derived:

$$f_{fu} = \frac{F_{R3}}{3} \quad 2.13$$

where

$$F_{R3} = \frac{3F_{(CMOD3)}L}{2bh_s^2} \quad 2.14$$

where $F_{(CMOD3)}$ is the force at $CMOD_3$, and L is the span length.

Linear post-cracking model: The linear post-cracking model is characterized by the f_{fs} and f_{fu} parameters which are defined through residual values of flexural strength using the following expressions (see Figure 2.8(b)):

$$f_{fs} = 0.45f_{R1} \quad 2.15$$

$$f_{fu} = f_{fs} - \frac{w_u}{CMOD_3} (f_{fs} - 0.5f_{R3} + 0.2f_{R1}) \geq 0 \quad 2.16$$

where

$$f_{R1} = \frac{3F_{(CMOD1)}L}{2bh_s^2} \quad 2.17$$

Di Prisco *et al* (2009) outlined a condition that must be achieved if the material is to be acceptable as a structural member to support loads, similar to that given by Naaman (2003), as follows:

$$\frac{f_{R1k}}{f_{Lk}} > 0.4 \text{ and } \frac{f_{R3k}}{f_{R1k}} > 0.5 \quad 2.18$$

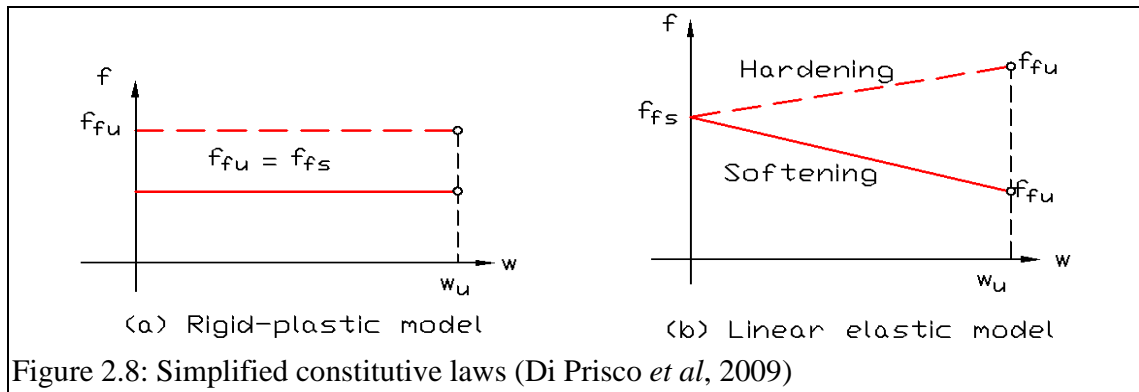


Figure 2.8: Simplified constitutive laws (Di Prisco *et al*, 2009)

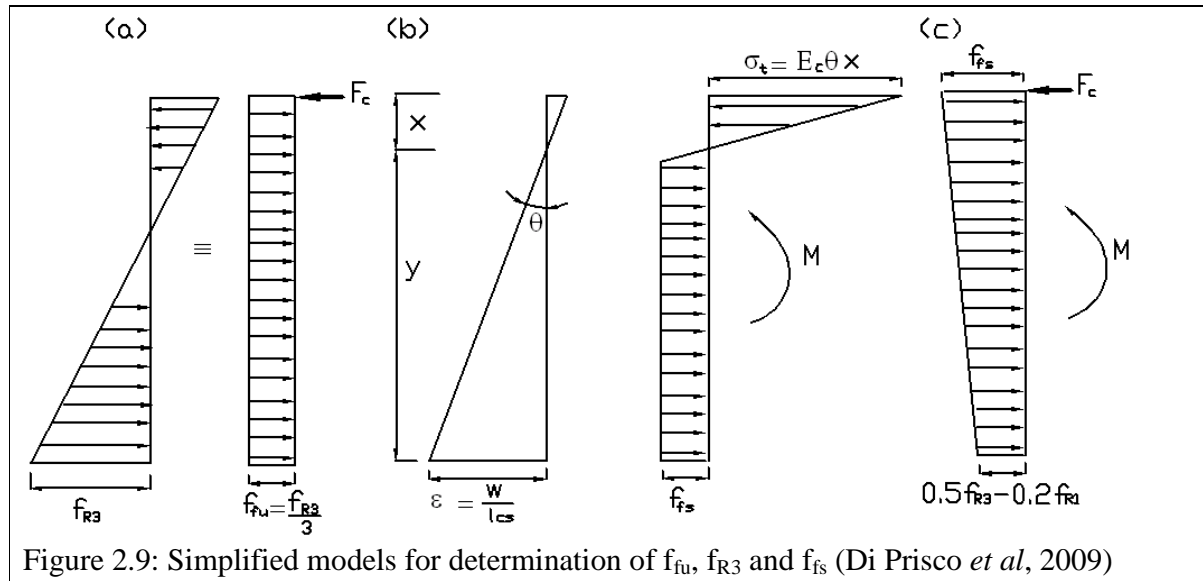


Figure 2.9: Simplified models for determination of f_{tu} , f_{R3} and f_{fs} (Di Prisco *et al*, 2009)

2.4 CURRENT FLEXURAL MODELS FOR SFRC BEAM SECTIONS

Much research has been done on flexural modelling of FRC. In this section, models developed by Soranakom and Mobasher (2007, 2008 and 2009), Naaman (2003), Henager and Doherty (1976) and Tan *et al* (1995) are reviewed. While the first two models are for SFRC, the model by Henager and Doherty is for steel bar reinforced SFRC. In addition to these models, a review of constitutive laws and the determination of stresses for flexural calculation as outlined in the Draft Model code (2010) and described by Di Prisco *et al* (2009), are discussed.

2.4.1 SORANAKOM AND MOBASHER APPROACH

Soranakom and Mobasher (2007, 2008 and 2009) developed closed form equations for the determination of the flexural capacity of strain-softening SFRC. The approach assumes a drop-down tensile model and a bilinear compressive model (as already illustrated in Figures 2.6(b) and 2.7(a)). In a drop-down tensile model, the concept of a normalised post-peak strength defined as the ratio of post-peak uniform tensile strength to peak tensile strength is used. For SFRC to exhibit deflection hardening, the normalised post-peak tensile strength must not be less than 0.40 ($\mu_{ft} \geq 0.40$). This condition is similar to that established by Naaman (2003). The following assumptions are made for this model:

- Young's modulus is the same for both compression and tension;
- the tension model consists of a linear stress-strain response up to cracking-strain, then a drop-down followed by a constant (average) post-crack response, f_{teq} ; and
- compressive strength is prescribed to be higher than tensile strength defined by using an elastic-perfectly plastic model.

Using a closed form approach, neutral axis depth ratio and normalised moment expressions were derived and are given in Table 2.4.

Table 2.4: Neutral axis depth ratio, normalised moment and curvature for SFRC model by Soranakom and Mobasher (2007)

Stage	k	m	θ
$0 \leq \zeta \leq 1$	$\frac{1}{2}$	$\frac{\zeta}{2k}$	$\frac{\zeta}{2k}$
$1 \leq \zeta \leq \xi$	$\frac{2\mu\zeta}{\zeta^2 + 2\mu(\zeta + 1) - 1}$	$\frac{(2\zeta^3 + 3\mu\zeta^2 - 3\mu + 2)k^2}{\zeta^2} - 3\mu(2k - 1)$	
$\xi \leq \zeta \leq \zeta_{cu}$	$\frac{2\mu\zeta}{-\zeta^2 + 2\zeta(\mu + \xi) + 2\mu - 1}$	$\frac{(3\xi\zeta^2 - \xi^3 + 3\mu\zeta^2 - 3\mu + 2)k^2}{\zeta^2} - 3\mu(2k - 1)$	

where

$$\xi = \frac{\epsilon_{cy}}{\epsilon_{ty}} = \frac{f_{cy}}{f_{ty}}$$

ζ is the normalised maximum compression strain.

$$\mu = \frac{f_{teq}}{\sigma_{cc}}$$

f_{teq} is an equivalent average post-cracking tensile strength for SFRC

k is the neutral axis depth ratio;

m is the normalised moment; and

θ is the normalised curvature.

The ultimate moment of resistance, M , is determined from the following expression:

$$M = mM_{cr} \quad 2.19$$

where M_{cr} is as defined in Equation 2.9.

At infinite curvature, the normalised moment can be simplified as follows:

$$m = \frac{3\xi\mu}{\xi + \mu} \quad 2.20$$

from which the nominal moment can be deduced with Equation 2.19. A reduction factor, ϕ , of 0.7 has been proposed to take account of the uncertainties arising from the use of post-cracking tensile strength in order to determine the ultimate moment capacity.

2.4.2 APPROACH PROPOSED BY A.E. NAAMAN

Naaman (2003) proposed three different approaches that can be used for the determination of the ultimate bending moment of resistance:

- 1) ACI rectangular stress block and perfectly plastic material in tension;
- 2) ACI rectangular stress block and triangular tensile stress profile; and
- 3) triangular compression stress block and perfectly plastic material in tension.

1) *ACI rectangular stress block and perfectly plastic material in tension* (see Figure 2.10(iii)). The compressive zone of concrete is represented by a rectangular stress block according to ACI (ACI Committee 318, 2002) and the concrete in tension is assumed to have a rectangular stress block with an average uniform stress, $\bar{\sigma}_{pc}$. With reference to Figure 2.10(iii), the ultimate bending moment of resistance of the section is defined as follows:

$$M = 3\bar{\sigma}_{pc} \left(\frac{bh^2}{6} \right) \left(1 - \frac{x}{h} \right) \left(1 + \frac{x}{h} (1 - \lambda_{cd}) \right) \quad 2.21$$

where

$$\frac{x}{h} = \frac{\bar{\sigma}_{pc}}{0.85f_{ck}\lambda_{cd} + \bar{\sigma}_{pc}} \quad 2.22$$

$$\frac{a}{h} = \frac{\lambda_{cd}\bar{\sigma}_{pc}}{0.85f_{ck}\lambda_{cd} + \bar{\sigma}_{pc}} \quad 2.23$$

a is the depth of compression stress block.

2) *ACI rectangular stress block and triangular tensile stress profile* (see Figure 2.10(iv)). This approach assumes an ACI rectangular stress block for compression zone and a linear stress distribution varying from maximum tensile strength, σ_{pc} , near the neutral axis to zero at the extreme tension fibre for the tension zone. The ultimate moment of resistance is defined as follows:

$$M = 3\sigma_{pc} \left(\frac{bh^2}{6} \right) \left(1 - \frac{x}{h} \right) \left(\frac{1}{3} + \frac{x}{h} \left(\frac{2}{3} - \frac{\lambda_{cd}}{2} \right) \right) \quad 2.24$$

where

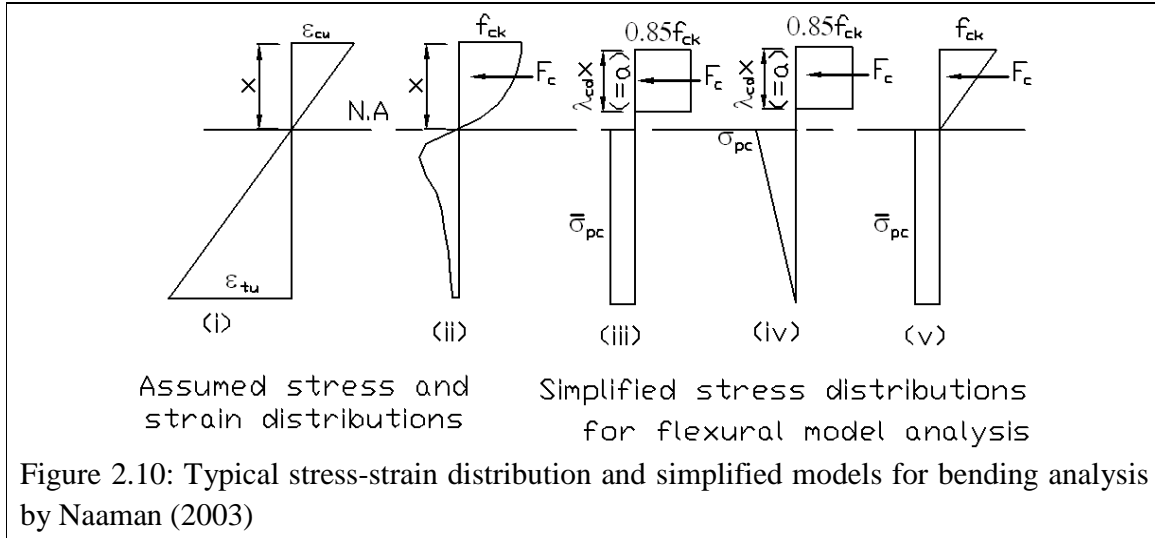
$$\frac{x}{h} = \frac{0.5\sigma_{pc}}{0.85f_{ck}\lambda_{cd} + 0.5\sigma_{pc}} \quad 2.25$$

3) *Triangular compression stress block and perfectly plastic material in tension* (see Figure 2.10(v)). This approach assumes a linear stress-strain curve of concrete in compression up to failure and a uniform stress distribution in tension with an average tensile stress of $\bar{\sigma}_{pc}$. The ultimate moment of resistance of the section is determined from:

$$M = 3\bar{\sigma}_{pc} \left(\frac{bh^2}{6} \right) \left(1 - \frac{x}{h} \right) \left(1 + \frac{x}{3h} \right) \quad 2.26$$

where

$$\frac{x}{h} = \frac{\bar{\sigma}_{pc}}{0.5f_{ck} + \bar{\sigma}_{pc}} \quad 2.27$$



2.4.3 APPROACH BY HENAGER AND DOHERTY

Henager and Doherty (1976) proposed a method that utilises a rectangular stress block for tension. The depth of the stress block is calculated based on strain compatibility for fibres and concrete, and force equilibrium. The basic design assumptions are shown in Figure 2.11. It should be noted that the ultimate compressive strain of 0.003 is used. However, various researchers (Williamson (1973); Pearlman (1983); Swamy & Al-Ta'an (1981) and Hassoun & Sahebjam (1985)) have recommended the use of greater values for ultimate compressive strain in the range of 0.0033 to 0.004 as opposed to 0.003, which may be conservative. The equation for the ultimate moment of resistance M of a singly reinforced SFRC beam is then as follows:-

$$M = A_s f_{sy} \left(d - \frac{a}{2} \right) + \sigma_{tf} b (h - e) \left(\frac{h}{2} + \frac{e}{2} - \frac{a}{2} \right) \quad 2.28$$

where

$$e = \frac{(\epsilon_t + 0.003)x}{0.003} \quad 2.29$$

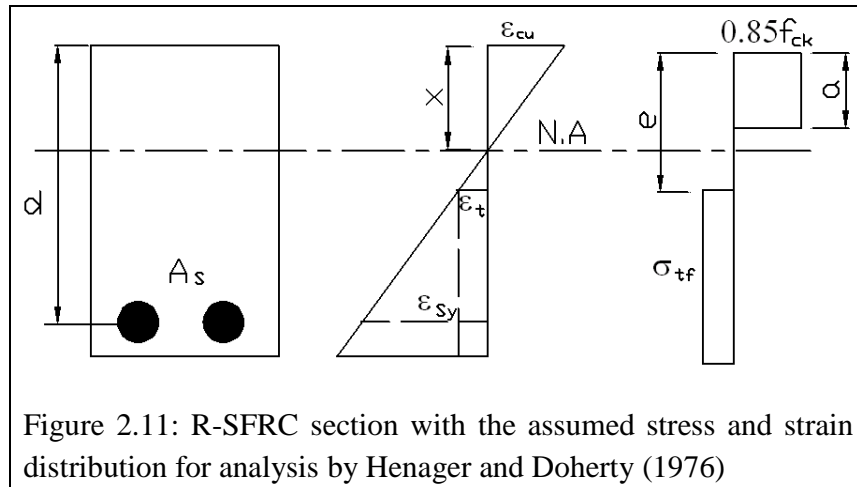
$$\sigma_{tf} = 0.00772 V_f F_{be} \frac{l_f}{d_f} \text{ (MPa)} \quad 2.30$$

$$\epsilon_t = \frac{\sigma_f}{E_s} \quad 2.31$$

F_{be} is the bond efficiency of fibres which varies between 1.0 and 1.2, depending on fibre characteristics;

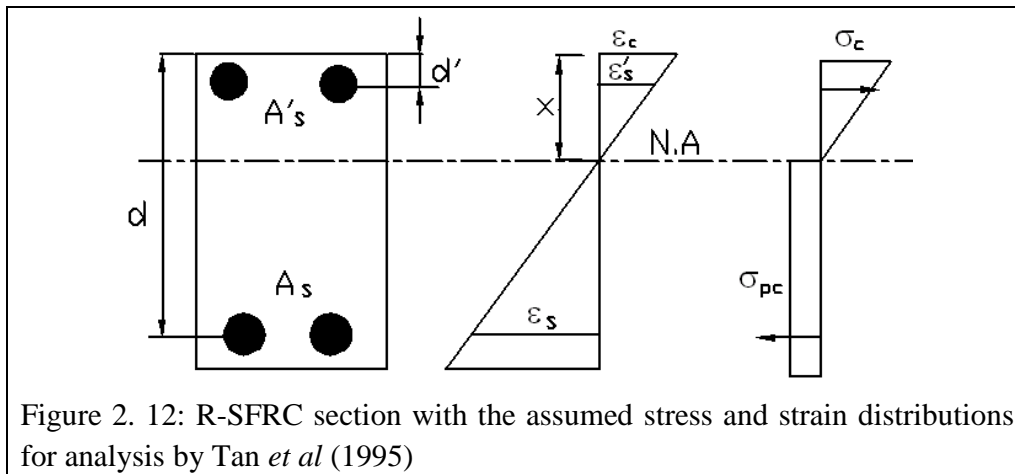
σ_{tf} is the tensile stress in fibrous concrete;

σ_f is the tensile stress developed at pull-out (dynamic bond stress of 2.3MPa); and E_s is the Young's modulus of steel bars.



2.4.4 APPROACH BY TAN *ET AL* (1995)

Tan *et al* (1995) outlined a procedure for determining the flexural capacity of a cracked SFRC section. A general approach was developed for SFRC with both tensile and compression reinforcement. Figure 2.12 shows the assumed stress distributions of SFRC in tension and compression. It should be noted that a uniform tensile stress smeared across the whole tensile section is assumed for tensile stress while a triangular block is assumed for concrete compression. The post cracking tensile strength is assumed to be independent of the crack opening because crack widths found in reinforced SFRC beams in flexure are relatively small (Tan *et al*, 1995).



Using equilibrium of forces and strain compatibility, the moment of resistance of a doubly reinforced section can be determined as follows:

$$M = \frac{1}{2} \sigma_c b x \left(\frac{2}{3} x + \frac{(h-x)}{2} \right) + E_s \epsilon_s A_s \left(d - x - \frac{(h-x)}{2} \right) + E_s \epsilon'_s A'_s \left(x - d' + \frac{(h-x)}{2} \right) \quad 2.32$$

and

$$x = \frac{E_s \varepsilon_s A_s - E_s \varepsilon'_s A'_s + \sigma_{pc} b h}{0.5 E_c \varepsilon_c b + \sigma_{pc} b} \quad 2.33$$

$$\varepsilon_s = \frac{d-x}{x} \varepsilon_c \leq \frac{f_{sy}}{E_s}, \quad \varepsilon'_s = \frac{x-d'}{x} \varepsilon_c \leq \frac{f'_{sy}}{E_s} \quad 2.34$$

where

f_{sy} and f'_{sy} are the yield strength of tension and compression reinforcement respectively; and A_s and A'_s are the areas of tension and compression reinforcement respectively.

Provision of reinforcement using this method follows an iterative process whereby the position of the neutral axis is first assumed and, using Equation 2.35 below, the value of maximum compressive strain in the section is calculated. Using this value of compressive strain, the strains in reinforcing bars are calculated, and then used to determine the position of the neutral axis using Equation 2.34 above. This process is repeated until the values of the neutral axis from Equations 2.33 and 2.35 converge. It should be noted that the same expression can be used for singly reinforced SFRC cracked sections if the area of compression steel bar is given as zero.

$$\varepsilon_c = \frac{M_a}{\frac{1}{2} E_c b x \left(\frac{h}{2} + \frac{x}{6} \right) + E_s \frac{(x-d')}{x} A'_s \left(\frac{x}{2} - d' + \frac{h}{2} \right) + E_s \frac{(d-x)}{x} A_s \left(d - \frac{x}{2} - \frac{h}{2} \right)} \quad 2.35$$

where M_a is the applied moment.

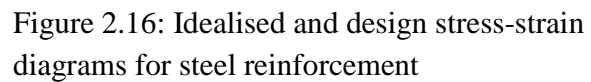
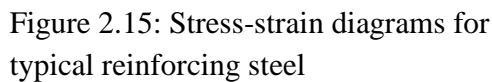
2.5 REVIEW OF DESIGN MODELS FOR NORMAL REINFORCED CONCRETE

Design approaches of normal reinforced concrete as outlined in Eurocode 2-Design of concrete structures, Part 1-1 (European standards, 2004) are given together with some methods available in other literature. Firstly, idealisation of the material parameters for both concrete and reinforcing steel is discussed, followed by structural analysis approaches adopted in the code.

2.5.1 CONCRETE AND REINFORCING STEEL MATERIAL PARAMETERS

In normal reinforced concrete, a compressive resistance is offered, while steel reinforcement offers tensile resistance to the flexural capacity of the beam. In order to use these materials in sectional analysis, idealised material models are used. For concrete compression behaviour, the compressive stress-strain distribution may be idealised as either a parabolic-rectangular stress distribution or a bilinear stress distribution (see Figures 2.13 and 2.14). For reinforcing steel, typical stress-strain curves of hot-rolled and cold-worked steel differ (see Figure 2.15). It is against this background that the tensile behaviour of reinforcing steel may be idealised as either elastic-perfect plastic behaviour or elastic-strain-hardening behaviour (see Figure 2.16). While characteristic values of material model parameters are used (5% fractile), determination of the design resistance values involves conversion of the characteristic values to design values. Of interest is the conversion of the idealised models from characteristic values to design values. For the concrete compression stress distribution, the yielding strain under characteristic parameters is

Figure 2.13: Parabolic-rectangular compression stress-strain distribution



The structural analysis of beams according to BS EN 1992-1-1(2004) follows four preliminary idealisations of the structure: linear elastic analysis, linear elastic analysis with limited moment redistribution, plastic analysis and non-linear analysis. For the purposes of this thesis, only linear elastic analysis and non-linear analysis will be discussed, together with a plastic analysis method for the determination of the ultimate moment resistance of the beam section.

2.5.2.1 LINEAR ELASTIC ANALYSIS

Under this approach, the determination of the moment capacity is done based on the following assumptions: (a) uncracked cross section of the beam, (b) linear stress-strain relationships and (c) mean value of the modulus of elasticity. With these assumptions, stresses are proportional to loads and therefore the superposition principle applies. While no limit on the ratio, x_u/d , has been considered, EC2 commentary (Jacobs, 2008) recommends observation of the limit consistent with the method of linear elastic analysis with limited redistribution, for which $x_u/d \leq 0.45$.

2.5.2.2 NON-LINEAR ANALYSIS

Tri-linear idealisation of the moment-curvature laws is adopted (see Figure 2.17).

State I (Elastic and linear state): This state is characterised by EI rigidity of the entire reaction section. It ends when the tensile strength of concrete is reached (i.e. at cracking moment, M_{cr}). For a singly reinforced concrete beam, the cracking moment and the corresponding curvature θ_{cr} can be determined from strain compatibility and equilibrium of forces as follows:

$$M_{cr} = \frac{1}{3} \epsilon_c E_c x^2 b + \frac{1}{3} \frac{(h-x)^3}{x} \epsilon_c E_c b + \frac{(d-x)^2 x}{x} \epsilon_c E_s A_s \quad 2.36$$

$$\theta_{cr} = \frac{\epsilon_c}{x} = \frac{\epsilon_{ty}}{h-x} \quad 2.37$$

where

$$x = \frac{(h + 2m\rho_g d)}{(2 + 2m\rho_g)} \quad 2.38$$

$$m = \frac{E_s}{E_c}; \rho_g = \frac{A_s}{bh}$$

ϵ_{ty} is the cracking tensile strain in concrete; and

ϵ_c in the compressive strain in concrete corresponding to the cracking tensile strain.

State II (Cracked state): This state ranges from the cracking moment to the moment corresponding to steel yielding. Moment increases are related to curvature increases on the basis of rigidity $E_s A_s Z(d-x)$, where A_s is the cross sectional area of tensional reinforcement, Z is the lever arm, x is the neutral axis depth from the compression face. Note that the rigidity can be increased by taking into account the contribution of concrete in tension between cracks (i.e. tension softening) but with caution in the case of load cycles. Kwak and Klim (2002) outlined an iterative procedure for the determination of the neutral axis at the point of yielding moment. In this case, the value of the neutral axis used for the determination of the total compression and tensile forces is changed until the difference between the tensile force and compressive force is less than the given tolerance. The expressions of the total compression force (F_c) and total tensile force (F_{t+s}) for a singly reinforced concrete section are given below:

$$F_c = \int_{Acc} \sigma_c dA \quad 2.39$$

$$F_{t+s} = \int_{Act} \sigma_t dA + f_{sy} A_s \quad 2.40$$

where

A_{cc} and A_{ct} represent the areas of concrete acted on by the compressive and tensile stresses respectively.

State III (Plastic state): This state starts from steel yielding to point of failure of the section. This corresponds to a θ_{pl} plastic rotation at critical section whose value can be deduced from Figure 5.6N in the EC2 given as a function of relative depth of the neutral axis. Apart from the use of the curves provided in the EC2, an approximate procedure would be to assume a constant bending stiffness of $E_{s2}I_{cr}$, where E_{s2} is the elastic modulus of steel after yielding and I_{cr} is the moment of inertia of the cracked section (Kwak & Klim, 2002). This assumes that the moment capacity of the section entirely depends on the structural behaviour of reinforcing steel in this state.

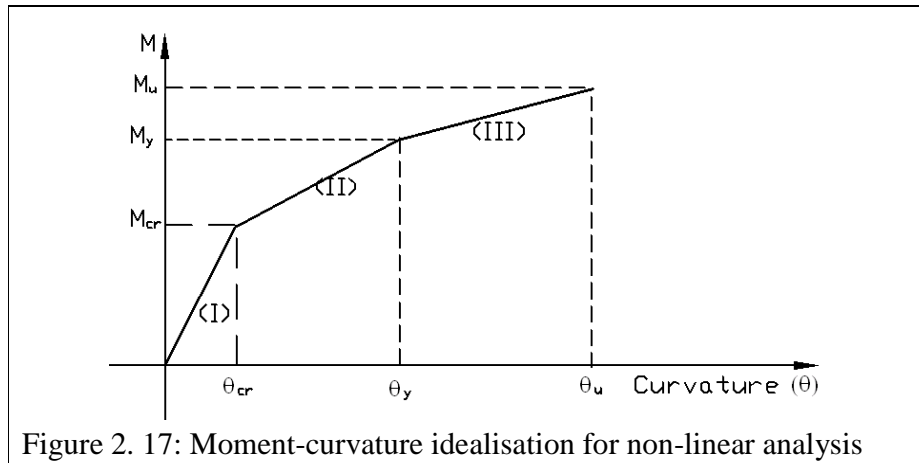


Figure 2. 17: Moment-curvature idealisation for non-linear analysis

2.5.2.3 ULTIMATE MOMENT OF RESISTANCE

Plastic analysis is used for the determination of the ultimate moment capacity of the beams. It should be acknowledged that there are three possible modes of failure for a reinforced concrete section (Bhatt *et al*, 2006), as discussed below:

Steel reinforcement yields first. This happens when the tensile force capacity of steel reinforcement is lower than the compression force capacity of concrete. Steel bars yield before the strain in concrete as the compression face reaches ultimate value. The beams continue to deform at a constant load (for elastic-perfect plastic steel) and the neutral axis moves up. This is the mode of failure that is encouraged in design as it allows for ductile mode of failure.

Simultaneous 'yielding' of steel reinforcement and concrete. In this stage, the tensile force capacity of steel reinforcement is higher than the previous stage and steel yielding is

simultaneously accompanied by the crushing of concrete. Unlike the previous failure mode, there is little warning before failure of the section. In design, this mode of failure should be avoided.

Concrete crushes first. In this mode of failure, the tensile force capacity of steel is so high that concrete crushes before the yielding of the steel reinforcement. This results in brittle failure as concrete is a fairly brittle material as compared to steel reinforcement. In design, this mode of failure should be avoided.

The following assumptions are made for determination of the ultimate moment resistance of reinforced concrete cross-sections:

- (i) plane cross-sections remain plane;
- (ii) the strain in bonded reinforcement, whether in tension or in compression, is the same as that in the surrounding concrete, i.e. no slip occurs; and
- (iii) the tensile strength of the concrete is ignored.

The stresses in the concrete in compression and stresses in the steel reinforcement in tension are derived from the design stress-strain relationship given in Section 2.5.1.

For a singly reinforced beam section, the ultimate moment of resistance is determined from the following expression:

$$M = A_s f_{sy} \left(d - \frac{\lambda_{cd} x}{2} \right) \quad 2.41$$

where the product $\lambda_{cd}x$ represents the depth of compression stress block and is determined as follows:

$$\lambda_{cd} x = \frac{A_s f_{sy}}{\eta_{cd} f_{ck} b} \quad 2.42$$

where λ_{cd} and η_{cd} are factors used to convert the compression stress distribution to an equivalent stress block as given in Eurocode 2 (2004).

2.6 REVIEW OF SPLITTING STRENGTH PARAMETERS

The splitting test is used as an indirect method for the determination of tensile properties of concrete. For concrete with steel fibres, splitting strength has been shown to vary based on the amount of steel fibres effectively crossing a crack and fibre orientation (Potrzebowski, 1983). Lofgren (2005) demonstrated the applicability of splitting parameters for material characterisation through the use of wedge-splitting method. The splitting test and flexural tests have been used to predict the axial tensile strength of concrete because they allow for a more stable test set-up as compared to direct tensile tests. While different test set-ups and specimen configurations (see Figure 2.18) are allowed in different Standards, all Standards use the same formula for determining the splitting strength as given in Equation 2.43. Thus the standards assume that the splitting strength of concrete is independent of such factors as bearing width and specimen geometry.

$$f_{isp} = \frac{2P_u}{\pi b h} \quad 2.43$$

Rocco *et al* (1998, 1999 and 2001) reviewed the splitting test standard methods and evaluated the size effect and the boundary conditions in the splitting test. They found that the splitting tensile strength depends on the specimen size and the boundary conditions of the test. As the size of the specimen increases and the relative width of the bearing strip decreases, the splitting strength tends asymptotically to a minimum value coincident with the tensile strength (Rocco *et al* 1998). A modification was therefore proposed to the formula adopted in standards so that the size effect and boundary conditions should be reflected. A linear elastic solution and a fracture mechanics approach were used resulting in two different formulations. Equation 2.44 gives the formula for direct tensile strength derived from splitting tests using the linear elastic method, while Equation 2.45 portrays the generalised relationship between splitting strength and direct tensile strength derived from the fracture mechanics approach.

$$f_t = \begin{cases} \frac{2P_u}{\pi b h} (1 - \beta^2)^{3/2} & \text{for cylindrical specimen} \\ \frac{2P_u}{\pi b h} [(1 - \beta^2)^{5/3} - 0.0115] & \text{for cubical specimen} \end{cases} \quad 2.44$$

$$f_{isp} = \frac{f_t}{c_1 + c_2(h/l_{chl})} + c_3 f_t \quad 2.45$$

where

$$\beta = \frac{b_r}{h} \text{ and } l_{chl} = \frac{E w_1}{2 f_t}$$

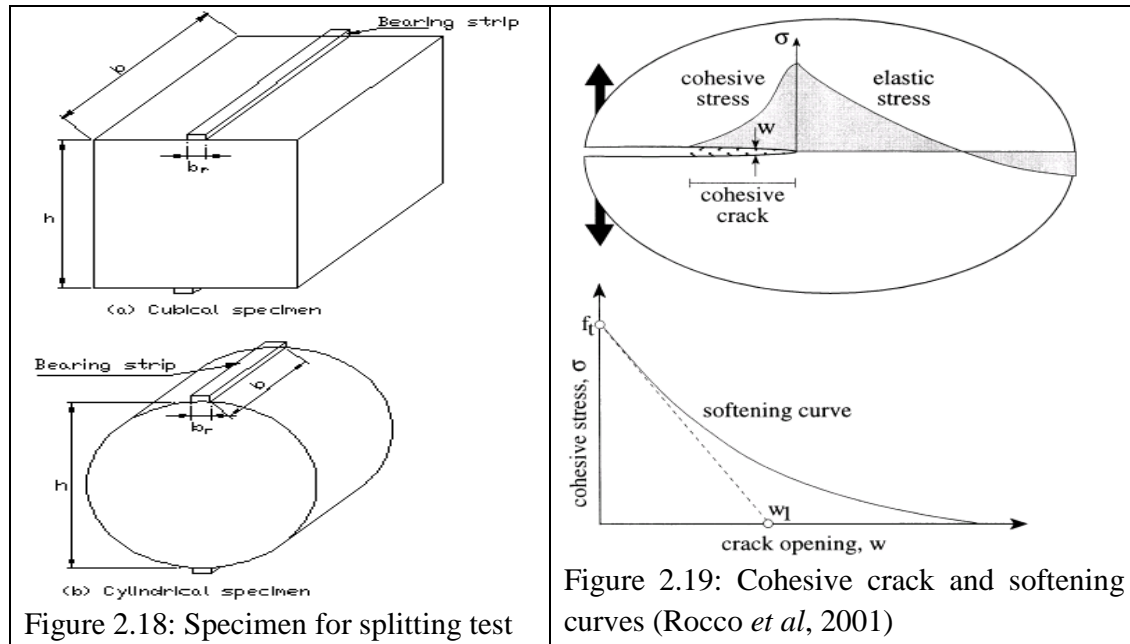
b_r is the bearing width;

l_{chl} is the reduced characteristic length;

w_1 is the horizontal intercept of the initial slope of the tensile stress-strain curve (see Figure 2.19); and

c_1 , c_2 and c_3 are coefficients depending on the specimen geometry and width of load bearing strips.

It should be noted that using equations derived from an elastic approach, the conversion factor for splitting strength to tensile strength within the standards prescribed strip widths and bearing width (i.e. $0.04 \leq \beta \leq 0.16$) is generally greater than 0.9 as recommended in different codes.



2.7 RELIABILITY BASED VERIFICATION OF MODELS

Principles of structural reliability are used mainly to provide a rational basis for improving the safety and economy of design practice with an extensive experience base (Dymond & Retief, 2010). The use of reliability principles in the development of design models for new materials ensures that the models provide acceptable safety in the absence of the broad experience base. Dymond and Retief (2010) outlined four basic steps for developing reliable design procedures for new innovative materials:

1. establish the material behaviour;
2. develop an analysis model;
3. verify the analysis model; and
4. ensure adequate reliability.

This thesis follows the above steps in developing the new model for flexural capacity of SFRC. Step One has been completed in this chapter, while Step Two is performed in Chapter 3. Step Three is discussed in Section 2.7.1 and will be implemented in Chapters 4 to 7. Since it is not within the scope of this thesis to adequately address the reliability analysis of the model, Step Four only proposes the next step of action for future refinement of the models.

2.7.1 VERIFICATION OF ANALYSIS MODELS

In order to verify the analysis model, a test program is developed to assess the bias and coefficient of variation in comparison to the test results. The experimental program may involve material characterisation tests and actual model verification tests. During the execution of the test program, it is very important to minimise the sources of uncertainties so that the difference between the experimental and theoretical results should represent the model uncertainty rather than incorporating the uncertainties and variations in the constituent parameters (Dymond &

Retief, 2010). In order to minimise sources of uncertainties in experimental data, it is necessary to ensure high quality control during the casting of concrete samples. It is furthermore important that accurate dimensions of each test specimen and measurements of actual loading points during testing are taken for utilisation in analysis. A two-step interpretation of experimental results has been outlined by Dymond and Retief (2010). These are discussed below.

Assessment of experimental results based on engineering judgement and reasoning. This step is performed in order to assess whether the results seem reasonable and if the analysis model acceptably predicts the outcome of the experiments. This is useful to eliminate any gross discrepancies between the predicted values and the experimental values. A scatter plot of the experimental data vs. theoretical predictions can be used for the correlation of the data points.

Statistical assessment of results. This step is performed after the first step has shown that the experimental results correlate well with predicted results. It is employed in order to determine the bias and uncertainty inherent in the theoretical model. EN 1990 (2002) outlines a statistical method for the determination of the bias and uncertainty inherent in the theoretical model. The prediction model uncertainty is described in terms of error term, δ_e , and model bias is described in terms of a correction factor, δ_c .

The correction factor, δ_c as defined in Equation 2.46 is the ‘least squares’ best fit to the slope as given in the scatter plot. It therefore measures the tendency of the model to systematically over- or under-predict the resistance of the element. Model uncertainty is expressed in terms of the coefficient of variation of the error term (m_{δ_e}) and is given in Equation 2.48, while the error term measures the relative scatter of the test results and is defined in Equation 2.47 for each test specimen.

$$\delta_c = \frac{\sum r_e r_t}{\sum r_t^2} \quad 2.46$$

$$\delta_{ei} = \frac{r_{ei}}{\delta_c r_{ti}} \quad 2.47$$

$$m_{\delta_e} = \sqrt{\exp(s_{\Delta}^2) - 1} \quad 2.48$$

where

$$s_{\Delta}^2 = \frac{1}{n-1} \sum_{i=1}^n (\Delta_i - \bar{\Delta})^2, \quad \bar{\Delta} = \frac{1}{n} \sum_{i=1}^n \Delta_i \quad \text{and} \quad \Delta_i = \ln(\delta_{ei}) \quad 2.49$$

$\bar{\Delta}$ is the estimate of the expected value;

s_{Δ}^2 is the estimate of the variance of the error term;

n is the number of test specimen used;

r_e is the experimental result; and

r_t is the theoretical prediction.

2.8 CONCLUSION

In this chapter, theoretical foundations on which the proposed analytical models for SFRC with and without steel bars will be based have been discussed. An in-depth evaluation of the material behaviour and the corresponding constitutive models and available analytical models for flexural capacity of SFRC have been given. Furthermore, a review was made of the splitting strength determination together with analytical models for normal reinforced concrete.

SFRC has a better ductility in both compression and tension than ordinary concrete. An increase in the steel fibres and steel fibre aspect ratio improves the toughness of SFRC. In order to characterise the material behaviour of SFRC, most characterisation methods used for normal concrete are employed. However, the material constitutive models, especially tensile constitutive models, may vary slightly from that of normal concrete. This is because SFRC tends to display strain-hardening with increasing amounts of steel fibres. This may imply that normal concrete models that ignore the post-cracking tensile strength of concrete may have to be refined to account for such changes if they are to be used for SFRC.

Several analytical models available in literature have been evaluated. Of interest is the way in which the tensile strength parameters are determined. While the use of experimental tests to determine tensile parameters is of paramount importance, some researchers have provided analytical formulas for the determination of tensile parameters of SFRC. This may reduce the amount of time and resources applied in characterising the material properties of SFRC. However, experience has shown that such analytical models tend to inherit uncertainties which are difficult to quantify, rendering reliability assessment of flexural models difficult. As indirect tensile strength methods are (reported to be) easier to perform, an understanding of the splitting strength, the effect of the boundary condition and the geometry of the specimen was necessary for the adoption of this test method in subsequent chapters. There is little information on how the post-cracking splitting stresses can be converted to direct tensile stresses. The review of the splitting strength parameters allows one to assess the possibility of using such a method to determine tensile stress parameters while understanding the potential errors derived from using such methods.

CHAPTER 3 DEVELOPMENT OF ANALYTICAL MODELS

3.1 INTRODUCTION

Flexural capacity models for SFRC beams are developed for rectangular sections using equivalent stress blocks for both tensile and compressive stresses. Parameters are defined allowing the conversion of stress-strain models into equivalent rectangular stress blocks, similar to Eurocode 2 (European Standards, 2004) for normal concrete. In the sections that follow, two different flexural models are developed for the determination of moment capacity for SFRC with and without reinforcing bars. Since the main principle for all the flexural models to be derived is based on the use of equivalent stress blocks, the derivation and analysis of the equivalent stress blocks are presented first. Characteristic values of model parameters are used throughout the derivation process, with the exception of Young's modulus which is given as a mean value.

3.2 DESIGN STRESS BLOCKS FOR SFRC

Determination of the moment capacity of SFRC may require consideration of the tensile stress distribution generated by the presence of steel fibres. Incorporation of such stress will modify the way the concrete section is designed, compared with standard reinforced concrete design practice. The paragraphs that follow outline how SFRC can be designed by defining a rectangular stress block for both compression and tension as it has been done for the compression zone in Eurocode 2 (European Standards, 2004).

A drop-down constant tensile stress (referred to as a drop-down tension distribution) used by Soranakom and Mobasher (2007) and a Rilem tension model (Vandewalle *et al*, 2002) have been used for tension, while a parabola-rectangular and a bilinear model have been used for compression. For the drop-down tension model, the post-peak parameters required to define the behaviour are the constant post-peak tensile strength, peak strength, cracking tensile strain and ultimate tensile strain. The use of equivalent stresses defined by Vandewalle and Dupont (2003) has been considered for the drop-down model. In the Rilem tension model, a multi-linear stress-strain relationship is defined by three pairs of parameters: peak tensile strength, initial post-peak tensile strength at a prescribed strain and final post-peak tensile strength and their corresponding strains.

3.2.1 DESIGN COMPRESSION STRESS BLOCKS

For normal concrete, the design compression stress distribution is simplified using conversion factors of λ and η applied to the design strength and its corresponding depth within the beam so that a rectangular stress block is generated from either a parabola-rectangular stress distribution or a bilinear stress distribution (European Standards, 2004). Since the compressive behaviour of SFRC will not vary significantly from that of normal concrete, the same concept can be used for SFRC in compression. The symbols used in this paper for the equivalent rectangular stress block parameters at any stress state are λ_c and η_c as shown in the Figure 3.1 below. The values of λ_c and η_c depend on the yield compressive strain, ϵ_{cy} and post-yield compressive strain, ϵ_{cp} .

When the ultimate compressive strain is used as a post-yield compressive strain, the design conversion factors λ_{cd} and η_{cd} are determined and can be used in flexural design. Both the yield and ultimate compressive strains may be assumed to vary depending on the grade of concrete as is the case with normal concrete.

3.2.1.1 PARABOLIC–RECTANGULAR STRESS–STRAIN MODEL

In order to be equivalent to the more realistic parabolic stress distribution, the derivation of the rectangular stress block is based on two conditions:

- the new stress block should have the same force; and
- the position of the resultant force should be the same.

It should be noted that the derivation for λ_{cd} and η_{cd} is applicable for $\varepsilon_{cp} > \varepsilon_{cy}$. Figure 3.1 illustrates how the rectangular stress block is converted from the parabola-rectangular stress-strain model. With reference to Figure 3.1, the following formulations are derived based on the above conditions and assuming a rectangular beam cross section.

A factor p is used to determine the depth of both the parabolic stress state section and rectangular stress state section and is determined as follows:

$$p = 1 - \frac{\varepsilon_{cy}}{\varepsilon_{cp}} \quad \text{for } \varepsilon_{cy} < \varepsilon_{cp} \leq \varepsilon_{cu} \quad 3.1$$

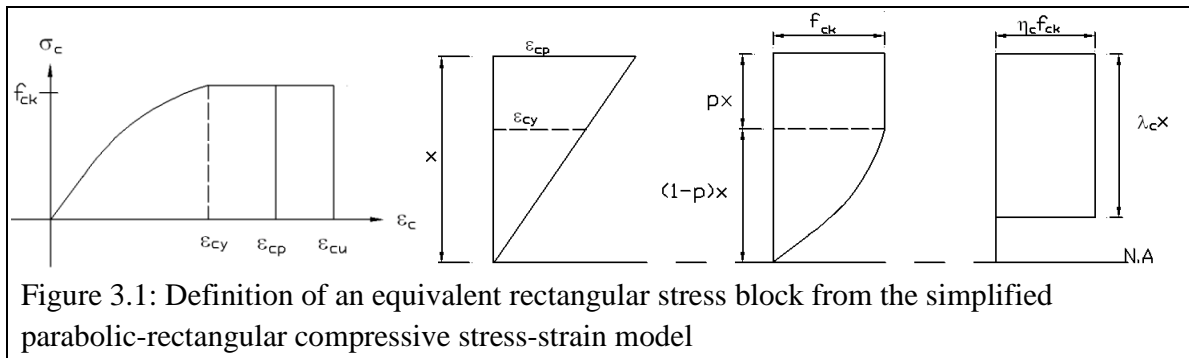
By stress integration over the section, the total compressive force for the section can be shown to be given by:

$$F_c = f_{ck} p x b + \frac{2}{3} (1 - p) x b f_{ck} = \left(\frac{p + 2}{3} \right) x b f_{ck} \quad 3.2$$

with b the beam section width, x the depth of neutral axis from compression face of the section and f_{ck} the characteristic cylinder compressive strength.

The total moment about the top edge of section can be shown to be given by:

$$M_c = f_{ck} \frac{(p x)^2}{2} + \frac{2}{3} (1 - p) x b f_{ck} \left(\frac{3}{8} (1 - p) x + p x \right) = \frac{(p^2 + 2p + 3)}{12} b x^2 f_{ck} \quad 3.3$$



For equivalence of the simplified rectangular stress block, the following can be shown:

$$\lambda_c = 2 \left(\frac{M_c}{F_c x} \right) = \frac{(p^2 + 2p + 3)}{2(p + 2)} \quad 3.4$$

$$\eta_c = \frac{F_c}{\lambda_c x b f_{cd}} = \frac{2(p + 2)^2}{3(p^2 + 2p + 3)} \quad 3.5$$

By defining the ratio of yield compressive to strain to outer fibre compressive strain (post-yield compressive strain) as follows:

$$\omega = \frac{\varepsilon_{cy}}{\varepsilon_{cp}} \quad 3.6$$

with which Equations 3.4 and 3.5 can be written as follows:

$$\lambda_c = \frac{\omega^2 - 4\omega + 6}{2(3 - \omega)} \quad 3.7$$

$$\eta_c = \frac{2(3 - \omega)^2}{3(\omega^2 - 4\omega + 6)} \quad 3.8$$

The product of the two ratios above, β_c , can be simplified as follows:

$$\beta_c = \lambda_c \eta_c = \frac{3 - \omega}{3} \quad 3.9$$

From Equations 3.7 and 3.8 above, it is apparent that the conversion factors λ_c and η_c depend on the ratio of yield compressive strain, ε_{cy} , to the post-yield compressive strain, ε_{cp} . If the ultimate compressive strain, ε_{cu} , is used as post-yield compressive strain in the above equations, the design conversion factors λ_{cd} and η_{cd} can be derived for the rectangular stress block equivalent to those given in the EN 1992-1-1. In this formulation, the design conversion factors are dependent on the compressive yield strain and ultimate strain as opposed to Eurocode approximation equations that depend on the concrete grade. It should be pointed out that the compressive yield strain and ultimate strains vary depending on the grade of concrete; hence the approximate values given by Equations 3.10 and 3.11 from EN 1992-1-1 are valid.

$$\lambda_{cd} = \begin{cases} 0.8 & \text{for } f_{ck} \leq 50 \text{ MPa} \\ 0.8 - \frac{f_{ck} - 50}{400} & \text{for } 50 \text{ MPa} < f_{ck} \leq 70 \text{ MPa} \end{cases} \quad 3.10$$

$$\eta_{cd} = \begin{cases} 1.0 & \text{for } f_{ck} \leq 50 \text{ MPa} \\ 1.0 - \frac{f_{ck} - 50}{200} & \text{for } 50 \text{ MPa} < f_{ck} \leq 70 \text{ MPa} \end{cases} \quad 3.11$$

RILEM recommends the values of 2.0‰ and 3.5‰ for compressive yield and ultimate strain for SFRC respectively for SFRC with strength not more than 50 MPa (Vandewalle *et al*, 2002). With these limiting strains, the value for conversion factors becomes $\lambda_{cd} = 0.83$ and $\eta_{cd} = 0.97$,

which are similar to the values for normal concrete with compressive strength of not more than 50MPa as given in EN 1992-1-1.

The values of λ_{cd} and η_{cd} , as calculated by Equations 3.7 and 3.8 and their corresponding approximations by the Eurocode, are plotted against characteristic compressive strength of concrete grades as shown in Figure 3.2 below.

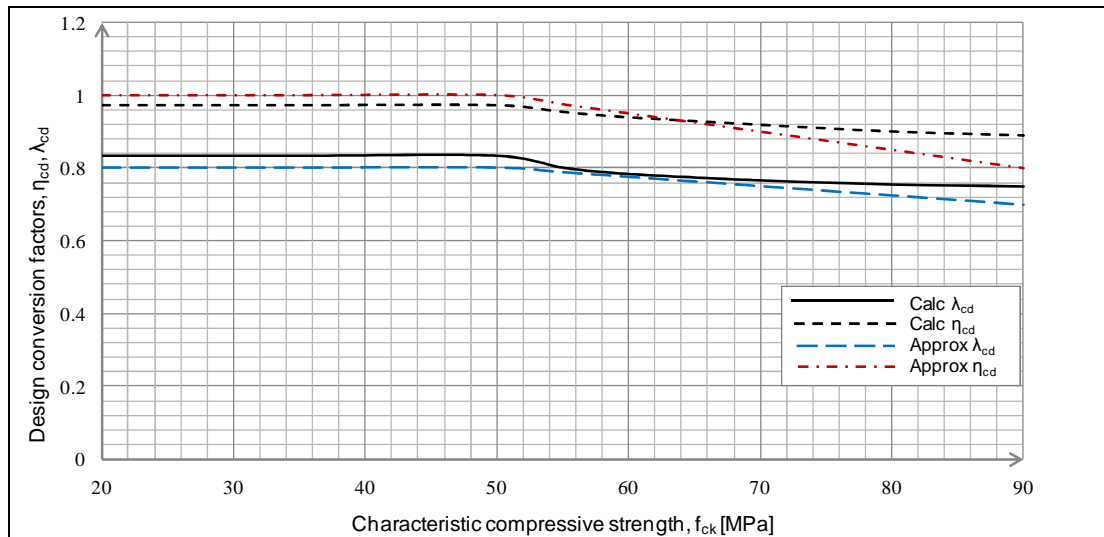


Figure 3.2: Values of the conversion factors λ_{cd} and η_{cd} for derivation of the rectangular stress block from a parabolic-rectangular compressive stress-strain model

3.2.1.2 BILINEAR COMPRESSIVE STRESS-STRAIN MODEL

Using a bilinear stress-strain model, a set of different relationships can be derived for a simplified rectangular stress block. Figure 3.3 illustrates how the rectangular stress block is converted from the bilinear compressive stress-strain model.

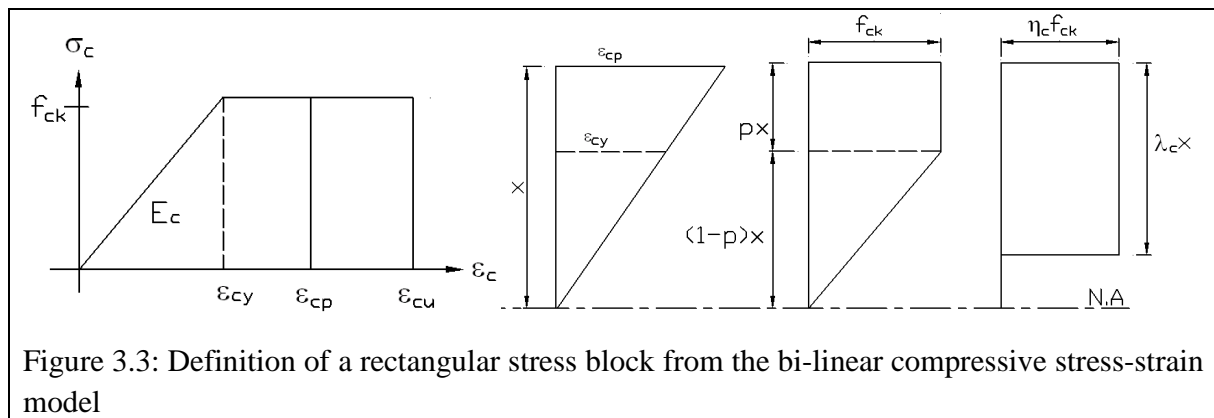


Figure 3.3: Definition of a rectangular stress block from the bi-linear compressive stress-strain model

With reference to Figure 3.3, the following formulae are derived in a similar manner as in Section 3.2.2.1. The derivation of the rectangular stress block is based on force equilibrium and maintenance of the position of the resultant force in the two systems. Based on these criteria and assuming a rectangular cross section for the beam element, the formulae are derived as follows: Recall that from Equation 3.1

$$p = 1 - \frac{\varepsilon_{cy}}{\varepsilon_{cp}} \quad \text{for } \varepsilon_{cy} < \varepsilon_{cp} \leq \varepsilon_{cu}$$

The total force for the section can be shown to be given by:

$$F_c = f_{ck} p x b + \frac{1}{2} (1 - p) x b f_{ck} = \frac{(p + 1)}{2} x b f_{ck} \quad 3.12$$

The total moment taken about the top edge of the section can be shown to be given by:

$$M_c = f_{ck} b \frac{(p x)^2}{2} + \frac{1}{2} (1 - p) x b f_{ck} \left(\frac{1}{3} (1 - p) x + p x \right) = \frac{(p^2 + p + 1)}{12} x^2 b f_{ck} \quad 3.13$$

For equivalence of the simplified rectangular stress block, the following can be shown:

$$\lambda_c = 2 \left(\frac{M_c}{F_c x} \right) = \frac{2(p^2 + p + 1)}{3(p + 1)} \quad 3.14$$

$$\eta_c = \frac{F_c}{\lambda_c x b f_{ck}} = \frac{3(p + 1)^2}{4(p^2 + p + 1)} \quad 3.15$$

and by substitution of Equation 3.6, Equations 3.14 and 3.15 respectively become

$$\lambda_c = \frac{2(\omega^2 - 3\omega + 3)}{3(2 - \omega)} \quad 3.16$$

$$\eta_c = \frac{3(2 - \omega)^2}{4(\omega^2 - 3\omega + 3)} \quad 3.17$$

and their product is given by

$$\beta_c = \lambda_c \eta_c = \frac{2 - \omega}{2} \quad 3.18$$

Figure 3.4 shows how the design conversion factors λ_{cd} and η_{cd} vary with concrete compressive strength. Note that the limiting strains at both cracking and ultimate state are based on values given in the EN 1992-1-1.

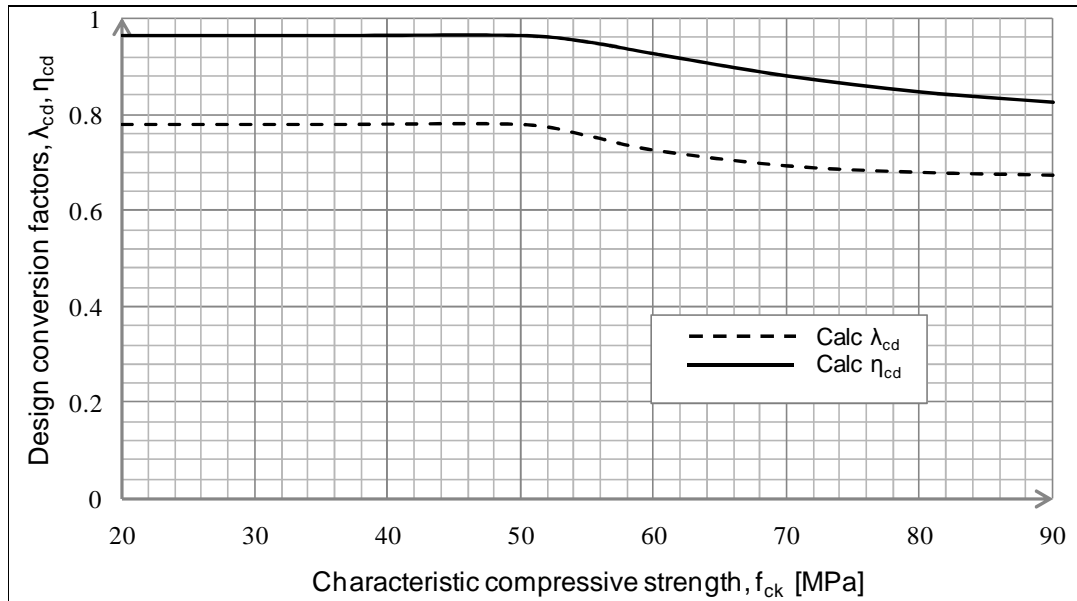


Figure 3.4: Values of the conversion factors λ_{cd} and η_{cd} for derivation of the rectangular stress block from a bi-linear compressive stress-strain model

3.2.2 DESIGN TENSILE STRESS BLOCKS

In the same manner as the compressive stress block, the tensile stress distribution is also converted to a rectangular stress block. It should be noted that the concept of a rectangular stress block for tensile stress distribution has been proposed by Naaman (2003) and Henager and Doherty (1976). However, the approaches they followed do not use the post-cracking behaviour as determined from experimental tests. The use of empirical analytical models by these authors to determine tensile behaviour may make it difficult to competently assess the model's uncertainties as more factors influence the post-cracking tensile behaviour of SFRC. It is against this background that the approach proposed here offers to use the tensile behaviour as determined from experiments so that any uncertainties within the proposed flexural model can be quantified to a greater degree of accuracy. Since the post-peak tensile behaviour of SFRC varies depending on the amount of fibres, the calculations that follow refer to strain-softening SFRC only.

3.2.2.1 DROP-DOWN CONSTANT MODEL

The drop-down constant tensile stress model, as proposed by Lim *et al* (1987b) and enhanced by Soranakom and Mobasher (2007), is used as shown in Figure 3.5 below. Generally, two stress parameters should be known if this model is to be used. These are ultimate tensile strength (peak tensile strength) and an assumed constant post-peak tensile strength. It is against this background that equivalent post-peak tensile parameters $f_{eq,2}$ and $f_{eq,3}$, defined by Vandewalle and Dupont (2003), can also be used. In SFRC, post-peak tensile behaviour does not substantially depend on the tensile strength of SFRC and therefore the grade of concrete will not be used as a basis for converting the stress distribution into a rectangular stress block. The post-peak tensile behaviour

for a particular grade of concrete will have to be determined through testing. It is assumed that for a specified sample, with consistency in mix design, the ratios of peak tensile strength to post-peak tensile strength, and that of cracking tensile strain to ultimate tensile strain, can be determined.

Factors λ_i and η_i are used to convert the drop-down constant stress distribution to a rectangular stress block, as shown in Figure 3.5. These values depend on the ratio of post-peak tensile strength to peak tensile strength, μ_i , and the ratio of yield tensile strain to post-yield tensile strain, ω' , which are assumed to fully define the post-peak material properties. Chapter 2 states that the constant post-peak tensile strength may be determined from toughness and crack width or strain over which the stress is averaged, the value of μ_i may differ for different strain states. Differentiation is made when calculating moment capacity at service and ultimate moment through the use of the subscripts s and u respectively. In cases where the material behaviour as observed from an experiment show a drop in tensile strength after the peak, followed by an almost uniform post-peak strength, exclusive utilisation of the drop-down tension model may be used without modifying values at different strains.

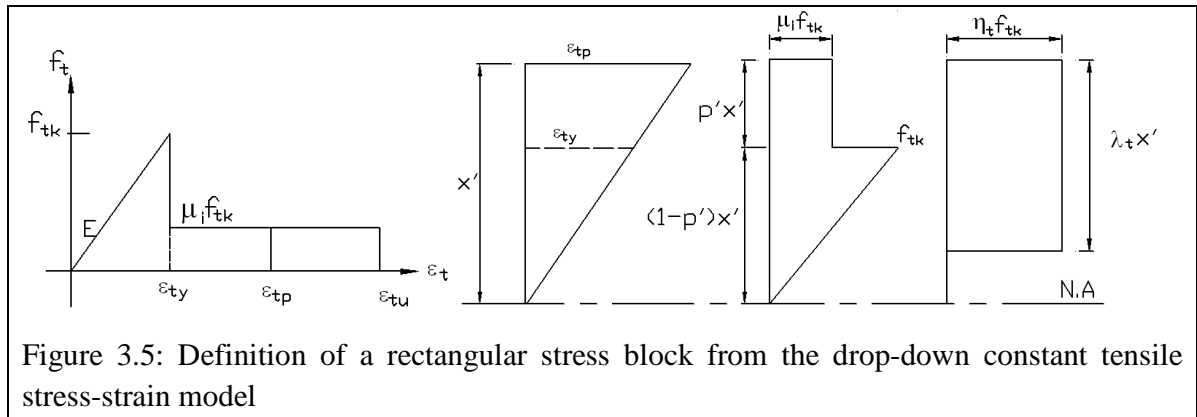


Figure 3.5: Definition of a rectangular stress block from the drop-down constant tensile stress-strain model

The derivation of an equivalent rectangular stress block is based on the two conditions, as outlined for the compression stress block, and the following expressions are therefore developed:

$$p' = 1 - \frac{\epsilon_{ty}}{\epsilon_{tp}} \quad \text{for } \epsilon_{ty} < \epsilon_{tp} \leq \epsilon_{tu} \quad 3.19$$

The total force for the section is given by:

$$F_t = \mu_i f_{tk} p' x' b + \frac{1}{2} (1 - p') x' b f_{tk} = \frac{(2\mu_i p' - p' + 1)}{2} x' b f_{tk} \quad 3.20$$

and the total moment about the top edge of the section is

$$M_t = \mu_i f_{tk} b \frac{(p' x')^2}{2} + \frac{1}{2} (1 - p') x' b f_{tk} \left(\frac{1}{3} (1 - p') x' + p' x' \right) = \frac{(1 + p' + p'^2 (3\mu_i - 2))}{6} b x'^2 f_{tk} \quad 3.21$$

As for compression, ensuring equivalence of the simplified rectangular stress block, the following can be shown:

$$\lambda_t = 2 \left(\frac{M_t}{F_t x'} \right) = \frac{2(1 + p' + p'^2(3\mu_i - 2))}{3(1 - p' + 2\mu_i p')} \quad 3.22$$

$$\eta_t = \frac{F_t}{\lambda_t x' b f_{tk}} = \frac{3(1 - p' + 2\mu_i p')^2}{4(1 + p' + p'^2(3\mu_i - 2))} \quad 3.23$$

Let the cracking tensile strain to post-cracking tensile strain ratio $\frac{\epsilon_{ty}}{\epsilon_{tp}}$ be ω' , whereby

Equations 3.22 and 3.23 become

$$\lambda_t = \frac{2(\omega'^2(3\mu_i - 2) + 3\omega'(1 - 2\mu_i) + 3\mu_i)}{3(\omega'(1 - 2\mu_i) + 2\mu_i)} \quad 3.24$$

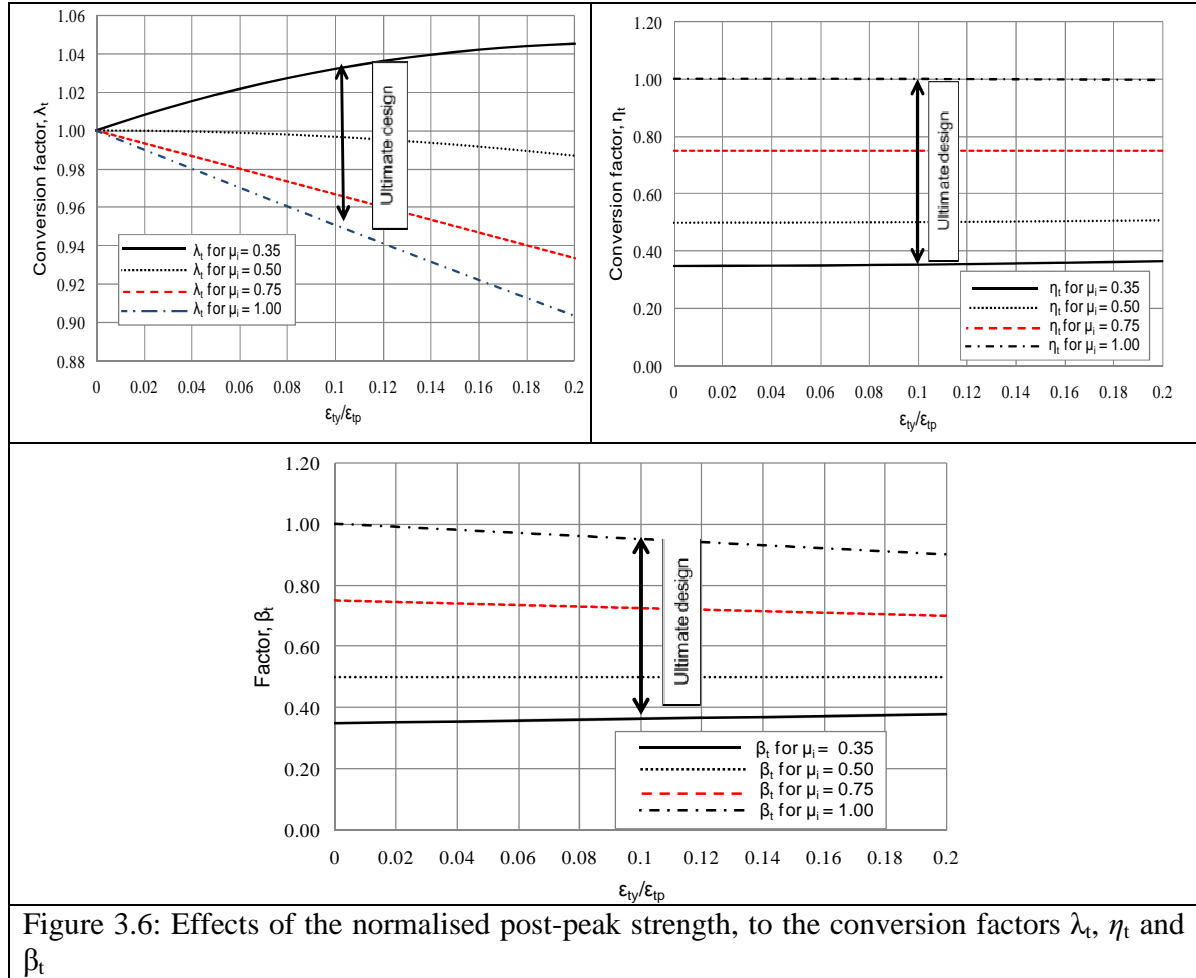
$$\eta_t = \frac{3(\omega'(1 - 2\mu_i) + 2\mu_i)^2}{4(\omega'^2(3\mu_i - 2) + 3\omega'(1 - 2\mu_i) + 3\mu_i)} \quad 3.25$$

The product of the two ratios above is defined as β_t , which can be shown to be given by

$$\beta_t = \lambda_t \eta_t = \frac{\omega'(1 - 2\mu_i) + 2\mu_i}{2} \quad 3.26$$

The conversion factor λ_t gives the relative depth of the tension stress block measured from extreme tensile fibre of the section. When λ_t is 1.0, the position of the resultant tensile force is at the middle of the depth of the tensile section and the tensile stress block is smeared throughout the whole tensile depth of the section. For λ_t less than 1.0, the position of the resultant tensile force moves away from the middle of the tensile section towards the extreme tension edge and the stress block is smeared over a fraction of the tensile depth of the section. When λ_t is greater than 1.0, the position of the resultant tensile force moves closer to the neutral axis, away from the middle of the tensile section. Physically, this may mean that the tensile stress block extends beyond the neutral axis, which is physically unacceptable but mathematically correct, so as to ensure equivalence of forces and moment for the drop-down stress distribution and the equivalent stress block.

Since different SFRC grades may have different ratios of the post-peak tensile strength to the peak tensile strength, the values of λ_t and η_t can be provided for different values of μ_i . A parametric study is conducted to observe the variability of parameters λ_t , η_t and β_t within practical range of the ratio of the cracking to the post-cracking tensile strain. Figure 3.6 shows effects of the normalised post-peak strength μ_i to the conversion factors λ_t , η_t and β_t within the practical range for the ratio of the cracking tensile strain to the post-yield tensile strain.



The range of 0.35 to 1.0 for μ_i has been chosen for two reasons: the ratio 0.35 is taken as the minimum ratio that achieves deflection-hardening in strain-softening SFRC, while the ratio 1.0 represents strain-hardening material with perfect plastic tensile strength, which is the maximum value that can be used by the proposed flexural models. Note that from literature, the critical flexural ratio $\mu_{cr,fl}$ varies between 0.343 and 0.353 (Soranakom & Mobasher, 2007). For the ultimate design of the section, the range of conversion factors has been shown in Figure 3.6 above. This range is based on the practical value over which the ratio of yield to post-yield tensile strain falls; the design conversion factor λ_{td} ranges from 0.95 for $\mu_i = 1.0$ to 1.03 for $\mu_i = 0.35$, while the factor η_{td} is approximately equal to the normalised post-peak tensile strength parameter μ_i .

3.2.2.2 RILEM TENSILE MODEL

The Rilem tension model (Vandewalle *et al*, 2002) defined the post-peak tensile behaviour of the SFRC using two post-peak tensile strengths and their corresponding strains, as shown in Figure 3.7. The model is applicable for concrete grades up to 50MPa (C50/60, i.e. 50MPa cylinder compressive strength, 60MPa cube compressive strength). The paragraphs that follow outline the derivation of an equivalent rectangular tensile stress block applicable to rectangular beam elements based on this tension model.

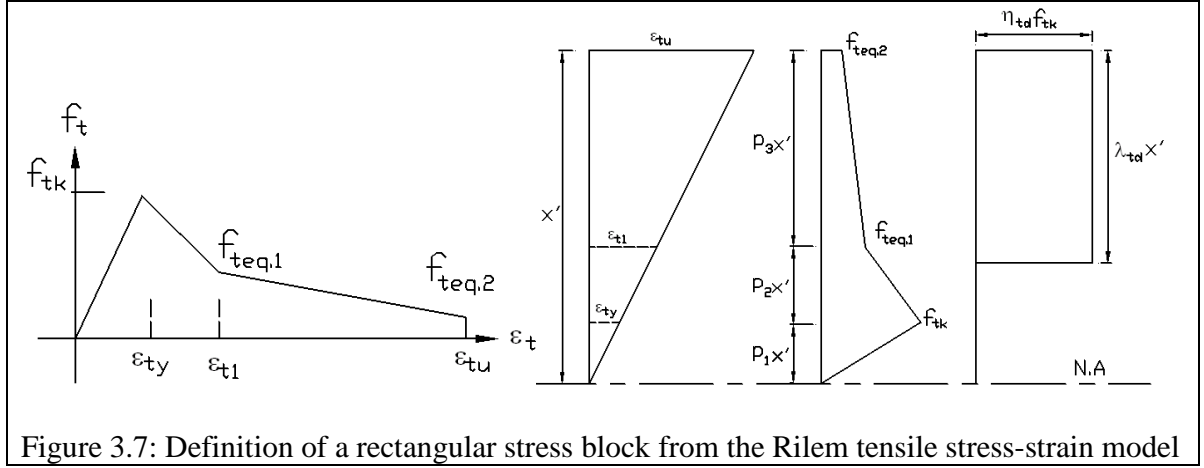


Figure 3.7: Definition of a rectangular stress block from the Rilem tensile stress-strain model

Considering stress-strain distribution at ultimate limit state: Defining the following terms with respect to the figure above:

$$\omega_{13} = \frac{\varepsilon_{ty}}{\varepsilon_{tu}}; \omega_{23} = \frac{\varepsilon_{t1}}{\varepsilon_{tu}}; \omega_{12} = \frac{\varepsilon_{ty}}{\varepsilon_{t1}} \quad 3.27$$

$$p_1 = \omega_{13}; p_2 = \omega_{23} - \omega_{13}; p_3 = 1 - \omega_{23} \quad 3.28$$

The total tensile force for the section is given by:

$$F_t = \frac{1}{2} (f_{tk} \omega_{23} + f_{teq1} + f_{teq2} - f_{teq1} \omega_{13} - f_{teq2} \omega_{23}) x' b \quad 3.29$$

Or

$$F_t = \frac{1}{2} (\omega_{23} + \mu_{R1} + \mu_{R2} - \mu_{R1} \omega_{13} - \mu_{R2} \omega_{23}) f_{tk} x' b \quad 3.30$$

$$\text{where } \mu_{R1} = \frac{f_{teq1}}{f_{tk}} \text{ and } \mu_{R2} = \frac{f_{teq2}}{f_{tk}}$$

The total moment at the top edge of the section is

$$M_t = \frac{f_{tk} b x'^2}{6} [\mu_{R1} (\omega_{13}^2 + \omega_{13} \omega_{23} - 3\omega_{13} - \omega_{23} + 2) + \mu_{R2} (\omega_{23}^2 - 2\omega_{23} + 1) + 3\omega_{23} - \omega_{13} \omega_{23} - \omega_{23}^2] \quad 3.31$$

and by equivalence of the simplified rectangular stress block, the following can be shown

$$\lambda_{td} = \frac{2[\mu_{R1}(\omega_{13}^2 + \omega_{13}\omega_{23} - \omega_{23} - 3\omega_{13} + 2) + \mu_{R2}(\omega_{23}^2 - 2\omega_{23} + 1) + 3\omega_{23} - \omega_{23}^2 - \omega_{13}\omega_{23}]}{3[\omega_{23} + \mu_{R1}(1 - \omega_{13}) + \mu_{R2}(1 - \omega_{23})]} \quad 3.32$$

$$\eta_{td} = \frac{3[\omega_{23} + \mu_{R1}(1 - \omega_{13}) + \mu_{R2}(1 - \omega_{23})]^2}{4[\mu_{R1}(\omega_{13}^2 + \omega_{13}\omega_{23} - \omega_{23} - 3\omega_{13} + 2) + \mu_{R2}(\omega_{23}^2 - 2\omega_{23} + 1) + 3\omega_{23} - \omega_{23}^2 - \omega_{13}\omega_{23}]} \quad 3.33$$

The product of the conversion factors is given by:

$$\beta_{td} = \frac{1}{2}[\mu_{R1}(1 - \omega_{13}) + \mu_{R2}(1 - \omega_{23}) + \omega_{23}] \quad 3.34$$

Considering stress-strain distribution at service limit state: Rilem defined f_{teq1} and ϵ_{tl} as service stress and strain respectively. Therefore, it can be shown that conversion factors at service are determined by adopting the following terms in the Equations 3.32 - 3.34:

$$\mu_{R1} = \mu_{R2}; \omega_{12} = \omega_{13} \text{ and } \omega_{12} = 1$$

Then, at service the conversion factors are determined as follows:

$$\lambda_{ts} = \frac{2[\mu_{R1}(2\omega_{12} - 1 - \omega_{12}^2) + \omega_{12} - 2]}{3[\mu_{R1}(\omega_{12} - 1) - 1]} \quad 3.35$$

$$\eta_{ts} = \frac{3[\mu_{R1}(\omega_{13} - 1) - 1]^2}{4[\mu_{R1}(1 - 2\omega_{12} + \omega_{13}^2) + 2 - \omega_{12}]} \quad 3.36$$

A complete derivation from first principles of these conversion factors at service has been provided in Appendix A.

The minimum acceptable values for ratios μ_{R1} and μ_{R2} may be derived from Equation 2.18 in Chapter 2 as recommended by Di Prisco *et al* (2009). Based on the definition of the tensile parameter ratios given in Section 2.3.3, the values of μ_{R1} and μ_{R2} allowed for the SFRC material to be considered to offer structural resistance are given as follows:

$$\mu_{R1} > 0.4 \text{ and } \mu_{R2} > 0.2 \quad 3.37$$

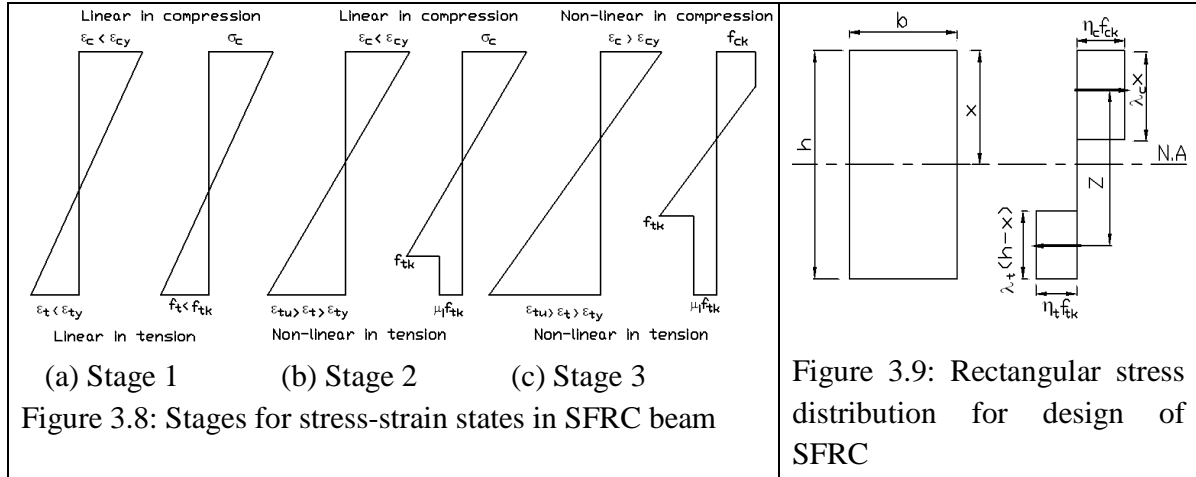
3.3 FLEXURAL MODELLING FOR SFRC RECTANGULAR BEAM SECTION

In this section, the derivation of flexural models for SFRC with and without reinforcing bars is outlined. The bilinear compression model and either the drop-down or the Rilem tension model have been used in the derivation of a flexural model for SFRC without reinforcing bars. A flexural model for SFRC with reinforcing bars has been derived from the bilinear compression model and drop-down tension model only.

3.3.1 FLEXURAL MODEL FOR SFRC BEAMS USING THE DROP-DOWN TENSION AND THE BILINEAR COMPRESSION MODELS

A beam element subjected to flexural loads may experience three basic stages of stress states as shown in Figure 3.8. The stages assume that the element will reach the first cracking strain in tension before reaching compression yield strain and are expressed as follows:

1. Stage 1: Linear elastic stress-strain relationship in both compression and tension, i.e. stress state before the material cracks in tension.
2. Stage 2: Linear elastic stress-strain relationship in compression while tension is in inelastic distribution, i.e. the stress state after the material has reached cracking strain before compression yield strain is reached.
3. Stage 3: Inelastic stress distribution for both compression and tension stress-strain fields, i.e. the stress state after the material has cracked in tension and yielded in compression.



Based on strain compatibility and force equilibrium, equations for the determination of the neutral axis, curvature and lever arm for different stages of stress-strain states are derived and are given in Table 3.1. Full derivations of the equations are outlined in Appendix A. In the equations, x is the neutral axis depth from compression face and h is the overall depth of the section, other terms are as defined before.

Table 3.1: Neutral axis, curvature and lever arm formulas using the bi-linear and the drop-down models

Parameter	Stage One	Stage two	Stage Three
$\frac{x}{h}$ (neutral axis ratio)	$\frac{1}{2}$	$\frac{2\beta_t \epsilon_{ty}}{\epsilon_c + 2\beta_t \epsilon_{ty}}$	$\frac{\beta_t \epsilon_{ty}}{\beta_c \epsilon_{cy} + \beta_t \epsilon_{ty}}$
$\frac{\epsilon_c}{x}$ (curvature)	$\frac{2\epsilon_c}{h}$	$\frac{\epsilon_c^2}{2h\beta_t \epsilon_{ty}} + \frac{\epsilon_c}{h}$	$\frac{\beta_c \epsilon_{ty} \epsilon_c}{h\beta_t \epsilon_{ty}} + \frac{\epsilon_c}{h}$
$\frac{Z}{h}$ (lever arm ratio)	$\frac{2}{3}$	$1 + \frac{x}{h} \left(\frac{\lambda_t}{2} - \frac{1}{3} \right) - \frac{\lambda_t}{2}$	$1 + \frac{x}{2h} (\lambda_t - \lambda_c) - \frac{\lambda_t}{2}$

By considering the simplified rectangular stress block (Figure 3.9), flexural capacity of the section can be derived. To ensure that moment capacity is derived from strains that do not exceed ultimate limits in either tension or compression, equivalent strains are determined from a strain compatibility equation and a force equilibrium equation. The minimum of the ultimate and

equivalent strains dictates the ultimate capacity of the section. It is assumed, based on practical values of strains, that the moment capacity for a SFRC without reinforcement will be limited by the tensile capacity of the section. Therefore, considering that the ultimate tensile strain is reached in either Stage Two or Stage Three, the equivalent compressive strains at failure are determined.

The position of the neutral axis moves as the section is being loaded. Since the yield strain in tension is less than that in compression, the neutral axis will move towards the compression face after yielding. The balanced strain ratio for ultimate strain compatibility, where both tension and compression zones will reach the ultimate strains at the same time, can be calculated below.

$$\frac{x}{h}(\text{balanced}) = \frac{\epsilon_{cu}}{\epsilon_{cu} + \epsilon_{tu}} \quad 3.38$$

Recall from Equation 3.18 that these parameters are directly related to material model parameters as follows:

$$\beta_c = 1 - \frac{\epsilon_{cy}}{2\epsilon_{cp}} \text{ and } \beta_{cd} = 1 - \frac{\epsilon_{cy}}{2\epsilon_{cu}}$$

and from Equation 3.26 that

$$\beta_t = \frac{\epsilon_{ty}}{2\epsilon_{tp}}(1 - 2\mu_i) + \mu_i \text{ and } \beta_{td} = \frac{\epsilon_{ty}}{2\epsilon_{tu}}(1 - 2\mu_u) + \mu_u$$

Stage Two:

Considering Stage Two strain compatibility:

$$\frac{\epsilon_{c2eq}}{\epsilon_{tu} + \epsilon_{c2eq}} = \frac{x}{h} \quad 3.39$$

and from force equilibrium, assuming a linear relation for the first stage, as follows:

$$\frac{2\beta_{tu}\epsilon_{ty}}{\epsilon_{c2eq} + 2\beta_{tu}\epsilon_{ty}} = \frac{x}{h} \quad 3.40$$

Solving the Equations 3.39 and 3.40 above yields the following expression

$$\epsilon_{c2eq} = \sqrt{2\beta_{tu}\epsilon_{ty}\epsilon_{tu}} \quad 3.41$$

Stage Three:

Setting the strain compatibility equation as follows:

$$\frac{\epsilon_{c3eq}}{\epsilon_{tu} + \epsilon_{c3eq}} = \frac{x}{h} \quad 3.42$$

and the force equilibrium equation, assuming a linear relation for the first stage, as follows:

$$\frac{\beta_{tu}\epsilon_{ty}}{\beta_{ceq}\epsilon_{cy} + \beta_{tu}\epsilon_{ty}} = \frac{x}{h} \quad 3.43$$

where β_{ceq} is calculated based on $\omega_{eq} = \frac{\epsilon_{cy}}{\epsilon_{c3eq}}$

Solving Equations 3.42 and 3.43 simultaneously for ϵ_{c3eq} yields:

$$\epsilon_{c3eq} = \frac{\beta_{tu} \epsilon_{ty} \epsilon_{tu}}{\epsilon_{cy}} + \frac{\epsilon_{cy}}{2} \quad 3.44$$

An appropriate value for equivalent strain calculated from Equations 3.41 and 3.44 is chosen if it meets the following criterion:

$$\epsilon_{c2eq} \leq \epsilon_{cy} \leq \epsilon_{c3eq} \leq \epsilon_{cu}$$

It is assumed that a value that meets the above criterion represents the compression strain at ultimate limit state of the section. The appropriate neutral axis depth to overall depth ratio to be used in the determination of moment capacity is therefore based on the appropriate value of equivalent compression strain at ultimate tensile strain, as calculated above. With the overall depth of the section known, the depth of the neutral axis and length of the lever arm are determined using the equations given in Table 3.1, and the moment resistance of the section is determined using the appropriate expression in Equation 3.45. When the beam fails in Stage Three, the moment values determined from either expression in Equation 3.45 should converge.

$$M = \begin{matrix} \beta_c x b Z f_{ck} & \text{ultimate failure, Stage Three stress state} \\ \beta_{tu} (h - x) b Z f_{tk} & \text{ultimate failure, Stages Two and Three stress states} \end{matrix} \quad 3.45$$

3.3.2 FLEXURAL MODEL FOR SFRC BEAMS USING THE RILEM TENSION AND THE BILINEAR COMPRESSION MODELS

Using the Rilem tensile model and the bilinear compression model, analytical formulae for flexural capacity of a rectangular beam can be derived for both at service and at ultimate limit state. In this section, only stress states for these two design situations (service and ultimate conditions) are considered. Two stress-strain situations are conceived for each of these design conditions as follows (see Figures 3.10 and 3.11):

Service condition:

Stage 1: Linear elastic stress-strain relationship in compression while service stress in tension is attained.

Stage 2: Inelastic stress distribution in compression while service stress in tension is attained.

Ultimate condition:

Stage 1: Linear elastic stress-strain relationship in compression while ultimate stress in tension is attained.

Stage 2: Inelastic stress distribution in compression while ultimate stress in tension is attained.

It should be noted that these stress-strain states assume that the SFRC section attains limiting tensile strains before concrete crushes in compression (i.e. before reaching the ultimate compressive strength). By considering the simplified rectangular stress blocks in tension and compression (similar to Figure 3.9), flexural capacity of the section can be derived. To ensure that moment capacity is derived from appropriate compressive strain for each design situation, equivalent compressive strains attained when the section reaches either service or ultimate tensile

strains are determined from a strain compatibility equation and a force equilibrium equation for the two stages of stress-strain states as follows:

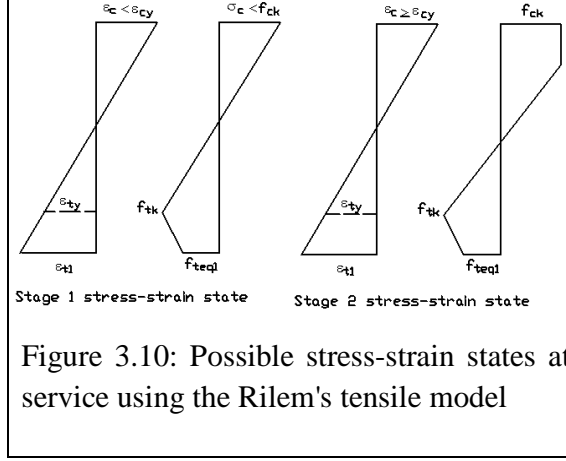


Figure 3.10: Possible stress-strain states at service using the Rilem's tensile model

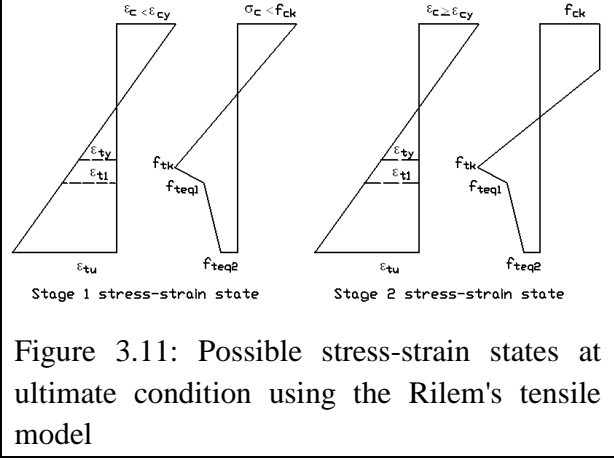


Figure 3.11: Possible stress-strain states at ultimate condition using the Rilem's tensile model

Recall from Equation 3.18 that these parameters are directly related to material model parameters as follows:

$$\beta_c = 1 - \frac{\epsilon_{cy}}{2\epsilon_{cp}} \text{ and the conversion factors at service and ultimate states are } \beta_{c1} = 1 - \frac{\epsilon_{cy}}{2\epsilon_{c1}}$$

and $\beta_{c,u} = 1 - \frac{\epsilon_{cy}}{2\epsilon_{c,u}}$ respectively.

Service state Stage 1 (with reference to Figure 3.10, Stage 1)

Considering strain compatibility, the ratio of the neutral axis to overall depth is defined as:

$$\frac{\epsilon_{cs1}}{\epsilon_{t1} + \epsilon_{cs1}} = \frac{x}{h} \quad 3.46$$

and from force equilibrium, assuming a linear relation for the first stage, as follows:

$$\frac{2\beta_{ts}\epsilon_{ty}}{\epsilon_{cs1} + 2\beta_{ts}\epsilon_{ty}} = \frac{x}{h} \quad 3.47$$

Solving the Equations 3.46 and 3.47 above yields the following expression

$$\epsilon_{cs1} = \sqrt{2\beta_{ts}\epsilon_{ty}\epsilon_{t1}} \quad 3.48$$

Service state Stage 2 (with reference to Figure 3.10, Stage 2)

Considering strain compatibility, the ratio of the neutral axis to overall depth is defined as:

$$\frac{\epsilon_{cs2}}{\epsilon_{tu} + \epsilon_{cs2}} = \frac{x}{h} \quad 3.49$$

and from force equilibrium, assuming a linear relation for the first stage, as follows:

$$\frac{\beta_{ts}\epsilon_{ty}}{\beta_{cs1}\epsilon_{cy} + \beta_{ts}\epsilon_{ty}} = \frac{x}{h} \quad 3.50$$

Solving the Equations 3.49 and 3.50 above yields the following expression:

$$\epsilon_{cs2} = \frac{\beta_{tu} \epsilon_{ty} \epsilon_{tu}}{\epsilon_{cy}} + \frac{\epsilon_{cy}}{2} \quad 3.51$$

An appropriate value for equivalent strain at service (ϵ_{c1}) is selected from Equations 3.48 and 3.51 if the calculated strain meets the following criterion:

$$\epsilon_{cs1} \leq \epsilon_{cy} \leq \epsilon_{cs2} \leq \epsilon_{cu}$$

Ultimate state Stage 1 (with reference to Figure 3.11, Stage 1)

Considering strain compatibility, the ratio of the neutral axis to overall depth is defined as:

$$\frac{\epsilon_{c,u1}}{\epsilon_{tu} + \epsilon_{c,u1}} = \frac{x}{h} \quad 3.52$$

and from force equilibrium, assuming a linear relation for the first stage, as follows:

$$\frac{2\beta_{tu} \epsilon_{ty}}{\epsilon_{c,u1} + 2\beta_{tu} \epsilon_{ty}} = \frac{x}{h} \quad 3.53$$

Solving the Equations 3.52 and 3.53 above yields the following expression

$$\epsilon_{c,u1} = \sqrt{2\beta_{tu} \epsilon_{ty} \epsilon_{tu}} \quad 3.54$$

Ultimate state Stage 2 (with reference to Figure 3.11, Stage 2)

Considering strain compatibility, the ratio of the neutral axis to overall depth is defined as:

$$\frac{\epsilon_{c,u2}}{\epsilon_{tu} + \epsilon_{c,u2}} = \frac{x}{h} \quad 3.55$$

and from force equilibrium, assuming a linear relation for the first stage, as follows:

$$\frac{\beta_{tu} \epsilon_{ty}}{\beta_{c,u2} \epsilon_{cy} + \beta_{tu} \epsilon_{ty}} = \frac{x}{h} \quad 3.56$$

Solving the Equations 3.55 and 3.56 above yields the following expression

$$\epsilon_{c,u} = \frac{\beta_{tu} \epsilon_{ty} \epsilon_{tu}}{\epsilon_{cy}} + \frac{\epsilon_{cy}}{2} \quad 3.57$$

An appropriate value for equivalent strain at ultimate state ($\epsilon_{c,u}$) is selected from Equations 3.54 and 3.57 if the calculated strain meets the following criterion:

$$\epsilon_{c,u1} \leq \epsilon_{cy} \leq \epsilon_{c,u2} \leq \epsilon_{cu}$$

Using the appropriate strains as calculated above, the appropriate neutral axis depth ratio is calculated from Equation 3.58, while the lever arm ratio for each stress state is given in Table 3.2.

$$\frac{x}{h} = \begin{cases} \frac{\epsilon_{c1}}{\epsilon_{c1} + \epsilon_{t1}} & \text{for service state} \\ \frac{\epsilon_{c,u}}{\epsilon_{c,u} + \epsilon_{tu}} & \text{for ultimate state} \end{cases} \quad 3.58$$

Table 3.2: Lever arm ratios at service and ultimate states using the bi-linear and the Rilem tensile models

	Service state, Stage 1	Service state, Stage 2	Ultimate, Stage 1	Ultimate, Stage 2
$\frac{Z}{h}$	$1 + \frac{x}{h} \left(\frac{\lambda_{t1}}{2} - \frac{1}{3} \right) - \frac{\lambda_{t1}}{2}$	$1 + \frac{x}{2h} (\lambda_{t1} - \lambda_{c1}) - \frac{\lambda_{t1}}{2}$	$1 + \frac{x}{h} \left(\frac{\lambda_{tu}}{2} - \frac{1}{3} \right) - \frac{\lambda_{tu}}{2}$	$1 + \frac{x}{2h} (\lambda_{tu} - \lambda_{c,u}) - \frac{\lambda_{tu}}{2}$

The resistance moment at either service state (M_{ser}) or ultimate (M) state can be determined using the general expression for moment as given in Equation 3.45 as rewritten below:

$$M_{ser} = \begin{cases} \beta_{c1} x b Z f_{ck} & \text{service state, Stage 2} \\ \beta_{t1} (h - x) b Z f_{tk} & \text{service state, Stage 1} \end{cases} \quad 3.59$$

$$M = \begin{cases} \beta_{c,u} x b Z f_{ck} & \text{ultimate state, Stage 2} \\ \beta_{tu} (h - x) b Z f_{tk} & \text{ultimate state, Stage 1} \end{cases} \quad 3.60$$

3.3.3 FLEXURAL MODELS FOR REINFORCED SFRC BEAMS

Three possible modes of failure for a reinforced concrete section (Bhatt *et al*, 2006) as outlined in Section 2.5.2.3 of Chapter 2 are considered for R-SFRC members. These are: steel reinforcement yields first, simultaneous ‘yielding’ of steel reinforcement and concrete in compression, and concrete crushes first. The codes recommend failure mode starting with yielding of steel bars before concrete crushes. A similar approach as outlined in Section 2.5.2.3 for nonlinear analysis of RC beams is adopted for R-SFRC beams. Five values of moment resistance for the beam will be considered. These are: cracking moment (M_{cr}), moment at ultimate tensile strength of concrete (M_{ut}), moment when steel yields (M_y), moment at the ultimate tensile strength of steel (M_p) and moment at ultimate compression strength of concrete (M_{uc}). Table 3.3 shows categories for various possibilities that are considered in order to calculate the moment values at the four points mentioned.

Table 3.3: Possible strain states combinations for determination of moments for R-SFRC beams

Category	Moment	Compression-tension stress condition in SFRC	Condition for one strain	Assumptions for other strains
A	M_{cr}	Elastic compression-elastic tension	ϵ_{ty} reached	$\epsilon_c < \epsilon_{cy}$, $\epsilon_s < \epsilon_{sy}$
B(I)	M_y	Elastic compression-plastic tension	ϵ_{sy} reached	$\epsilon_c < \epsilon_{cy}$, $\epsilon_{t(u)} > \epsilon_{ty}$
B(II)		Plastic compression-plastic tension	ϵ_{sy} reached	$\epsilon_c > \epsilon_{cy}$, $\epsilon_{t(u)} > \epsilon_{ty}$
C(I)	M_{ut}	Elastic compression-plastic tension	ϵ_{tu} reached	$\epsilon_c < \epsilon_{cy}$, $\epsilon_s < \epsilon_{sy}$
C(I)*		Elastic compression-plastic tension	ϵ_{tu} reached	$\epsilon_c < \epsilon_{cy}$, $\epsilon_s > \epsilon_{sy}$
C(II)		Plastic compression-plastic tension	ϵ_{tu} reached	$\epsilon_c > \epsilon_{cy}$, $\epsilon_s < \epsilon_{sy}$
C(II)*		Plastic compression-plastic tension	ϵ_{tu} reached	$\epsilon_c > \epsilon_{cy}$, $\epsilon_s > \epsilon_{sy}$
D(I)	M_p	Elastic compression-plastic tension	ϵ_{uk} reached	$\epsilon_c < \epsilon_{cy}$, $\epsilon_{t(u)} > \epsilon_{ty}$
D(II)		Plastic compression-plastic tension	ϵ_{uk} reached	$\epsilon_c > \epsilon_{cy}$, $\epsilon_{t(u)} < \epsilon_{ty}$
E(I)	M_{uc}	Plastic compression-plastic tension	ϵ_{cu} reached	$\epsilon_s \leq \epsilon_{sy}$, $\epsilon_{t(u)} > \epsilon_{ty}$
E(I)*		Plastic compression-plastic tension	ϵ_{cu} reached	$\epsilon_s > \epsilon_{sy}$, $\epsilon_{t(u)} > \epsilon_{ty}$

*Steel reinforcement has yielded; the change in formulations is the determination of steel bar forces for strain-hardening reinforcing bars only.

Cracking moment (M_{cr}): This is the moment when the SFRC reaches cracking tensile strain. This may be assumed to occur before concrete yields in compression (see Figure 3.12). A linear analysis formula similar to that for normal RC is applicable as follows:

$$M_{cr} = \frac{1}{3} \epsilon_c E_c x^2 b + \frac{1}{3} \frac{(h-x)^3}{x} \epsilon_c E_c b + \frac{(d-x)^2}{x} \epsilon_c E_s A_s \quad 3.61$$

Where ϵ_c is calculated from the relations $\frac{\epsilon_c}{x} = \frac{\epsilon_{ty}}{h-x}$ and $x = \frac{(h + 2m\rho_g d)}{(2 + 2m\rho_g)}$ for which $\epsilon_c \leq \epsilon_{cy}$

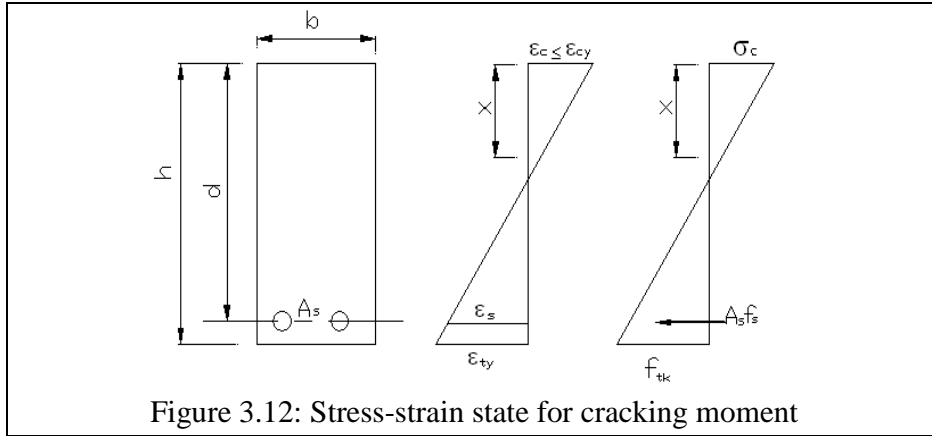


Figure 3.12: Stress-strain state for cracking moment

Moment when steel yields (M_y): This is the moment when the steel reinforcement reaches yielding strain. Two possibilities considered are elastic compression with corresponding plastic tension, and plastic compression and tension combinations (see Figure 3.13). Using strain compatibility and force equilibrium, the following expressions are derived:

Strain compatibility:

$$\frac{\epsilon_{t(u)}}{\epsilon_{sy}} = \frac{h-x}{d-x}, \frac{\epsilon_c}{\epsilon_c + \epsilon_{sy}} = \frac{x}{d} \quad 3.62$$

Force equilibrium for elastic compression-plastic tension case:

$$\frac{1}{2} \sigma_c b x = \beta_t f_{tk} (h-x) b + A_s f_{sy} \quad 3.63$$

Recall that $\beta_t = \frac{\epsilon_{ty}}{2\epsilon_{t(u)}} (1 - 2\mu_i) + \mu_i$ from Equation 3.26 for a drop-down model

Solving Equations 3.62 and 3.63 for x yields a quadratic expression with the solution of the form:

$$x = \frac{-B \pm \sqrt{B^2 - 4AC}}{2A} \quad 3.64$$

where

$$A = b(-E_c \epsilon_{sy}^2 + f_{tk} \epsilon_{ty} - 2\mu_i f_{tk} \epsilon_{ty} + 2\mu_i f_{tk} \epsilon_{sy})$$

$$B = bd \left(-2f_{tk}\epsilon_{ty} + 4\mu_i f_{tk}\epsilon_{ty} - 2\mu_i f_{tk}\epsilon_{sy} \frac{h}{d} - 2\mu_i f_{tk}\epsilon_{sy} \right) - 2A_s f_{sy} \epsilon_{sy}$$

$$C = f_{tk} bd^2 \left(\epsilon_{ty} - 2\mu_i \epsilon_{ty} + 2\mu_i \epsilon_{sy} \frac{h}{d} \right) + 2A_s f_{sy} \epsilon_{sy} d$$

Force equilibrium for plastic compression-plastic tension case:

$$\beta_c f_{ck} x b = \beta_t f_{tk} (h - x) b + A_s f_{sy} \quad 3.65$$

Solving Equations 3.62 and 3.65 for x yields the following expression:

$$x = \frac{d \left(f_{ck} \epsilon_{cy} + f_{tk} \epsilon_{ty} - 2\mu_i f_{tk} \epsilon_{ty} + 2\mu_i f_{tk} \epsilon_{sy} \frac{h}{d} + 2\rho f_{sy} \epsilon_{sy} \right)}{2f_{ck} \epsilon_{sy} + f_{ck} \epsilon_{cy} + f_{tk} \epsilon_{ty} - 2\mu_i f_{tk} \epsilon_{ty} + 2\mu_i f_{tk} \epsilon_{sy}} \quad 3.66$$

Using Equation 3.62 and the value of x determined from Equations 3.64 and 3.66, the potential value of ϵ_c is determined. The value of ϵ_c used will follow the basic assumptions in the derivation, i.e. ϵ_c from linear-plastic $\leq \epsilon_{cy}$ and ϵ_c from plastic-plastic $> \epsilon_{cy}$. The appropriate moment when steel yields is determined as follows:

$$M_y = \begin{cases} \frac{1}{3} \sigma_c b x^2 + \frac{1}{2} \beta_t f_{tk} (h - x)^2 b + A_s f_{sy} (d - x) & \text{for elastic - plastic condition} \\ \frac{1}{2} \beta_c f_{ck} b x^2 + \frac{1}{2} \beta_t f_{tk} (h - x)^2 b + A_s f_{sy} (d - x) & \text{for plastic - plastic condition} \end{cases} \quad 3.67$$

where $\sigma_c = \epsilon_c E_c$

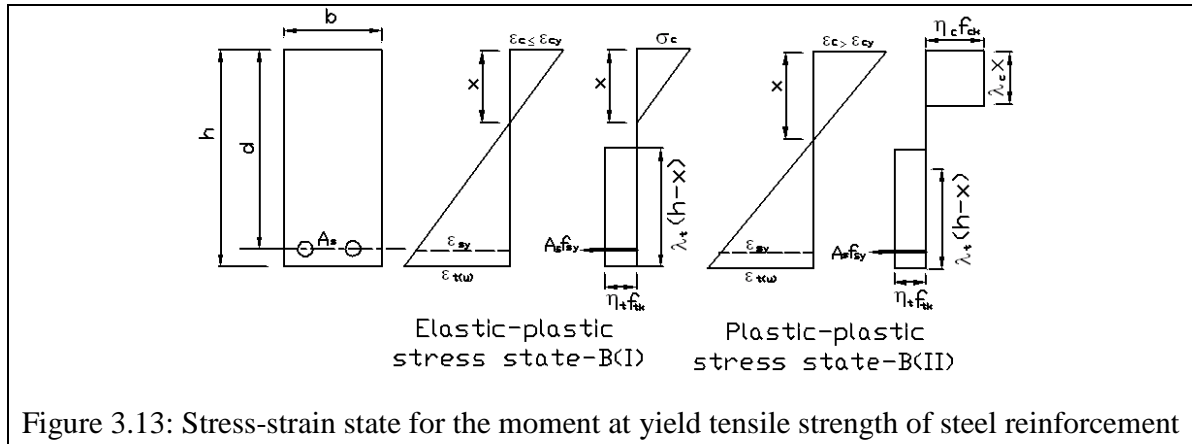


Figure 3.13: Stress-strain state for the moment at yield tensile strength of steel reinforcement

Moment at ultimate tensile strength of concrete (M_{ut}): This is the moment when the SFRC reaches the ultimate tensile strain. Two main possibilities considered are elastic compression with plastic tension, and plastic compression and tension (see Figure 3.14). Of these two possibilities, it may be possible that steel reinforcement may either have or have not yielded. Using strain compatibility and force equilibrium, the following expressions are derived:

Strain compatibility:

$$\frac{\epsilon_s}{\epsilon_{tu}} = \frac{d - x}{h - x}, \frac{\epsilon_c}{\epsilon_c + \epsilon_{tu}} = \frac{x}{h} \quad 3.68$$

Force equilibrium for elastic compression-plastic tension case:

$$\frac{1}{2}\sigma_c b x = \beta_{tu} f_{tk} (h - x)b + A_s f_s \quad 3.69$$

Solving Equations 3.68 and 3.69 for x yields a quadratic expression with the solution of the

$$\text{form: } x = \frac{-B \pm \sqrt{B^2 - 4AC}}{2A} \quad 3.70$$

where

$$A = b(-E_c \epsilon_{tu}^2 + f_{tk} \epsilon_{ty} - 2\mu_i f_{tk} \epsilon_{ty} + 2\mu_i f_{tk} \epsilon_{tu})$$

$$B = bh(-2f_{tk} \epsilon_{ty} + 4\mu_i f_{tk} \epsilon_{ty} - 4\mu_i f_{tk} \epsilon_{tu}) - 2A_s E_s^* \epsilon_{tu}^2$$

$$C = f_{tk} b h^2 (\epsilon_{ty} - 2\mu_i \epsilon_{ty} + 2\mu_i \epsilon_{tu}) + 2A_s E_s^* \epsilon_{tu}^2 d$$

$$E_s^* = \begin{cases} E_s & \text{for } \epsilon_s \leq \epsilon_{sy} \\ E_{s1} & \text{for } \epsilon_s > \epsilon_{sy} \end{cases}$$

E_{s1} is the gradient of the stress-strain curve of steel reinforcement after yielding

$$f_s = E_s \epsilon_{sy} + E_{s1} (\epsilon_s - \epsilon_{sy})$$

Force equilibrium for plastic compression-plastic tension case:

$$\beta_c f_{ck} x b = \beta_{tu} f_{tk} (h - x)b + A_s f_s \quad 3.71$$

Solving Equations 3.68 and 3.71 for x yields a quadratic expression of the form:

$$x = \frac{-B \pm \sqrt{B^2 - 4AC}}{2A} \quad 3.72$$

where

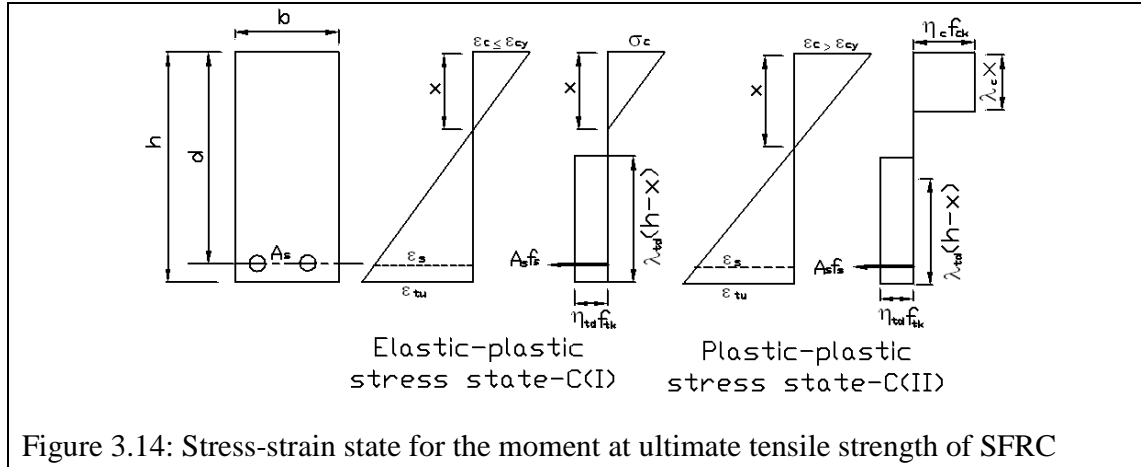
$$A = b(2f_{ck} \epsilon_{tu} + f_{ck} \epsilon_{cy} + 2\beta_{tu} f_{tk} \epsilon_{tu})$$

$$B = -2bh(f_{ck} \epsilon_{tu} + f_{ck} \epsilon_{cy} + 2\beta_{tu} f_{tk} \epsilon_{tu}) - 2A_s E_s^* \epsilon_{tu}^2$$

$$C = b h^2 (f_{ck} \epsilon_{cy} + 2\beta_{tu} f_{tk} \epsilon_{tu}) + 2A_s E_s^* \epsilon_{tu}^2 d$$

Using Equation 3.68 and the value of x determined from Equations 3.70 and 3.72, the potential value of ϵ_c is determined. The value of ϵ_c to be used will follow the basic assumptions in the derivation (i.e. ϵ_c from linear-plastic $\leq \epsilon_{cy}$ and ϵ_c from plastic-plastic $> \epsilon_{cy}$). The appropriate moment at ultimate tensile strength is given as follows:

$$M_{ut} = \begin{cases} \frac{1}{3}\sigma_c b x^2 + \frac{1}{2}\beta_{tu} f_{tk} (h - x)^2 b + A_s f_s (d - x) & \text{for elastic - plastic condition} \\ \frac{1}{2}\beta_c f_{ck} b x^2 + \frac{1}{2}\beta_{tu} f_{tk} (h - x)^2 b + A_s f_s (d - x) & \text{for plastic - plastic condition} \end{cases} \quad 3.73$$



Moment at ultimate tensile strength of steel (M_p): This is the moment when the steel reinforcement reaches its ultimate tensile strain. Two possibilities considered are elastic compression with corresponding plastic tension, and plastic compression and tension combinations (see Figure 3.15). Using strain compatibility and force equilibrium, the following expressions are derived:

Strain compatibility:

$$\frac{\epsilon_{t(u)}}{\epsilon_{uk}} = \frac{h-x}{d-x}, \frac{\epsilon_c}{\epsilon_c + \epsilon_{uk}} = \frac{x}{d} \quad 3.74$$

Force equilibrium for elastic compression-plastic tension case:

$$\frac{1}{2} \sigma_c b x = \beta_t f_{tk} (h-x)b + A_s f_{uk} \quad 3.75$$

Recall that $\beta_t = \frac{\epsilon_{ty}}{2\epsilon_{t(u)}} (1 - 2\mu_i) + \mu_i$ from Equation 3.26 for a drop-down model

Solving Equations 3.74 and 3.75 for x yields a quadratic expression of the form:

$$x = \frac{-B \pm \sqrt{B^2 - 4AC}}{2A} \quad 3.76$$

where

$$\begin{aligned} A &= b \left(-E_c \epsilon_{uk}^2 + f_{tk} \epsilon_{ty} - 2\mu_i f_{tk} \epsilon_{ty} + 2\mu_i f_{tk} \epsilon_{uk} \right) \\ B &= bd \left(-2f_{tk} \epsilon_{ty} + 4\mu_i f_{tk} \epsilon_{ty} - 2\mu_i f_{tk} \epsilon_{uk} \frac{h}{d} - 2\mu_i f_{tk} \epsilon_{uk} \right) - 2A_s f_{uk} \epsilon_{uk} \\ C &= f_{tk} bd^2 \left(\epsilon_{ty} - 2\mu_i \epsilon_{ty} + 2\mu_i \epsilon_{uk} \frac{h}{d} \right) + 2A_s f_{uk} \epsilon_{uk} d \end{aligned}$$

Force equilibrium for plastic compression-plastic tension case:

$$\beta_c f_{ck} x b = \beta_t f_{tk} (h-x)b + A_s f_{uk} \quad 3.77$$

Solving Equations 3.74 and 3.77 for x yields the following expression

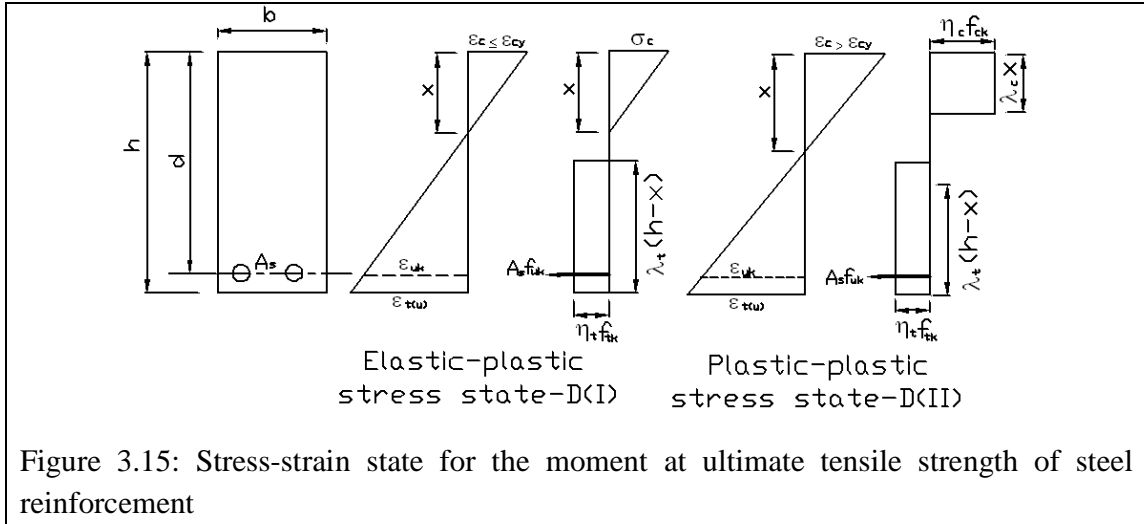
$$x = \frac{d \left(f_{ck} \epsilon_{cy} + f_{tk} \epsilon_{ty} - 2\mu_i f_{tk} \epsilon_{ty} + 2\mu_i f_{tk} \epsilon_{uk} \frac{h}{d} + 2\rho f_{uk} \epsilon_{uk} \right)}{2f_{ck} \epsilon_{uk} + f_{ck} \epsilon_{cy} + f_{tk} \epsilon_{ty} - 2\mu_i f_{tk} \epsilon_{ty} + 2\mu_i f_{tk} \epsilon_{uk}} \quad 3.78$$

where

f_{uk} and ϵ_{uk} are the ultimate tensile strength and strain of steel reinforcement respectively.

Using Equation 3.74 and the value of x determined from Equations 3.76 and 3.78, the potential values of ϵ_c are determined. The value of ϵ_c to be used will follow the basic assumptions in the derivation, i.e. ϵ_c from linear-plastic $\leq \epsilon_{cy}$ and ϵ_c from plastic-plastic $> \epsilon_{cy}$. The appropriate moment at steel ultimate tensile strength is given as follows:

$$M_p = \begin{cases} \frac{1}{3} \sigma_c b x^2 + \frac{1}{2} \beta_t f_{tk} (h-x)^2 b + A_s f_{uk} (d-x) & \text{for elastic-plastic condition} \\ \frac{1}{2} \beta_c f_{ck} b x^2 + \frac{1}{2} \beta_t f_{tk} (h-x)^2 b + A_s f_{uk} (d-x) & \text{for plastic-plastic condition} \end{cases} \quad 3.79$$



Moment at ultimate compressive strength of SFRC (M_{uc}): This is the moment when the SFRC reaches its ultimate compression strain. It is assumed that the cracking tensile strain of concrete would have been exceeded while strain in steel reinforcement may either have yielded or not. Therefore, only one situation is considered as shown in Figure 3.16. Using strain compatibility and force equilibrium, the following expressions are derived:

Strain compatibility:

$$\epsilon_{t(u)} = \epsilon_{cu} \frac{h-x}{x} \quad \epsilon_s = \epsilon_{cu} \frac{d-x}{x} \quad 3.80$$

Force equilibrium:

$$\beta_{cd} f_{ck} x b = f_s A_s + \beta_t f_{tk} b h - \beta_t f_{tk} b x \quad 3.81$$

Solving for x gives a quadratic expression with solutions given in the form:

$$x = \frac{-B \pm \sqrt{B^2 - 4AC}}{2A} \quad 3.82$$

where

$$A = 2\beta_{cd}f_{ck}\epsilon_{cu} - f_{tk}\epsilon_{ty} + 2\mu f_{tk}\epsilon_{ty} + 2\mu f_{tk}\epsilon_{cu}$$

$$B = 2d\left(\rho E_s^* \epsilon_{cu}^2 - \mu f_{tk}\epsilon_{cu} \frac{h}{d}\right)$$

$$C = -2\rho E_s^* \epsilon_{cu}^2 d^2$$

E_s^* is as defined in Equation 3.62

Using Equation 3.80 and the value of x determined from Equation 3.82 the values of $\epsilon_{t(u)}$ and ϵ_s are determined. The moment at ultimate compression strength of SFRC is given as follows:

$$M_{uc} = \frac{1}{2}\beta_{cd}f_{ck}bx^2 + \frac{1}{2}\beta_t f_{tk}(h-x)^2b + A_s f_s(d-x) \quad 3.83$$

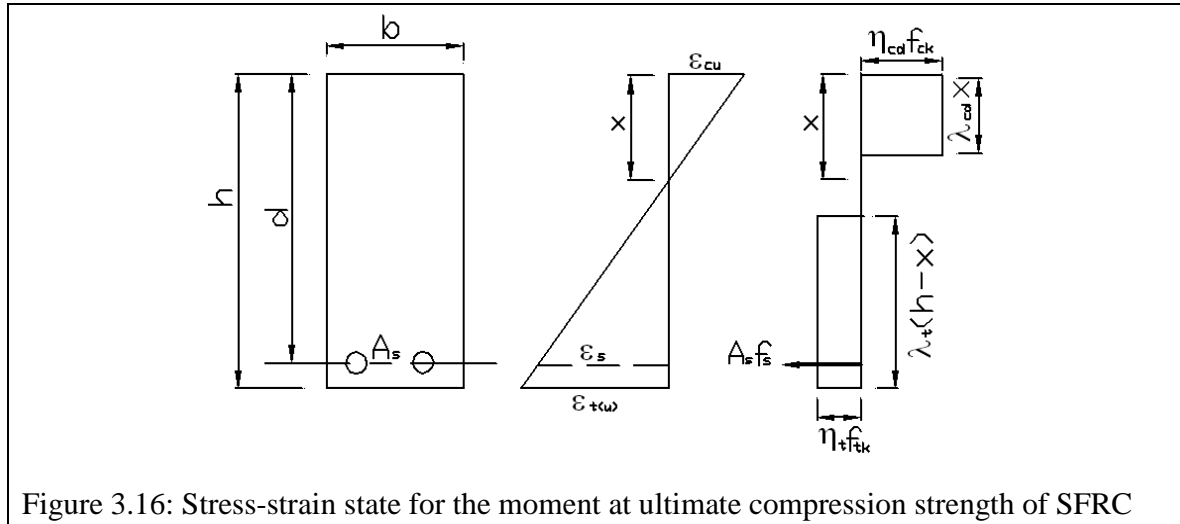


Figure 3.16: Stress-strain state for the moment at ultimate compression strength of SFRC

3.3.4 CONSIDERATION FOR PROVISION OF REINFORCEMENT IN SFRC BEAMS

Provision of reinforcement may not necessarily follow the expressions given in Section 3.3.2. In practice, the grade of concrete is selected and then used for the design of the section for normal reinforced concrete. In SFRC, the same approach will be used. In addition to knowledge of the grade of concrete, information must be furnished to the designer on the tensile properties of SFRC. When reinforcement is provided, a section may fail in three possible modes: steel reinforcement yielding first before concrete crushes; simultaneous yielding of steel reinforcement and crushing of concrete; concrete crushes first before steel yields. Following these modes of failure, three strain states are considered as under-reinforced, over-reinforced and a balanced state section (see Figure 3.17). Note that this strain state configuration utilises the ultimate compression force capacity for SFRC when designing the section.

For a balanced state, the strain state may be derived from Equation 3.84. Thus, for high yield steel reinforcement with a yield strain of 0.002, and using ultimate compression strain of 0.0035, the limiting neutral axis depth is given by 0.636d. Failure of the section at this state may not allow for adequate warning. Therefore, design standards recommend limiting the value of the neutral axis to 0.5d for sections with less than 10% moment redistribution (Bhatt *et al*, 2006, European Standards, 2004 and SABS 0100, 2000). This limit will be assumed for SFRC as well as the limits depending on the ultimate compression strain of concrete and the yield strain of steel reinforcement not influenced by the addition of steel fibres. However, subsequent use of the limiting value for K (≤ 0.156) may not be applicable as the stress states are different at this condition due to fibre contribution.

The position of the neutral axis for a balanced strain state is given as follows:

$$\frac{x}{d}(\text{balanced}) = \frac{\epsilon_{cu}}{\epsilon_{cu} + \epsilon_{sy}} \quad 3.84$$

and the maximum tensile strain in SFRC at the balanced strain state is given by

$$\epsilon_{tu*} = \frac{h}{d}(\epsilon_{cu} + \epsilon_{sy}) - \epsilon_{cu} \quad 3.85$$

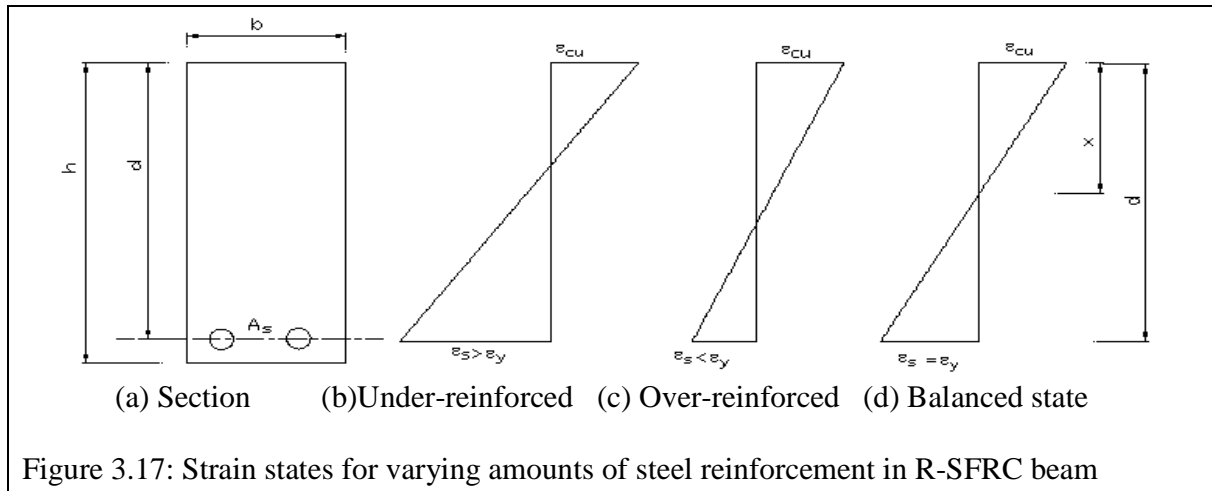


Figure 3.17: Strain states for varying amounts of steel reinforcement in R-SFRC beam

For a specified section dimension, the values of ϵ_{cu} , ϵ_{tu*} , and ϵ_{sy} are known and the variation of the position of the neutral axis with respect to the amount of steel reinforcement at balanced state can be deduced. From a force equilibrium expression for the section at this stress state:

$$\beta_{cd} f_{ck} x b = \beta_{td*} f_{tk} (h - x) b + A_s f_{sy} \text{ from which } \frac{x}{d} = \frac{\rho f_{sy} + \beta_{td*} f_{tk} \frac{h}{d}}{\beta_{cd} f_{ck} + \beta_{td*} f_{tk}} \quad 3.86$$

From Equation 3.86, the neutral axis ratio depends on the compression and tension capacity of the SFRC section and the amount of steel reinforcement provided. This is different for normal reinforced concrete in which the ratio of the neutral axis depends on the compression capacity of the SFRC section and the amount of steel reinforcement provided as follows:

$$\eta_{cd} \lambda_{cd} x b f_{cd} = A_s f_s \Leftrightarrow \frac{x}{d} = \frac{\rho f_s}{\beta_{cd} f_{ck}} \quad 3.87$$

For a specified section with material properties of SFRC known, a parametric study of the effect of the amount of reinforcing bars on the position of the neutral axis could be conducted. Figure 3.18 shows the result of a parametric study of the effect of the amount of reinforcing bars on the position of the neutral axis for concrete with characteristic compressive strength of 30MPa, compressive strains $\epsilon_{cu} = 0.0035$, $\epsilon_{cy} = 0.00125$ (as recommended by Rilem) and selected characteristic tensile strength, f_{tk} , of 4MPa, yield tensile strain, $\epsilon_{ty} = 0.000125$ and $\mu_i = 0.6$ for a section size, $h = 150\text{mm}$, $d = 120\text{mm}$ as compared with a section of the same size but without steel fibre contribution. The left figure shows the variation in the neutral axis depth when normalised tensile strength is varied.

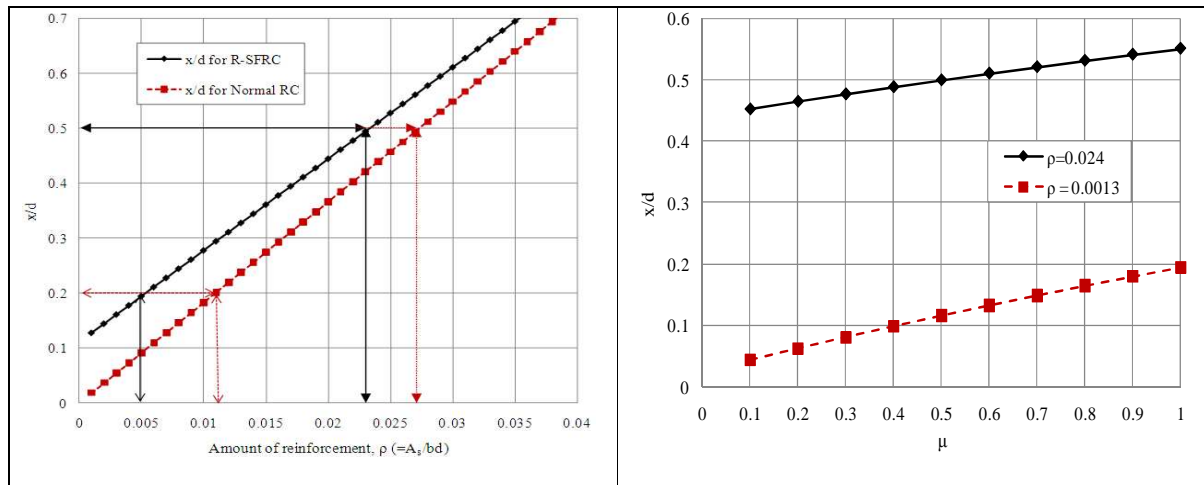


Figure 3. 18: Effects of fibres on the neutral axis ratio; Left: Comparison with NRC at $\mu_i=0.6$; Right: Comparison for varying normalised post-peak (drop-down) tensile strength ratio

As apparent from the figure, the amount of reinforcing steel is reduced when SFRC is used instead of normal concrete. At a prescribed limiting neutral axis depth of $0.5d$, NRC requires 2.7% of reinforcement ($\rho = 0.027$), while R-SFRC requires 2.4% of steel reinforcement ($\rho = 0.027$).

3.3.5 PROVISION OF REINFORCEMENT IN SFRC BEAMS

In order to ensure that the whole compression force from concrete is used in designing a section, two limiting tensile strains may be imposed: that dictated by SFRC and the limiting values for steel reinforcement. This is similar to the determination of the moment at yield steel (stress state B(II)), the moment at ultimate tensile strength of concrete (stress state C(II)) and the moment at ultimate compression strength of concrete (stress state E(I)) but considering that the strain in steel reinforcement is not fixed (see Figure 3.19).

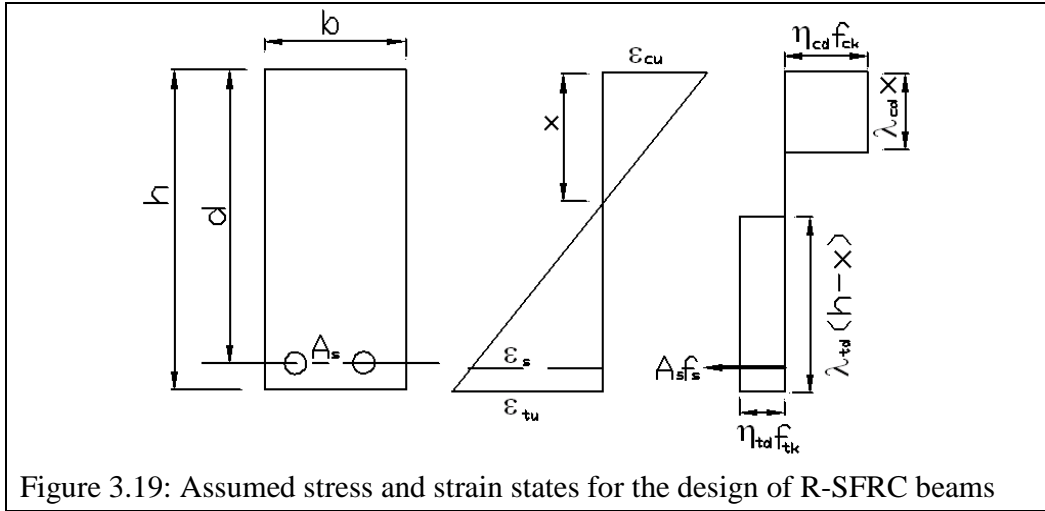


Figure 3.19: Assumed stress and strain states for the design of R-SFRC beams

A flexural model for the provision of steel reinforcement is developed. The limiting tensile strain of SFRC, ε_{tu} is used while the limiting tensile strain of steel reinforcement may either be ε_{sy} for steel bars with elastic-plastic tensile behaviour and ε_{uk} for strain hardening steel bars. Referring to Figure 3.19, the expressions for equilibrium of forces and strain compatibility can be shown to be

Force equilibrium:

$$\beta_{cd} f_{ck} x b = f_s A_s + \beta_{td} f_{tk} b h - \beta_{td} f_{tk} b x \quad 3.88$$

Strain compatibility:

$$\varepsilon_s = \varepsilon_{cu} \frac{d-x}{x} \leq \varepsilon_{sy} \text{ or } \varepsilon_s = \varepsilon_{cu} \frac{d-x}{x} \leq \varepsilon_{uk} \quad 3.89$$

Solving for x gives a quadratic expression with solutions given in the form:

$$x = \frac{-B \pm \sqrt{B^2 - 4AC}}{2A} \quad 3.90$$

where

$$A = b(\beta_{cd} f_{ck} + \beta_{td} f_{tk})$$

$$B = A_s E_s^* \varepsilon_{cu} - \beta_{td} f_{tk} b h$$

$$C = -A_s E_s^* \varepsilon_{cu} d$$

E_s^* is as defined in Equation 3.62

Using Equation 3.89 and the value of x determined from Equation 3.90 the value of ε_s is determined. The moment at ultimate compression strength of SFRC is given as follows:

$$M = \frac{1}{2} \beta_{cd} f_{ck} b x^2 + \frac{1}{2} \beta_{td} f_{tk} (h-x)^2 b + A_s f_s (d-x) \quad 3.91$$

3.4 CONCLUSION

Flexural capacity of SFRC with or without reinforcement can be assessed analytically as outlined in this chapter. Since the tensile properties of SFRC are required for design, more and complex design procedures are required. Two analytical models have been developed for flexural capacity of SFRC: with steel reinforcement, and without steel reinforcement. The flexural models are developed based on equivalent rectangular stress blocks for both compression and tension. Conversion of the material models to equivalent rectangular stress blocks requires the use of conversion factors λ_t , η_t , and β_t for tension and λ_c , η_c , and β_c for compression, which may depend on yield strains, post-yield strain and normalised tensile strength. While both parabolic and bilinear compressive stress-strain models were considered, the bilinear model has been used in further development of flexural models due to its simplicity. For tension, Rilem's multi-linear model and drop-down model were considered. However, for further development of flexural models, only the drop-down model was used as it requires fewer parameters to be defined and is hence easier to develop closed form equations for modelling.

Equilibrium of forces and strain compatibility were used to develop the models. Bernouli's assumptions for strains were intrinsically adopted in the formulations. Parametric studies have been performed to assess the sensitivity of parameters involved in conversion factors and also to assess the potential benefits of using SFRC. For example, the tensile conversion factor, λ_t , varies from 1.0 to 1.03 for the drop-down model, and from 1.0 to 1.2 for Rilem's model. The conversion factor, η_t , is approximately equal to the normalised tensile strength, μ_t , for the drop-down model, while it is slightly below average for the two post-peak normalised strength parameters, μ_{R1} and μ_{R2} , for Rilem's model. The use of R-SFRC offers more benefits, especially at low x/d (or low rebar amounts) rather than at high x/d (or high rebar amounts). Furthermore, when SFRC is used together with steel reinforcement, the maximum amount of reinforcement for the section to avoid brittle failure (due to concrete crushing before rebar yielding) is reduced.

Flexural models for R-SFRC have been outlined at different strain states as given in Table 3.3. Using the analytical models derived in Section 3.3.3, bending moments and their corresponding curvatures are determined that can be used to derive a moment vs. curvature curve for a particular section. When using the analytical models derived in Section 3.3.3, the appropriate limiting strains must be considered if the resulting solution is to be accepted. For example, a moment value determined at ultimate tensile strain of concrete while the corresponding compression strain exceeds the ultimate compression strain may be rejected. However, if the ultimate tensile strain of SFRC is exceeded, the equivalent post-peak tensile strength appropriate at such strain may have to be used. When providing steel reinforcement to a section, all limiting strains should not be exceeded as outlined in Section 3.3.5. Strain-hardening steel bars may generate greater moment capacity in the beam section than elastic-perfect plastic steel bars and therefore, appropriate consideration should be taken during design.

CHAPTER 4.0 EXPERIMENTAL DESIGN AND METHODOLOGY

4.1 INTRODUCTION

This chapter outlines the design of the experimental program and procedures, and statistical methods. The general experimental strategy is explained under experimental design while experimental procedures and statistical methods used are discussed under methodology. Concrete grade C30/37 is used throughout the experiments.

4.2 EXPERIMENTAL DESIGN

Two models have been proposed in Chapter 3. These models are verified through a systematic experimental program that has been divided into two phases, namely a preliminary experimental phase and a model verification phase. Under the preliminary experimental phase, the material is characterised and the normalised post-peak tensile strength, μ_i , is determined for various fibre contents. Mixes whose normalised post-peak tensile strength surpasses critical flexural values are selected for the model verification phase (see Figure 4.1).

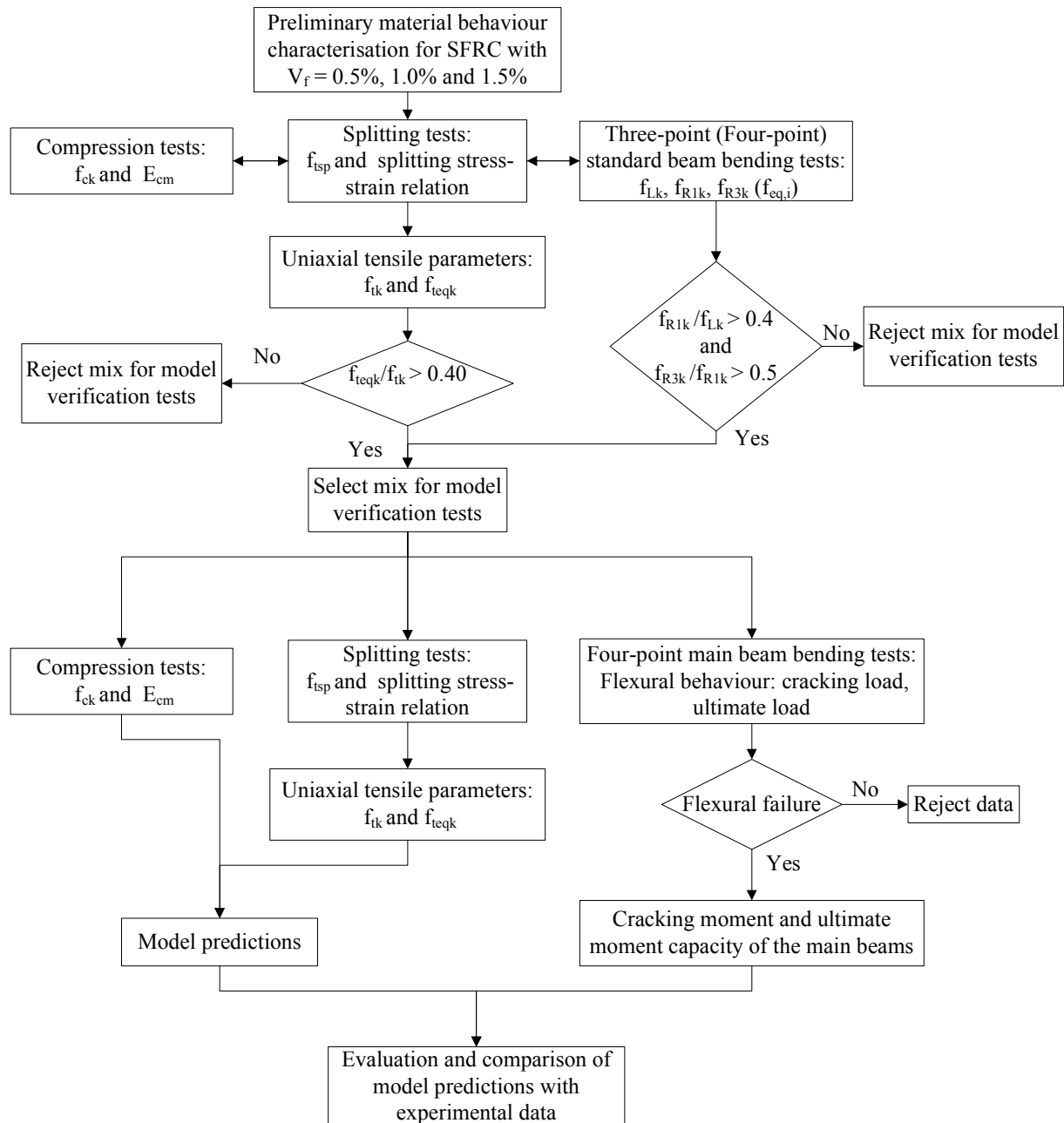


Figure 4.1: Flowchart for research methodology execution

4.2.1 PHASE I: PRELIMINARY EXPERIMENTAL PHASE

The main aim of the preliminary experimental phase is the selection of appropriate mix proportions for model verification through material characterisation of SFRC. The mix proportions for SFRC (in terms of volume of steel fibres) yielding a post-tensile to peak tensile ratio greater than the critical value ($\mu_i \geq 0.40$) for the drop-down model (Soranakom &

Mobasher, 2009) or meet the condition $\frac{f_{R1k}}{f_{Lk}} > 0.40$ and $\frac{f_{R3k}}{f_{R1k}} > 0.50$ for the Rilem tensile model (Vandewalle *et al*, 2002) are selected for Phase II. Only one compressive strength class of concrete is used with varying amounts of steel fibres, as shown in Table 4.1. Sample groups with steel fibre volumes of 0.5%, 1.0% and 1.5% are used. A control sample group is used with no steel fibres.

Table 4.1: Sample groups for preliminary material characterisation tests

Fibre volume	$V_f = 0.0\%$	$V_f = 0.5\%$	$V_f = 1.0\%$	$V_f = 1.5\%$
Sample group	PC0.0%	PC0.5%	PC1.0%	PC1.5%

These preliminary material characterisation tests formed part of a recent test series conducted by Zeranka (2010) in the same research group and the material mix designed used by Zeranka was adopted for this research. For the samples made by Zeranka, compression tests were conducted by the author, while four-point bending tests and splitting tests were conducted by Zeranka. Three-point bending by Jarratt (2011, in preparation) was also considered for the preliminary analysis as the same mix design was used. Table 4.2 shows characterisation tests that were conducted together with the sample size and specimen dimensions.

Table 4.2: Sample size and specimen dimensions for material characterisation tests (Phase I)

Test	Specimen size (mm)	Test sample group			
		PC0.0%	PC0.5%	PC1.0%	PC1.5%
Cube compressive test	100x100	3	3	3, 3*	3
Splitting test(indirect tension test)	100x100	-	-	3	3
4-Point bending test	100x100x500	-	-	3	3
3-Point bending test	150x150x750	-	-	6*	-

* Set of experiments conducted by Jarratt (2011 in preparation) using the same mix design

4.2.2 PHASE II: EXPERIMENTAL PROGRAM FOR MODEL VERIFICATION

The aim of this experimental program is to generate data used in the verification of the proposed models through four-point bending tests on main beams discussed later in Section 4.3.3.2. In order to reduce uncertainties, additional characterisation tests were conducted from samples made from the same batch of concrete used for the main beams.

A preliminary analysis of results from the Phase I experimental program determined the normalised post-peak tensile strength, μ_i , for each sample group with a specified fibre volume. As discussed in Section 4.3.4, the value of μ depends on how the drop-down model is derived from the experimental tensile stress-strain results. The samples that meet the engineering criteria outlined for Phase I will theoretically achieve a deflection-hardening behaviour. From a preliminary analysis of material characterisation data outlined in Appendix C, the normalised post-peak tensile strength for samples with steel fibre volumes of 1.0% and 1.5% exceeded the critical value and hence was selected for model verification experiments. It should be noted that

SFRC with fibre volumes as low as 0.75% could result in strain-hardening behaviour though not pronounced over a large strain range (Suwannakarn, 2009). Table 4.3 shows sample groups for four-point flexural tests while Table 4.4 shows sample size and specimen dimensions for various characterisation tests and verification tests performed for each sample group. Note that samples from each group were prepared from the same batch.

Table 4.3: Sample groups of the bending test program for Phase II

Amount of Rebar	Steel fibre volume		
	$V_f = 0\%$	$V_f = 1.0\%$	$V_f = 1.5\%$
No rebar	-	MB0-C1.0% (or C)	MB0-E1.5% (or E)
2Y10 ($\rho = 0.4475\%$)	MB2-A0.0% (or A), MB2-F0.0% (or B)	MB2-B1.0% (or B)	MB2-D1.5% (or D)

Table 4.4: Sample size and specimen dimensions for Phase II tests

Test	Specimen size- in mm	Test sample group					
		A	B	C	D	E	F
Cube compressive test	100x100	4	4	4	6	6	6
Splitting test	100x100	4	3	4	4	6	6
4-Point bending test	150x300x750	3	3	3	3	3	3

4.3 METHODOLOGY

The material mix proportions, casting and curing procedures for samples, testing methods and statistical methods employed are described in the sections that follow.

4.3.1 MATERIAL MIX DESIGN, CASTING AND CURING PROCEDURES

The mix proportions for concrete grade C30 are given in Table 4.5. Wiremix® ZL30/0.5 steel fibres were used for batches B to E. The properties of these steel fibres as provided by the supplier are given in Table 4.6, while photographs of these fibres together with other materials used in the mix are shown in Figure 4.2. In order to facilitate mixing and ensure reasonable consistency in fluidity and workability of SFRC, superplasticiser was added for mixes with steel fibre percentages of 1.0% and a volume of 1.5%. The water/binder ratio was kept constant to control compressive and tensile (first cracking) strength and stiffness (Van Zijl & Boshoff, 2006 and Van Zijl & Song, 2005).

Table 4.5: Concrete mix proportions used in the experimental program

Mix constituents	RD	Amount of mix constituents in kg/m ³			
		$V_f = 0\%$	$V_f = 0.5\%$	$V_f = 1.0\%$	$V_f = 1.5\%$
Surebuild cement (CEM II 32.5)	3.1	292	292	292	292
Fly Ash	2.8	89	89	89	89
Stone 13.2mm (40%)	2.7	406.3	403.3	400.1	396.5
Stone 6.7mm (60%)	2.7	609.5	605	600.1	594.8
Sand	2.65	815.7	809.7	803.2	796.1
Water	1	190	190	190	190
Chryso Fluid Premia SP 100	1.2	0	0	0.292	0.876
Chryso Optima SP 100	1.2	0	0	0.292	0.876
ZP 305 Dramix® and ZL30/0.5	7.85	0	39.25	78.5	117.75
Wiremix® steel fibres					
TOTAL		2403	2428	2453	2478
Sand/Total aggregate(volume)		0.45	0.45	0.45	0.45
Total aggregate/Total mix(volume)		0.684	0.679	0.674	0.668
Water/cement(volume)		0.65	0.65	0.65	0.65
water/binder (volume)		0.5	0.5	0.5	0.5



Table 4.6: Properties of Wiremix® ZL30/0.5

Fibre length (mm)	30
Fibre thickness (mm)	0.5
Young's modulus (GPa)	200
Fibre strength (MPa)	1050

All cubes and beams for material characterisation were cast in plastic moulds and metallic moulds respectively. After 24 hours' protection in the moulds, the samples were demoulded and put in a curing water container with water kept at a temperature of $23\pm 2^{\circ}\text{C}$. The samples were removed for testing from the curing container at the age of 28 days. The main beams were cast in wooden moulds. After 24 hours, the beams were demoulded and water-cured on the floor by covering them with wet blankets for the duration of the curing time. The samples were cured for a further 27 days, and tested at the age of 28 days.

4.3.3 TESTING METHODS

Standard testing methods were employed to characterise the material and also to determine the flexural capacity of main beams for model verification. Details of both the characterisation test and verification test are outlined below.

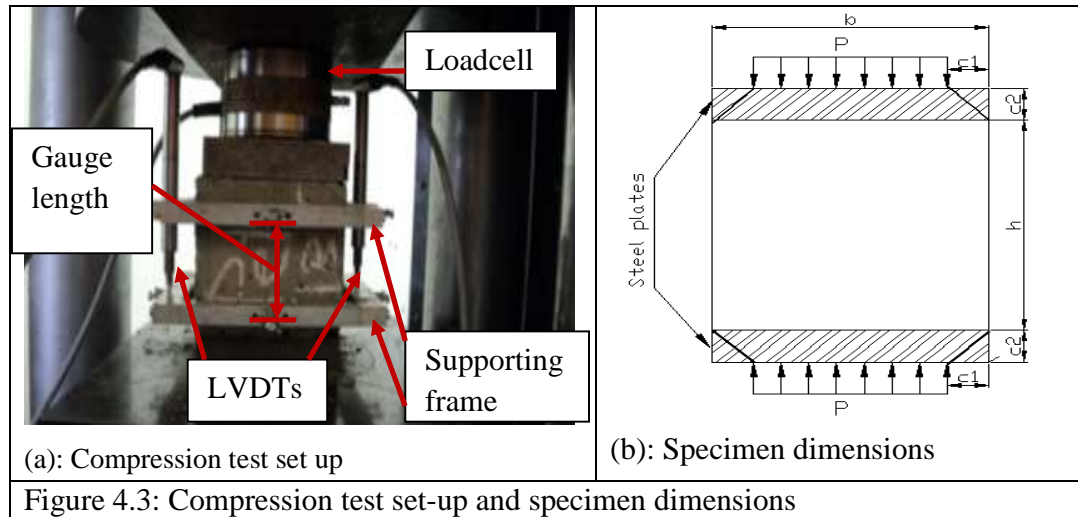
4.3.3.1 MATERIAL CHARACTERISATION TESTS

For the preliminary experimental program, three characterisation tests were conducted. These are a compression test, a splitting test for indirect tension and a four-point bending test for flexural characterisation. In addition to the four-point bending test, results from a three-point bending test (using the same mix but with only 1.0% steel fibres by volume) were considered.

Compression test

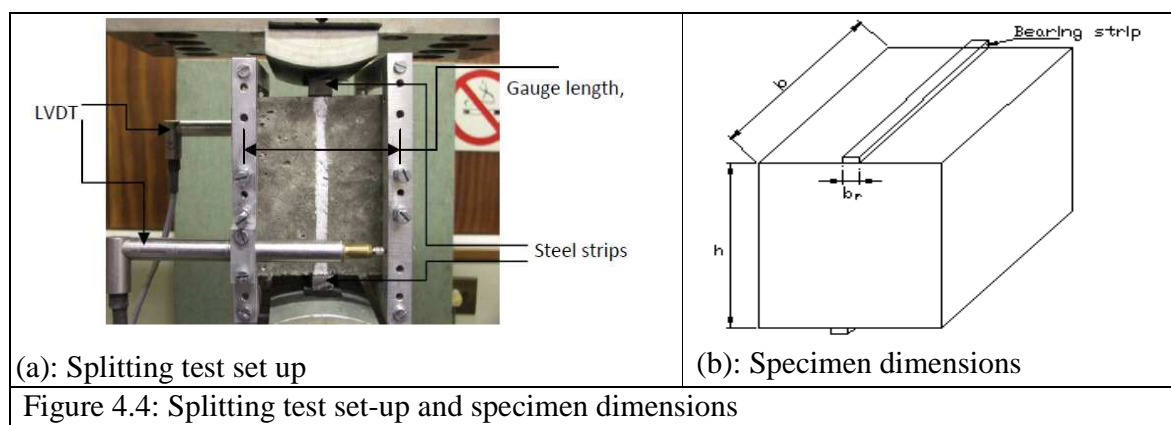
Compressive testing was conducted according to SANS 5863 (2006). A prismatic specimen, 100mm sides, was used for the test. Both the compressive strength and Young's modulus of elasticity were required for the specimen. The load was applied on the opposite sides of the specimen through steel plates so that an evenly distributed loading could be achieved for the whole cross section of the specimen as shown in Figure 4.1. At least two cycles of loading to 40% of the expected maximum load were applied until the loading and unloading curves coincided to eliminate stress nonlinearities. This test was performed using the Contest 2MN Materials Testing Machine. Since the force-displacement behaviour of the specimen was required, LVDTs and a load cell were used in order to record the displacements and loading in a Spider8 data capturing system. Two LVDTs were placed on opposite sides of the cube and were supported by an aluminium frame, as shown in Figure 4.3. The frames were positioned at a fixed distance and were tightly screwed to the cubes before testing started. It is acknowledged that prism/cylindrical specimens with height to width/diameter ratio of 2 are preferred to attain a uniform stress field over the mid-part of the specimen. However, only 150mm diameter x 300mm height cylindrical moulds were available at the time, which would require large volumes of material. 100mm x 200mm cylindrical moulds have been ordered for future work. In addition,

height restrictions in the Contest Materials Testing Machine (MTM) demands a new MTM with sufficient capacity, which is foreseen to be bought and installed in the next academic year.



Splitting test

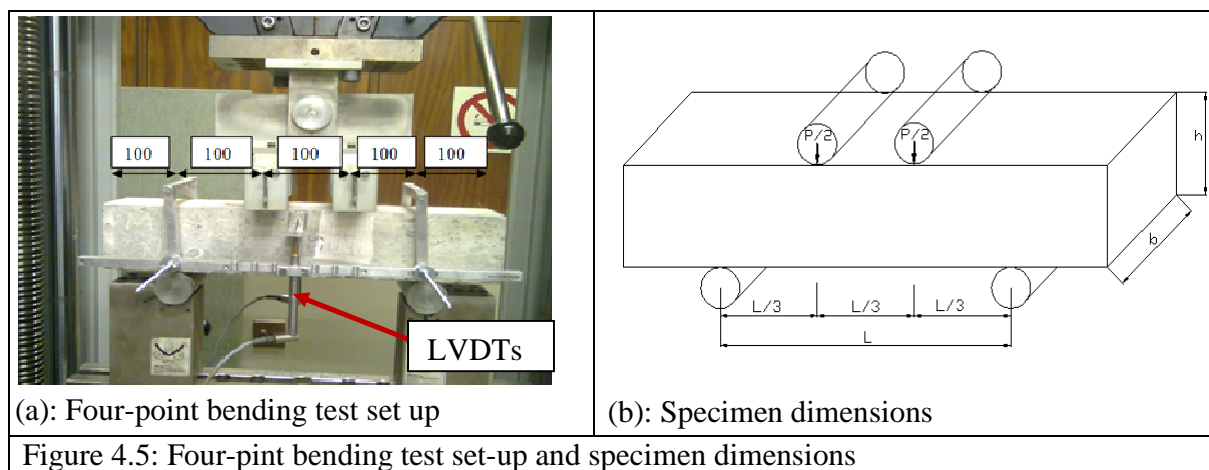
A prismatic specimen, with sides of 100mm, was used to conduct the splitting test according to SANS 6253 (2006) with a slight modification where steel bearing strips were used instead of hardwood strips. This was done as the hardwood strips were being severely damaged during testing. The load was applied along the opposite sides on the middle of the specimen as shown in Figure 4.4. In order to prevent multiple cracking and crushing at the points of load application, the loading was distributed through two bearing steel strips of 13mm in width. This test was performed using the Zwick Universal Material Testing Machine (UMTM). Since the post-peak characteristics were also required, the testing procedure was modified so that data for post-cracking behaviour was recorded. In order to measure the displacements, two LVDTs were placed on opposite sides of the cube and were supported by an aluminium frame as shown in Figure 4.4. The frames were positioned at a same distance apart and were tight-screwed to the cubes before testing started.



It is acknowledged that the large gauge length includes non-uniform deformation. Only once cracking starts, the deformation is dominated by the crack opening. Also, the tensile stress-crack width response is influenced by orthogonal compression, which may increase the pull-out resistance of the fibres, whereby the tensile response is overestimated by this test method. A direct tensile test is preferred, but its development was considered to fall beyond the scope of the current work. It should be pointed out that the use of LVDTs was restricted to samples that were expected to show ductile failure, i.e. those containing a sufficient amount of steel fibres. Therefore, LVDTs were not used for samples with 0.5% steel fibres or less.

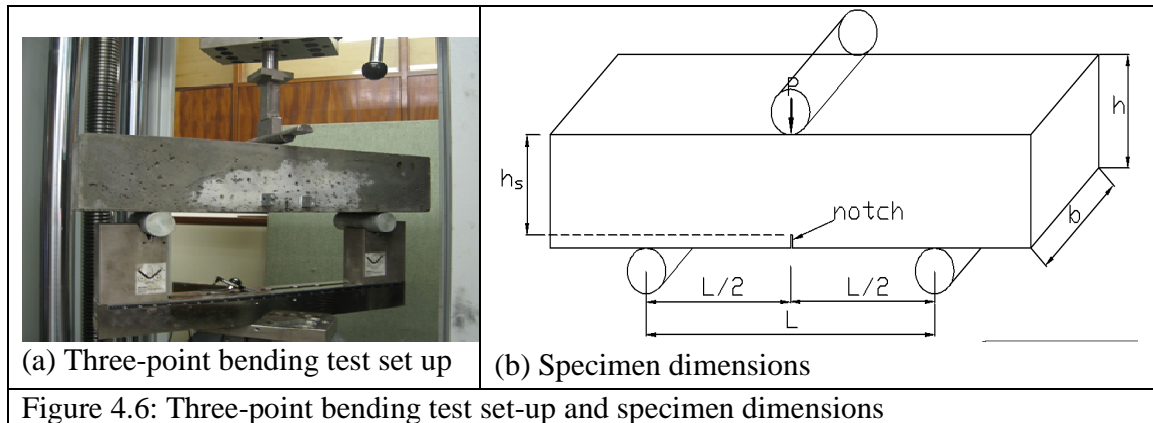
Four-point bending test

Four-point bending tests were performed on unnotched beams according to SANS 5864 (2006), with slight modifications, using the Zwick UMTM. Prismatic specimens, 100mm in width and 500mm in length were used for the test. Loads were applied at equal distances of 100mm apart through cylindrical bearings so that there was free movement of the specimen with respect to the loading (see Figure 4.5). In order to capture the load-displacement behaviour of the specimen, two LVDTs supported by aluminium frames were placed in the middle of the beams on opposite sides as shown in Figure 4.5(a).



Three-point bending test

Three-point bending tests were performed on notched beams according to SANS 5864 (2006) using the Zwick UMTM. Prismatic specimens, 150mm in width and 750mm in length with a 25mm deep notch were used for the test. Loads were applied at equal distances of 150mm apart through circular bearings so that there was free movement of the specimen with respect to the loading (see Figure 4.6). In order to capture the load-displacement behaviour of the specimen, two LVDTs, supported by aluminium frames, were placed in the middle of the beams on opposite sides (Figure 4.6(a) shows the three-point bending set-up before LVDTs were placed).

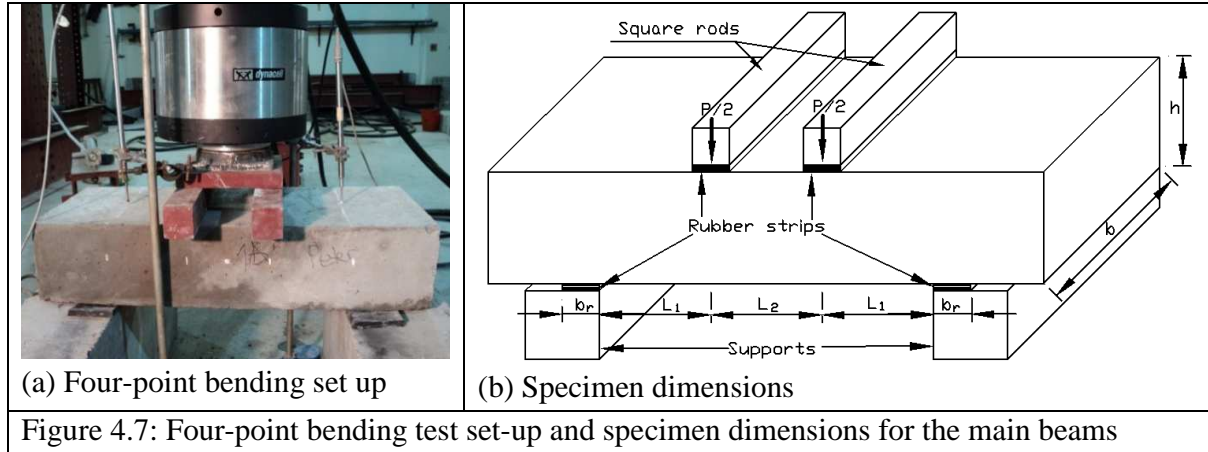


4.3.3.2 MODEL VERIFICATION-FLEXURAL TEST

The four-point flexural bending test according to SANS 5864 (2006), with slight deviation, was used to obtain data for model verification. This test was performed on the Instron Universal MTM (Instron). The test set-up and specimen dimensions are shown in Figure 4.7. Loads were applied at specified distances through square rods with 5mm rubber strips in between the rods and the specimen. Rubber strips were used in order to avoid concrete crushing and cracking at points of load application (see Figure 4.7). The Instron has its own load recording system and measures total displacement at the point of contact with the specimen. Therefore, in order to have effective displacement, LVDTs were placed at the support so that support displacements are measured separately, and recorded in a Spider8 data capturing device. This was necessary for displacement (due to compression of the rubber strips placed at the supports) to be known and removed from the total displacement measured by the Instron. This method does not acknowledge the displacements that occur in the loading frame and rubber strips placed at loading points. The distances between loading points and the width of an 8mm thick rubber bearing strips (as shown in Figure 4.7(b)) for different batches are illustrated in Table 4.7.

Table 4.7: Spacing for loading points and support bearing widths for the four-point bending test

Batch	Load spacing L_1 (mm)	Load spacing L_2 (mm)	Bearing width b_r (mm)
A, B, C	150	150	85
D, E and F	200	150	100



4.3.4 DATA ANALYSIS

Compression strength and Young's modulus

Ultimate compressive strength of concrete is determined from

$$f_{uc} = \frac{P_u}{A} \quad 4.1$$

where A is the cross sectional area of the specimen ($A = \text{breadth} \times \text{length}$) and P_u is the ultimate compressive force measured in the compressive crushing test.

Young's modulus is determined from the stress-strain curve recorded in the compression test as follows:

$$E_c = \frac{\sigma_1 - \sigma_0}{\epsilon_1 - \epsilon_0} \quad 4.2$$

where

σ_1 and ϵ_1 are stress and corresponding strain at 40% of the maximum compressive strength, ϵ_0 is a small compressive strain, taken as 0.00005 in this work and σ_0 is the corresponding stress.

Splitting tensile strength and post-peak equivalent tensile strength

Determination of ultimate splitting strength as given in the code (SANS 6253, 2006) is as follows:

$$f_{tsp} = \frac{2P_u}{\pi b h} \quad 4.3$$

where P_u is the maximum load applied on the splitting specimen and b and h are specimen dimensions as shown in Figure 4.4, which define the crack surface size.

Direct tensile strength can be derived from the splitting strength as outlined by Standards as follows (European Standards, 2004):

$$f_{tu} = 0.9 f_{tsp} \quad 4.4$$

Research performed by Rocco *et al* (2001) showed that the splitting strength of concrete using different specimen configurations but the same formula, is specimen-size dependent and also

depends on the size of the bearing strips. Therefore, the following formula, developed from an elastic theory approach for the cubical specimen, is considered for direct tensile strength derived from a splitting test:

$$f_{tu} = \frac{2P_u}{\pi b h} \left[\left((1 - \beta^2) \right)^{5/3} - 0.0115 \right] \quad 4.5$$

where $\beta = b_r / h$

with b_r the bearing strip width.

Equivalent post-peak tensile strength, f_{teq} , is determined from integration of a stress crack width curve over a prescribed limit of crack width, w_{lim} , and is given as follows:

$$f_{teq} = \frac{1}{w_{lim}} \int_0^{w_{lim}} f_t(w) dw \quad 4.6$$

Conversion of the splitting post-peak tensile stress, $f_{ts}(w)$, to direct tensile stress, $f_t(w)$, was based on the conversion of peak (elastic) tensile strengths for splitting and direct tension, i.e. use of 0.9 as a conversion factor. In this case two approaches are considered:

- working from the peak splitting strength and applying a factor of 0.9 to get equivalent maximum direct tensile strength, then subtracting a uniform value of $0.1f_{isp}$ from stress values beyond the peak strength (as shown in Figure 4.8); and
- adopting the formula by Rocco *et al* (2001) for the post-cracking region of splitting stress-displacement curve.

As outlined before, this expression (Equation 4.5) is based on the elastic theory approach and may not be the best approximation for the conversion of splitting stress to direct stress in the post-cracking region. In Chapter 2, an equation for tensile strength based on fracture mechanics as proposed by Rocco *et al* (2001) was outlined. This is considered to be a more efficient method of establishing post-cracking tensile stresses, but could not be used in this study as it requires prior knowledge of the toughness of the material. It should be noted that the approach outlined above is based on normal concrete which is quasi-brittle. It is widely known that the tensile behavior of FRC is similar to that of normal concrete up to initial crack formation beyond which fibre mechanisms in bridging the cracks are activated.

From Equation 4.6 it is apparent that the stress-crack width relationship is required for the determination of equivalent post-cracking strength. During the splitting test, only one crack is assumed to occur when concrete reaches cracking strength. Based on this assumption, a crack width at any post-cracking stress may be calculated as follows:

$$w = w_T - \epsilon_m L_g \quad 4.7$$

where w_T is the total displacement measured from the splitting test, ϵ_m is the strain at maximum splitting strength during the test and L_g is the gauge length.

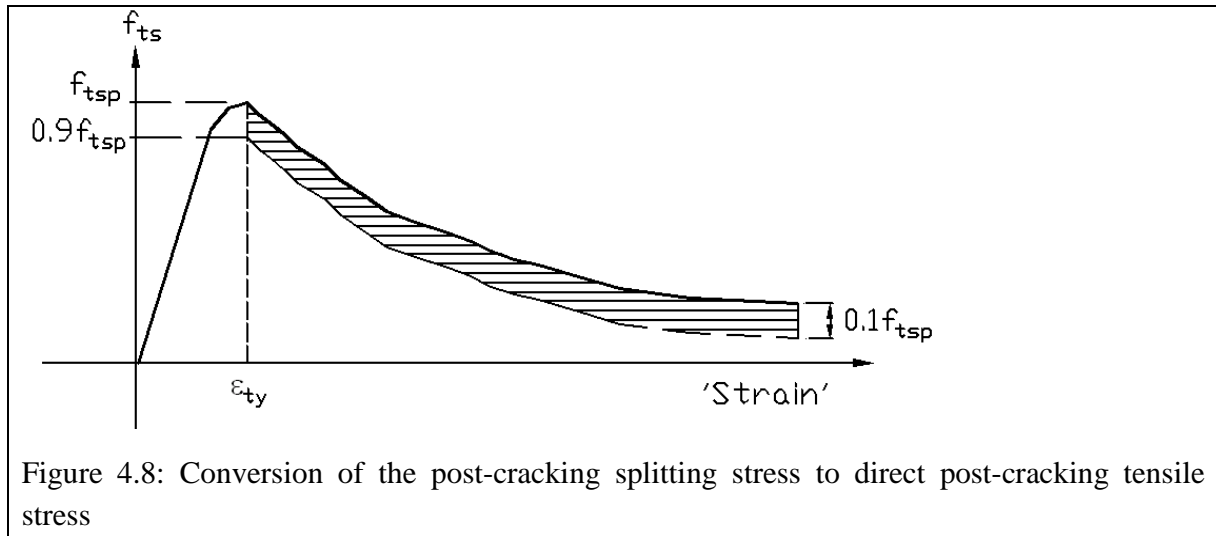


Figure 4.8: Conversion of the post-cracking splitting stress to direct post-cracking tensile stress

Flexural strength and equivalent post-peak flexural strengths from four-point bending

Expression of the flexural strength of the beams in terms of modulus of rupture assumes that the stress increases linearly from the neutral axis. Maximum flexural strength of the beam is calculated from the four-point bending results using the following formula (with notations as shown in Figure 4.5):

$$f_{fu} = \frac{3P_u L}{2bh^2} \quad 4.8.$$

Where P_u is the maximum point load recorded within the first 0.05mm deflection (see Figure 4.9).

Equivalent post-peak flexural strength

Post-peak flexural strength can be determined from either a force-displacement curve or force-CMOD curve if an un-notched beam or a notched beam is used respectively. For the execution of the four-point bending, only un-notched beams were used. Also, the post-peak flexural strength will be the equivalent flexural parameters defined by Vandewalle and Dupont (2003), with some modifications to the formula as a four-point bending has been used in this research.

Equivalent post-peak flexural strength at service state

The equivalent flexural strength is taken at a deflection of $\delta_L + 0.65\text{mm}$ in accordance with Rilem's recommendations and is given as

$$f_{eq,2} = \frac{T_s^f}{0.5} \frac{L}{bh^2} \quad 4.9$$

where T_s^f is the area under force-displacement curve taken up to a deflection of $\delta_L + 0.65\text{mm}$ b and h are section dimensions and δ_L is maximum elastic deflection.

Equivalent post-peak flexural strength at ultimate state

The equivalent flexural strength is taken at a deflection of $\delta_L + 2.65\text{mm}$ in accordance with Rilem's recommendations and is given as

$$f_{eq,3} = \frac{T_u^f}{2.5} \frac{L}{bh^2} \quad 4.10$$

where T_u^f is the area under force-displacement curve taken up to a deflection of $\delta_L + 2.65\text{mm}$ (see Figure 4.9c).

Flexural strength and residual flexural strengths from three-point bending

Determination of the flexural strength of a beam from a three-point bending test is similar to that of a four-point bending test in which the stress is assumed to increase linearly from the neutral axis. Maximum flexural strength of the beam is calculated as follows:

$$f_{fu} = \frac{3P_u L}{2bh_s^2} \quad 4.11$$

where P_u is the maximum point load recorded within the first 0.05mm deflection; and

b is the breadth of the beam and h_s is the distance from the tip of the notch to the top of the beam cross section (see Figure 4.4.6b).

Equivalent post-peak flexural strength

The equivalent post-peak flexural strength for a three-point bending of a notched beam is calculated as follows:

- at service state

The equivalent flexural strength is taken at a deflection of $\delta_L + 0.65\text{mm}$ in accordance with Rilem's recommendations and is given as

$$f_{eq,2} = \frac{3 T_s^f}{2 \cdot 0.5} \frac{L}{bh_s^2} \quad 4.12$$

where T_s^f is the area under force-displacement curve taken up to a deflection of $\delta_L + 0.65\text{mm}$ and b and h_s are section dimensions as earlier defined and δ_L is maximum elastic deflection.

-at ultimate state

The equivalent flexural strength is taken at a deflection of $\delta_L + 2.65\text{mm}$ in accordance with Rilem's recommendations and is given as

$$f_{eq,3} = \frac{3 T_u^f}{2 \cdot 2.5} \frac{L}{bh_s^2} \quad 4.13$$

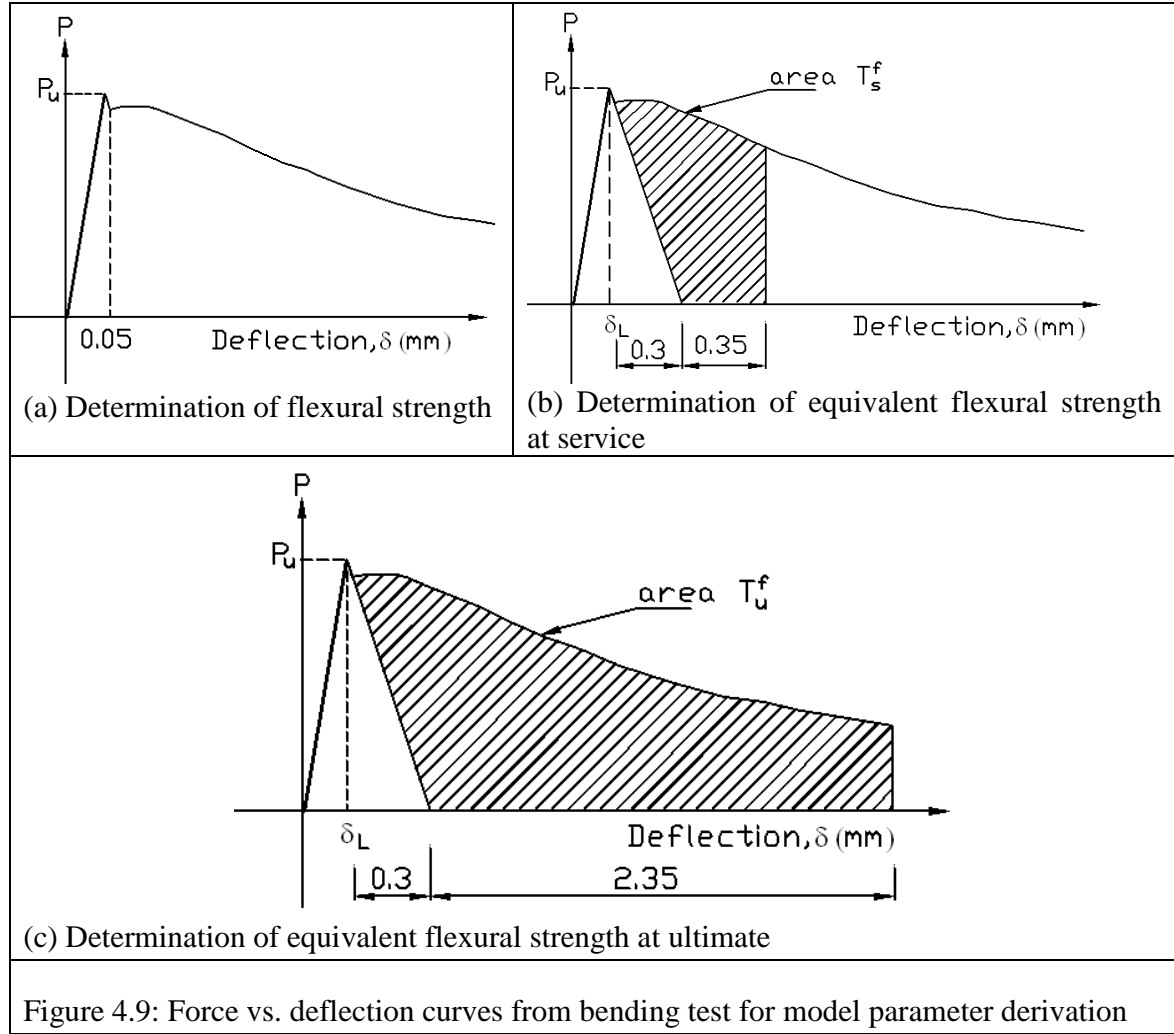
where T_u^f is the area under force-displacement curve taken up to a deflection of $\delta_L + 2.65\text{mm}$; and b and h_s are section dimensions as defined before and δ_L is maximum elastic deflection.

Residual flexural strengths

Residual strength is determined from the following expression:

$$f_{R,i} = \frac{3 F_{R,i} L}{2 bh_s^2} \quad 4.14$$

where $F_{R,i}$ is the load recorded at deflection $\delta_{R,i}$ or CMOD_i .



Moment for model verification: The four-point flexural test gives force-displacement data. This data can be used to determine either cracking moment or maximum moment of the beam section. The experimental cracking moment $M_{cr,exp}$ and maximum moment $M_{u,exp}$ of the beam are determined from Equations 4.15 and 4.16 respectively:

$$M_{cr,exp} = \frac{1}{2} P_{cr} (L_1 + \alpha_b b_r) \quad 4.15$$

$$M_{u,exp} = \frac{1}{2} P_u (L_1 + \alpha_b b_r) \quad 4.16$$

where

P_{cr} and P_u are the recorded cracking load and maximum load from the four-point bending test; L_1 is the distance from loading point to the nearest support as shown in Figure 4.7(b); and $\alpha_b = 0.3$, is the factor defining the position of the resultant reaction from interior face of support determined from a non linear Finite Element Analysis (see Appendix C).

4.3.5 VERIFICATION OF ANALYSIS MODELS

Assessment and determination of model parameters

The data that is used as input model parameters for the model verification exercise is subjected to both engineering assessment and statistical assessment. Only data that satisfies engineering criteria (engineering judgment and reasoning) for each type of parameter is used for statistical assessment before adopting the data for model verification. A flow chart outlining the assessment procedure is given in Figure 4.10.

After calculating the mean values and standard deviations for all models' parameters from different batches, one can verify the sample from a population as being normally distributed by applying the 'goodness-of-fit' test developed by *Kolmogorov-Smirnov*. However, due to limited sample sizes used in different batches, this test cannot be performed and the material strength parameters are assumed to follow the normal distribution. Measured values that clearly deviate from other values are found by freak test. In this case a value is deemed an outlier when it is more than twice the standard deviation away from the mean. To ensure that the different samples belong to a common population and may therefore be unified to an overall sample, a *t*-test was used - a statistical evaluation requiring several iterations (as illustrated in Figure 4.10). The characteristic parameters are derived from the overall mean and standard deviation according to EN 1990, based on the 5th percentile of the material strength (European standards, 2002). The following expression is used in determining the characteristic strength parameters:

$$X_c = X_m - K_n \sigma \quad 4.15$$

where X_c is characteristic strength parameter for the material;

X_m is sample mean;

K_n is fractile estimator and depends on the sample size and the required level of confidence (in this case 95% is used for characteristic strength parameters); and

σ is the sample standard deviation.

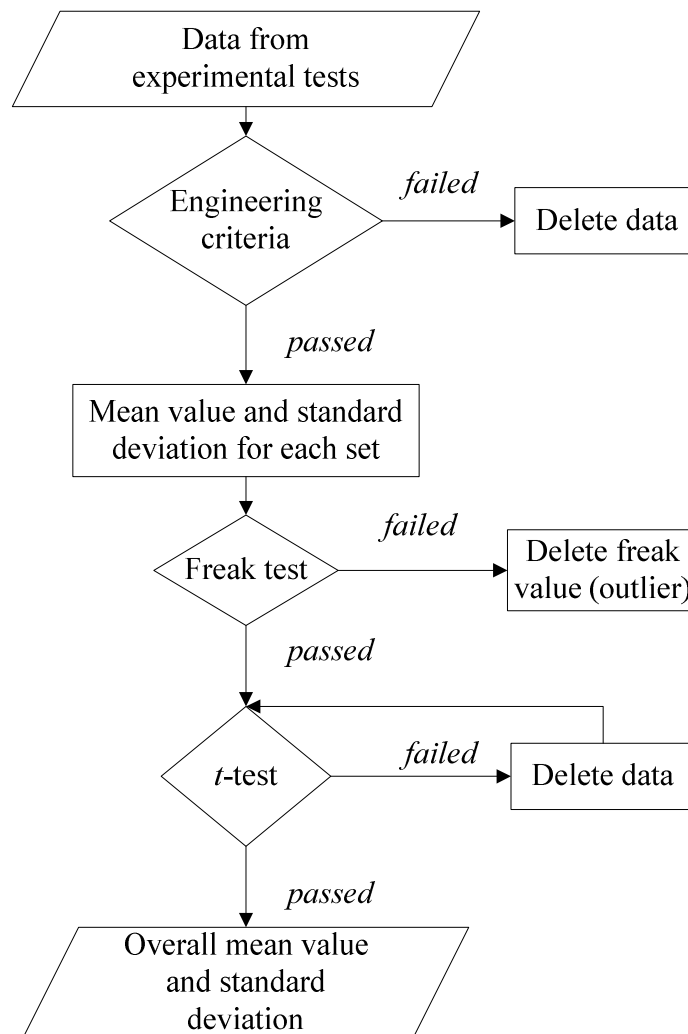


Figure 4.10: Flowchart for statistical evaluation procedure

Statistical assessment of model predictions and experimental results

In order for this step to be performed there must be a strong correlation between the model predictions and experimental results (see Section 2.7.1) and the model must accurately predict the outcome of the experiments. This step is important as it ensures that the bias and uncertainty inherent in the theoretical model are determined. Using the coefficient of variation and correlation factor (as outlined in Section 2.7.1), the accuracy of the proposed model will be assessed.

4.4 CHALLENGES AND LIMITATIONS

While wider grades of concrete would give a better indication of the performance of the models in predicting flexural capacity, only concrete grade C30/37 was used as the testing equipment did not have the capacity for testing concrete grades of C50/60 and greater. Furthermore, due to the limited capacity of the concrete mixer available, fewer samples were used in each batch. The

samples that meet statistical requirements as outlined in Section 6.2 were combined so that an overall sample size for each batch would be improved. Another limitation was the use of one size of steel fibres. According to the literature, aspect ratio affects the post-peak behaviour of SFRC (ACI Committee 544-4R-88, 1988).

Tensile properties used for model verification were derived from indirect testing (splitting test), as the equipment for direct tensile testing was not available at the time of experimental execution.

4.5 UNCERTAINTIES WITH EXPERIMENTAL DATA ACQUISITION

Certain uncertainties were noted during the data acquisition phase, as set out below.

A slight variation in curing conditions. Main beams were cured on the floor by covering them with blankets which were constantly kept wet for the entire curing time, while characterisation samples were cured in a container with water at a controlled temperature. Slight fluctuations of the room temperature to which the main beams were subjected might have occurred as compared to the controlled temperature in the curing of the characterisation samples.

The calibration of equipment. The contest machine used for compressive testing allows the user to provide a parallel load measurement system apart from the in-built load recording system. It was noted that the reading of these two systems differed. Where only one reading was measured, appropriate reference is made.

Data uncertainties occurred. The conversion of splitting strength parameters to direct tensile strength parameters created some uncertainties within the experimental data. While a factor of 0.9 is widely recommended in the code for conversion of splitting strength to direct strength, there is no literature on the conversion of post peak splitting parameters to direct post peak tensile parameters.

4.6 CONCLUSION

In this chapter, both material characterisation tests and model verification tests were outlined. It is apparent that while the tensile strength parameters are derived from a splitting test, it is unknown whether the conversion of splitting test to direct tensile parameters will follow the approach used in normal concrete. This is a source of uncertainty imbedded in the experimental data used for tensile strength parameters.

Another point of importance is the fact that cubes are used in the determination of the compressive strength. In order to get equivalent cylinder strengths from cube strengths, a conversion factor of 0.8 is used as is the case for normal concrete (BS EN1992-1-1:2004). This has been adopted as literature reports that the compressive behaviour of SFRC with small amounts of steel fibres does not significantly change and hence the conversions used in normal concrete may apply for these SFRC samples (Di Prisco *et al*, 2009).

CHAPTER 5.0 EXPERIMENTAL RESULTS

5.1 INTRODUCTION

This chapter provides all the results obtained from various experiments performed in this research, conducted in two phases. Phase I is intended for evaluation towards the understanding of the material behaviour through material characterisation processes. Using standard specimens, material characterisation experiments for concrete involved indirect tensile tests (splitting tests), four-point bending tests and compression tests. The results from this phase are used to select the appropriate concrete mix (fibre content) for eventual model verification, which is the purpose of Phase II. Most of these preliminary experiments were conducted in conjunction with Zeranka (2010). The stress-strain behaviour of reinforcing bars was also determined through direct tensile tests. A four-point bending test is used to determine the flexural capacity of large beams. Since the input parameters for the model are determined from characterisation experiments, it was decided that in addition to the material characterisation results obtained from Phase I, material characterisation in Phase II would involve only compression and splitting tests for samples. These were made from the same batch from which the main beams are produced, with the same mix proportion as in Phase I. This would reduce uncertainties within the input data for the proposed models.

5.2 MATERIAL CHARACTERISATION

As outlined in Chapter 4, three tests were conducted for preliminary material characterisation (whose samples are denoted by PC followed by percentage of steel fibres used). These are compression tests, splitting tests and flexural tests. The compression tests were conducted using a 100mm cube specimen in order to determine the compression strength and Young's modulus of concrete. Both splitting tests on a 100mm cube specimen and the flexural tests on 100 x 100 x 500 mm standard beams were used as indirect methods for the determination of the tensile properties of concrete. Using data obtained from splitting tests, another set of Young's modulus was determined to compare with the one established from compression data. These indirect tests were used to determine tensile strength (axial and flexural) and post-cracking tensile strengths. In model verification characterisation tests (whose samples are denoted by MC followed by batch identification and steel fibre percentage used), only compression tests and splitting tests were conducted. A slump test was conducted for each mix to assess the workability of the concrete mix since the flowability of fresh SFRC has a great influence on fibre distribution and potential segregation. Photos showing cross sections of some cubes after splitting tests, given in Appendix C, display aggregate and fibre distribution and, therefore, extent of segregation. Table 5.1 summarises the slump test results, showing that mixes MC-C1.0% have significantly higher slump values, which could be due to new aggregate stock. An error in the weighing of ingredients is ruled out, as Jarratt (2011, in preparation) experienced similar problems in his work, independent from the author of this research. In later sections, the mechanical properties of these mixes are reported and their further use in model verification evaluated.

Table 5.1: Slump of concrete sample groups

Sample name	Slump (mm)
PC0.0%	70
PC0.5%	65
PC1.0%	60
PC1.5%	60
MC-A0.0%	80
MC-B1.0%	40
MC-C1.0%	120
MC-D1.5%	40
MC-E1.5%	85
MC-F0.0%	65

5.2.1 CONCRETE COMPRESSIVE BEHAVIOUR

Four categories of SFRC representing different steel fibre contents of 0%, 0.5%, 1.0% and 1.5% were tested. Figure 5.1 shows the results of all the compression tests in terms of stress vs. strain. From these results, compression model parameters, the compression strength and the Young's modulus were determined using expressions given in Section 4.3.4, and the mean values and their standard deviations are given in Table 5.2. Complete data showing the compression strength and the Young's modulus for each sample is given in Appendix B. Samples of normal concrete (without steel fibres) show greater consistency in their compressive strength and Young's modulus. Generally, there is an increase in compressive strength with increasing amount of steel fibres. The Young's modulus does not significantly change with increase in steel fibres. Samples with steel fibres show some consistency within the group for both compressive strengths and Young's modulus, with the exception of samples belonging to MC-C1.0%. It should be noted that MC-C1.0% is the batch that displayed very high slump, potentially influencing constituents' segregation and overall mechanical properties of the concrete.

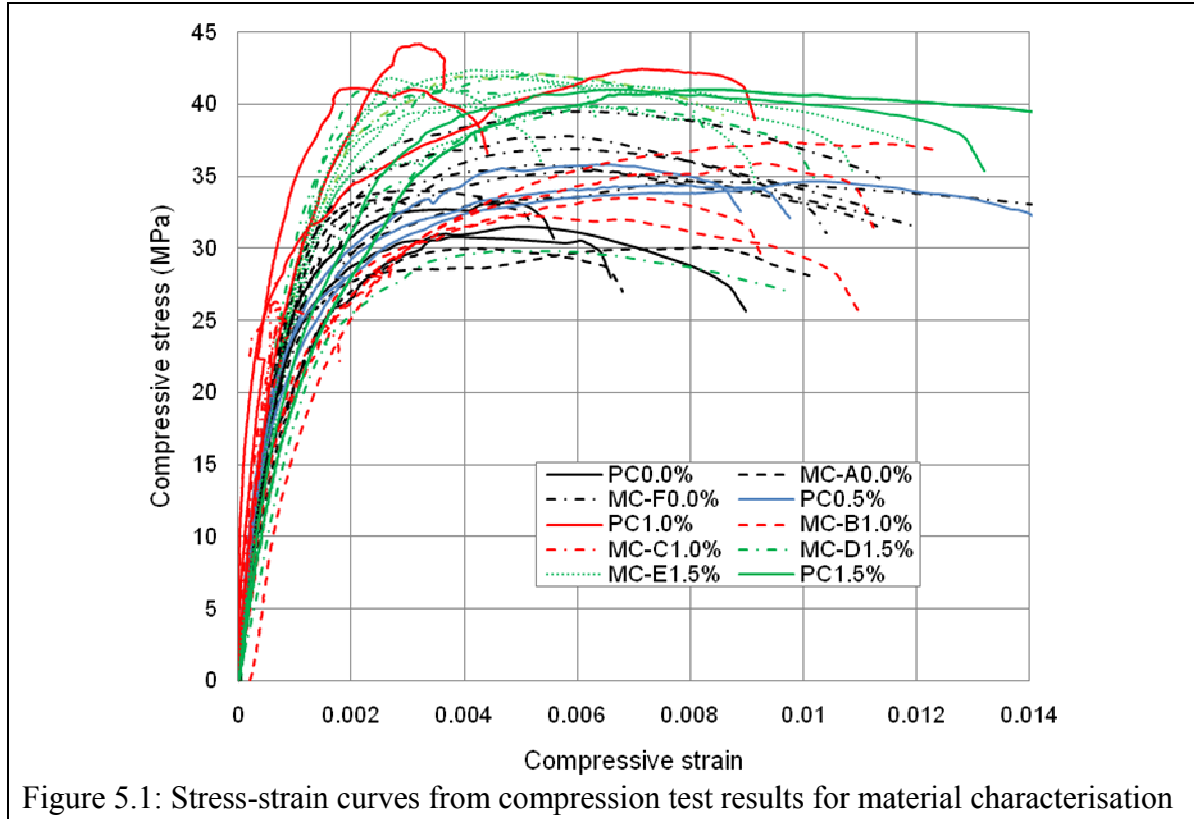


Table 5. 2: Compression strength and Young's modulus from material characterisation tests

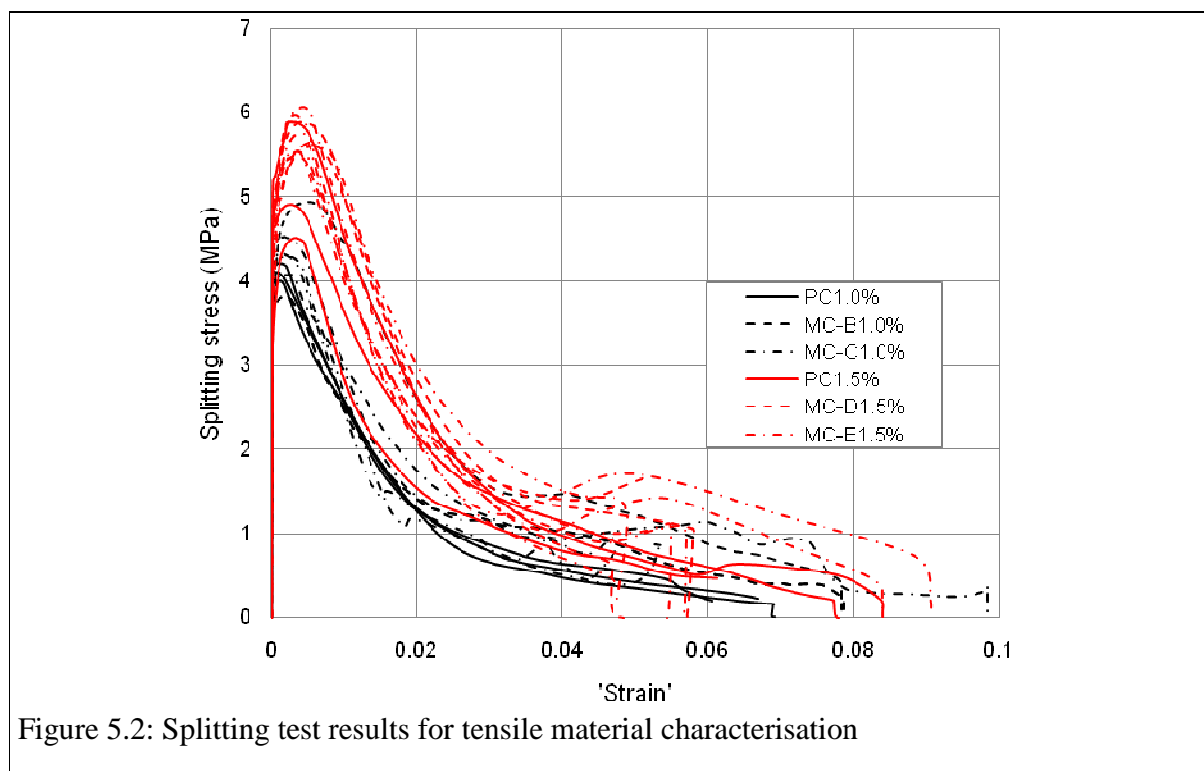
Sample name	Maximum cube strength (MPa)			Young's modulus (GPa) from compression data		Young's modulus (GPa) from tensile data		
	<i>n</i>	f_{cm} (mean)	CoV	E_{cm}	CoV	<i>n</i>	E_{cm}	CoV
PC0.0%	3	31.84	0.039	32.79	0.110	-	NA	-
MC-A0.0%	4	31.87	0.068	31.94	0.117	-	NA	-
MC-F0.0%	6	36.61	0.050	34.82	0.099	-	NA	-
PC0.5%	3	34.93	0.022	36.48	0.162	-	NA	-
PC1.0%	3	42.58	0.036	40.70	0.157	3	34.58	0.192
MC-B1.0%	4	34.68	0.068	31.68	0.053	2	31.5	0.121
MC-C1.0%	3	25.60	0.032	42.54	0.063	3	36.7	0.101
PC1.5%	2	42.18	0.037	32.23	0.072	3	35.15	0.169
MC-D1.5%	5	41.20	0.022	33.75	0.071	3	35.67	0.104
MC-E1.5%	6	41.20	0.027	31.89	0.049	5	32.63	0.145

5.2.2 CONCRETE TENSILE BEHAVIOUR

Results from splitting tests are shown in Figure 5.2. The splitting behaviour for samples with steel fibre content ranging from 0%, 0.5%, 1.0% and 1.5% are reported. The results include splitting results from the preliminary characteristic tests (denoted by PC) and the model-verification characterisation tests (denoted by MC). In order to prevent damage to LVDTs during specimen failure, displacements for samples with 0% and 0.5% steel fibres were not taken.

From the splitting test results, splitting strengths and direct tensile parameters were determined as described in Section 4.3.4. Mean values of the splitting strengths and direct tensile strengths determined, using both codified definition and the formula derived from an elastic approach by Rocco *et al* (2001), are given in Table 5.3. The two approaches outlined in Section 4.3.4 for conversion of post-cracking splitting stress to direct tensile stress are used to obtain post-cracking tensile stresses. The total post-cracking 'strain' is converted to crack width as outlined in Chapter 4. Results for direct tensile behaviour as calculated using the method by Rocco *et al* (2001) are shown in Figure 5.3.

As outlined in Section 4.3.4, the toughness parameter from which the equivalent post-cracking tensile strength is evaluated, depends on the limiting crack width. In this research the limiting crack width is taken at an ultimate tensile strain of 25‰. Table 5.4 outlines the toughness parameters at this limiting strain with the corresponding crack widths determined from Equation 4.7 for all samples with 1.0% and 1.5% steel fibres. A typical variation of the toughness/direct stresses vs. crack width is shown in Figure 5.4.



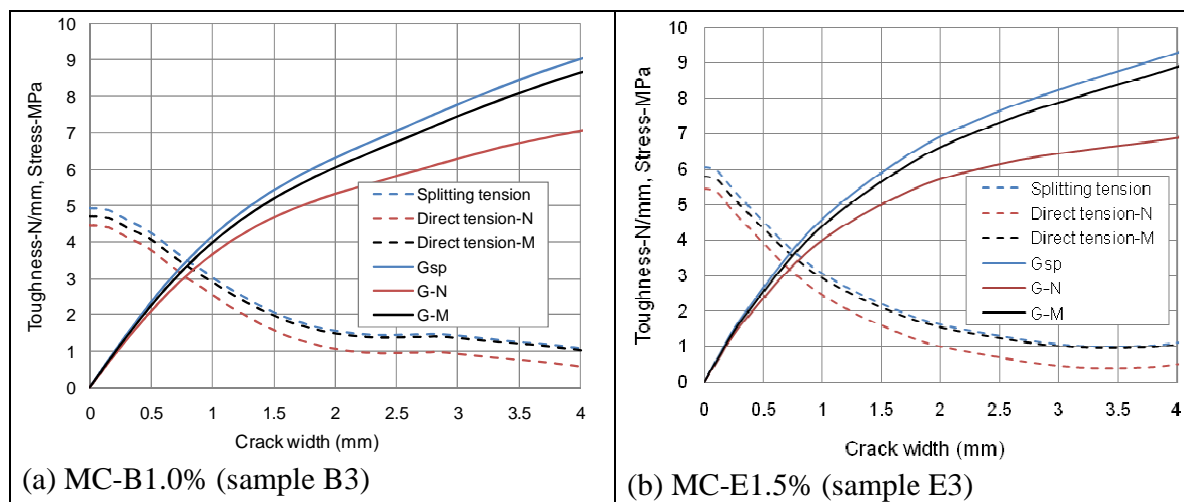
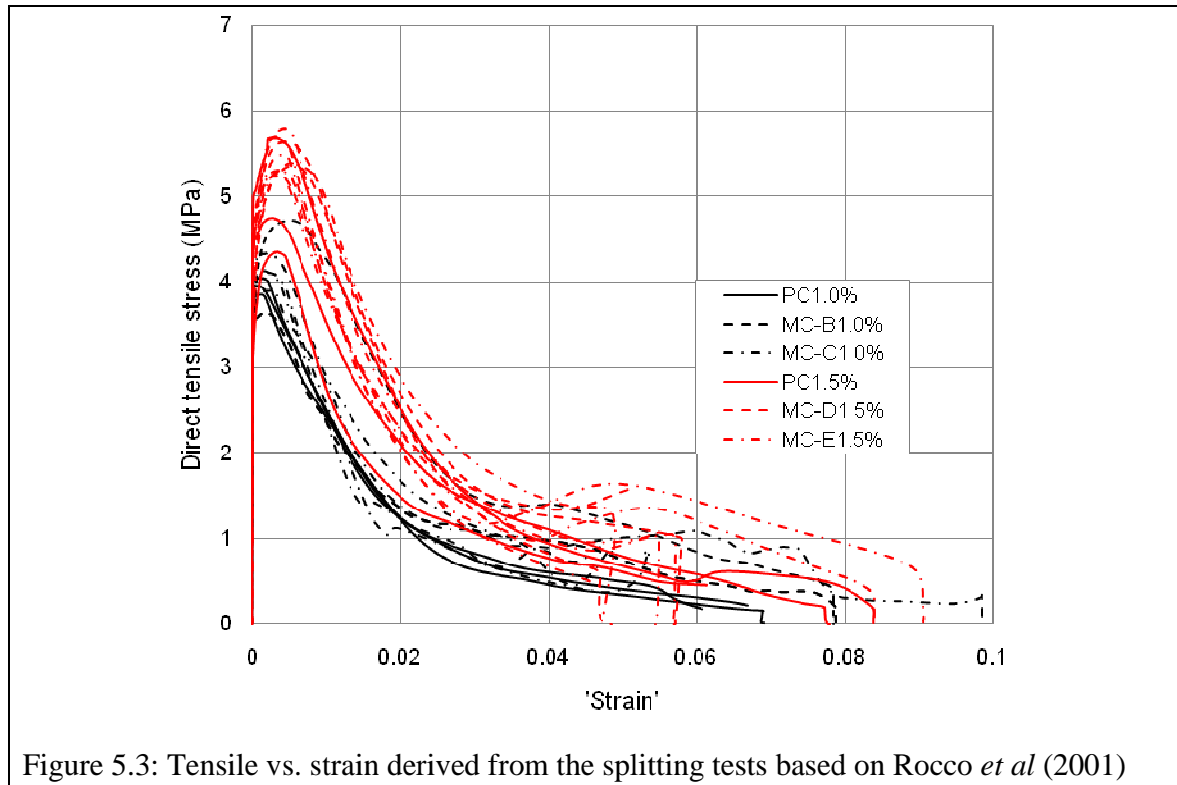


Figure 5.4: Typical post-cracking tensile stress vs. crack width curves superimposed on toughness (denoted G, for fracture energy) vs. crack width curves

Table 5.3: Tension strength parameters from the splitting tests

Sample name	<i>n</i>	Splitting strength (MPa)		Tensile strength, Code definition (MPa)		Tensile strength, Rocco <i>et al</i> (2001) (MPa)	
		f_{isp} (mean)	CoV	f_t (mean)	CoV	f_t (mean)	CoV
PC0.0%	3	3.80	0.030	3.42	0.030	3.66	0.030
MC-A0.0%	4	3.72	0.083	3.35	0.083	3.56	0.083
MC-F0.0%	6	3.80	0.084	3.42	0.084	3.64	0.084
PC0.5%	3	3.77	0.075	3.39	0.075	3.63	0.075
PC1.0%	3	4.10	0.025	3.69	0.025	3.96	0.025
MC-B1.0%	2	4.37	0.183	3.93	0.183	4.18	0.183
MC-C1.0%	4	4.31	0.043	3.88	0.043	4.12	0.043
PC1.5%	3	5.08	0.143	4.57	0.143	4.90	0.143
MC-D1.5%	3	5.66	0.038	5.09	0.038	5.41	0.037
MC-E1.5%	6	5.74	0.038	5.17	0.038	5.49	0.039

Table 5.4: Toughness and ultimate crack widths at ultimate tensile strain of 25‰ for SFRC

Sample name	<i>n</i>	Crack width, w_{lim} (mm) (mean value)	Toughness, Code definition (N/mm)		Toughness, Rocco <i>et al</i> (2001) (N/mm)	
			G (mean)	CoV	G (mean)	CoV
PC1.0%	3	1.993	3.76	0.046	4.40	0.045
MC-B1.0%	2	1.990	4.12	0.240	4.65	0.215
MC-C1.0%	4	1.993	3.71	0.151	4.32	0.133
PC1.5%	3	1.989	4.87	0.253	5.58	0.236
MC-D1.5%	3	1.987	5.28	0.057	5.94	0.048
MC-E1.5%	6	1.987	4.99	0.049	5.69	0.041

5.2.3 CONCRETE FLEXURAL BEHAVIOUR

Flexural tests for material characterisation were performed on the Phase I samples only. Four-point bending tests on unnotched 100 x 100 x 500 mm standard beams were conducted to determine the flexural response of SFRC. Four categories representing different amounts of steel fibres by volume 0%, 0.5%, 1.0% and 1.5% were tested with each category consisting of three samples. In order to avoid damage of the LVDTs due to abrupt failure of beams without steel fibres, the tests were stopped just after reaching ultimate flexural strength. Figure 5.5(a) shows the force vs. mid span deflection for the four-point bending tests. Model parameters were determined from the four-point bending tests as taken at prescribed mid-span displacements of 0.05mm, 0.46mm, 1.31mm, 2.15mm and 3.00mm and their mean values and standard deviations are reported in Table 5.5. It is clear from the Figure 5.5 that concrete with 1.0% and 1.5% steel fibres show some deflection-hardening behaviour, hence selected for the model verification.

In addition to this test, a three-point bending test performed by Jarratt (2011, in preparation) is reported for comparison purposes, where a similar mix proportion as in this research (1.0% steel fibres) was applied. Jarratt used 150 x 150 x 750 mm standard beams with a 25mm notch at the

mid-span to initiate cracking. Both deflection and CMOD were measured (see Figures 5.5(b) and 5.5(c)). From the three-point bending tests, values of limit of proportionality (LOP), residual forces at $CMOD_1$ and $CMOD_3$, as recommended by Rilem (Vandewalle *et al*, 2002), were determined and are displayed in Table 5.6.

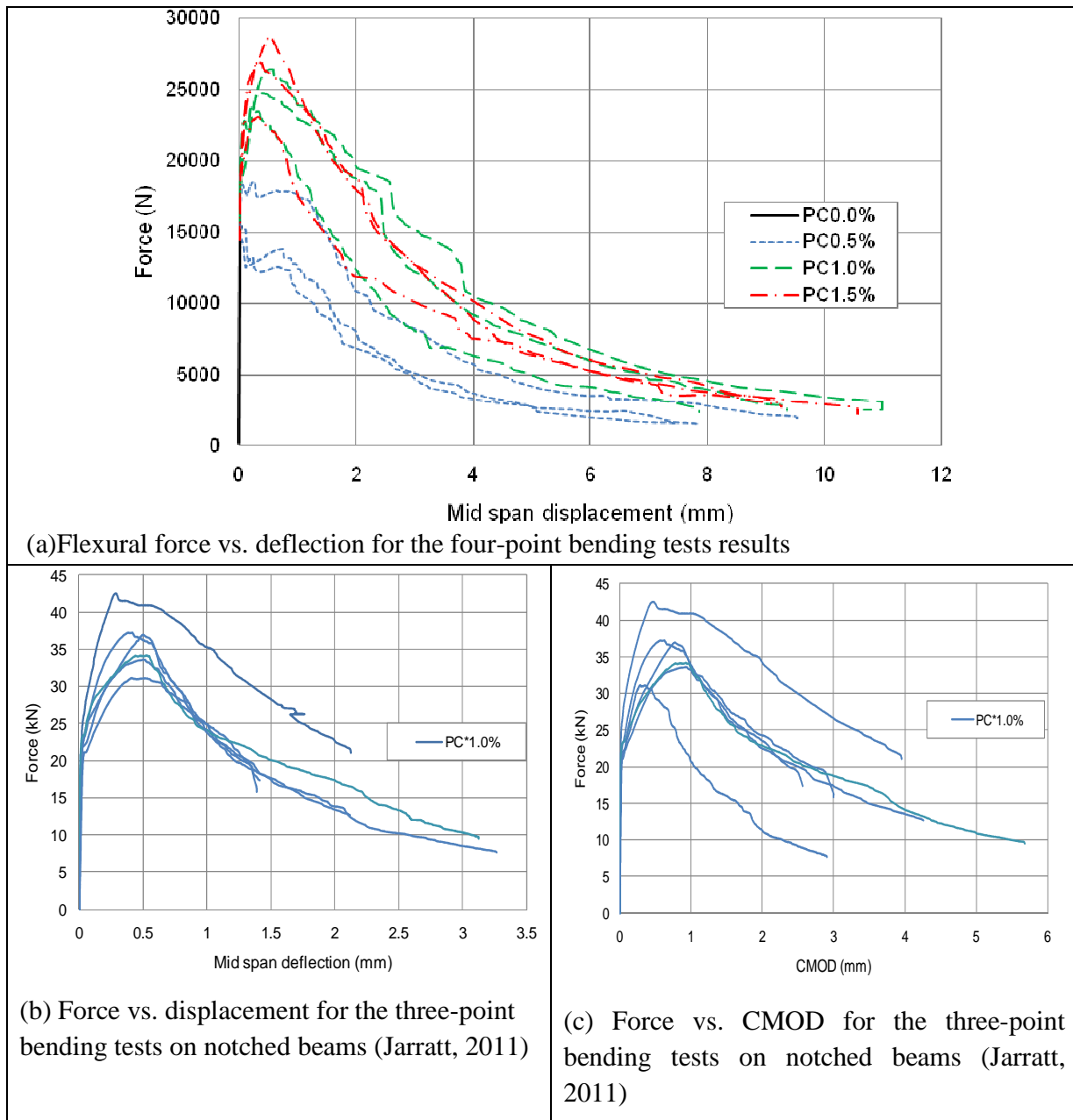


Figure 5.5: Flexural test results

Flexural Modelling of Steel Fibre-Reinforced Concrete With and Without Steel Bars

Table 5.5: Four-point flexural characterisation data for varying volumes of steel fibres

Displace. δ (mm)	PC0.0%		PC0.5%		PC1.0%		PC1.5%	
	P-kN (mean)	Std dev	P-kN (mean)	Std dev	P-kN (mean)	Std dev	P-kN (mean)	Std dev
0.05	15.852	0.660	15.94	1.795	19.797	1.199	19.592	0.566
0.46	15.849	0.670	14.415	2.827	24.536	1.795	25.705	2.898
1.31	-	-	12.598	3.304	20.671	3.318	20.256	3.849
2.15	-	-	8.169	2.131	16.52	4.2	15.316	3.046
3.00	-	-	6.04	1.895	11.854	3.548	11.885	1.526

Table 5.6: Three-point flexural characterisation data for SFRC with 1.0% steel fibres

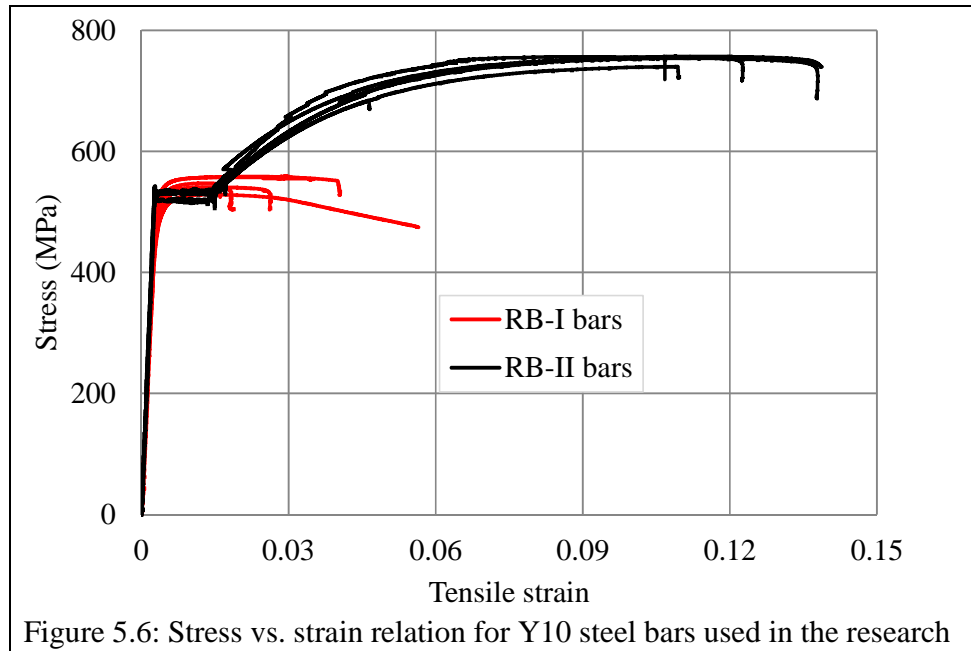
Sample No	LOP		CMOD ₁ (0.5mm)		CMOD ₃ (2.5mm)	
	P(kN)	f_L (N/mm ²)	P (kN)	f_{R1} (N/mm ²)	P (kN)	f_{R3} (N/mm ²)
1	28.55	9.14	42.27	13.53	30	9.6
2	21.93	7.02	31.35	10.03	21	6.72
3	22.167	7.09	33.13	10.60	19.27	6.17
4	23.6	7.55	36.85	11.79	20.01	6.40
5	23.41	7.49	31.58	10.11	20.5	6.56
6	21.13	6.76	29.64	9.48	19	6.08
Mean	23.46	7.51	34.14	10.92	21.63	6.92
Std Dev.	2.66	0.85	4.67	1.49	4.17	1.33
COV	0.1134	0.1134	0.1368	0.1368	0.1927	0.1927

5.2.4 TENSILE RESPONSE OF REINFORCING BARS

A direct tensile test for reinforcing bars was performed employing an HBM DD1 extensometer for deformation measurement. A gauge length of 50mm was used in the tests. Two sets of batches classified as reinforcing bar –type I (RB-I) and reinforcing bar type II (RB-II) were identified based on visual properties of the steel bars. Data from the direct tensile experiment was used to determine the yielding stresses and strains, as well as the post-yielding behaviour of the steel bars used in the model verification experiments. Figure 5.6 shows the results from the tensile test and Table 5.7 gives the tensile yield strengths and strains for both reinforcement types and the ultimate strengths and strains for RB-II reinforcement. Two distinct behaviours are clear. Firstly, RB-I reinforcement has elastic behaviour up to an average yield strength of 545.50MPa, followed by a perfect plastic behaviour. On the other hand RB-II reinforcement has elastic behaviour up to an average yield strength of 535.74MPa, followed by strain-hardening behaviour and displaying greater ductility than RB-I reinforcement.

Table 5.7: Tensile parameters for Y10 steel reinforcement

Sample name	Yield strength (MPa)		Yield strain		Ultimate strength (MPa)		Ultimate strain	
	f_{sy} (mean)	CoV	ϵ_{sy} (mean)	CoV	f_u (mean)	CoV	ϵ_u (mean)	CoV
RB-I	545.50	0.021	0.0027	0.021	NA	NA	NA	NA
RB-II	535.74	0.016	0.0027	0.024	752.22	0.009	0.1054	0.107



5.3 MODEL VERIFICATION FLEXURAL TEST RESULTS

Flexural tests for the model verification were conducted on main beams (denoted by MB followed by number of Y10 steel bars, batch name and volume of steel fibres used). As outlined in Section 5.2, the model parameters relevant for verification purposes were derived from characterisation experiments conducted on samples made from the same batches as the main beams. The amount of steel fibres were 0%, 1.0% and 1.5%, while the numbers of steel reinforcement were 0 and 2Y10, with 85mm c/c R8 shear links provided in all beams with steel bars. All flexural tests conducted for the model verification are outlined in Table 5.8. Note that samples without steel bars were used as control experiments. Two sets of control experiments were conducted at different times as outlined under “Methodology” in Chapter 4.

Table 5.8: Model verification flexural tests sample groups

Sample name	<i>n</i>	Sample description
MB2-A0.0%	3	2Y10 RB-II steel bars, no steel fibres- control experiment
MB2-F0.0%	3	2Y10 RB-II steel bars, no steel fibres- control experiment
MB0-C1.0%	3	1.0% Wiremix® ZL30/0.5 steel fibre, no steel bars
MB0-E1.5%	3	1.0% Wiremix® ZL30/0.5 steel fibre, no steel bars
MB2-B1.0%	3	2Y10 RB-II steel bars, 1.0% Wiremix® ZL30/0.5 steel fibre
MB2-D1.5%	3	2Y10 RB-II steel bars, 1.5% Wiremix® ZL30/0.5 steel fibre

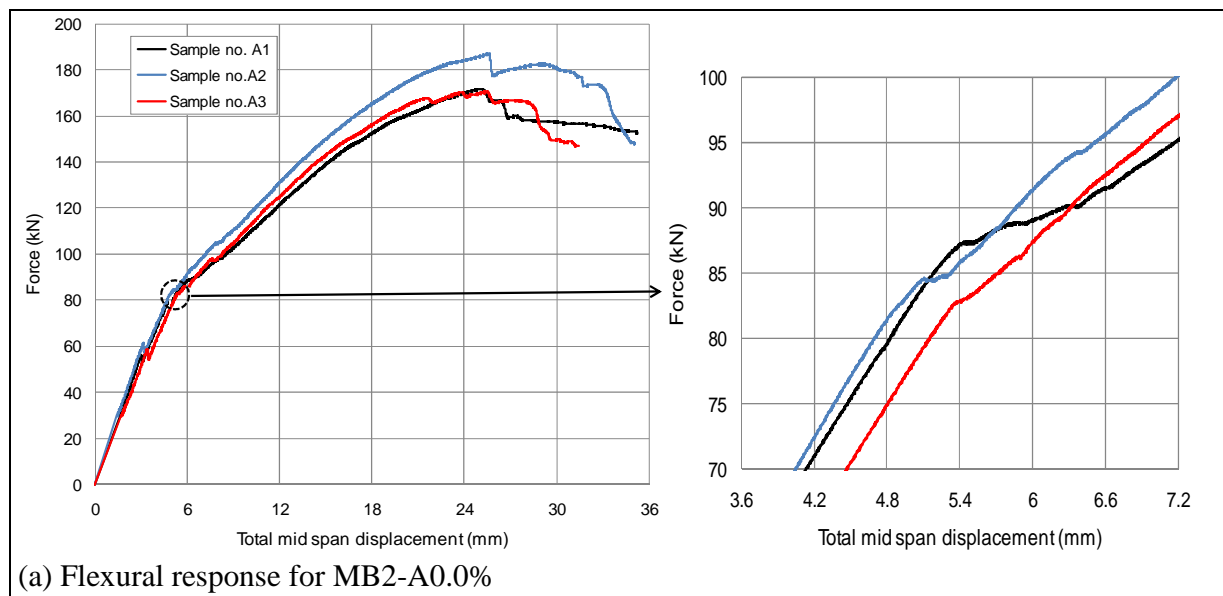
5.3.1 FLEXURAL RESPONSE FOR MB2-A0.0% AND MB2-F0.0%

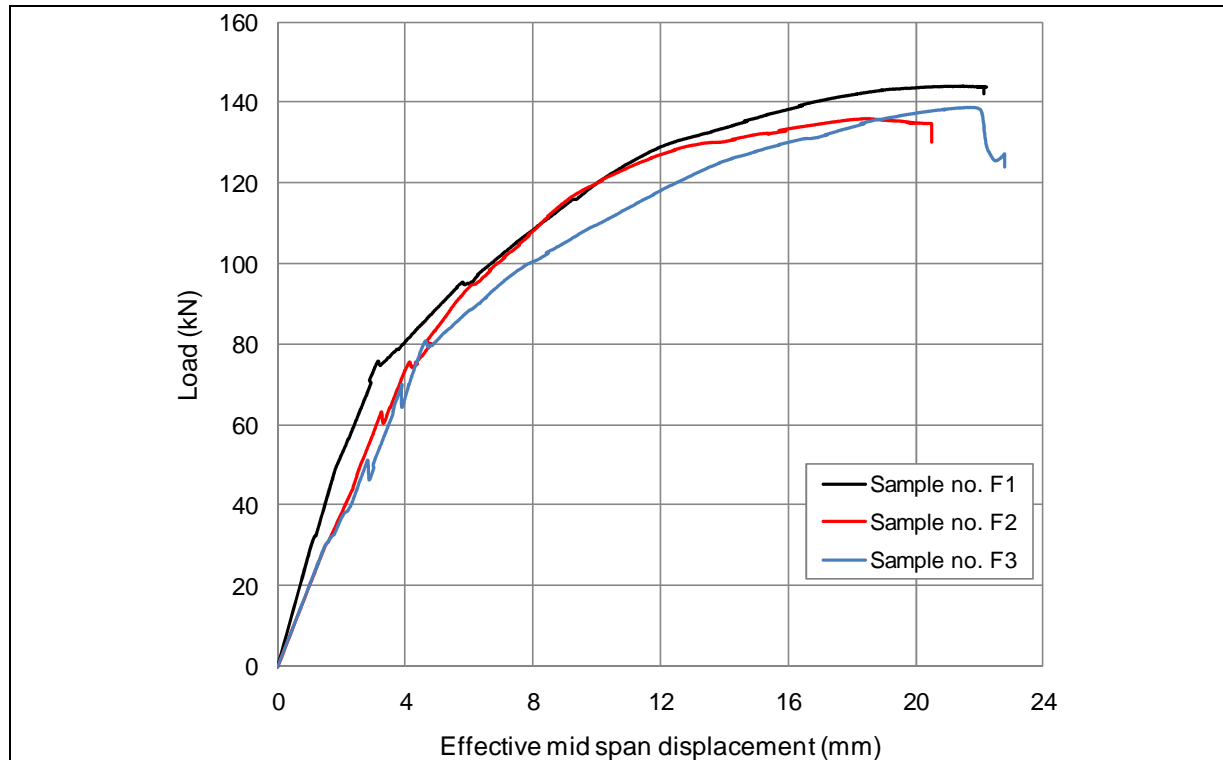
Sample groups MB2-A0.0% and MB2-F0.0% were used as control experiments. Three specimens in each sample group containing 2Y10 RB-II steel bars each were used. The spacing between the loading points and the nearest support is 150mm for MB2-A0.0% and 200mm for

MB2-F0.0% and, therefore, only bending moment values can be compared across the sample groups. Bending moment is calculated using Equations 4.15 and 4.16 given in Section 4.3.4. Both forces and moments at cracking point (denoted by P_{cr-exp} and M_{cr-exp} respectively) and maximum flexural capacity (denoted by P_{u-exp} and M_{u-exp} respectively) of the beams are outlined in Table 5.9. While the concrete might have started to crack at lower forces, the cracking force in this paper is taken as the value where a noticeable change in stiffness of the force-displacement curve is observed (see Figure 5.7). From Table 5.9, beams from batch F have greater cracking moments than beams from batch A but there is insignificant difference in the ultimate moments for these two batches.

Note that the mid-span displacement for MB2-A0.0% is taken from vertical displacement of the Instron-head. It therefore contains displacements due to the compression of rubber strips at support and loading points and deflection of the steel frame supporting the Instron as outlined in Chapter 4. The effective mid-span displacement for MB2-F0.0% is taken from vertical displacement of the Instron-head minus displacements due to the compression of the rubber strips, but includes deflections in the steel frame supporting the Instron. Therefore, the displacements for all these flexural tests results are not to be considered for any evaluation.

All the beams in these sample groups failed by flexure while shear cracks were seen developing in most of the beams. A full description of experimental data observations exhibited by these beams is outlined in Appendix B, but typical cracking patterns for selected beams are shown in Figure 5.8.







(b) Flexural response for MB2-F0.0%

Figure 5.7: Flexural response for MB2-A0.0% and MB2-F0.0% beams

Table 5.9: Flexural response for MB2-A0.0% and MB2-F0.0% beams

Sample name	Sample No.	Cracking force (kN)	Maximum force (kN)	Cracking moment (kNm)	Maximum moment (kNm)
		P_{cr}	P_u	M_{cr-exp}	M_{u-exp}
MB2-A0.0%	A1	79	171.65	6.93	15.06
	A2	84	186.91	7.37	16.40
	A3	86	170.56	7.55	14.97
MB2-F0.0%	F1	74	142.81	8.51	16.42
	F2	76	135.88	8.74	15.63
	F3	80	138.82	9.20	15.96

Sample No.	Intermediate cracking mode	Final failure state
(a) MB2-A0.0% (Sample no. A3)		

(b) MB2-F0.0%
(Sample no. F1)



Figure 5.8: Typical cracking patterns for selected beams from MB2-A0.0% and MB2-F0.0%

5.3.2 FLEXURAL RESPONSE FOR MB0-C1.0% AND MB0-E1.5%

Sample groups MB0-C1.0% and MB0-E1.5% were used as verification experiments for the flexural capacity model without reinforcing bars. Three specimens containing 1.0% and 1.5% steel fibres as denoted by the sample groups were used in each sample group. The loading, spacing and bearing widths used for the determination of moment capacity are given in Section 4.3.3.2. Figure 5.9 displays force displacement curves from experimental results. Maximum forces and their corresponding bending moments are shown in Table 5.10. From Table 5.10, beams from batch E have greater maximum moments than beams from batch C. It should be noted that batch E has higher compressive and tensile properties than batch C as reported in Section 5.2.

All the beams in these sample groups failed by flexure without visual concrete crushing in the compression zone. No shear cracks developed up to failure. A full description of the experimental response exhibited by these beams is outlined in Appendix B, but typical cracking patterns for selected beams are shown in Figure 5.10. All samples show consistency in flexural strength and stiffness, with the exception of Sample no. E3. Deflection data at the supports for this sample could not be retrieved and hence overall displacement was used, possibly influencing the ‘observed’ less stiffness.

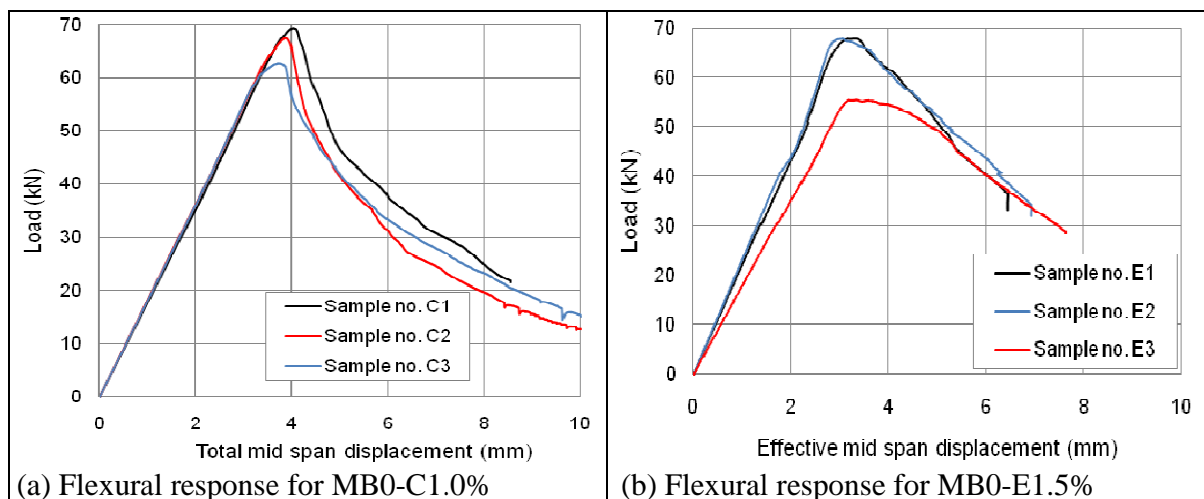


Figure 5.9: Flexural response for MB0-C1.0% and MB0-E1.5% beams

Table 5.10: Flexural response for MB0-C1.0% and MB0-E1.5% beams

Sample name	Sample No.	Maximum force	Maximum moment
		P_u (kN)	M_{u-exp} (kNm)
MB0-C1.0%	C1	69.44	6.09
	C2	67.46	5.92
	C3	62.69	5.50
MB0-E1.5%	E1	68.12	7.83
	E2	67.16	7.72
	E3	55.48	6.38





Sample No.	Intermediate cracking mode	Final failure state
(a): MB0-C1.0% (Sample no. C3)		
(b): MB0-E1.5% (Sample no. E3)		

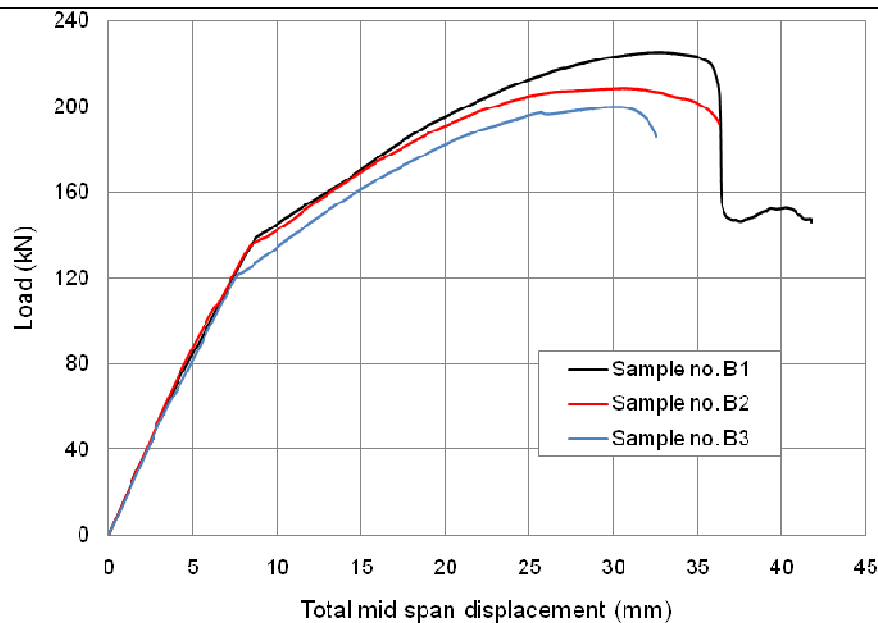
Figure 5.10: Typical cracking patterns for selected beams from MB0-C1.05 and MB0-E1.5%

5.3.3 FLEXURAL RESPONSE FOR MB2-B1.0% AND MB2-D1.5%

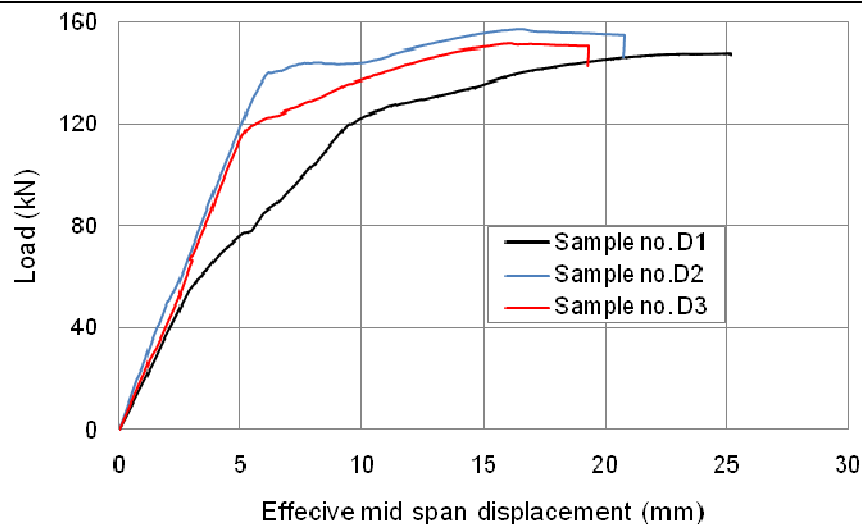
Sample groups MB2-B1.0% and MB2-D1.5% were used as verification experiments for the flexural capacity model with reinforcing bars. Three specimens with 2Y10 RB-II steel bars containing 1.0% and 1.5% steel fibres as denoted by the sample groups were used in each sample group. The loading, spacing and bearing widths used for the determination of moment capacity are given in Section 4.3.3.2. Figure 5.11 shows the force-displacement curves from experimental results. Both forces and moments at cracking point and maximum flexural capacity of the beams are outlined in Table 5.11. From Table 5.11, beams from batch D have greater cracking moments than beams from batch B but there is insignificant difference in the ultimate moments for these two batches.

MB2-B1.0% beams exhibited flexural shear cracks with one or more cracks developed at failure, while in MB2-D1.5% beams only one flexural crack developed with little or no visual shear cracks observed. The final failure for both sample groups was flexure. A full description of experimental data observations exhibited by these beams is outlined in Appendix B, but typical cracking patterns for selected beams are shown in Figure 5.12. Generally, samples with more

cracks at failure exhibited greater flexural capacity. Samples from MB2-1.5% show greater cracking moments as compared to samples from MB2-B1.5% while there is little difference in the maximum flexural moments. While beams MB2-D1.5% showed stronger material properties (Section 5.2) than MB2-B1.0%, the weaker beams have slightly better maximum flexural strength due to more cracks developed before failure as compared to MB2-D1.5%.



(a) Flexural response for MB2-B1.0% beams



(b) Flexural response for MB2-D1.5% beams

Figure 5.11: Flexural response for MB2-B1.0% and MB2-D1.5% beams

Table 5.11: Flexural response for MB2-B1.0% and MB2-D1.5% beams

Sample name	Sample No.	Cracking force (kN)	Maximum force (kN)	Cracking moment (kNm)	Maximum moment (kNm)
		P_{cr}	P_u	M_{cr-exp}	M_{u-exp}
MB2-B1.0%	B1	139	225.7	12.20	19.81
	B2	136	208.6	11.93	18.30
	B3	122	199.9	10.71	17.54
MB2-D1.5%	D1	120	147.8	13.80	17.00
	D2	120	148.8	13.80	17.11
	D3	140	151.2	16.10	17.39





Sample No.	Intermediate cracking mode	Final failure state
(a) MB2-B1.0% (Sample no. B1)		
(b) MB2-D1.5% (Sample no. D1)		

Figure 5.12: Typical cracking patterns for selected beams from MB2-b1.0% and MB2-D1.5%

5.4 CONCLUSION

The concrete material has been characterised through standard methods as outlined in the Codes. There is an increase in compression strength with an increase in the amount of steel fibres for both preliminary characterisation data and model verification characterisation data, with the exception of mixes MC-F0.0% and MC-C1.0%. The MC-F0.0% samples show a relatively higher compressive strength compared to other samples without steel fibres. This could be explained by the relatively low slump in mix MC-F0.0%, as compared to other mixes that do not contain steel fibres. Samples from mix MC-C1.0%, however, show relatively lower compressive strengths as compared to other samples with 1.0% steel fibres. The lower compressive strength may have been influenced by possible segregation as shown in photos given in Appendix C. While compression strength increases with increase in steel fibres, there is no clear trend in the Young's modulus. The Young's modulus as calculated from compression data and splitting data correlate well with each other. The Young's modulus obtained from the compression data will be used in the subsequent chapters.

Two procedures have been employed for the determination of direct tensile stress parameters, which give very different values at both ultimate tensile strength and post-cracking state. The methods proposed by Rocco *et al* (2001), together with the method recommended in the Standards have been used. The method proposed by Rocco *et al* (2001) may not satisfactorily predict the post-cracking behaviour as it is based on the elastic theory approach. The second approach uses the code conversion of the maximum splitting strength to the direct tensile strength. In this approach, the post-cracking direct tensile stress is deduced from the post-cracking splitting stress by inferring a uniform stress equal to the difference between the maximum splitting strength and the direct tensile strength. The use of these indirect methods for the determination of tensile parameters creates some uncertainty in the tensile parameters. As a means to ascertain which of these two sets of data gives a better representation of the direct tensile parameters, a nonlinear finite element analysis is performed in Chapter 6. Physical and statistical evaluation of all the material properties for the determination of relevant model parameters is also outlined in Chapter 6.

In addition to concrete tests, a direct tensile test was conducted for the steel bars used in the model verification experiments. This ensures that appropriate model parameters are used for verification of SFRC flexural models with reinforcing bars. The tensile properties of steel bars show two different distinct behaviours: elastic-perfect plastic behaviour and elastic-strain-hardening behaviour.

Results from four-point bending tests conducted on beams for model verification have been outlined. All the beams failed in flexure (as expected), only with differences in the number of cracks formed before failure. Samples that developed more cracks before failure show superior flexural capacity to those that displayed less cracks before failure. This could be explained by an increased fracture energy required to develop more cracks.

CHAPTER 6. ANALYSIS OF EXPERIMENTAL RESULTS

6.1 INTRODUCTION

Chapter 5 indicated that some data from the ‘same’ mix proportions was acquired at different phases of the experimental program. It is therefore against this background that in addition to the evaluation of material properties as outlined in the previous chapter, the *t*-test is employed to group samples based on a prescribed risk acceptance level. Furthermore, this chapter evaluates and establishes patterns (if any) within population groups and across different populations from model verification experiments. Parameters useful for model verification are derived from the analysis of the experimental data. Based on the understanding that the same material mix proportions were used, preliminary population categories are developed to represent the amount of fibres used for each population. These categories are as follows:

- Category I: concrete without steel fibres;
- Category II: concrete with 1.0% steel fibres;
- Category III: concrete with 1.5% steel fibres.

6.2 EVALUATION OF MATERIAL BEHAVIOUR

The general material behaviour has been characterised under Section 5.2. Both compressive behaviour and tensile behaviour are outlined. For the tensile behaviour, indirect methods are used to determine the tensile properties, including flexural and splitting test data. While the bending test was only employed for the preliminary characterisation test, the splitting test was used throughout the experimental program. As explained under Methodology in Chapter 4, these tests were conducted under different experimental set-ups. Each experimental set-up may afford a varying degree of accuracy and hence cause uncertainty within the experimental data. It is against this background that the compressive strength and flexural strength data may be deemed as more accurate than the Young’s modulus and the splitting strength data. This is due to the stability of the test set-up and testing procedures. In addition to these tests, a slump test for material flowability was performed.

Engineering judgment and reasoning are used to assess the data from material characterisation tests. Since the compressive strength data is more reliable, evaluation of other parameters will be based on analytical expressions, recommended by Eurocode (European standards, 2004) and Rilem TC 162-TDF (Vandewalle, 2003) which depend on the compressive strength. The standardised values for the Young’s modulus obtained from analytical expressions given in the Eurocode are merely indicative. It is well established that the Young’s modulus not only dependent of compressive strength, but also other factors, including the aggregate type. The slump value may be referred to as it may enhance the segregation of concrete constituents in addition to depicting the potential amount of water available in the concrete.

6.2.1 COMPRESSIVE BEHAVIOUR

Category I

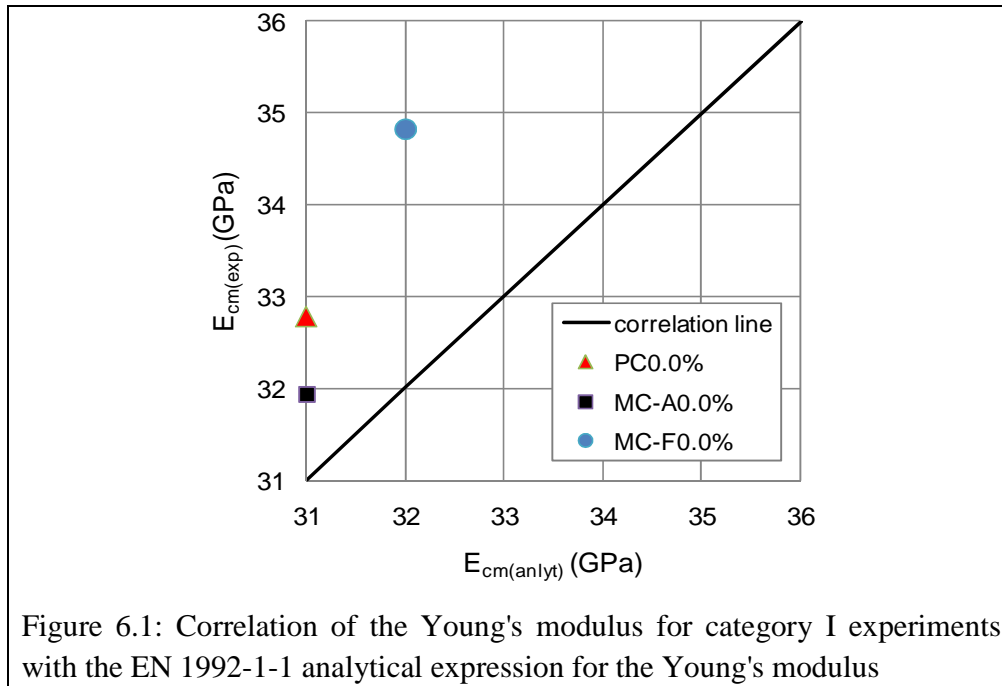
Sample groups PC0.0%, MC-A0.0% and MC-F0.0% belong to this category. The slumps within these batches vary between 65mm and 80mm. Concrete with lower slump has the highest compressive strength (see Table 6.1). This may mean that even though the same water/cement ratio was used, practical implementation of such may bring slight variation in the mortar fraction. Sample group MC-F0.0% may have the least amount of water followed by PC0.0%. Another reason could be the amount of entrained air within the matrix.

At target strength of 30MPa, sample groups PC0.0% and MC-A0.0% could be assumed to belong to the same population. It should be noted that samples belonging to MC-F0.0% were cast three and half months after MC-A0.0% samples (MC-A0.0% samples were cast on 12 October 2010 and MC-F0.0% samples were cast on 25 January 2011). The fact that the slump for MC-F0.0% is the smallest, may imply that the actual amount of free water was slightly less than in the other batches. This may have resulted in the smaller slump and higher compressive strength as reported in Table 6.1.

The values for the Young's modulus for sample groups PC0.0% and MC-A0.0% correlate well with corresponding values from the EN 1992-1-1 analytical expression (see Figure 6.1). For sample group MC-F0.0%, there is a substantial diversion from the value of the analytical expression provided in EN1992-1-1, as illustrated in Figure 6.1. The variations in the values of Young's modulus from those determined from analytical expressions provided in the EN 1992-1-1 are expected, as cubes were used in the compression tests and they generated stress confinement. Stress confinement may affect the Young's modulus. In addition, mechanical properties of the concrete constituents also affect the Young's modulus.

Table 6.1: Compression test results summary for category I, with CoV in brackets

Property	PC0.0%	MC-A0.0%	MC-F0.0%
Slump (mm)	70	80	65
Average compressive strength (MPa)	31.84 (0.039)	31.87(0.068)	36.61(0.050)
Average Young's modulus (GPa)	32.79(0.110)	31.94(0.117)	34.82(0.099)



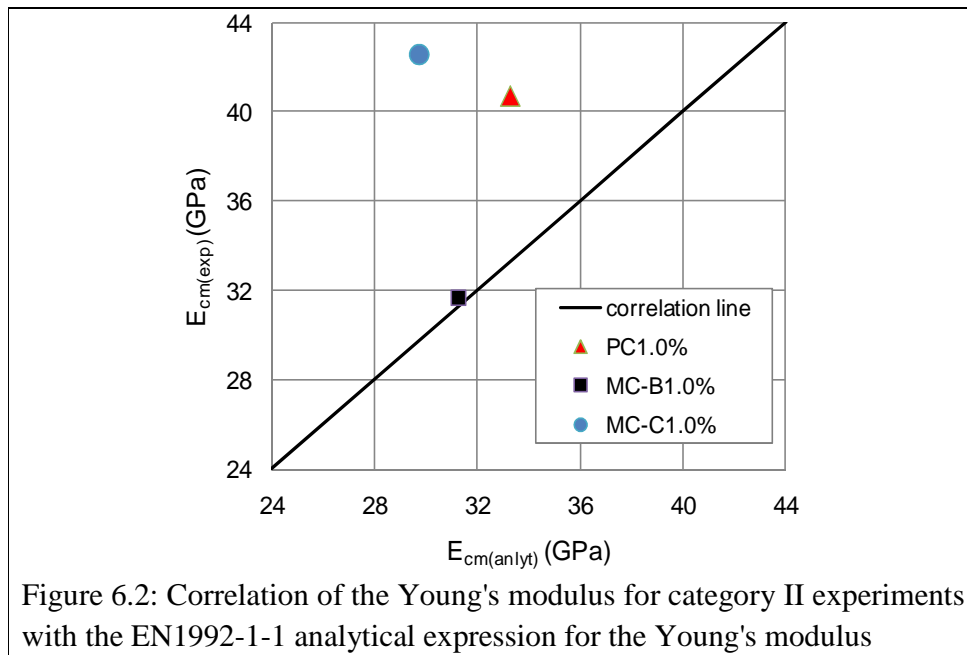
Category II

Sample groups PC1.0%, MC-B1.0% and MC-C1.0% belong to this category. The slumps within these batches vary between 40mm and 120mm. There is no trend in the compressive strength values with the slumps (see Table 6.2). The variations in compressive strength are so high that the concrete batches could not be treated as coming from the same population. For the sample groups in this category, mixes with higher flowability (high slump value) tend to have lower compression strength.

The values for the Young's modulus for the sample groups in this category do not correlate well with corresponding values from the EN 1992-1-1 analytical expression (see Figure 6.2) with the exception of beams from batch MC-B1.0%. The variations in the values of Young's modulus from those determined from analytical expressions provided in the EN 1992-1-1 are expected, as cubes were used in the compression tests and they generated stress confinement. Stress confinement may affect the Young's modulus. For MC-C1.0% samples, aggregate segregation and poor distribution of steel fibres may have affected the results for both compression strength and Young's modulus. This sample group had very high slump value as compared to other samples.

Table 6.2: Compression test results summary for category II, with Cov in brackets

Property	PC1.0%	MC-B1.0%	MC-C1.0%
Slump (mm)	60	40	120
Average compressive strength (MPa)	42.58(0.036)	34.68(0.068)	25.60(0.032)
Average Young's modulus (MPa)	40.70(0.157)	31.68(0.053)	42.54(0.063)

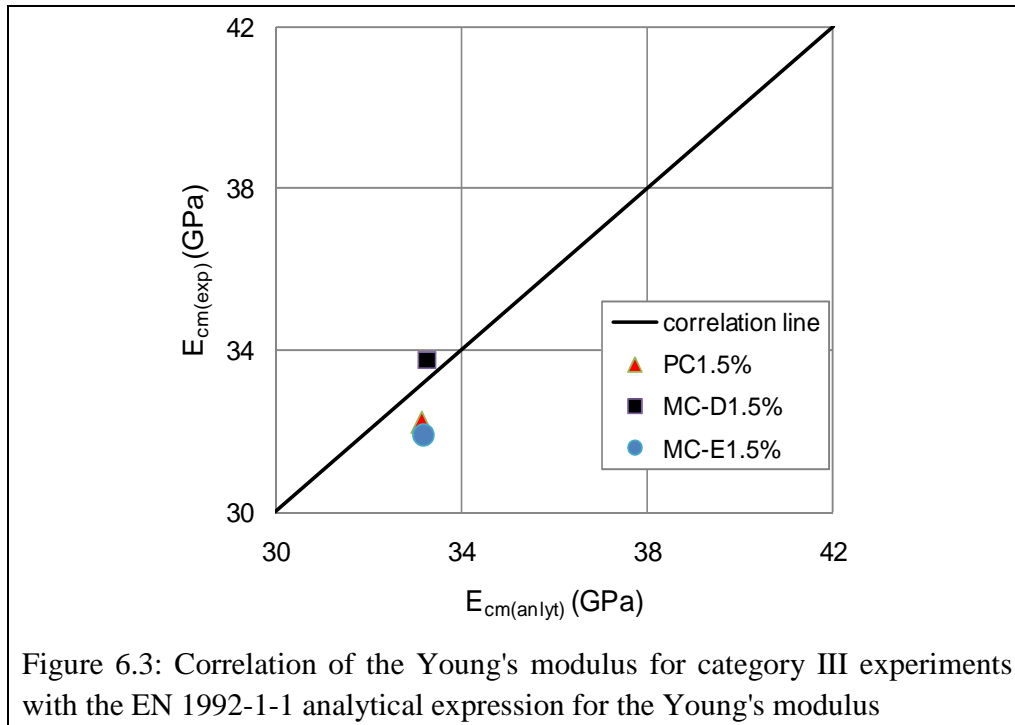


Category III

Sample groups PC1.5%, MC-D1.5% and MC-E1.5% belong to this category. The slumps within these batches vary between 40mm and 85mm. There is no clear trend in the compressive strength to slump flow relation (see Table 6.3). The Young's modulus for all batches are generally lower than the values provided by the analytical expression used in EN1992-1-1, as illustrated in Figure 6.3. It should be noted that the Young's modulus as determined from tensile data reported in Section 5.2.1 are higher than the ones reported here.

Table 6.3: Compression test results summary for category III, with CoV in brackets

Property	PC1.5%	MC-D1.5%	MC-E1.5%
Slump (mm)	60	40	85
Average compressive strength (MPa)	42.18(0.037)	41.20(0.022)	41.2(0.027)
Average Young's modulus (MPa)	32.23(0.072)	33.75(0.071)	31.89(0.049)



6.2.2 TENSILE BEHAVIOUR

The tensile behaviour of concrete materials is influenced by the matrix properties, amount, type, distribution and orientation of steel fibres used. All these factors, except for fibre distribution and orientation, can be easily determined. In this research fibre orientation was assumed to be in 3D and evenly distributed for all samples containing steel fibres. Evaluation of tensile behaviour will follow the same categories outlined under Section 6.1. In this section, the direct tensile strength as based on the code recommendations and modified elastic approach by Rocco *et al* (2001), is used to access the elastic tensile behaviour of concrete. Furthermore, compression behaviour will be referred to as there is a relation between the compressive strength and the tensile strength of concrete (European standards, 2004; Vandewalle, 2003). The post-cracking behaviour is evaluated from the toughness of concrete at a strain of 0.025, as outlined in the experimental results.

Category I

There is a very slight variation in tensile parameters across the sample groups, with mean tensile strengths varying from 3.35MPa to 3.42MPa for a code definition, and 3.56MPa to 3.66MPa for an elastic approach definition respectively (see Table 6.4). However, it should be noted that mixes PC0.0% and MC-A0.0% belong to the same population of concrete Class C20/25, while mix MC-F0.0% belongs to concrete Class C25/30, based on characteristic compressive strength values as outlined in Appendix B. Using analytical expressions given in EN 1992-1-1, the corresponding mean tensile strengths are determined (see Table 6.4). Both methods used to determine the direct tensile strength from splitting strength over-predict the tensile strength. The

code approach ‘over-predicts’ the strength by 28% to 41%, while the elastic approach ‘over-predicts’ by 36% to 50%. Such an over-prediction from a codified method would only have resulted from the use of cube compression strength which has inherent weakness in predicting the compressive behaviour of concrete as compared to cylindrical samples.

Table 6.4: Tension test results summary for Category I, with CoV in brackets

Sample name	Average tensile strength, (MPa)			Experimental/Analytical	
	Code definition	Rocco <i>et al</i> (2001)	Analytical (EN1992-1-1)	Code definition	Rocco <i>et al</i> (2001)
PC0.0%	3.42(0.030)	3.66(0.030)	2.47	1.38	1.48
MC-A0.0%	3.35(0.083)	3.56(0.083)	2.38	1.41	1.50
MC-F0.0%	3.42(0.084)	3.64(0.084)	2.68	1.28	1.36

Category II

There is a very slight variation in tensile parameters across the sample groups with the mean tensile strength varying from 3.69MPa to 3.88MPa for the code definition and 3.96MPa to 4.18MPa for the elastic approach definition respectively (see Table 6.5). In this category, all the sample groups are treated as belonging to different concrete strength classes due to their compression strength parameters. Using analytical expressions given in EN1992-1-1, the corresponding tensile strengths are determined (see Table 6.5). Tensile strength determined from an elastic theory ‘over-predicts’ the tensile strength by 32% to 91%. The code definition ‘over-predicts’ tensile strength by 23% and 80% respectively. The toughness values of concrete for mixes PC1.0% and MC-C1.0% are close to each other as compared to mix MC-B1.0%. An apparent trend is an increase in the toughness with increasing tensile strength.

Table 6.5: Tension test results summary for Category II, with CoV in brackets

Sample name	Average tensile strength, (MPa)			Experimental strength		Toughness (N/mm)	
				Analytical strength			
	Code definition	Rocco <i>et al</i> (2001)	Analytical (EN1992-1-1)	Code definition	Rocco <i>et al</i> (2001)	Code definition	Rocco <i>et al</i> (2001)
PC1.0%	3.69(0.025)	3.96	3.01	1.23	1.32	3.76(0.05)	4.40(0.05)
MC-B1.0%	3.93(0.183)	4.18	2.52	1.56	1.66	4.12(0.240)	4.65(0.2)
MC-C1.0%	3.88(0.043)	4.12	2.16	1.80	1.91	3.71(0.15)	4.32(0.13)

Category III

As observed in Categories I and II, there is a very slight variation of tensile parameters across the mixes in this category with mean tensile strengths varying from 4.57MPa to 5.17MPa for the code definition, and 4.90MPa to 5.49MPa for the elastic approach definition respectively (see Table 6.6) in all the mixes. In this category, mixes PC1.5%, MC-D1.5% and MC-E1.5% may be deemed to belong to the same population of concrete (C25/30), based on characteristic compressive strengths as given in Appendix B. Using the analytical expression given in EN1992-1-1, the corresponding tensile strengths are determined (see Table 6.6). Both methods used to

determine the direct tensile strength from splitting strength over-predict the tensile strength. The code approach ‘over-predicts’ the strength by 54% to 73% while the elastic approach over-predicts by 65% to 84%. Toughness of concrete for mixes PC1.5%, MC-D1.5% and MC-E1.5% are close to each other and increases with increasing tensile strength as is the case with Category I.

Table 6.6: Tension test results for Category III, with CoV in brackets

Sample name	Average tensile strength, (MPa)			Experimental strength		Toughness (N/mm)	
				Analytical strength			
	Code definition	Rocco <i>et al</i> (2001)	Analytical (EN1992-1-1)	Code definition	Rocco <i>et al</i> (2001)	Code definition	Rocco <i>et al</i> (2001)
PC1.5%	4.57(0.143)	4.90	2.98	1.54	1.65	4.87(0.25)	5.58(0.24)
MC-D%1.5	5.09(0.038)	5.41	3.00	1.70	1.80	5.28(0.06)	5.94(0.048)
MC-E1.5%	5.17(0.038)	5.49	2.98	1.73	1.84	4.99(0.05)	5.69(0.04)

6.3 STATISTICAL ANALYSIS OF MATERIAL CHARACTERISATION DATA

Statistical properties of the material strength are used to determine characteristic values as well as design values and partial material factors (Dymond & Retief, 2010). In this paper only the characteristic values are employed, as further research on reliability is required for comprehensive model verification. Since statistical properties depend on sample size, it is beneficial to combine data groups belonging to the same population considering that few small sample sizes were used. Concrete compression strengths and tensile strengths are drawn upon as leading properties of concrete for assessing whether the sample groups belong to the same population. Samples will be deemed to belong to the same population if both the compression and the tensile strengths qualify as such. The use of these two parameters is justified since the model verification exercise requires the application of these parameters concurrently. Furthermore, post-cracking parameters are assumed to be influenced by the concrete grade and steel fibre volume. Therefore, using fibre content as a criterion for the classification of categories ensures that appropriate sample groups are made. Three categories are considered as outlines in Section 6.1.

A *t*-test is used to determine whether samples belong to the same population, taking a risk level (α) of 0.05. The *t*-test is applied to check whether the variations in means and standard deviation are as a result of statistical variability or material property. Since concrete strength has been widely assumed to have the same variance across the strength, it is reasonable to assume that population variances from which the samples are drawn, are equal for all properties of concrete. A pooled estimate of population variances is therefore used and the formula for the *t*-test using Difference of Two-means is given as follows (Montgomery & Ruger, 2007):

$$t = \frac{\bar{X}_1 - \bar{X}_2}{\sqrt{\frac{n_1 s_1^2 + n_2 s_2^2}{n_1 + n_2 - 2} \sqrt{\frac{n_1 + n_2}{n_1 n_2}}}} \quad 6.1$$

Where

\bar{X}_1 , s_1 and n_1 are the mean, the standard deviation and the size of the first sample group; and

\bar{X}_2 , s_2 and n_2 are the mean, the standard deviation and the size of the second sample group.

A null hypothesis (H_0) and an alternative hypothesis (H_1) are used. The null hypothesis assumes that there is no difference in the means of two populations, while the alternative hypothesis assumes that there is in fact a difference in the means of two populations. The two hypotheses used are mathematically written as follows:

$$H_0 : \mu_1 - \mu_2 = 0 \text{ and } H_1 : \mu_1 - \mu_2 \neq 0$$

Where

μ_1 and μ_2 are the means for the first and second populations respectively.

6.3.1 COMPRESSION TEST RESULTS

Category I: concrete without steel fibres

Three sample groups were reported under Chapter 5 and have statistical properties as outlined in Table 6.7 below. Since the Difference of Two-means test is used, three pairs of analysis are derived as follows: a-b, a-c and b-c with reference to Table 6.7. Using Equation 6.1, t -values for these pairs are determined and reported in Table 6.8. A decision for each case is made based on the risk level of 0.05. Table 6.8 indicates that only a-b will be combined to represent mix MC-A0.0%, while mix MC-F0.0% will be treated as coming from a different population in subsequent analysis.

Table 6.7: Statistical values for the compression strength of Category I concrete

Parameter	Compressive strength for Category I		
	(a) PC0.0%	(b) MC-A0.0%	(c) MC-F0.0%
Mean, \bar{x}_i	31.84	31.87	36.61
Standard deviation, s	1.22	2.16	1.84
Sample size, n	3	4	6

Table 6.8: Results from a t -test for the compression strength of Category I concrete

Group pairs	ν	$t_{df,0.05}$	t	Comment
a-b	5	2.015	-0.019	Accept hypothesis of no difference
a-c	7	1.895	-3.720	Reject hypothesis of no difference
b-c	8	1.860	-3.222	Reject hypothesis of no difference

Category II: concrete with 1.0% steel fibres

Three sample groups were reported in Chapter 5 and have statistical properties as outlined in Table 6.9 below. Since the Difference of Two-means test is used, three pairs of analysis are derived as follows: a-b, a-c and b-c with reference to Table 6.9. Using Equation 6.1, t -values for these pairs are determined and reported in Table 6.10. A decision for each case is made based on the risk level of 0.05. Table 6.10 indicates that samples in this category will not be combined as they are deemed to come from different populations, based on the statistical analysis performed at a risk level of 0.05. Therefore, mixes PC1.0%, MC-B1.0% and MC-C1.0% will be treated as mixes coming from different populations.

Table 6.9: Statistical values for the compression strength of Category II concrete

Parameter	Compressive strength for Category II		
	(a) PC1.0%	(b) MC-B1.0%	(c) MC-C1.0%
Mean, \bar{x}_i	42.58	34.68	25.60
Standard deviation, s	1.54	2.36	0.81
Sample size, n	3	4	3

Table 6.10: Results from a t -test for the compression strength of Category II concrete

Group pairs	ν	$t_{df,0.05}$	t	Comment
a-b	5	2.015	4.266	Reject hypothesis of no difference
a-c	4	2.132	13.801	Reject hypothesis of no difference
b-c	5	2.015	5.399	Reject hypothesis of no difference

Category III: Concrete with 1.5% steel fibres

Four sample groups were reported in Chapter 5 and have statistical properties as outlined in Table 6.11 below. Since the Difference of Two-means test is used, six pairs of analysis are derived as follows: a-b, a-c and b-c, with reference to notations in Table 6.11. Using Equation 6.1, t -values for these pairs are determined and reported in Table 6.12. Based on the risk level of 0.05, a decision for each case is made. From results given in Table 6.12, compression strength from mixes MC-D1.5% and MC-E1.5% will be combined in the subsequent analysis.

Table 6.11: Statistical values for the compression strength of Category III concrete

Parameter	Compressive strength for Category III		
	(a) PC1.5%	(b) MC-D1.5%	(c) MC-E1.5%
Mean, \bar{x}_i	42.18	41.2	41.2
Standard deviation, s	1.56	0.09	1.11
Sample size, n	2	5	6

Table 6.12: Results from a t -test for the compression strength of Category III concrete

Group pairs	ν	$t_{df,0.05}$	t	Comment
a-b	5	2.015	1.182	Accept hypothesis of no difference
a-c	6	1.943	0.840	Accept hypothesis of no difference
b-c	9	1.833	0.000	Accept hypothesis of no difference

6.3.2 SPLITTING TEST RESULTS

The parameter chosen to classify categories is the tensile strength. While post-cracking tensile behaviour depends not only on the class of concrete, it is possible to view tensile strength as the main factor influencing post-cracking behaviour because fibre content determines categorisation. It should be known that literature shows great correlation between tensile strength and compression strength (European standards, 2004; Vandewalle, 2003). Based on this understanding, a combination of samples based on categorisation as outlined in Section 6.1 will be followed. A t -test is conducted for the tensile strength as derived from code definition.

Category I: concrete without steel fibres

Three sample groups were reported in Chapter 5 and have statistical properties as outlined in Table 6.13 below. Using the Difference of Two-means test, three pairs of analysis are derived as follows: a-b, a-c and b-c with reference to Table 6.13. Using Equation 6.1, t -values for these pairs are determined and reported in Table 6.14. A decision for each case is made based on the risk level of 0.05. The results from the t -test show that for this category all tensile parameters come from the same population. However, since under analysis of compression strength in Section 6.3.1 only a-b qualified, the decision made from compression analysis stands.

Table 6.13: Statistical values for the tensile strength of Category I concrete

Parameter	Concrete direct tensile strength (MPa) for Category I		
	(a) PC0.0%	(b) MC-A0.0%	(c) MC-F0.0%
Mean, \bar{x}_i	3.42	3.35	3.42
Standard deviation, s	0.25	0.28	0.29
Sample size, n	3	4	6

Table 6.14: Results from a t -test for the tensile strength of Category I concrete

Group pairs	ν	$t_{df,0.05}$	t	Comment
a-b	5	2.015	0.290	Accept hypothesis of no difference
a-c	7	1.895	0.000	Accept hypothesis of no difference
b-c	8	1.860	-0.339	Accept hypothesis of no difference

Category II: concrete with 1.0% steel fibres

Three sample groups were reported in Chapter 5 and have statistical properties as outlined in Table 6.15 below. Using the Difference of Two-means test, three pairs of analysis are derived as follows: a-b, a-c and b-c, with reference to the Table 6.15. Using Equation 6.1, t -values for these pairs are determined and reported in Table 6.16. A decision for each case is made based on the risk level of 0.05. The results from t -test show that for this category all tensile parameters come from the same population. However, since under the analysis of compression strength parameters in Section 6.3.1 none of the sample groups qualified to have come from the same population, the decision made from the compression strength analysis stands.

Table 6.15: Statistical values for the tensile strength of Category II concrete

Parameter	Concrete direct tensile strength (MPa) for Category II		
	(a) PC1.0%	(b) MC-B1.0%	(c) MC-C1.0%
Mean, \bar{x}_i	3.69	3.93	3.88
Standard deviation, s	0.09	0.72	0.17
Sample size, n	3	2	4

Table 6.16: Results from a t -test for the tensile strength of Category II concrete

Group pairs	ν	$t_{df,0.05}$	t	Comment
a-b	3	2.353	-0.442	Accept hypothesis of no difference
a-c	5	2.015	-1.487	Accept hypothesis of no difference
b-c	4	2.132	0.108	Accept hypothesis of no difference

Category III: Concrete with 1.5% steel fibres

Four sample groups were reported in Chapter 5 and have statistical properties as outlined in Table 6.17 below. Using the Difference of Two-means test, six pairs of analysis are derived as follows: a-b, a-c and b-c, with reference to notations in Table 6.17. Using Equation 6.1, t -values for these pairs are determined and reported in Table 6.18. Based on the risk level of 0.05, a decision is made for each case. From the t -test results, tensile strength from PC1.5%, MC-D1.5% and MC-E1.5% may be combined. This agrees with the t -test results for compression strength and the decision stands.

Table 6.17: Statistical values for the tensile strength of Category III concrete

Parameter	Concrete direct tensile strength (MPa) for Category III		
	(a) PC1.5%	(b) MC-D1.5%	(c) MC-E1.5%
Mean, \bar{x}_i	4.57	5.09	5.17
Standard deviation, s	0.65	0.19	0.20
Sample size, n	3	3	6

Table 6.18: Results from a t -test for the tensile strength of Category III concrete

Group pairs	ν	$t_{df,0.05}$	t	Comment
a-b	4	2.132	-1.086	Accept hypothesis of no difference
a-c	7	1.895	-1.828	Accept hypothesis of no difference
b-c	7	1.895	-0.507	Accept hypothesis of no difference

6.4 PARAMETERS FOR MODEL VERIFICATION PROCESS

Model verification will be performed using two sets of data: mean parameters and characteristic parameters. Since the confidence of ensuring that these parameters closely represent the material may depend on the statistical properties, use of an increased sample size has been sought through the combination of samples deemed to come from the same population (as outlined in Section 6.3). A material characteristic value is determined from the Equation 4.15 given in Section 4.3.5. For material characteristic value, a 95% percentile is used and the fractile estimator K_n depends on the sample size (Holicky, 2009) as given in Table 6.19. In this paper the population standard deviation is assumed to be known.

Table 6.19: Coefficients K_n for 5% characteristic value

Coefficient	Sample size n										
	1	2	3	4	5	6	8	10	20	30	∞
σ known	2.31	2.01	1.89	1.83	1.80	1.77	1.74	1.72	1.68	1.67	1.64
σ unknown	-	-	3.37	2.63	2.33	2.18	2.00	1.92	1.76	1.73	1.64

Concrete compression parameters

Parameters for compression material behaviour are compression strength, yield compression strain and Young's modulus of elasticity. Since knowledge of any two of the parameters allows one to determine the remaining parameter, only compression strength and Young's modulus are outlined in Table 6.20.

Table 6.20: Compression parameters for the model

Combined sample group	n	Average value (MPa)		Standard deviation		Characteristic
		Compressive strength	Young's modulus	Compressive strength	Young's modulus	Compression Strength(MPa)
'MC-A0.0%'	7	31.86	32301	1.68	3390	28.88
'MC-B1.0%'	4	34.68	31678	2.36	1680	30.36
'MC-C1.0%'	3	25.50	42540	0.81	2688	24.07
'MC-D(or E)1.5%'	13	41.35	32658	1.06	2051	39.54
'MC-F0.0%'	6	36.61	34842	1.84	3453	33.35

Concrete tension parameters

Parameters for tension behaviour of concrete are tensile strengths and the equivalent post-peak tensile strengths. The equivalent post-peak tensile strength is derived from toughness parameters and corresponding crack width as shown in Equation 6.2. In this paper, a crack width corresponding to a recommended ultimate tensile strain of 0.025 at the position of steel bars is used (Vandewalle, 2003). Based on the gauge length of 80mm used during the splitting test, the total displacement corresponding to this limiting strain is 2.0mm. At the extreme edge, the crack width will vary, depending on the position of the neutral axis in the beam but should not exceed 3.5mm (Vandewalle, 2003).

In Chapter 3, flexural models for SFRC with reinforcing bars have been outlined. The models not only predict the capacity of the beams but also determine bending moments at cracking of concrete, yielding of steel bars and maximum tensile strength of steel bars. A drop-down assumes a constant post-peak strength determined at a given crack width, according to Equation 6.2. The value of the equivalent post-peak strength may therefore change, depending on the selected crack width. Plastic displacements (crack width) are calculated for each sample based on each sample's cracking strains. Tables 6.21 and 6.22 supply a summary of the tension parameters as determined by code definition and theory of elasticity approach respectively. This is based on a limiting strain of 0.025 and complete data for this analysis is given in Appendix C. The equivalent post-peak tensile strength, f_{teq} , is determined from the following expression:

$$f_{teq} = \frac{\int_0^{w_{lim}} \sigma(w) dw}{w_{lim}} \quad 6.2$$

where w_{lim} is the limiting crack width and $\sigma(w)$ is the stress-crack width material law.

A case study is conducted to assess the variability of the equivalent post-peak tensile strength for SFRC with 1.0% and 1.5% steel fibres as given in Figures 6.4 and 6.5. It is clear that the crack width used to determine the post-peak tensile strength influences its value. Generally, for the greater crack width the rate of change in post peak-strength is minimal as compared to small crack widths. It should be noted that the shape of the graphs depends solely on the experimental data realised from the splitting test. If direct tensile data with a steeper gradient just after cracking, followed by an almost flat curve was used, the shape of the graph may change.

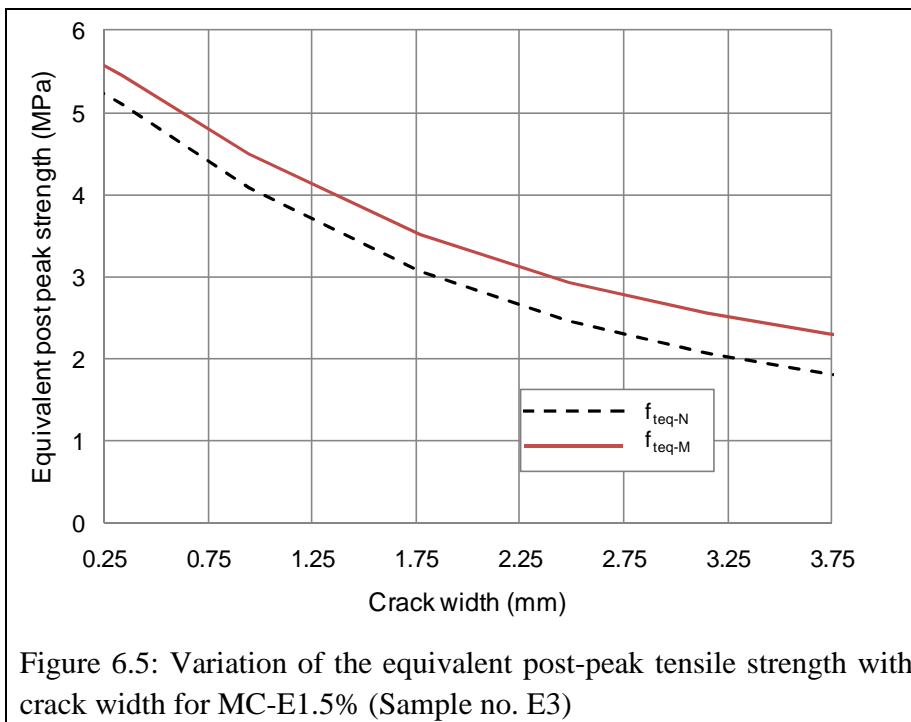
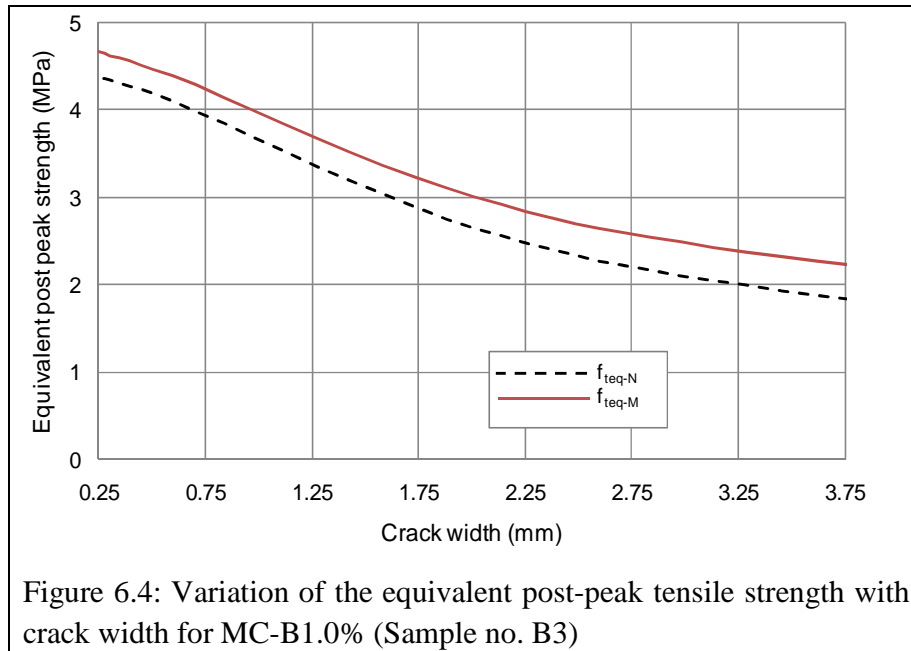


Table 6.21: Tension parameters for the model based on the Code definition

Combined sample group	n	Average strength (MPa)			Standard dev.		Characteristic strength (MPa)		
		f_{t-N}	f_{teq}	μ_u	f_{t-N}	f_{teq}	f_{tk-N}	f_{teqk}	μ_u
'MC-A0.0%'	7	3.38	-	-	0.21	-	3.01	-	-
'MC-B1.0%'	2	3.93	2.08	0.527	0.72	0.50	2.48	1.07	0.431
'MC-C1.0%'	4	3.88	1.87	0.481	0.17	0.28	3.57	1.33	0.373
'MC-D(or E)1.5%'	12	5.00	2.53	0.506	0.41	0.30	4.29	2.02	0.471
'MC-F0.0%'	6	3.42	-	-	0.29	-	2.91	-	-

Table 6.22: Tension parameters for the model based the theory of elasticity by Rocco *et al* (2001)

Sample group	n	Average strength (MPa)			Standard dev.		Characteristic strength (MPa)		
		f_{t-N}	f_{teq}	μ_u	f_{t-N}	f_{teq}	f_{tk-N}	f_{teqk}	μ_u
'MC-A0.0%'	7	3.60	-	-	0.22	-	3.20	-	-
'MC-B1.0%'	2	4.18	2.34	0.560	0.77	0.50	2.64	1.33	0.502
'MC-C1.0%'	4	4.12	2.17	0.526	0.18	0.29	3.79	1.62	0.428
'MC-D(or E)1.5%'	12	5.32	2.88	0.541	0.43	0.31	4.59	2.35	0.512
'MC-F0.0%'	6	3.64	-	-	0.31	-	3.10	-	-

Steel bar tensile parameters

Two types of steel bars were used in the experiment. While it was the intention of the author to have only one type, the supplied bars showed two distinct behaviours as illustrated in Chapter 5. The main parameters for model verification from this test are yield strength, yield strain and or Young's modulus (E_s) as given in Table 6.23. As stated in Chapter 5, the Young's modulus for both steel bar types is 200GPa. In addition to these parameters, the strain-hardening behaviour displayed that RB-II bars may also be useful in some analyses. For RB-II bars, the gradient of the post-yield stress-strain curve (E_{s1}) is 2.11GPa and may be used together with the ultimate strength and strain. The simplified stress-strain relations to be used for the analysis are bilinear stress-strain relations with perfect-plastic behaviour for RB-I bars and strain-hardening behaviour for RB-II bars (as shown for the typical behaviour in Figure 6.6).

Table 6.23: Tensile parameters for Y10 steel reinforcement

Sample name	n	Average strength (MPa)		Standard deviation		Characteristic strength (MPa)		Average strain		Post-yield E_{s1} (GPa)
		Yield f_{sy}	Ultimate f_u	f_{sy}	f_u	f_{sy}	f_u	ϵ_{sy}	ϵ_u	
RB-I	6	545.50	NA	11.51	NA	525.12	NA	0.0027	NA	NA
RB-II	6,5*	535.74	752.22	8.61	7.02	520.5	739.58	0.0027	0.1054	2.11

* Number of samples used for the determination of ultimate strength.

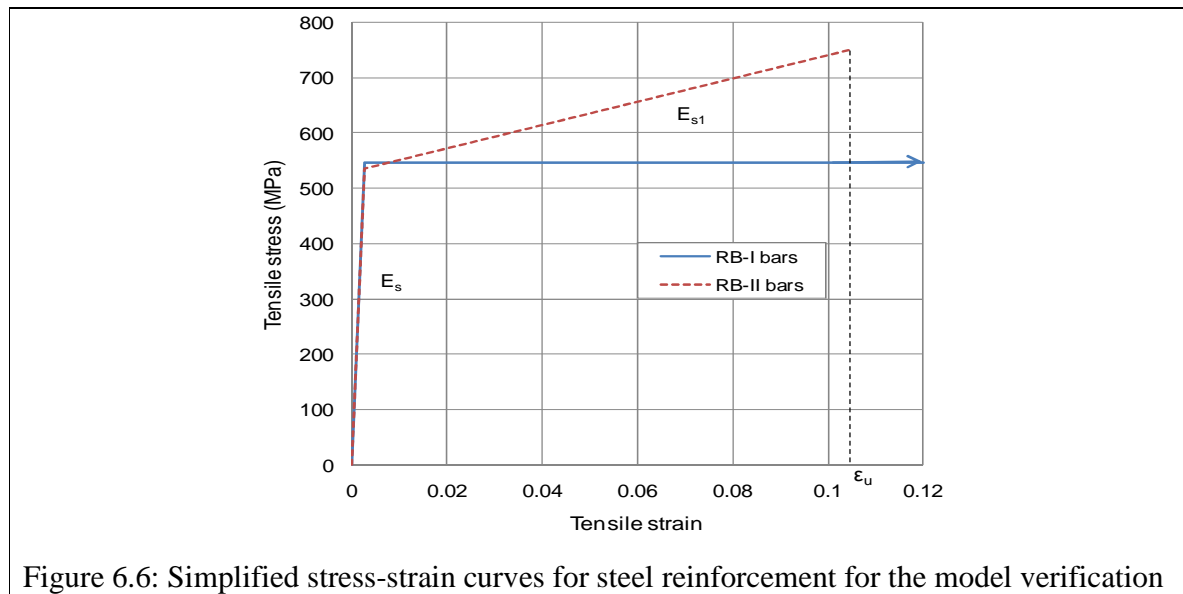


Figure 6.6: Simplified stress-strain curves for steel reinforcement for the model verification

6.5 INVERSE ANALYSIS FOR VERIFICATION OF TENSILE CONSTITUTIVE MODEL

Tensile behaviour of SFRC can be characterised by either direct methods or indirect methods. In this thesis, indirect tensile behaviour through the splitting test has been established. The use of the splitting test is widely accepted for the determination of the ultimate tensile strength of concrete (strength up to failure) but little information is available for the post-cracking parameters. The use of the splitting test for post-cracking behaviour may therefore need further research so that appropriate correction factors are used for the post-cracking parameters. In this section, the inverse analysis approach is used to verify the assumed constitutive model for tension (a drop-down constant tensile model) by varying the data obtained from the splitting tests. Since the post-cracking tensile strength in the drop down constant model is derived from the material toughness, a toughness dependent post-cracking material model by Hordijk (1991) has been adopted in the FEA in combination with elastic compression properties. Four-point bending results obtained from mixes PC1.0% and PC1.5% for standard beams as outlined in Section 5.2.3, are used for verification. The flowchart in Figure 6.7 shows the procedure followed in executing the inverse analysis procedure.

In this analysis, the value of tensile strength is kept constant (either using tensile strength from code definition or based on the elastic approach by Rocco *et al*) while changing the post-cracking parameters (toughness and equivalent post-peak tensile strength). The starting toughness values are those determined for mixes PC1.0% and PC1.5% as given in Chapter 5. Using DIANA, an iterative process is followed until the results from the numerical analysis fairly correlate well with the force-displacement curve obtained for the four-point flexural tests.

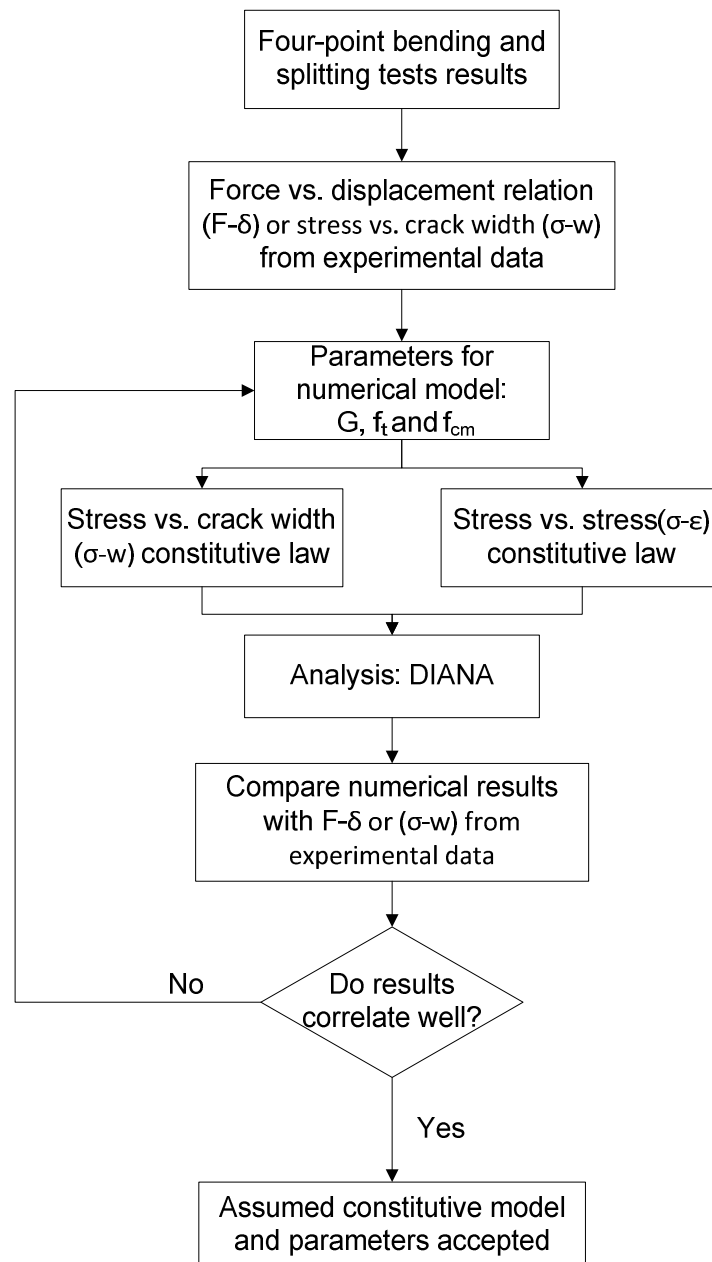


Figure 6.7: Inverse analysis procedure for constitutive model verification

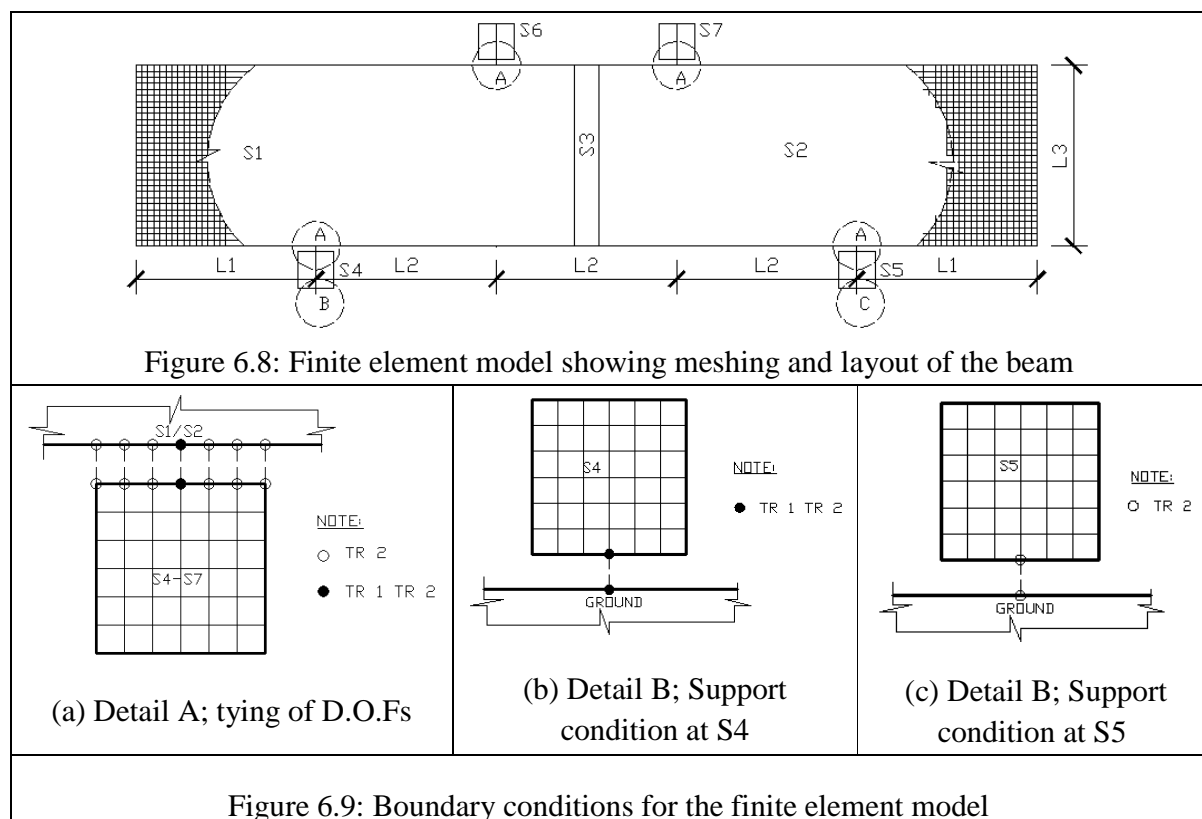
6.5.1 FINITE ELEMENT MODELLING APPROACH

Plane stress theory is applied in the development of the finite element models used in this research. During the four-point bending test for the standard beams only one visible crack developed up to failure. It is against this background that a weaker strip at the middle of finite element beam model is induced by ensuring that the surrounding elements have slightly higher model parameters than that of the middle strip.

Finite element model schematisation for the four-point bending

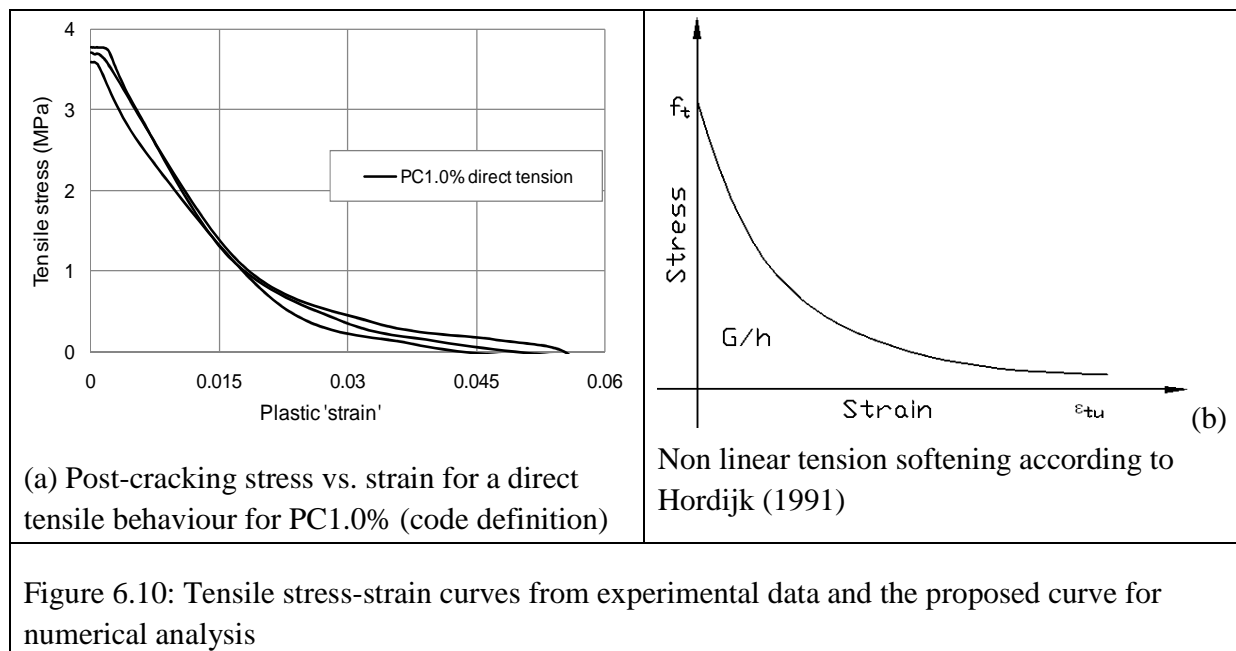
The beam element is subjected to two point loads (4-point bending) allowing the middle span of the beam to be subjected to an equal moment so that the weakest part will crack first. In order to induce development of a single crack, a strip of weaker elements is improvised into the finite element model along the mid section, denoted by S3 in Figure 6.8. Four-noded membrane elements 4mm x 4mm are used to model the standard beam. Points of contact for loading and supporting the beam are provided by use of a square metal rod (denoted by S4 -S7 in Figure 6.8) with contact width of 30mm representing bearings in the actual experimental set up.

Since the experiments are conducted on a simply supported beam, the model is developed to take this into account. The boundary conditions are provided such that the beam is allowed to move laterally. To achieve this only vertical translation is restrained at one node of one support (bottom left bearing). Boundary conditions are modelled to reflect to a greater extent the physical behaviour while ensuring development of structurally stable system. In this regard, some nodes provide restraint in vertical translation while others provide restraint in both lateral and vertical translation as indicated in the Figure 6.9. Furthermore, the connection between bearings and the beam is made such that the material in the beam at the bearing does not experience excessive stresses. This is done by tying degrees of freedom appropriately as shown in the figure.



Material modelling for Steel fibre-reinforced concrete

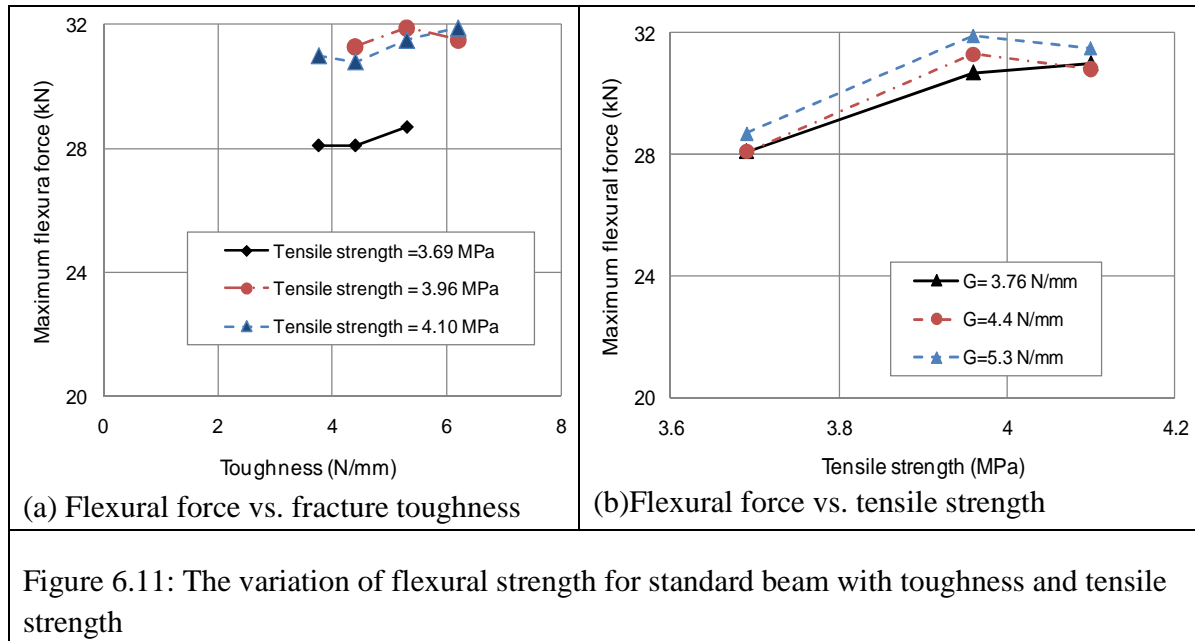
Steel fibre-reinforced concrete is modelled using a total strain model, with elastic-perfect plastic stress-strain law for compression, and Hordijk for tension. Note that for the elastic-perfect plastic compression model, the yield stress was assumed to be equal to the maximum compressive strength. Based on tension softening behaviour obtained from the tension tests carried out during characterisation test (given in Figure 6.10a) it was decided that the tension softening model according to Hordijk (1991) better represented the actual behaviour of the material in tension. The softening model developed by Hordijk requires that the material fracture energy and peak tensile strength be known as indicated in Figure 6.10(b).

**6.5.2 INVERSE ANALYSIS RESULTS AND EVALUATION**

Compression and tensile characterisation data obtained from PC1.0% and PC1.5% were used for a numerical model. Table 6.24 shows a matrix of parameters and cases studied in the numerical analysis in order to establish any correlation between flexural strength and characterisation parameters. Note that parameters from batch PC1.5% have been indicated with an asterisk (*). A preliminary analysis conducted to assess the effect of changing either the toughness or the tensile strength showed that the maximum flexural strength of a beam is more sensitive to the tensile strength than fracture toughness (see Figure 6.11).

Table 6.24: Program for the numerical analysis showing different cases

Fracture Toughness, G (N/mm)	f_{teq} (MPa)	Tensile strength, f_t (MPa)			
		3.69	3.96	4.57*	4.90*
3.76	1.89	A	-	F	-
4.4	2.21	-	D	-	I
4.87*	2.45	B	-	G	-
5.58*	2.81	-	E	-	J



With the trend obtained from the preliminary numerical analysis, only cases A, D, G and J are reported and their force vs. displacement curves compared with experimental data. Figures 6.12 and 6.13 compare the numerical solutions as obtained using toughness-dependent tensile model by Hordijk (1991) with the experimental data for PC1.0% and PC1.5% respectively. From the figures, two distinct issues arise, namely;

1. The numerical solution slightly over-predicts the flexural strength of the beams.
2. The numerical solution reliably predicts the stiffness of the beam up to peak strength. The post-peak behaviour as obtained from the numerical solution is less stiff while the experimental results show greater toughness after cracking.

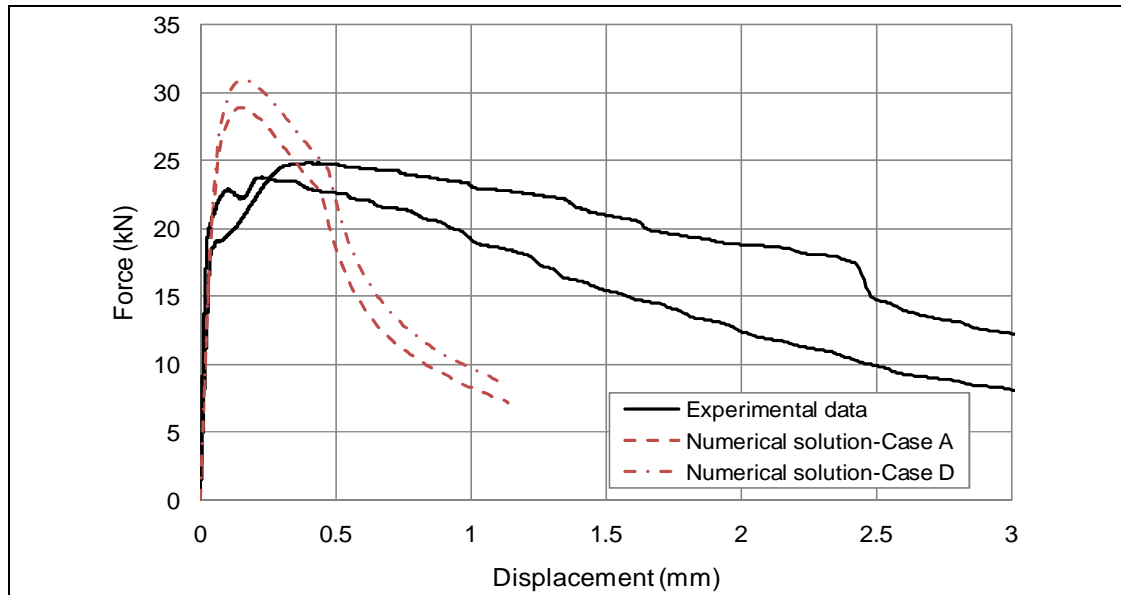


Figure 6.12: Comparison of the numerical solution with experimental data for PC1.0%

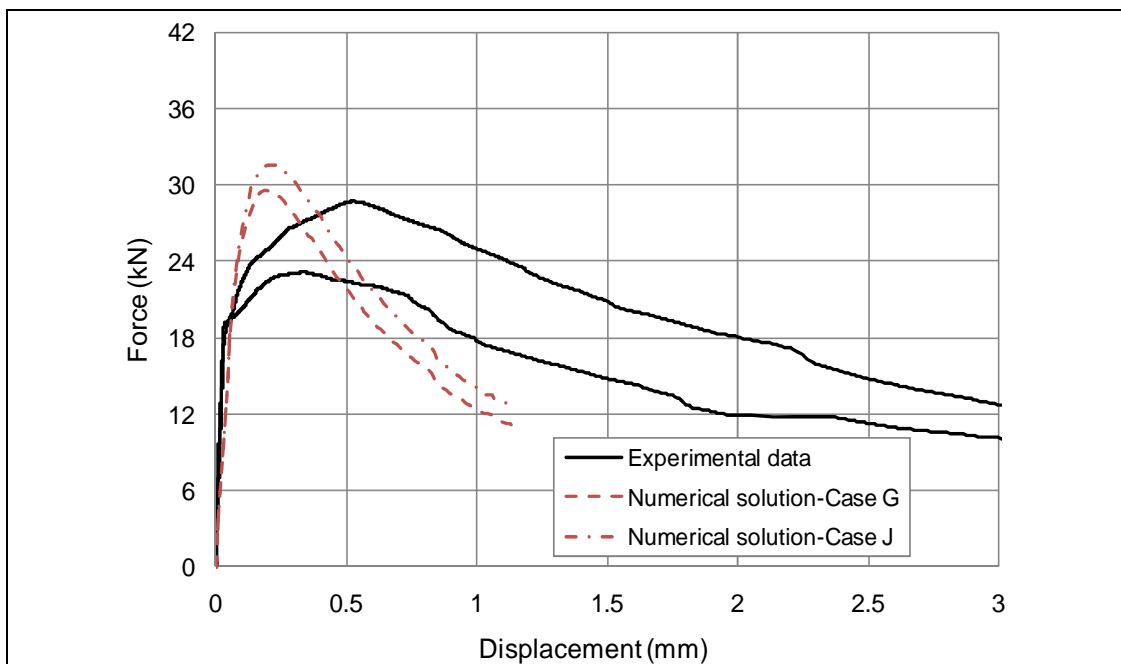
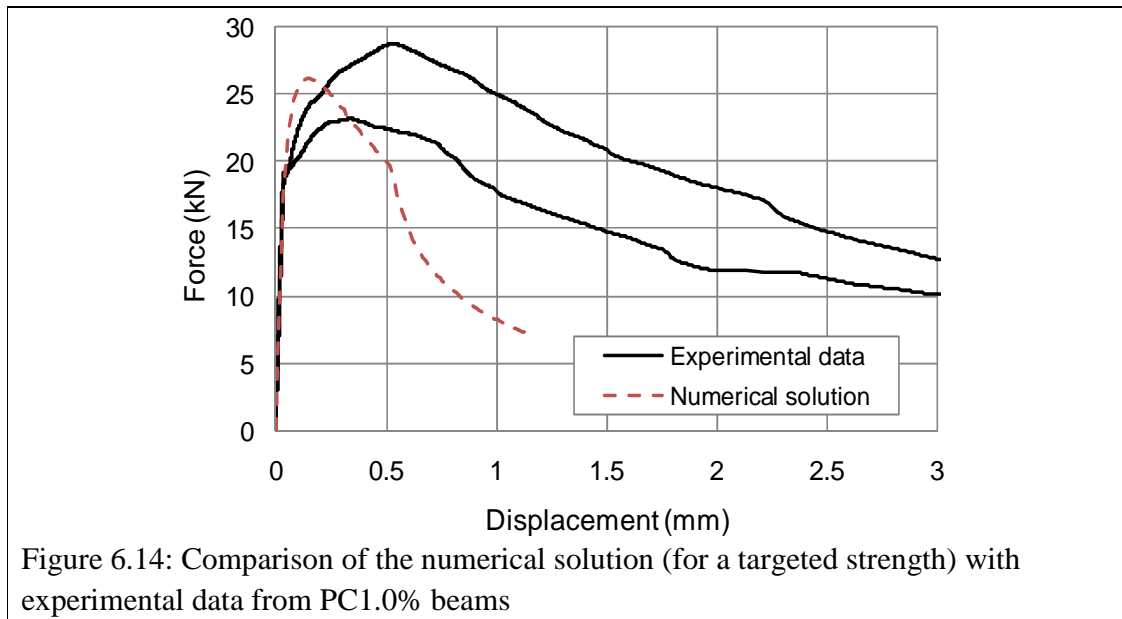


Figure 6.13: Comparison of the numerical solution with experimental data for PC1.5%

For a target average flexural strength of 25kN (for beams from batch PC1.0%), an iterative process was followed to determine appropriate tensile strength to be used in the analysis. A tensile strength of 3.3MPa was identified to closely predict the beam's flexural strength when tensile parameters derived from code definition are used (this was done by extrapolation of the results shown in Figure 6.11). Figure 6.14 compares the numerical solution derived from

the projected tensile strength with the experimental data for PC1.0% beam. From the results, it is clear that in order to reliably predict the flexural strength of the beam, a lower value for the tensile strength is required. For the beam's post-peak stiffness, greater toughness values may be required. It should be noted, however, that the post-peak behaviour obtained in a numerical analysis may be affected by the material model used. In this case, an appropriate tensile model that fairly represents the tensile behaviour of SFRC may be ideal.

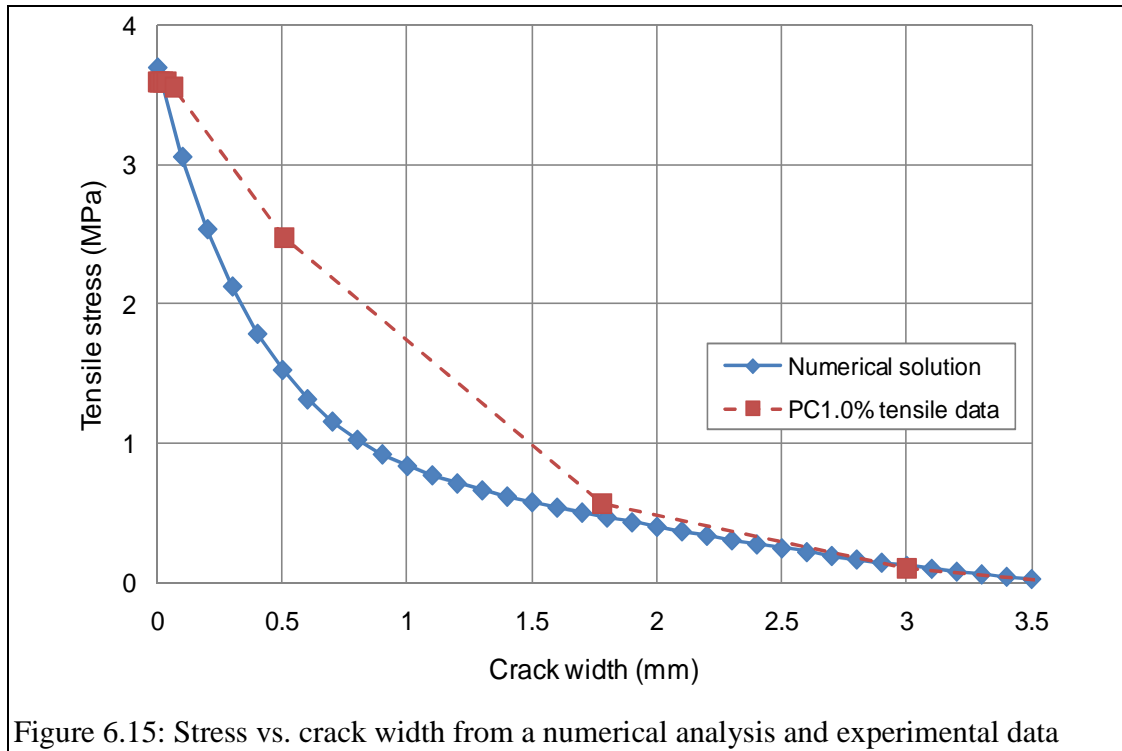


From numerical analysis on a four-point bending test reported in this section, the higher stiffness in the analysis after cracking may be attributed to the following factors:

- (i) compressive hardening which is not included in the simplified bilinear-rectangular compression model used in the numerical analysis (see compression stress vs. strain curves given in Figure 5.1);
- (ii) there may also be some tensile hardening before the peak (cracking) which is not included in the simple tensile model used in the numerical analysis; and
- (iii) there may be a few smaller cracks in the experimental beam, which are also dissipating energy, and reducing the stiffness before the peak.

In order to assess whether the selected tensile model (Hordijk) used in the numerical analysis closely reflects the tensile behaviour derived from the splitting test, a simple one element test was conducted in DIANA. An elastic-plastic model for compression with yield strength of 34.06MPa and an elastic behaviour up to peak tensile strength followed by tension softening defined by Hordijk for tension softening were used. A single element, 1mm x 1mm supported to allow uniaxial (x) lengthening and Poisson (y-direction shortening) and subjected to uniaxial tension (x-direction) under displacement control was used. Figure 6.15 compares the results from the numerical analysis with the experimental data. Note that parameters from PC1.0% were used

in the analysis and the stress vs. crack width from experimental data is based on code definition approach. The stress vs. crack width relation from the numerical analysis correlates well with experimental results with the exception of tensile toughening just after cracking. The numerical model shows less toughness as compared to the experimental results for the initial portion of the curve.



6.6 ANALYSIS OF MODEL VERIFICATION EXPERIMENTAL DATA

Force-deflection results from four-point bending tests on main beams have been investigated in Chapter 5. For these results to be used for model verification, the flexural failure mode is a prerequisite. Therefore, a few cases highlighted in this section represent results from beams which failed in flexure. From the force-displacement behaviour outlined in Chapter 5, moment-displacement curves for the selected beams are drawn in this section. Moment has been applied for comparison because of variations in the loading point for some beams. The position of the resultant force of the reaction from the inner face of the support is given by a factor, α_b , determined from a FEA using DIANA as given in Appendix C. From the distribution of reaction forces at nodes of a finite element model developed, a value of 0.3 for α_b is determined for both cracking and maximum load applied to the beams. Since it is difficult to assess the position of the resultant reaction for all data points, the factor of 0.3 is assumed and used for all data points.

6.6.1 FLEXURAL BEHAVIOUR FOR REINFORCED CONCRETE BEAMS WITHOUT STEEL FIBRES

Two mixes, MB2-A0.0% and MB2-F0.0%, were used as control experiments and only contained reinforcing bars without steel fibres. During the flexural tests, the beams MB2-A0.0% had loading points spaced at 0.15m away from nearest supports, while beams MB2-F0.0% had the loading spacing from the nearest support of 0.2m, as given in Chapter 4. A comparison of the typical flexural behaviour of beams from these two sample groups is shown in Figure 6.16, where moment vs. displacement is used. Moments for the beams are calculated using Equation 4.15 with applied load recorded from the bending test used. Note that total displacement is used for MB2-A0.0% beams while effective displacement is employed for MB2-F0.0%. Therefore, comparison is made on moment values only without referring to displacements.

Beam F1 shows a better flexural response than A1 with both cracking and ultimate strength greater than that of A1. This could be attributed to greater compressive strength properties of concrete for mix with beams MB-F0.0%, as reported in Section 5.2.1. Note that MC-A0.0% and MC-F0.0% are mixes for material characterisation for mixes MB2-A0.0% and MB2-F0.0% respectively. In Sample no. F1, flexural results were obtained up to failure, while post-peak behaviour is evident in Sample A1. Two phases of flexural behaviour up to failure can be deduced from the moment–displacement curves. The first portion is linear up to cracking moment and thereafter a nonlinear phase starts and continues up to the point of failure. The main sources of nonlinearity are crack formation, but slipped bolted connections of the test frame in the case of beam F1, where the total mid-span movement of the Instron cross-head is plotted on the horizontal axis, also contributes. Despite these differences in the deformation measure, the force measurement is reliable and used for further analysis.

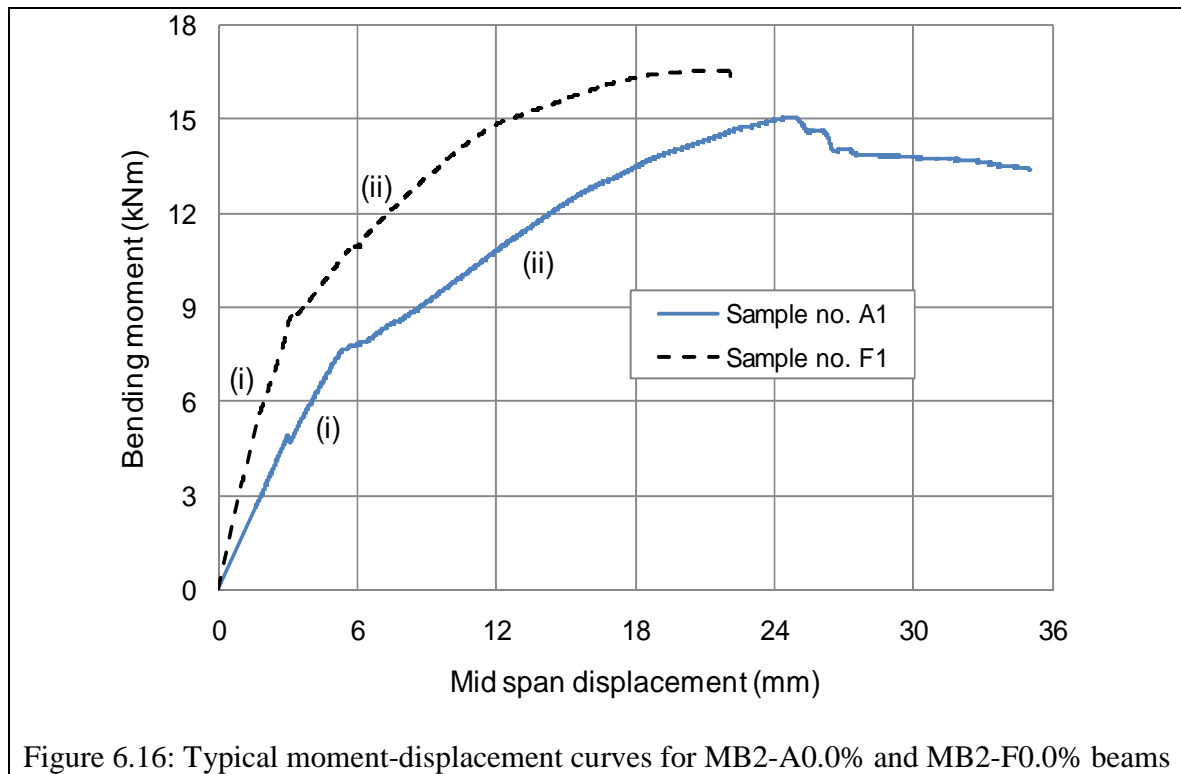


Figure 6.16: Typical moment-displacement curves for MB2-A0.0% and MB2-F0.0% beams

6.6.2 FLEXURAL BEHAVIOUR FOR STEEL REINFORCED CONCRETE BEAMS

Two mixes, MB0-C1.0% and MB-E1.5%, were used to establish the flexural behaviour of SFRC beams without reinforcing bars. The loading points for all beams in this section were spaced at 0.20m away from the inner face of the nearest support (as given in Chapter 4). Moments for the beams are calculated using Equations 4.15 with applied load recorded from the bending test used. Note that total displacement is used for MB0-C1.0% beams while effective displacement is used for MB0-E1.5%. Therefore, a comparison is made on moment values only, without referring to displacements.

Figure 6.17 shows that both beams exhibit almost an elastic response up to maximum flexural strength, beyond which the flexural capacity reduces at different rates. Both beams have almost equal flexural capacities, with beam E2 showing better post-cracking behaviour (part of the curve that is beyond maximum flexural capacity). The reason for better post-cracking behaviour for beam E2 may be better post-cracking tensile properties and higher compressive strength of concrete as outlined in Section 5.2 (note that MC-C1.0% and MC-E1.5% are mixes for material characterisation for mixes MB0-C1.0% and MB0-E1.5% respectively).

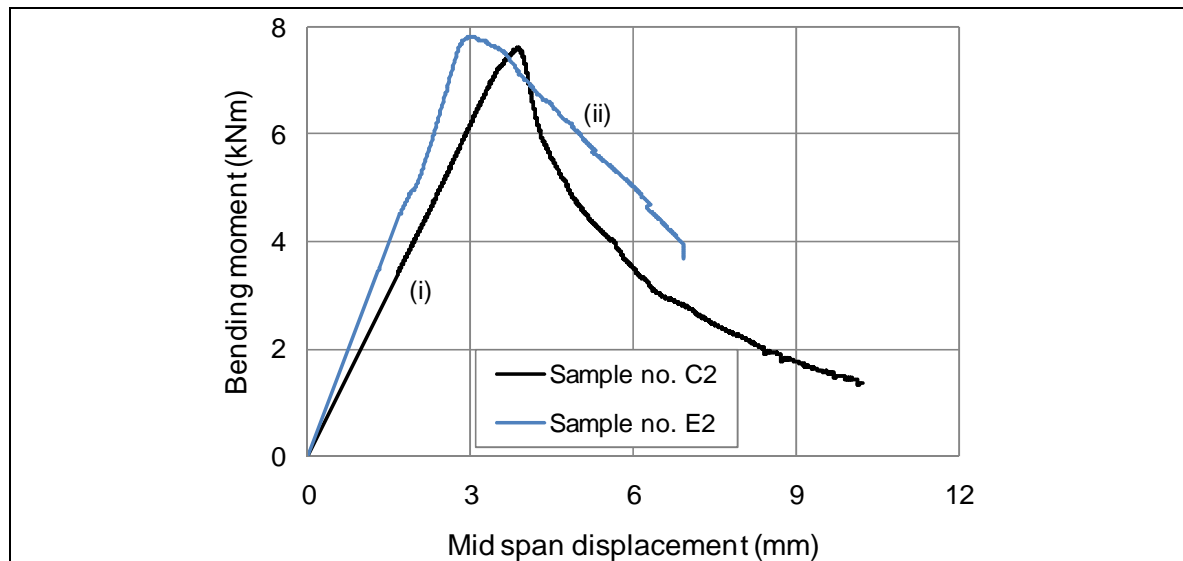


Figure 6.17: Typical moment-displacement curves for MB0-C1.0% and MB0-E1.5% beams

6.6.3 FLEXURAL BEHAVIOUR FOR SFRC BEAMS WITH REINFORCING BARS

Two mixes, MB2-B1.0% and MB2-D1.5%, were used to establish the flexural behaviour of SFRC beams with reinforcing bars. For these two mixes the amount of steel reinforcement was kept constant (2Y10 RB-II bars), while varying the amount of steel fibres (1.0% and 1.5%). During the flexural tests, the beams MB2-B1.0% had loading points spaced at 0.15m away from the inner face of the nearest supports, while beams MB2-D1.50% had the loading spacing from the nearest support of 0.2m, as given in Chapter 4. The position of the resultant force of the reaction from the inner face of the support is given by a factor of 0.3 for both the cracking and the maximum forces respectively, as determined from DIANA (see Appendix C). A comparison of the typical flexural behaviour of beams from these two sample groups is shown in Figure 6.18, where moment vs. displacement is used. Moments for the beams are calculated using Equation 4.15 with applied load recorded from the bending test used. Note that total displacement is used for MB2-B1.0% beams, while effective displacement is used for MB2-D1.50%.

Beam B1 has a greater maximum flexural capacity while beam D3 has a greater cracking moment, as denoted by the point where the curve shows considerable change in gradient (see Figure 6.18). The greater cracking value in beam D1 could be attributed to the greater compressive and tensile strength properties of concrete for mix with beams MB2-D1.50%, as reported in Section 5.2 of material characterisation of the two mixes (note that MC-B1.0% and MC-D1.5% are mixes for material characterisation for mixes MB2-B1.0% and MB2-D1.5% respectively). A lower maximum moment in beam D3 might be due to the use of RB-I bars, which have less superior strength properties, especially after the yielding of the steel bars (this information could not be verified as no such data was available on the type of rebar used in Sample no. D3). In Sample no. D2, flexural results were obtained up to failure, while some post-peak behaviour was evident in Sample no. B1. Two phases of flexural behaviour up to failure

can be deduced from the moment–displacement curves. The first portion is linear up to cracking moment and thereafter a nonlinear phase starts and continues up to the point of failure. The source of nonlinearity is the development of cracks. It should be noted that the total mid-span movement of the Instron cross-head is plotted on the horizontal axis for beam B1 hence the difference in stiffness. Despite these differences in the deformation measure, the force measurement is reliable and used for further analysis.

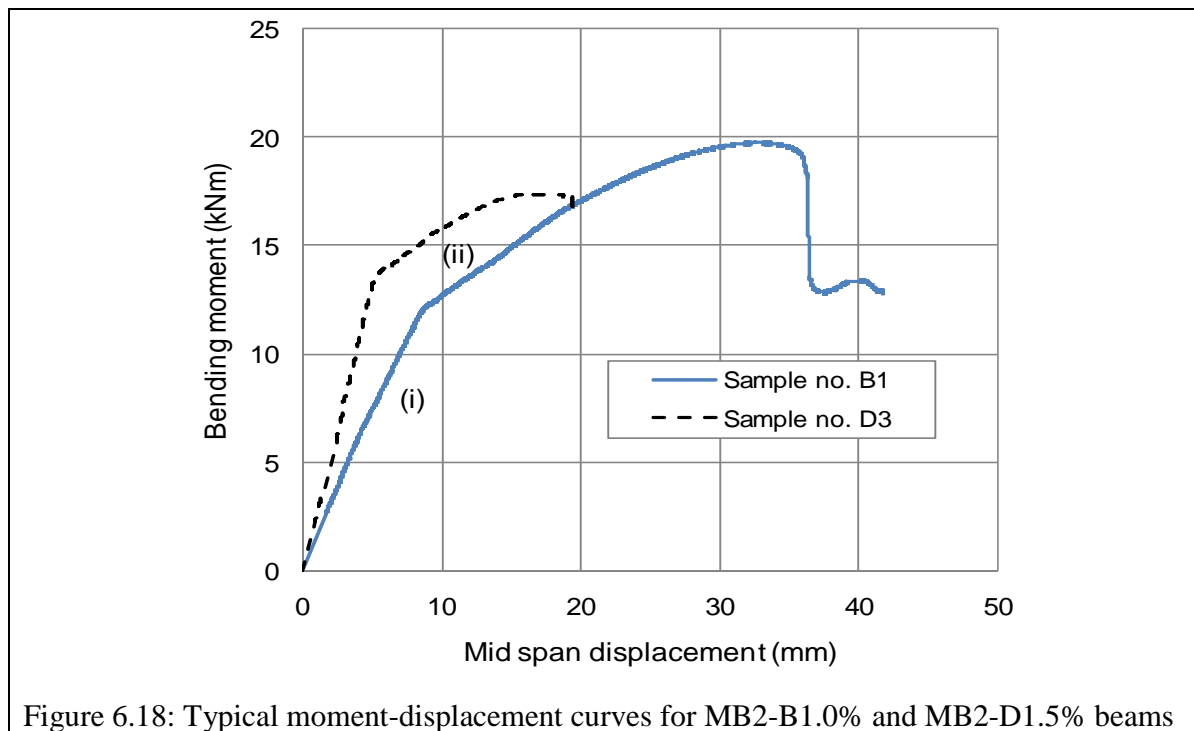


Figure 6.18: Typical moment-displacement curves for MB2-B1.0% and MB2-D1.5% beams

6.7 CONCLUSION

Parameters for model verification have been determined and analysed from both physical and statistical perspectives. Based on engineering reasoning and statistical analysis, some samples have been combined to represent the same population. Concrete Batch C belongs to concrete Class C16/20, Batches A and B can be combined as they seem to belong to the same population, concrete Class C20/25. Batches D, E and F can also be combined to represent a single population, concrete Class C25/30. With this variation in compressive strength, the use of normalised values may be helpful in evaluating the moment capacity predictions across the concrete classes. By assessing data originating from the same population, an increased amount of characterisation data has been obtained in some instances. This ensures that characterisation properties of the material are more representative. The overall statistical data properties have been used to determine characteristic parameters to be used in model verification as outlined in Chapter 7.

Compression strengths show greater variability as compared to tensile strengths which were more consistent. While use of cubes generates stress confinement which affects the compression

and tensile properties of concrete, a possible variation in the physical properties of the constituents of concrete may have affected the properties of concrete. Stress confinement results in greater values for concrete compression properties. A conversion factor may be used for compression strength but there is no such provision for the Young's modulus and such greater values determined may still be used in subsequent analysis. Equivalent post-peak tensile strengths used in the drop-down model have been established. Since the post-peak tensile strength depends on the toughness and crack width at which it is evaluated, the variation in the value of the post-peak tensile strength with crack width shows a greater change at small crack widths, with a reduced rate of change at large crack widths. It is clear that for proper use of the drop-down model, it is ideal to determine the equivalent post-peak strength based on the anticipated crack width (i.e. there can be different values for service stress and ultimate stresses). In the case of the proposed analytical models for flexural capacity of SFRC with reinforcing bars, it is possible to determine and vary the equivalent post-peak strengths depending on the anticipated strains.

An attempt was made to verify the constitutive model adopted for tension (the drop-down constant model) by an inverse analysis. Since the post-cracking parameters in the drop down model are derived from fracture toughness, a tensile model developed by Hordijk(1991) was used. For the clearly defined modelling strategy, material models, finite element size, loading arrangement and simplified support conditions adopted, a particular result was found. The numerical solution does not clearly agree with the experimental results. Some tentative trends (Figure 6.11) have been established which may be useful for the development of more accurate finite element analyses in the future. The numerical analysis results show that the tensile strength derived from code definition may have to be reduced in order for the model to reliably predict the flexural strength of the beam. However, experimental data showed better ductility than the numerical solution.

Analysis of the results from the main beams for flexural verification highlighted a challenge: the size of the beams was generally so small that any error in the measurement of loading spacing could result in substantial difference in the calculated bending moments. In this regard, care has been taken to ensure that a reasonable value is used for the calculation of bending moments. This was achieved by conducting a non linear finite element analysis (FEA) using DIANA, ensuring that the contribution of the bearing strip on the supports to the overall length for the determination of bending moments is ascertained. Results and analysis of the finite element model is reported in Appendix C. Comparison of moment capacities shows that concrete with greater material strength as characterised in Section 5.2, has greater flexural behaviour. This is observed both at cracking and at ultimate for all beams, except for MB2-B1.0% and MB2-D1.5%, where such trend is only observed at cracking but the beams show minimal differences in maximum flexural strengths. The only possible explanation is the possibility of combining RB-I and RB-II bars in the beams.

CHAPTER 7. MODEL VERIFICATION AND DISCUSSIONS

7.1 INTRODUCTION

This chapter verifies the proposed analytical models using the experimental data. Two analytical models for the determination of the bending moment capacity of SFRC have been proposed in Chapter 3. These are flexural models for SFRC with and without reinforcing bars. In addition to the moment capacity prediction for SFRC with reinforcing bars, analytical models for the determination of concrete's moments at cracking, yielding of steel bars and maximum tensile strength of steel bars have been outlined in Chapter 3. In this chapter these models are verified using experimental results. Control experiments were carried out for normal reinforced concrete. This has been done to assess the accuracy of both the characterisation properties and the current analytical model for normal reinforced concrete, as the new models are developed based on the same principles. It is against this background that an evaluation of the flexural capacity of the normal reinforced concrete beams is given first.

In addition to verification using experimental data obtained in this research, the proposed models are compared with current models available in literature. From Chapter 2, it is clear that some of the models available in literature do not require the post-cracking experimental characterisation of SFRC, but rather use analytical expressions to determine the post-peak strength. Wherever possible, the use of analytical expressions for the determination of the post-cracking strength will be implemented and compared with values found in this research.

7.2 FLEXURAL BEAM CAPACITY FOR REINFORCED CONCRETE-2Y10

Chapter 2 indicated that the analytical models for flexural capacity of a reinforced concrete beam section are based on strain compatibility and force equilibrium. Moment capacity for normal reinforced concrete is usually given by

$$M = A_s f_{sy} \left(d - \frac{a}{2} \right) \quad 7.1$$

where $a = \frac{A_s f_{sy}}{0.85 f'_c b}$ and f'_c is ultimate uniaxial cylinder compressive strength, and the

assumption has been made that the rebar has reached yield stress.

The value of a can also be determined from a force equilibrium equation, ignoring the factor 0.85 in Equation 7.1 accounting for (a) differences between standard testing on the cylinders and strength development in the beams (in-situ), and (b) long term effects.

$$\eta_{cd} f'_c \lambda_{cd} x b = A_s f_y \Leftrightarrow a = \lambda_{cd} x = \frac{A_s f_{sy}}{\eta_{cd} b f'_c} \quad 7.2$$

where λ_{cd} and η_{cd} are equivalent stress block conversion factors given as 0.8 and 1.0 respectively for $f_{ck} \leq 50\text{MPa}$ in EN 1992-1-1.

In laboratory conditions where both the beams and the cubes were subjected to similar exposure conditions, the value of a as given in Expression 7.2 will be used.

Since cube strength has been used in experiments in this thesis, ultimate uniaxial cylinder compressive strength will be replaced with $0.8f_{cu}$ as adopted in SABS 0100 (2000), to account for the difference between standard testing on cubes and cylinders.

For these beams, $d = 117\text{mm}$ and $A_s = 157\text{mm}^2$ and other material parameters are given in Table 7.1, along with other input parameters for the model. Mean values are supplied for the two batches, while characteristic values (where appropriate) are shown in brackets. Note that for steel bars, Young's modulus of 200GPa is used throughout. These parameters represent MB2-A0.0% and MB2-F0.0%. From the experimental results of the flexural capacity of these beams, it was observed that concrete crushed in compression in all these beams.

Table 7.1: Model input parameters for MB2-A0.0% and MB2-F0.0% beams

Sample group	Concrete properties			Steel bar
	Compressive strength (MPa)	Tensile strength (MPa)	Young's modulus (GPa)	Yield strength (MPa)
MB2-A0.0%	31.9 (28.9)	3.38(3.01)	32.3	535.7(520.5)
MB2-F0.0%	36.6(33.4)	3.42(2.91)	34.8	535.7(520.5)

Using the material parameters from Table 7.1 in Equation 7.1, the predicted moment capacities for the beams using both mean and characteristic parameters are given in Table 7.2. Table 7.3 summarises both the cracking moments and the ultimate moments determined from experiments and compare them with the predictions obtained from Table 7.2. At cracking, only the Young's modulus and tensile strength contribute to the concrete cracking moment. The greater the ratio of the concrete's Young's modulus to steel bars' Young's modulus the greater the neutral axis depth which may result in an increased the predicted cracking strength. A greater tensile strength increases the cracking strength of the beam. The tensile strengths from both sample groups do not differ significantly, but their Young's modulus differs, resulting in MB2-A0.0%, predicted to have a slightly better cracking strength contrary to our expectation from the experimental results. This case indicates the sensitivity of the Young's modulus in obtaining a reliable value for cracking strength. The model for cracking moment over-predicts the cracking moment by an average of 30% and 46% when characteristic and mean parameters are used respectively for beams MB2-A0.0%; and it over predict the cracking moment by an average of 2% and 20% when characteristic and mean parameters are used respectively for beams MB2-F0.0%. The maximum moment (or rather the moment at yielding of steel bars) is however under-predicted by 39% and 41% for beams MB2-A0.0% and MB2-F0.0% respectively when mean values are used.

When either mean values or characteristic values are used, the analytical models under-predict the maximum moment capacity of the beam. For example, in MB2-A0.0%, the model under-predicts the moment capacity by an average of 39%-41%, while in MB2-F0.0% it under-predicts by an average of 41% to 43%. Generally, there is a slight difference in the predicted moment when either mean values or characteristic values are used. This may be due to narrow scatter of material characterisation parameters as observed in the coefficients of variations reported in

Chapter 5. It should be noted that the prediction model for ultimate strength assumes the following:

- steel bars yield;
- the post yield strength remains constant; and
- yielding strength makes the moment when steel yields the same as the ultimate moment.

All of these factors may account for very low predicted moment capacity for these beams.

Table 7.2: Predicted moment capacity for MB2-A0.0% and MB2-F0.0% beams

Sample group	Cracking moment (kNm)		Compression block depth, a (mm)		Ultimate moment (kNm)	
	Mean	Characteristic	Mean	Characteristic	Mean	Characteristic
MB2-A0.0%	10.64	9.48	11.00	11.80	9.38	9.08
MB2-F0.0%	10.56	8.99	9.58	10.21	9.44	9.15

Table 7.3: Comparison of experimental and predicted moment capacity for MB2-A0.0% and MB2-F0.0% beams

Sample no.	Cracking moment (kNm)		$M_{cr(pred)}/M_{cr(exp)}$		Ultimate moment (kNm)		$M_{u(pred)}/M_{u(exp)}$	
	MB2-A0.0%	MB2-F0.0%	MB2-A0.0%	MB2-F0.0%	MB2-A0.0%	MB2-F0.0%	MB2-A0.0%	MB2-F0.0%
1	6.93	8.51	1.54(1.37)	1.24(1.06)	15.06	16.42	0.62(0.60)	0.57(0.56)
2	7.37	8.74	1.44(1.29)	1.21(1.03)	16.4	15.63	0.57(0.55)	0.60(0.59)
3	7.55	9.20	1.41(1.26)	1.15(0.98)	14.97	15.96	0.61(0.59)	0.59(0.57)
Mean	7.28	8.82	1.46(1.30)	1.20(1.02)	15.48	16.00	0.61(0.59)	0.59(0.57)
Std Dev.	0.319	0.351	-	-	0.801	0.397	-	-
CoV	0.044	0.040	-	-	0.052	0.025	-	-

7.3 FLEXURAL BEAM CAPACITY FOR SFRC

Beams tested under this category are MB0-C1.0% and MB0-E1.5%; representing 1.0% steel fibres and 1.5% steel fibres respectively. As discussed in Chapter 6, the material characterisation properties for PC1.0%, MC-D1.5% and MC-E1.5% have been combined to provide more accurate statistical data as the properties have been deemed to belong to the same population. In addition to the use of the combined properties, individual material characterisation properties are also used and compared with the combined properties to assess whether such a combination improves the accuracy of prediction of the model. Flexural models proposed in Chapter 3 are used to predict the cracking moment, moments at yielding and ultimate strength of steel bars and moments at ultimate tensile and compression strength of SFRC. Equations defined in Section 3.3.1 are used to calculate moment capacity for the SFRC beam. It should be noted that a factor of 0.8 is used to convert cube compressive strengths to cylinder compressive strengths.

7.3.1 FLEXURAL BEAM CAPACITY FOR SFRC WITH 1.0% STEEL FIBRES-MB0-C1.0%

Table 7.4 gives the material characterisation parameters to be used for beams in Batch C and the predicted ultimate moment. As noted in Chapter 6, no sample combination was done for Batch C. Post-peak tensile strength has been replaced with normalised post-peak strength, μ_u , (given by $\mu_u = f_{teq} / f_{tk}$). Young's modulus of 42.5GPa, ultimate tensile strain and ultimate compressive strain of 0.025 and 0.0035 respectively, are used for both characteristic values and mean values (see Section 6.4). Note that relevant compressive yield strains are used in either characteristic or mean parameters. In the prediction of the moment capacity, analytical models using the tensile strength parameters are used and are given in Table 7.4.

Table 7.4: Model input parameters for SFRC beams, MB0-C1.0%

Parameter	Tension properties			Compression, cube	Ultimate moment
	f_t (MPa)	μ	ϵ_{ty}	f_c (MPa)	M_{pred} (kNm)
Mean value	3.88	0.480	0.00009	25.6	5.77
Characteristic	3.57	0.378	0.00008	24.1	4.20

Table 7.5 gives the ultimate moments determined from experiments and compares them with the predictions obtained from Table 7.4. When either mean values or characteristic values are used, the analytical models under-predict the moment capacity. In Table 7.5 comparison is made only for tension derived moment values. The results indicate that the model under-predicts by an average of 1.0% when mean values are used, while it under-predicts by an average of 28% when characteristic values are used. The difference may be attributed to poor characterisation properties used for the model prediction and the greater scatter of characterisation properties as observed in the coefficient of variations given in Chapter 5. The simplicity of the models used (compression bilinear model and tension drop-down model) and the uncertainty of relations between standard test strength measures and the strength developed in the beams could also contribute to the difference in predicted values and the experimental values obtained.

Table 7.5: Comparison of experimental and predicted moment capacity for MB0-C1.0% beams

Sample	Ultimate moment (kNm)	M_{pred} / M_{exp} (mean)	M_{pred} / M_{exp} (characteristic)
1	6.09	0.95	0.69
2	5.92	0.97	0.71
3	5.50	1.05	0.76
Mean	5.84	0.99	0.72
Std Dev.	0.304	-	-
CoV	0.052	-	-

7.3.2 FLEXURAL BEAM CAPACITY FOR SFRC WITH 1.5% STEEL FIBRES

Table 7.6 illustrates the material characterisation parameters for combined MC-E1.5% and MC-D1.5% and the predicted ultimate moment from the MB0-E1.5% beams. The material characterisation parameters from MC-E1.5% only and the predicted ultimate moment from the MB0-E1.5% beams are indicated by Table 7.7. Post-peak tensile strength has been replaced by normalised post-peak strength, μ , as defined in Equation 7.4. Young's modulus of 32.7GPa for the combined sample group, 31.9GPa for MC-E1.5%, ultimate tensile strain and ultimate compressive strain of 0.025 and 0.0035 respectively are used for both characteristic values and mean values (refer to Section 6.4 of Chapter 6). Note that relevant compressive yield strains are used in both characteristic and mean parameters. The predictions for both the combined and the single sample group cases are consistent. There is a reduction in the predictions from characteristic values when combined sample parameters are used, probably due to reduced tensile parameters and an increased coefficient of variation realised after combining the sample groups.

Table 7.6: Model predictions using the combined characterisation parameters for MB0-E1.5% beams

Parameter	Tension properties			Compression, cube	Ultimate moment
	f_t (MPa)	μ	ϵ_{ty}	f_c (MPa)	M_{pred} (kNm)
Mean value	5.00	0.506	0.00015	41.35	7.91
Characteristic	4.29	0.471	0.00013	39.54	6.39

Table 7.7: Model predictions for MB0-E1.5% using characterisation parameters from batch MC-E1.5% only

Parameter	Tension properties			Compression, cube	Ultimate moment
	f_t (MPa)	μ	ϵ_{ty}	f_c (MPa)	M_{pred} (kNm)
Mean value	5.17	0.485	0.00016	41.20	7.85
Characteristic	4.82	0.475	0.00015	39.23	7.19

Table 7.8 shows the ultimate moments determined from experiments and compares those with the predictions obtained from Tables 7.6 and 7.7. When mean values are applied, the analytical model over predicts by an average of 8% and 9% for single and combined sample groupings respectively. When characteristic values are used, the analytical models under-predict the moment capacity. For example, the model under-predicts by an average of 12% and 1% for the combined and the single sample groups respectively. The difference may be attributed to poor characterisation properties drawn upon for the model prediction, in addition to the simplicity of the models used (compression bilinear model and tension drop-down model) and the uncertainty of relation between standard test strength measures and the strength developed in the beams. Sample no. E3 has lower flexural capacity when compared to other samples.

Table 7.8: Comparison of the experimental and predicted moment capacity for MB0-E1.5% beams

Sample	Ultimate moment(kNm)	M_{pred}/M_{exp}		M_{pred}/M_{exp}	
		(Combined sample groups case)		(single sample group case)	
		(mean)	(characteristic)	(mean)	(characteristic)
1	7.83	1.02	0.82	1.00	0.92
2	7.72	1.02	0.83	1.02	0.93
3	6.38	1.23	1.00	1.23	1.13
Mean	7.31	1.09	0.88	1.08	0.99

7.4 FLEXURAL BEAM CAPACITY FOR REINFORCED SFRC

Beams tested under this category are MB2-B1.0% and MB2-D1.5%. As discussed in Chapter 6, the material characterisation properties for PC1.0%, MC-D1.5% and MC-E1.5% have been combined to demonstrate improved statistical data as the properties have been deemed to belong to the same population. Hence, values from Table 7.6 will be used for MB2-D1.5% in addition to single group properties given for each case.

As outlined in Section 3.3.3, there are five different moment values that can be determined based on the considered strain state. The following states can be defined as strain states: when concrete cracks in tension (M_{cr}), when ultimate tensile strain of concrete is reached (M_{ut}), when ultimate compression strain of concrete is reached (M_{uc}), when yielding strain of steel bars is reached (M_y) and when ultimate strain of steel bars is reached (M_p). It should be noted that these analytical models illustrated in Section 3.3.3 only predict possible bending moments at prescribed strain levels during loading of the beam. In providing reinforcement for a beam, a slightly different analytical model is used, ensuring that both the compression and tensile capacity of concrete are fully used before collapse of the section.

7.4.1 FLEXURAL BEAM CAPACITY FOR R-SFRC WITH 1.0% STEEL FIBRES, 2Y10-MB2-B1.0%

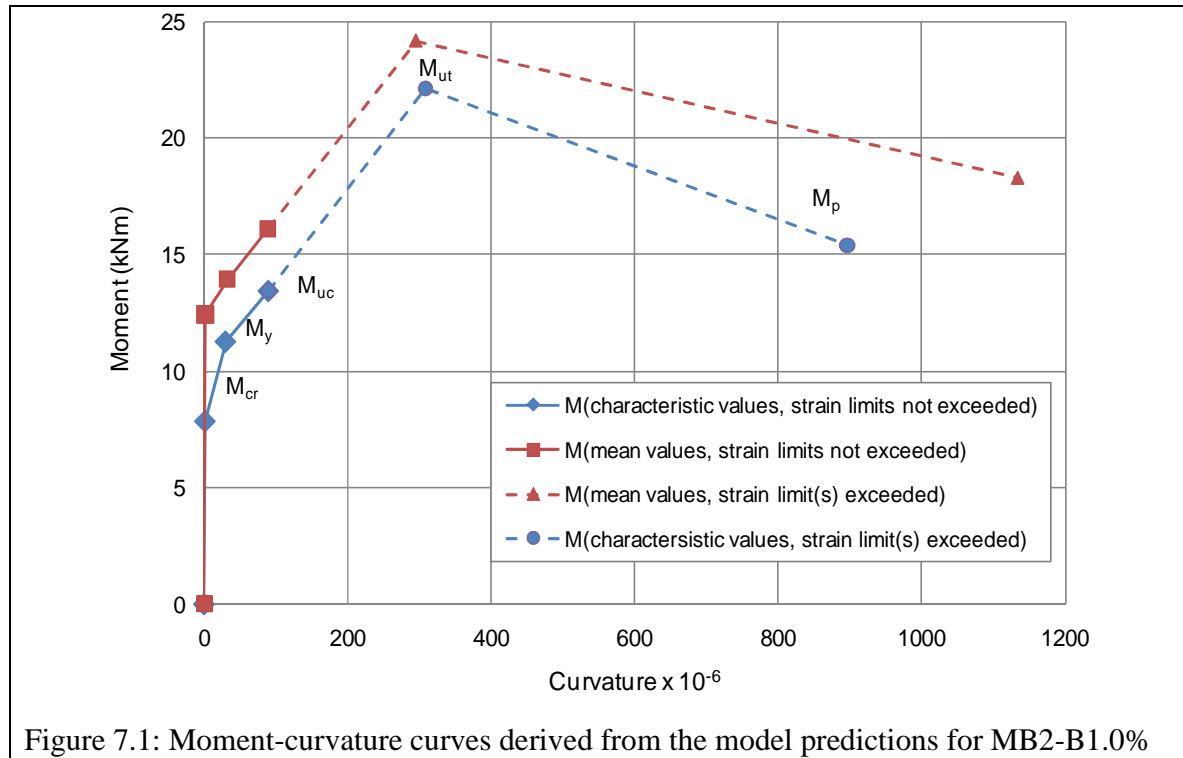
Five moment values for beams MB2-B1.0% are determined using the analytical models proposed in Section 3.3.3. These moments are: at cracking, at yielding of steel bars, at ultimate tensile strength of SFRC, at ultimate compression strength of SFRC and at ultimate strength of steel bars. Both the mean input parameters and the results from the analytical model are given in Table 7.9, while characteristic values are given in brackets. From the Table 7.9, the cracking moment has a least value while the moment at the ultimate tensile strength of SFRC has the largest value. Moment capacity when steel bars reach ultimate strength has a lower value than M_{ut} , but a greater value than both the cracking and the steel yielding moments. The values of M_{ut} is reached after concrete exceeded its ultimate compression strain of 0.0035, while the value of M_p is reached after exceeding the ultimate tensile and compression strains of SFRC of 0.025 and 0.0035 respectively. With the limiting strains exceeded in the prediction of both M_{ut} and M_p , it is likely that the actual maximum capacity for the beam lies between M_y and M_{ut} , with the value of

the ultimate tensile strain of concrete properly adjusted to ensure that the ultimate compression strain is not exceeded. Therefore, the value of M_{uc} may be taken as the ultimate moment capacity of the beam section. There is an increase in the curvature as the moment values change from M_{cr} to M_p through M_y and M_{ut} . The moment vs. curvature relation is illustrated in Figure 7.1. This illustration indicates that the stiffness of the beam reduces when the beam cracks and further reduces when steel yields. This reduction in stiffness was observed in the analysis of the experimental data as given in Chapter 6.

Table 7.9: Model input parameters and moment predictions for MB2-B1.0% beams

Parameter	Parameters for M_{cr}	Parameters for M_y	Parameters for M_{uc}	Parameters for M_{ut}	Parameters for M_p
f_c -cube(MPa)	NA	34.68(30.36)	34.68(30.36)	34.68(30.36)	34.68(30.36)
ϵ_{cy} ($\times 10^{-3}$)	NA	0.88(0.77)	0.88(0.77)	0.88(0.77)	0.88(0.77)
ϵ_{cu} ($\times 10^{-3}$)	NA	NA	3.50	NA	NA
f_t (MPa)	3.93(2.48)	3.93(2.48)	3.93(2.48)	3.93(2.48)	3.93(2.48)
ϵ_{ty} ($\times 10^{-3}$)	0.12(0.08)	0.12(0.08)	0.12(0.08)	0.12(0.08)	0.12(0.08)
E_c (GPa)	31.68	31.68	31.68	31.68	31.68
ρ_g (%)	0.35	NA	NA	NA	NA
A_s (mm ²)	NA	157	157	157	157
f_{sy} (MPa)	NA	535.74(520.50)	535.74(520.50)	535.74(520.50)	NA
ϵ_{sy} ($\times 10^{-3}$)	NA	2.68(2.60)	2.68(2.60)	2.68(2.60)	NA
E_s (GPa)	200	200	200	200	200
E_{s1} (GPa)	NA	NA	2.1	2.1	2.1
μ	NA	0.524(0.429)	0.524(0.429)	0.524(0.429)	0.524(0.429)
ϵ_{tu} ($\times 10^{-3}$)	NA	NA	NA	25.00	NA
f_s (MPa)	-	-	544.31(529.56)	562.15(546.20)	-
ϵ_s ($\times 10^{-3}$)	-	-	6.87(6.91)	15.25(14.84)	-
$\epsilon_{(tu)}$ ($\times 10^{-3}$)	-	3.73(3.58)	9.80(9.85)	-	142.83(114.64)*
ϵ_c ($\times 10^{-3}$)	0.13(0.08)	1.04(0.88)	-	19.31(21.18)*	27.30(19.80)*
Curvature ($\times 10^{-6}$)	1.7(1.1)	31.8(29.7)	88.7(89.0)	295.0(308.0)	1134.2(896.2)
M_{pred} (kNm)	12.44(7.85)	13.93(11.27)	16.09(13.44)	24.16(22.13)	18.28(15.39)

* Strain limits exceeded.



Both the cracking moment and maximum moment of the experimental data have been demonstrated. Table 7.10 shows the values of cracking moments and ultimate moments determined from experiments, and compares them with the predictions obtained from Table 7.6. When mean values are used for predicting the cracking moment, the model over-predicts by an average of 7%, while under-prediction of the cracking moment by an average of 32% occurs when characteristic values are used. At ultimate moment capacity of the section, the model under-predicts the maximum moment capacity by an average of 13% and 27% when mean values and characteristic values are used respectively.

Table 7.10: Comparison of the experimental and the predicted moment capacity for MB2-B1.0% beams

Sample no.	Moments from experiment (kNm)		$\frac{M_{cr-pred}}{M_{cr-exp}}$		$\frac{M_{u-pred}}{M_{u-exp}}$	
	M_{cr-exp}	M_{u-exp}	(mean)	(characteristic)	(mean)	(characteristic)
B1	12.2	19.81	1.02	0.64	0.81	0.68
B2	11.93	18.30	1.04	0.66	0.88	0.73
B3	11.61	17.54	1.16	0.73	0.92	0.77
Mean	11.61	18.55	1.07	0.68	0.87	0.73

7.4.2 FLEXURAL BEAM CAPACITY FOR R-SFRC WITH 1.5% STEEL FIBRES, 2Y10-MB2-D1.5%

MB2-D1.5% beams were used to verify the proposed models for reinforced SFRC outlined in Section 3.3.3. Moment predictions are derived from two cases, namely using combined characterisation parameters and using characterisation parameter for Batch MB2-D1.5% only. Using the combined characterisation properties, the mean input parameters and results from the analytical models are summarised in Table 7.11, while characteristic values are shown in brackets. Table 7.13 summaries the input parameters and results from analysis of the analytical models using characterisation parameters for Batch MB2-D1.5% only.

Predictions for the combined characterisation parameters

From the five moment values taken at different strains, the cracking moment has a least value, while the moment at the ultimate tensile strength of SFRC has the largest value with the exception of the yielding moment prediction from mean model parameters. Moment capacity when steel bars reach ultimate strength has a lower value than M_{ut} but greater than both the cracking and the steel yielding moments. The value of M_{ut} is reached after concrete exceeded its ultimate compression strain of 0.0035, while the value of M_p is reached after exceeding the ultimate tensile and compression strains of SFRC (0.025 and 0.0035 respectively). With the limiting strains exceeded in the prediction of both M_{ut} and M_p , it is likely that the maximum capacity for the beam lies between M_y and M_{ut} . The value of the ultimate tensile strain of concrete must be properly adjusted to ensure that the ultimate compression strain is not exceeded as is provided by M_{uc} . There is an increase in the curvature as the moment values change from M_{cr} to M_p through M_y and M_{ut} . Moment vs. curvature relation is illustrated in Figure 7.2. From Figure 7.2, it is clear that the model could not ably predict the decrease in stiffness as the section cracks as denoted by gradient of the line connecting cracking and steel yielding moments (circled portion in Figure 7.2). This may be attributed to the uncertainties inherent in the model input parameters.

Flexural Modelling of Steel Fibre-Reinforced Concrete With and Without Steel Bars

Table 7.11: Model input parameters and moment predictions for MB2-D1.5% beams using the combined characterisation parameters

Parameter	Parameters for M_{cr}	Parameters for M_y	Parameters for M_{uc}	Parameters for M_{ut}	Parameters for M_p
f_c (MPa)	NA	41.35(39.54)	41.35(39.54)	41.35(39.54)	41.35(39.54)
ϵ_{cy} ($\times 10^{-3}$)	NA	1.01(0.97)	1.01(0.97)	1.01(0.97)	1.01(0.97)
ϵ_{cu} ($\times 10^{-3}$)	NA	NA	3.50	NA	NA
f_t (MPa)	5.00(4.29)	5.00(4.29)	5.00(4.29)	5.00(4.29)	5.00(4.29)
ϵ_{ty} ($\times 10^{-3}$)	0.15(0.13)	0.15(0.13)	0.15(0.13)	0.15(0.13)	0.15(0.13)
E_c (GPa)	32.66	32.66	32.66	32.66	32.66
ρ_g (%)	0.35	NA	NA	NA	NA
A_s (mm ²)	NA	157	157	157	157
f_{sy} (MPa)	NA	535.74(520.50)	535.7(520.5)	535.7(520.5)	NA
ϵ_{sy} ($\times 10^{-3}$)	NA	2.68(2.60)	2.68(2.60)	2.68(2.60)	NA
f_u (MPa)	NA	NA	NA	NA	752.22(739.58)
ϵ_u ($\times 10^{-3}$)	NA	NA	NA	NA	105.40(85.06)
E_s (GPa)	200	200	200	200	200
E_{s1} (GPa)	NA	NA	2.1	2.1	2.1
μ	NA	0.506(0.471)	0.506(0.471)	0.506(0.471)	0.506(0.471)
ϵ_{tu} ($\times 10^{-3}$)	NA	NA	NA	25.00	NA
f_s (MPa)	-	-	545.34(530.69)	563.55(548.30)	-
ϵ_s ($\times 10^{-3}$)	-	-	7.36(7.46)	15.92(15.84)	-
$\epsilon_{(tu)}$ ($\times 10^{-3}$)	-	3.73(3.61)	10.43(10.55)	-	142.10(114.30)*
ϵ_c ($\times 10^{-3}$)	0.16(0.13)	1.06(0.98)	-	16.29(16.64)*	24.72(18.75)*
Curvature ($\times 10^{-6}$)	2.1(1.8)	32.0(30.6)	92.9(93.6)	275.0(278.0)	1112.2(887.2)
M_{pred} (kNm)	15.70(13.47)	15.09(13.64)	17.61(16.19)	25.08(23.92)	19.80(18.24)

* Strain limits exceeded.

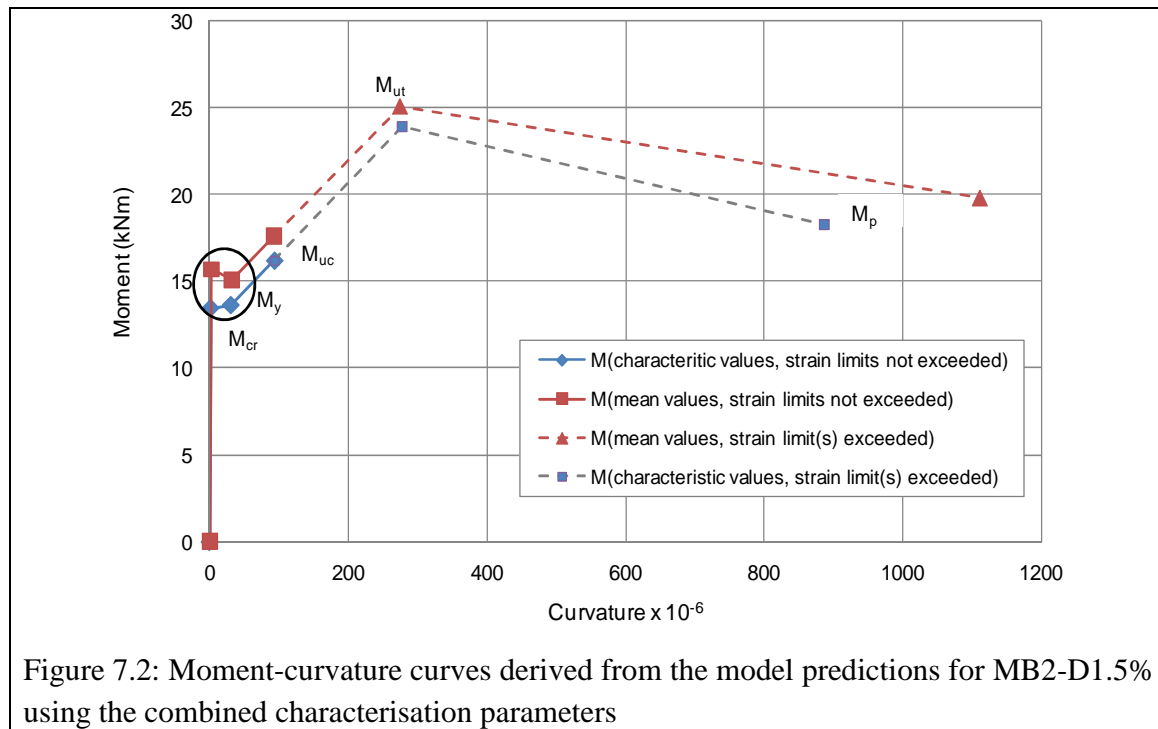


Table 7.12 explains the cracking moment and the ultimate moment determined from experiments and compares with the predictions obtained from Table 7.11. When mean values are used for predicting the cracking moment, the model over-predicts by an average of 8%, while when characteristic values are used, it under-predicts the cracking moment by an average of 5%. At ultimate moment capacity of the section, the model over-predicts the maximum moment capacity by an average of 6% when mean values are used, while it under-predicts by an average of 2% when characteristic values are used.

Table 7.12: Comparison of the experimental and the predicted moment capacity for MB2-D1.5% beams using the combined characteristic parameters

Sample no.	Moments from experiment (kNm)		$\frac{M_{cr(pred)}}{M_{cr(exp)}}$		$\frac{M_{u(pred)}}{M_{u(exp)}}$	
			(mean)	(characteristic)	(mean)	(characteristic)
D1	13.80	17.00	1.14	0.98	1.04	0.95
D2	13.80	17.11	1.14	0.98	1.03	0.95
D3	16.10	17.39	0.98	0.84	1.02	0.93
Mean	14.57	17.17	1.08	0.93	1.03	0.94

Predictions using characterisation parameters from Batch MC-D1.5%

From the five moment values taken at different strains, the cracking moment has the smallest value, while the moment at the ultimate tensile strength of SFRC has the largest value with the exception of the yielding moment prediction from mean model parameters. Moment capacity

when steel bars reach ultimate strength has a lower value than M_{ut} but greater than both the cracking and the steel yielding moments. The value of M_{ut} is reached after concrete exceeded its ultimate compression strain of 0.0035, while the value of M_p is reached after exceeding the ultimate tensile and compression strains of SFRC (0.025 and 0.0035 respectively). With the limiting strains exceeded in the prediction of both M_{ut} and M_p , it is likely that the maximum capacity for the beam lies between M_y and M_{ut} . The value of the ultimate tensile strain of concrete must be properly adjusted to ensure that the ultimate compression strain is not exceeded as is provided by M_{uc} . There is an increase in the curvature as the moment values change from M_{cr} to M_p through M_y and M_{ut} . Moment vs. curvature relation is illustrated in Figure 7.3. From Figure 7.3, it is clear that the model could not ably predict the decrease in stiffness as the section cracks as denoted by gradient of the line connecting cracking and steel yielding moments (circled portion in Figure 7.3). This may be attributed to the uncertainties inherent in the model input parameters.

Table 7.13: Model parameters and moment predictions for MB2-D1.5% beams using characterisation parameters from MC-D1.5% only

Parameter	Parameters for M_{cr}	Parameters for M_y	Parameters for M_{uc}	Parameters for M_{ut}	Parameters for M_p
f_c (MPa)	NA	41.20(39.60)	41.20(39.60)	41.20(39.60)	41.20(39.60)
ϵ_{cy} ($\times 10^{-3}$)	NA	0.98(0.94)	0.98(0.94)	0.98(0.94)	0.98(0.94)
ϵ_{cu} ($\times 10^{-3}$)	NA	NA	3.50	NA	NA
f_t (MPa)	5.09(4.74)	5.09(4.74)	5.09(4.74)	5.09(4.74)	5.09(4.74)
ϵ_{ty} ($\times 10^{-3}$)	0.15(0.14)	0.15(0.14)	0.15(0.14)	0.15(0.14)	0.15(0.14)
E_c (GPa)	33.75	33.75	33.75	33.75	33.75
ρ_g (%)	0.35	NA	NA	NA	NA
A_s (mm ²)	NA	157	157	157	157
f_{sy} (MPa)	NA	535.74(520.50)	535.7(520.5)	535.7(520.5)	NA
ϵ_{sy} ($\times 10^{-3}$)	NA	2.68(2.60)	2.68(2.60)	2.68(2.60)	NA
f_u (MPa)	NA	NA	NA	NA	752.22(739.58)
ϵ_u ($\times 10^{-3}$)	NA	NA	NA	NA	105.40(85.06)
E_s (GPa)	200	200	200	200	200
E_{s1} (GPa)	NA	NA	2.1	2.1	2.1
μ	NA	0.521(0.501)	0.521(0.501)	0.521(0.501)	0.521(0.501)
ϵ_{tu} ($\times 10^{-3}$)	NA	NA	NA	25.00	NA
f_s (MPa)	-	-	545.23(530.35)	563.48(548.17)	-
ϵ_s ($\times 10^{-3}$)	-	-	7.31(7.30)	15.88(15.78)	-
$\epsilon_{(tu)}$ ($\times 10^{-3}$)	-	3.73(3.62)	10.36(10.34)	-	142.29(114.74)*
ϵ_c ($\times 10^{-3}$)	0.15(0.14)	1.06(1.01)	-	16.44(16.92)*	25.40(20.16)*
Curvature ($\times 10^{-6}$)	2.0(1.9)	32.0(30.8)	92.4(92.3)	276.0(279.0)	1118.0(899.3)
M_{pred} (kNm)	15.84(14.75)	15.41(14.50)	17.87(16.98)	25.33(24.65)	20.09(19.12)

* Strain limits exceeded.

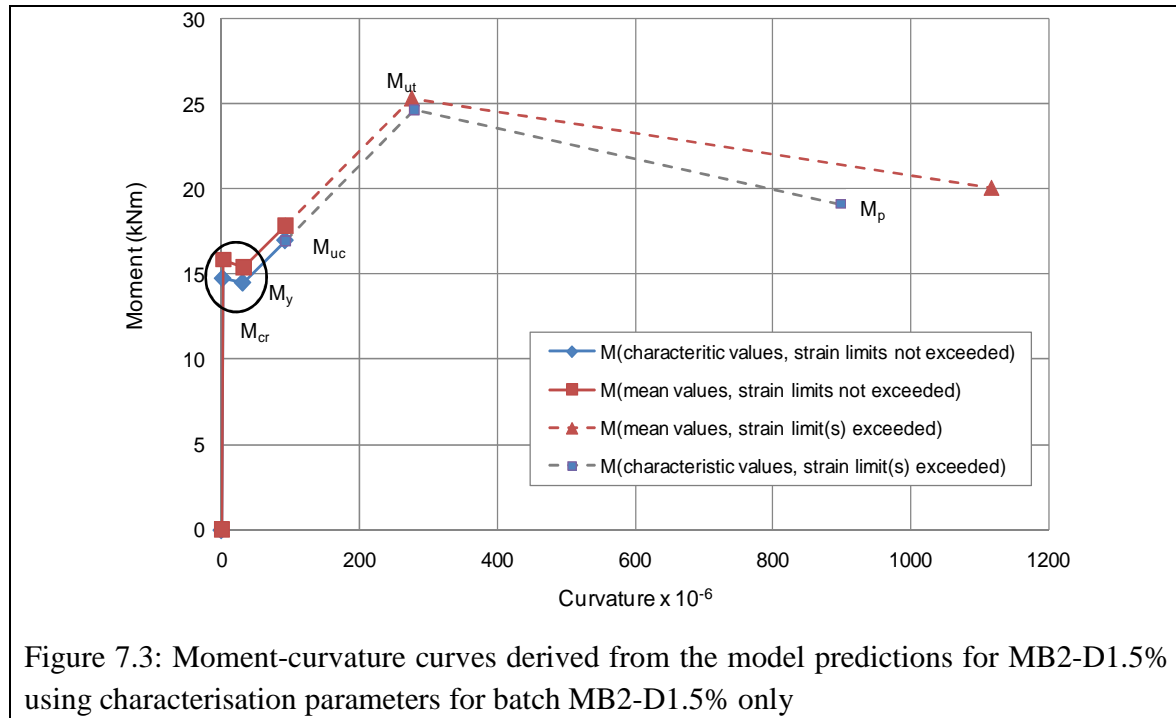


Table 7.14 explains the cracking moment and the ultimate moment determined from experiments and compares with the predictions obtained from Table 7.13. When mean values are used for predicting the cracking moment, the model over-predicts by an average of 9% , while when characteristic values are used, it over-predicts the cracking moment by an average of 2%. At ultimate moment capacity of the section, the model over-predicts the maximum moment capacity by an average of 4% when mean values are used, while it under-predicts by an average of 1% when characteristic values are used.

Table 7.14: Comparison of the experimental and the predicted moment capacity for MB2-D1.5% beams using characterisation parameters from MC-D1.5% only

Sample no.	Moments from experiment (kNm)		$\frac{M_{cr-pred}}{M_{cr-exp}}$		$\frac{M_{u-pred}}{M_{u-exp}}$	
	M_{cr-exp}	M_{u-exp}	(mean)	(characteristic)	(mean)	(characteristic)
D1	13.80	17.00	1.15	1.07	1.05	1.00
D2	13.80	17.11	1.15	1.07	1.04	0.99
D3	16.10	17.39	0.98	0.92	1.023	0.98
Mean	14.57	17.17	1.09	1.02	1.04	0.99

7.5 COMPARISON OF THE MODEL PREDICTION WITH OTHER MODELS

The proposed model for predicting the flexural capacity for SFRC is compared with models developed by Namaan (2003) and that of Soranakom and Mobasher (2009). In this section, two sets of data will be used: experimental data derived from the author's experiments and experimental data acquired from literature. The flexural model proposed for reinforced SFRC

will be compared with the models developed by Tan *et al* (1995) and Henager and Doherty (1976) reported in Chapter 2. Models proposed by all these authors except Soranakom and Mobasher use empirical formulae to derive the ultimate post cracking tensile strength, σ_{pc} . It is against background that post cracking tensile strength is determined first.

7.5.1 DETERMINATION OF POST CRACKING TENSILE STRENGTH USING EMPIRICAL METHODS

The post cracking tensile strength will be determined using two expressions outlined in Chapter 2. Recall that the post-cracking tensile strength as defined by Naaman (2003) is given by Equation 2.2 while that developed by Li *et al* (1990, 1992a) is given by Equation 2.4 given in Chapter 2 rewritten here as follows:

$$\sigma_{pc} = \frac{\lambda_{pc} \tau V_f l_f}{d_f} \quad (\text{Naaman, 2003})$$

$$\sigma_{pc} = \frac{1}{2} g \tau V_f \frac{l_f}{d_f} \quad (\text{Li et al, 1990 and 1992a})$$

Note that the factor, $\frac{1}{2}$ in the expression by Li *et al* represents fibre orientation for randomly distributed fibres in 3D. The snagging factor, g , is taken as 2.0 for steel fibres (Li *et al*, 1990 and 1992a) and the bond strength is taken as 5.1MPa for hooked steel fibres (Suwannakarn 2009). The value of the efficient factor, λ_{pc} , varies depending on the steel fibre content as outlined by Suwannakarn (2009). Using expressions for steel fibres given in Table 2.1, the values of are 2.024 and 1.746 for fibre volumes of 1.0% and 1.5% respectively. Table 7.15 gives the post-cracking tensile strength derived from the empirical expressions.

Table 7.15: The post-cracking tensile strength for SFRC derived from the empirical expressions

Expression	σ_{pc} for $V_f = 1.0\%$	σ_{pc} for $V_f = 1.5\%$
Naaman (2003)	6.19	8.01
Li <i>et al</i> (1990, 1992a)	3.06	4.59

From Table 7.15, it is clear that use of empirical expressions brings more uncertainties since the post-cracking tensile strength determined by these two expressions differ a lot. Use of the expression proposed by Naaman over estimates the tensile strength due to a higher value for efficiency factor λ_{pc} . This was also noted by Suwannakarn (2009).

7.5.2 COMPARISON OF THE PROPOSED SFRC FLEXURAL MODEL WITH OTHER MODELS

The flexural model proposed by Soranakom and Mobasher (2009) uses the same parameters as the current model. Table 7.16 shows comparison of these models based on data from literature, while Table 7.17 shows comparison of these models based on characterisation data for Batches C and E. From the results, it is clear that both the proposed model and the model developed by

Soranakom and Mobasher reliably predict the moment capacity. It is clear from the results given in the tables that the proposed model reasonably predicts the moment capacity of SFRC beams.

Table 7.16: Comparison of the current SFRC model with the model by Soranakom and Mobasher (2009) using experimental data from literature (Soranakom & Mobasher, 2009)

Mix	Fibre content kg/m ³	Model parameters			Bending moment (kNm)		
		f_{ck}, f_{tk} (MPa)	μ	ϵ_{ty} (%)	Current model	Model [*]	Expe. [**]
NSC	25	30.2, 3.5	0.31	0.011	4.19	4.25	4.64-5.34
NSC	50	26.6, 4.2	0.48	0.014	7.62	7.44	5.42-7.61
HSC	60	52.9, 6.2	0.5	0.016	11.65	11.71	9.6 -12.68

[*] Predictions based on Soranakom and Mobasher (2009).

[**] Experimental results for model verification reported by Soranakom and Mobasher (2009).

Table 7.17: Comparison of the current SFRC model with the model by Soranakom and Mobasher (2009) using current experimental data

Batch	Model parameters				Bending moment (kNm)		
	f_{ck}, f_{tk} (MPa)	μ	ϵ_{ty} (%)	ϵ_{cy} (%)	Current model	Model [*]	Exp.
C (mean)	20.48, 3.88	0.481	0.009	0.06	5.77	5.89	5.50-6.09
C(characteristic)	19.28, 3.57	0.373	0.008	0.06	4.20	4.26	5.50-6.09
E (mean)	32.96, 5.17	0.485	0.016	0.06	7.85	8.02	6.38-7.83
E (characteristic)	31.38, 4.82	0.475	0.015	0.04	7.19	7.32	6.38-7.83

[*] Predictions based on Soranakom and Mobasher (2009) model.

Flexural models proposed by Naaman (2003) uses post cracking strength derived from empirical expressions. Using the ACI rectangular stress block and triangular tensile stress profile as outlined in Section 2.4.2, moment predictions are determined. The Table 7.18 compares the moment predictions from the current model with that of Naaman (2003). Model input parameters for both models are also given in the table. Note that characteristic properties of concrete have been used.

Table 7.18: Comparison of the current SFRC model with the model by Naaman (2003)

Batch	Naaman (2003) Model			Current model	Experiment
	f_c (MPa)	σ_{pc} (MPa)	Moment (kNm)	Moment (kNm)	Moment (kNm)
C-characteristic	14.56	3.06	3.23	4.12	5.50-6.09
	14.56	6.19	6.13	4.12	5.50-6.09
E- characteristic	31.38	4.59	4.94	7.19	6.38-7.83
	31.38	8.01	8.35	7.19	6.38-7.83

7.5.3 COMPARISON OF THE PROPOSED R-SFRC FLEXURAL MODEL WITH OTHER MODELS

Flexural models for R-SFRC proposed by Henager and Doherty (1976), and Tan *et al* (1995) are outlined in Chapter 2. Only the model proposed by Henager and Doherty (1976) is considered as it is the only one that enables one to predict the flexural capacity of a beam while the model by

Tan et al (1995) is useful for provision of reinforcement only. The flexural model makes use of post cracking tensile strength derived from Equation 2.30. Assuming a bond efficiency of 1.2 for hooked steel fibres, the post cracking tensile strengths for 1.0% and 1.5% steel fibre volumes are 0.56MPa and 0.83MPa respectively. Table 7.19 summaries the moment predictions by the model based in characteristic values for model characterisation parameters derived from batches MC-B1.5% and MC-D1.5%. Note that the moment capacity can be taken as moment at yielding of steel bars as denoted by the use of yield strength of steel bars in the formula. The moment predicted using the flexural model by Henager and Doherty (1976) are more conservative compared to the current model. This is may be attributed to the small value of the tensile stress, σ_{tf} , determined using an empirical expression.

Table 7.19: Comparison of the current R-SFRC model with the model by Henager and Doherty (1976)

Batch	Henager and Doherty(1976) model				Current model	
	f_{ck} (MPa)	f_{sy} (MPa)	σ_{tf} (MPa)	A_s (mm ²)	Moment (kNm)	Moment, M_y (kNm)
B (characteristic)	24.29	520.50	0.56	157	10.36	11.27
D (characteristic)	31.68	520.50	0.83	157	11.22	14.50

7.6 STATISTICAL ASSESSMENT OF MODEL PREDICTIONS AND EXPERIMENTAL RESULTS

As discussed in Chapter 2, the bias of the model predictions can be assessed using statistical methods. This statistical procedure is possible for models whose predictions have been verified through experimental processes. In this case, models for prediction of the maximum moment capacity for SFRC without steel bars and flexural capacity of SFRC with reinforcement bars are assessed. Beams MB-C1.0% and MB-E1.5% have been used to derive experimental data against which the theoretical predictions for the flexural model of SFRC without steel bars are assessed. For flexural models of SFRC with reinforcing bars, beams MB2-B1.0% and MB2-D1.5% have been used. Using both results obtained from mean and characteristic model parameters scatter plots for the model predictions and experimental results are displayed in Figure 7.4 and 7.5. Only predictions at maximum moment capacity for the beams are considered. The gradients of the scatter plots, defined as ‘least square’ best fit to the scatter plot (δ_c), are indicated in each figure. The gradient of more than unity indicates that the model is conservative in predicting the bending moment of the beam.

Flexural Modelling of Steel Fibre-Reinforced Concrete With and Without Steel Bars

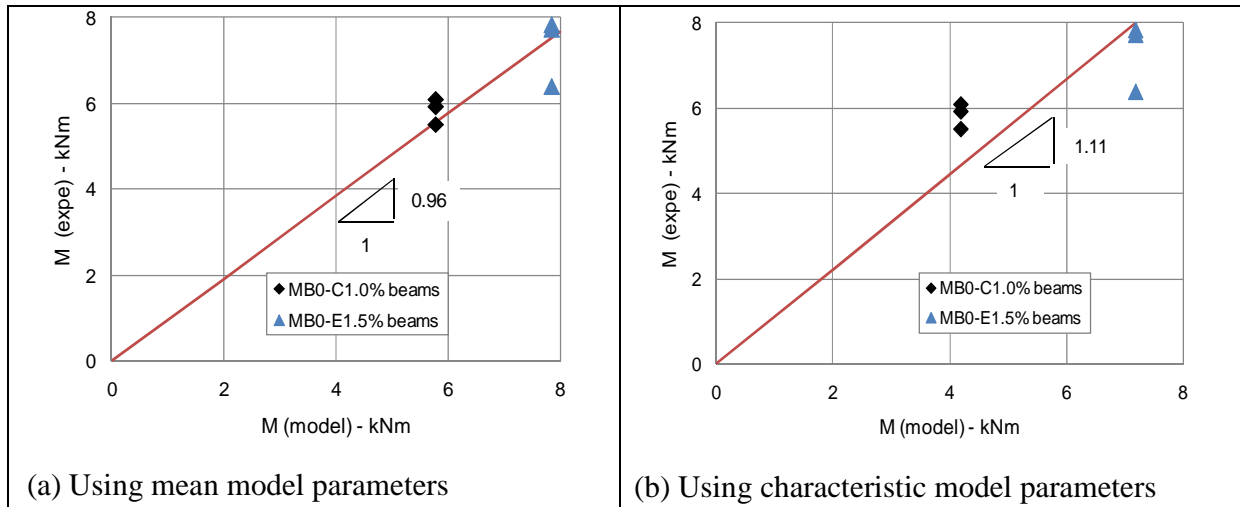


Figure 7.4: Scatter plot of experimental and model predictions for SFRC without steel bars (MB0-C1.0% and MB0-E1.5% beams)

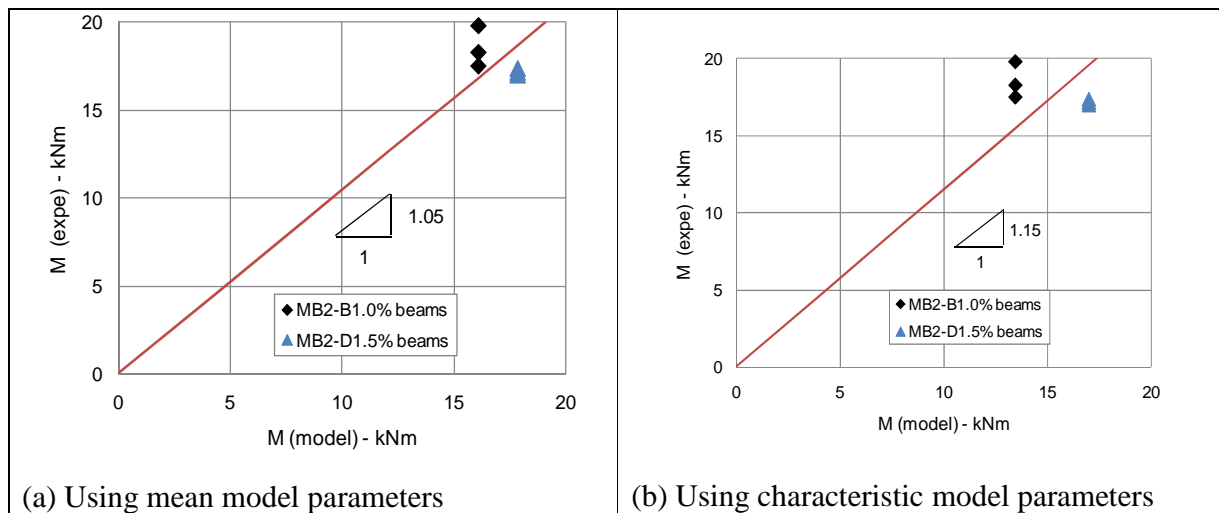


Figure 7.5: Scatter plot of experimental and model predictions for R-SFRC (MB2-B1.0% and MB2-D1.5% beams)

Table 7.20 summarises the statistical assessment of the model predictions. The model correction factors (shown in Figures 7.4 and 7.5 as gradients of the scatter plot) and the coefficient of variation of the error term are given in the table for the analytical models. Model correct factors of magnitudes greater than unity are reported in the table, indicating that the model predictions are conservative. Predictions obtained from mean parameters of material characterisation show closer values to experimental values as indicated by the correction factors close to unity. Another aspect highlighted by the statistical results is the measure of scatter of the results indicated by the coefficient of the error term, m_{δ_e} . Mean values more accurately predict the moment capacity of

the beam as compared to characteristic values (indicated by a larger m_{δ_e} value for characteristic predictions as compared to mean predictions).

Table 7.20: Correction factors and coefficient of variations of the error term for the current models

Parameter	SFRC model without rebar		SFRC model with rebar	
	(mean)	(characteristic)	(mean)	(characteristic)
Model correction factor (δ_c)	0.96	1.11	1.05	1.15
Coefficient of variation of error term (m_{δ_e})	0.09	0.19	0.14	0.28

7.7 CONCLUSION

The two analytical models proposed in this thesis have been verified by means of four-point bending experiments on beams. Generally, all the proposed models are conservative in predicting the bending moment of the beam. When mean model parameters are used, moment predictions are closer to experimental results than when characteristic model parameters are used as indicated by a smaller coefficient of variation of the error term. This may be due to larger scatter of the material characterisation data, which results in greatly reduced characteristic values. In batches where the scatter in characterisation data was minimal, the predictions did not show a great difference when either the mean or the characteristic model parameters were used. This is the case with predictions from batch MB0-E1.5% when characterisation data obtained from the batch were used.

When experimental data obtained from literature is used for the verification of SFRC model, the current model fairly predicts the moment capacity. The predicted moments are generally conservative and do not differ much from the predictions obtained when using the model developed by Soranakom and Mobasher (2009). A comparison of the model predictions using current experimental data show similar trend with the proposed model fairly conservative with the exception of the results obtained from batch MB0-E1.5%. Relevant model parameters were derived for use in the model proposed by Naaman (2003). However, it is clear that the selection of relevant parameters for determination of the post-cracking tensile strength is vital. Two different approaches by Li *et al* (1990, 1992a), and Naaman (2003) and Suwannakarn (2009) give completely different values for post-cracking tensile strength. A more conservative value is obtained when using the formula by Li *et al* (1990, 1992a). When using the post-cracking strength obtained based on Li *et al* (1990, 1992a), the model by Naaman under-predicts the flexural capacity of the beams, while when the post-cracking strength obtained based on Naaman (2003) and Suwannakarn (2009) are used, Naaman's model over-predicts the flexural strength of the beam.

In SFRC with reinforcing bars, five moment values were determined; namely, moment at cracking, moment at steel bar yielding, moments at ultimate tensile and compression strength

and moment at ultimate tensile strength of steel bars. Batch MB2-B1.0% displayed a good correlation of moment predictions compared to the experimental results with the stiffness of the beam section decreasing from cracking up to failure. However, moment predictions for batch MB2-D1.5% could not clearly depict such a trend as the predicted cracking moment was more or equal to the moment at yielding of steel bars. One reason for such a discrepancy could be the uncertainties in the input model parameters used. It should be recalled that all the input model parameters were derived from ‘indirect’ methods; cubes were used for compressive strength and Young’s modulus while splitting test was employed to determine tensile parameters. The current model fairly predicts the maximum bending moment of the beam. At maximum bending moment, the current model shows that the concrete compression strength dictated failure in all beams with ultimate compression strain reached prior to ultimate tensile strain.

The current flexural models for R-SFRC fairly predict the bending strength of the beam compared to available model in literature. While two models for R-SFRC have been reviewed in Chapter 2, only the model by Henager and Doherty (1976) was used for comparison. The other model by Tan *et al* (1995) is useful for provision of reinforcement as it requires knowledge of the maximum moment to be applied on the beam. Just as was the case with the model by Naaman (2003), the model by Henager and Doherty (1976) also requires determination of tensile properties using an empirical expression. Using the tensile properties obtained from the empirical expression, the flexural model by Henager and Doherty (1976) under-predicts the bending resistance of the beam. It is clear that one of the reasons for the smaller moment predicted by this model is the use of a small tensile stress obtained by the empirical expression.

It should be noted that the derivation of the model for SFRC with reinforcing bars assumed the addition of separate resistance effects from both concrete and reinforcing bars. This ignores the synergetic effect that might exist due to the use of both steel fibres and reinforcing bars. While the synergetic effect may exist when steel fibres are used together with reinforcing bars, such an effect may easily be ignored for small steel fibre volumes as the model predictions and the experimental results do not show substantial differences.

CHAPTER 8 CONCLUSIONS AND RECOMMENDATIONS

Various literatures have been reviewed in order to establish the general behaviour of SFRC. SFRC may exhibit either strain hardening or strain softening behaviour depending on the amount and properties of the steel fibres used. An assessment of the available models used for determination of the flexural capacity of SFRC with and without steel bars has revealed that all the reviewed models use empirical expressions for the determination of the tensile properties of SFRC. Two phases of model development have been followed in the previous chapters: development of analytical models and a verification process. The verification stage examined two steps in acquiring experimental data, which are to determine characterisation properties and actual beam flexural capacity for verification of the analytical models. This chapter discusses conclusions and recommendations for each of the stages outlined.

8.1 CONCLUSIONS

8.1.1 ANALYTICAL MODELS

Development of analytical models for flexure of SFRC with and without reinforcing bars in this thesis followed the basic mechanics of the materials approach in which Bernoulli's strain theory is used for strains, wherein strain compatibility and force equilibrium equations are implemented. Using a bilinear compression stress-strain distribution and drop-down tension stress-strain distribution, equivalent stress distributions were developed through the use of conversion factors λ_t , η_t , and β_t for tension and λ_c , η_c , and β_c for compression which may depend on yield strains, post-yield strain and normalised tensile strength, μ_i . These conversion factors can be determined for SFRC with strain softening behaviour for which compression strain and tension strain are greater than yielding strain and cracking strain respectively.

Parametric studies for the conversion factors at ultimate state agree with the assumed stress block used in literature for both tension and compression stress distributions. A value of 1.0 for λ_{td} means that the tensile stress block is smeared over the whole tensile depth of the beam section. The conversion factor, η_{td} , is approximately equal to the normalised tensile strength, μ_i , for a drop-down tensile model while it is slightly below average of the two post-peak normalised strength parameters, μ_{R1} and μ_{R2} , for a Rilem's tensile model. From the parametric studies, it is clear that incorporation of tensile contribution in the flexural capacity of R-SFRC beams may increase the flexural capacity of the beams, especially at low x/d (or low rebar amounts) rather than at high x/d (or high reinforcing bar amounts).

Flexural models for R-SFRC have been outlined at five different strain states corresponding to cracking moment, moment at yielding of steel bars, moment at ultimate compression and tension strength and moment at ultimate tensile strength of steel bars. Using the proposed models, the moment vs. curvature curves were established showing the trend in the moment capacity development as the beam is being loaded. Such a trend was similar to what is theoretically expected with exception of some circumstances in which poor model parameters affected the

outcome of the analysis. While these five moment values may be considered in order to determine the moment capacity of a beam with specified reinforcement, provision of reinforcement in a beam may require a slightly modified approach as outlined in Section 3.3.5. An iterative process is required if appropriate reinforcement is to be provided for the beam section, ensuring that limiting strains are not exceeded. Strain-hardening steel bars may generate greater moment capacity in the beam section than elastic-perfect plastic steel bars and therefore, appropriate consideration should be taken during design.

8.1.2 MATERIAL CHARACTERISATION AND MODEL VERIFICATION DATA

Material characterisation data was obtained through compression tests and splitting tests on cubes. The use of cubes in both compression and splitting data may generate additional stresses due to stress confinement. An appropriate factor has been used in order to convert the compression strength to represent cylindrical compressive strength in analyses. The splitting test is an indirect means of acquiring direct tensile strength. For post-cracking behaviour, conversion of the splitting behaviour to direct tension behaviour involves more uncertainties. The conversion factor recommended in literature for peak strength is assumed to be valid for post-cracking behaviour. Improved tensile characterisation requires direct uniaxial tension testing, or inverse analysis from flexural test response. Through limited finite element analysis in this thesis (in which mean model parameters were used), it has been shown that the use of the splitting tensile response as axial tensile response, after the simple adjustments applied in this thesis, may lead to slightly higher flexural capacity predictions as compared to the measured flexural capacity. This agrees with the general model predictions where mean model parameters are used as outlined in Chapter 7. Further research is required in this regard.

Model verification experiments involving larger SFRC beams with and without steel reinforcing bars were conducted using four-point bending tests. Having a region of constant moment along the beam ensured that a correct failure mode could easily be deduced from the experiments. The spanning of the beams was short with the loading spacing at between 150mm and 200mm, equating to a loading distance to section depth ratio of about 1.3 – 1.7. With this amount of spanning; it is likely that a small magnitude of error in placing of loading points can have a substantial effect on the bending moments generated in the beams. It is against this background that a non linear finite element analysis was conducted in order to determine the position of the resultant reaction forces at the supports of the beams. During the four-point bending tests, the deflections were measured indirectly through the use of overall mid-span deflections (Instron deflection) and support deflections measured from the top of the beam. The application of deflections ignores deflections due to the compression of the rubber strips and the movement of the frame supporting the Instron. Therefore, the deflections given in the thesis for the larger beams do not represent actual mid span deflections of the beams. In the standardised small beam tests, correct measurement of true mid-span deflection was ensured by appropriate design and application of a deformation measurement device frame.

8.1.3 CURRENT MODELS PREDICTIONS, VERIFICATION AND COMPARISON WITH AVAILABLE MODELS IN LITERATURE

The proposed models have been verified by means of four-point bending tests on beams. Two sets of characterisation data were used; namely mean parameters and characteristic parameters. Generally all the analytical models proposed in this thesis fairly predict the moment resistance. The models offer better procedures for the determination of moment resistances as compared to models reviewed from literature. The user is allowed to modify the ultimate strains based on the required design function of a structural member, thereby offering flexibility. When mean model parameters are used, moment predictions are closer to experimental results than when characteristic model parameters are used. A larger scatter in the material characterisation data results in a significantly reduced characteristic value.

It should be noted that the derivation of the model for SFRC with reinforcing bars assumed the addition of separate resistance effects from both concrete and reinforcing bars. While the synergetic effect may exist when steel fibres are used together with reinforcing bars, such an effect may easily be ignored for small steel fibre volumes as the model predictions and the experimental results do not show substantial differences.

When experimental data obtained from literature is used for the verification of the SFRC model, the current model fairly predicts the moment capacity being slightly more conservative than the model developed by Soranakom and Mobasher (2009). Relevant post-cracking strength was derived for use in the models proposed by Naaman (2003) and Henager and Doherty (1976). The post-cracking strength determined from empirical expressions depends on the selection of relevant parameters. This results in differences in the post-cracking strength which affect the predictions of the models. It is difficult to quantify the risks associated with the post-cracking strength that is derived from empirical expressions hence making reliability assessment of these models difficult.

8.2 RECOMMENDATIONS

8.2.1 ANALYTICAL MODELS

While reliable predictions can be made from SFRC model, further research is required for reliability studies of this model. Design values taking both the material variability and the model variability into account need to be developed. In this case, since post-cracking tensile behaviour is investigated, the appropriate factors for these properties as outlined in the *Draft Model code 2010* need to be considered.

Since the development of R-SFRC flexural models ignores the synergetic effect of using both steel fibres and steel bars, studies into the synergetic effect should be conducted. Such studies may have to incorporate high volume steel fibre contents in SFRC and high compression strength SFRC. Incorporation of the synergetic effect of using SFRC with rebar should then be considered.

8.2.2 MODEL VERIFICATION DATA

Two experiments were mainly conducted for material properties characterisation. These include the indirect tensile test (splitting test) and the compression test. From the analytical model it is clear that more data is required than is the case when determining the flexural capacity of normal concrete. Additional data needed would largely be the post-cracking tensile data for concrete. Ideally, the direct tensile test would be used as a reliable procedure for determining the tensile properties. However, due to difficulties in executing such an experiment, a splitting test was used which brought with it some uncertainties within the data. Therefore, the following recommendations are made for the determination of tensile properties of SFRC:

- a) Research is required to determine and characterise the post-cracking tensile properties of SFRC using both the splitting test and the direct test. If this can be performed, models similar to that developed by Rocco *et al* (2001) that use the fracture mechanics approach and characteristic length of concrete can be determined for SFRC.
- b) As an alternative to the direct tensile test, inverse analysis for the determination of the tensile parameters should be used. In this case a four-point bending test on unnotched beam may be performed together with the splitting test. Using the approach proposed by Rossello *et al* (2006), comparative studies can be performed to check whether there is any correlation between the post cracking parameters obtained from a bending test and a splitting test. A four-point bending test on unnotched beams is preferred because of the absence of internal shear forces in the constant moment zone which is not the case for a three-point bending test. Furthermore, the absence of a notch ensures that no stress concentrations exist in the constant moment region.
- c) As an alternative to performing experiments, a numerical procedure can be performed for both splitting and direct tension as long as all data required for such an exercise is available. This data could then be compared with bending behaviour of the beam obtained through numerical methods. The only drawback to this approach is the availability of relevant data for the biaxial behaviour of SFRC to be used in the splitting numerical method.
- d) Another source of error in the results from the splitting test was the use of a large gauge length. As a recommendation, a smaller gauge length can be used to minimise the effects of stress gradients over a larger gauge length.

The four-point bending test can be employed satisfactorily for model verification. However, a larger beam span would offer reduced errors in determining applied moments. Furthermore, the data capturing mechanism for deflection should be done on the sample itself where deflections are taken from the centre of the sample.

REFERENCE

- ACI Committe 318, 2002. Building Code Requirements for Structural Concrete (ACI 318-02) and Commentary (ACI 318R-02). Farmington Hills, Michigan: American Concrete Institute.
- ACI Committe 544, 1996. Design Considerations for Steel Fibre Reinforced Concrete. In *ACI 544.4R-88*. Farmington Hills, MI. American Concrete Institute.
- ACI Committe 544-4R-88, 1988. ACI manual of concrete practice (Reapproved, 1999). Farmington Hills, Michigan, . American Concrete Institute.
- ACI Committee 318, 2005. Building Code Requirements for Structural Concrete. In *ACI 318-05*. Farmington Hills, MI. American Concrete Institute.
- Barros, J.A.O. & Figueiras, J., 1999. Flexural behaviour of steel fibre reinforced concrete: testing and modelling. *Journal of Materials in Civil Engineering*, 11(4), pp.331-39.
- Bazant, Z. & Cedolin, L., 1983a. Finite element modelling of crack band propagation. *ASCE Journal Structures and Engineering*, 109(1), pp.69-92.
- Bazant, Z. & Novak, D., 2003. Stochastic models for deformation and failure of quasi-brittle structures. In Bicanic, N.*et al*, eds. *Recent advances and new directions, Computational modelling of concrete structures*. Lisse: Swets and Zeitlinger. pp.583-98.
- Bazant, Z. & Oh, B., 1983b. Crack band theory for fracture of concrete. *Materials and Structures*, 16(93), pp.155-77.
- Bazant, Z. & Pijaudier-Cabot, G., 1988. Non-local continuum damage. localisation instability and convergence. *ASME Journal of Applied Mechanics*, 55, pp.287-93.
- Bencardino, F., Rizzuti, L., Spadea, G. & Swamy, R.N., 2007. Stress-strain behaviour of steel fibre-reinforced concrete in compression. *ASCE Journal of Materials in Civil Engineering*, 20(3).
- Bentur, A. & Mindess, S., 1990. *Fibre reinforced cementitious composites*. London, England: Elsevier Applied Science.
- Bhatt, P., MacGinley, T.J. & Choo, B., 2006. *Reinforced concrete: Design theory and examples*. 3rd ed. London: Taylor and Francis.
- CEB-FIP Model code, 2010. *Draft 2010 Model code*. London.
- CNR-DT 204, 2006. *Guidelines for design, construction and production control of fibre reinforced concrete structures*. Italy: National Research council of Italy.

- De Borst, R., Mulhaus, H., Pamin, J. & Sluys, L., 1992. Computational modelling of localisation of deformation. In D.R.J. Owen & *et. al*, eds. *Proceedings on the computational plasticity fundamentals and applications, Part II*. Swansea: Pineridge Press.
- De Oliveira, F., 2010. *Design-oriented constitutive model for steel fibre reinforced concrete*. Phd Thesis. Universitat Politecnica de Catalunya.
- Di Prisco, M., Felicetti, R. & Gambarova, P.G., 1999. Evaluation of the characteristic length in high strength concrete. In A. Azizinamini, D. Darwin & C. French, eds. *High strength concrete*. Kona, Hawaii: ASCE. pp.377-90.
- Di Prisco, M., Plizzari, G. & Vandewalle, L., 2009. Fibre reinforced concrete: new design perspective. *Materials and structures*, 42, pp.1261-81.
- Dupont, D. & Vandewalle, L., 2002. Characterisation of steel fibre concrete with stress-strain relation. In *Proceedings of the 4th International PhD symposium in Civil Engineering*. Munich.
- Dymond, J.S. & Retief, J.V., 2010. Towards a reliability based development program for SHCC design procedures. In van Zijl, G.P.A.G. & Boshoff, W.P., eds. *Advances in Cement-Based Materials*. London. Taylor and Francis Group.
- European standards, 2002. *EN 1990: Eurocode- Basis of structural design*. Brussels. European Committee of Standardisation.
- European standards, 2004. *BS EN 1992-1-1: Eurocode 2- Design of concrete structures: Part 1-1: General rules and rules for buildings*. Brussels. European Committee for Standardisation.
- Ezeldin, A. & Balagurur, P., 1992. Normal-high strength fibre reinforced concrete under compression. *Journal of Materials in Civil Engineering*, 4(4), pp.415-29.
- Fokwa, D. & Berthaud, Y., 1993. Heterogeneous materials: experimental analysis of localisation and influence of size of the heterogeneities on the behaviour in tension. *Materials and Structures*, 26, pp.136-43.
- Gopalatnam, V. & Shah, S., 1985. Softening response of plain concrete in direct concrete. *ACI Journal*, 82(3), pp.310-23.
- Hassoun, M.N. & Sahebjam, K., 1985. Plastic hinge in two-span reinforced concrete beams containing steel fibres. In *Canadian Society for Civil Engineering*. Montreal.
- Henager, C., Doherty, T. J, 1976. Analysis of reinforced fibrous cement beams. *ASCE*, 12(ST1), pp.177-88.

- Hillerborg, A., Modeer, M. & Peterson, P., 1976. Analysis of crack formation and crack growth by means of fracture mechanics and finite elements. *Cement and Concrete Research*, 6, pp.773-82.
- Holicky, M., 2009. *Reliability analysis for structural design*. 1st ed. Stellenbosch, South Africa: SUN MeDIA.
- Hordijk, D.A., 1991. *Local Approach to Fatigue of Concrete*. PhD Thesis. Delft University of Technology.
- Jacobs, J.-P., ed., 2008. *Eurocode 2 Commentary*. Brussels: European Concrete Platform ASBL.
- Jarratt, R., 2011 (In preparation). *Feasibility of using self compacting SFRC in the construction of in situ members*. Msc. Thesis. University of Stellenbosch.
- Kosa, K. & Naaman, A., 1990. Corrosion of steel fibre reinforced concrete. *ACI Materials Journal*, 2(1), pp.27-37.
- Kuneida, M., Kamanda, T. & Rokungo, K., 2002. Size effect on the flexural failure behaviour of ECC members. In *Proceedings of the JCI workshop on Ductile Fibre Reinforced Cement Composite (DFRCC)-Applications and Evaluations*. Tokyo, Japan, Japan Concrete Institute.
- Kwak, H.-G. & Klim, S.-P., 2002. Nonlinear analysis of reinforced concrete beams based on moment-curvature relationship. *Computers and Structures*, 80, pp.615-28.
- Li, V.C., 1992a. Post cracking scaling relations for fibre reinforced cementitious composites. *ASCE Journal of materials in Civil Engineering*, 4(1), pp.41-57.
- Lim, T., Paramasivam, P. & Lee, S., 1987b. Bending behaviour of steel fibre reinforced beams. *ACI Structures Journal*, 84(6), pp.524-36.
- Lim, T., Paramasivan, P. & Lee, S., 1987a. Analytical model for tensile behaviour of steel fibre concrete. *ACI Materials Journal*, 84(4), pp.286-98.
- Li, V.C., Wang, Y. & Backer, S., 1990. Effects of inclined angle bundling and surface treatment on synthetic fibre pull-out from cement matrix. *Composites*, 21(2), pp.132-40.
- Li, V.C. & Wu, H.C., 1992. Conditions for pseudo strain -hardening in fibre reinforced brittle matrix composites. *Journal of Applied Mechanics Review*, 45(8), pp.390-98.
- Li, V.C. *et al.*, 2002. Interface tailoring for strain-hardening Polyvinyl Alcohol Engineered Cementitious Composites (PVA-ECC). *ACI Materials Journal*, 99(2), pp.463-72.
- Löfgren, I., 2005. Fibre-reinforced concrete for industrial construction- a fracture mechanics approach to material testing and structural analysis. PhD Thesis, Chalmers University of technology, Department of Civil and Environmental Engineering.

- Lok, T. & Xiao, L., 1998. Tensile behaviour and moment-curvature relationship of steel fibre reinforced concrete. *Magazine of Construction Research*, 50(40), pp.359-68.
- Manie, J. & Kikstra, W. P., eds., 2010. DIANA: Finite element analysis, User's manual release 9.4.2 Material library, Delft, The Netherlands.
- Montgomery, D. & Ruger, G., 2007. *Applied statistics and Probability for Engineers*. 4th ed. USA: JW Wiley and Sons.
- Naaman, A., 2003. High Performance Fibre Reinforced Cement Composites. In Naaman, A.E. & Reihardt, H., eds. *HPFRCC 4, PRO 30*. Bagnaux, France. RILEM Publications, S.A.R.L.
- Nataraja, M., Dhang, N. & Gupta, A., 1999. Stress-strain curve for steel fibre reinforced concrete under compression. *Cement and Concrete Composites*, 21, pp.383-90.
- Pearlman, S.L., April 1983. *Flexural performance of reinforced steel fibre-reinforced concrete beams*. Msc Thesis. Pittsburg: Carnegie-Mellon University.
- Potrzebowski, J., 1983. The splitting test applied to steel fibre-reinforced concrete. *International Journal of Cement Composites and Light weight Concrete*, 5(1), pp.49-53.
- Rocco, C., Guinea, G., Planas, J. & Elices, M., 2001. Review of the splitting-test standards from a fracture mechanics point of view. *Cement and Concrete Research*, 31, pp.73-82.
- Rocco, C., Guinea, G., Planas, J. & Elices, M., 1999. Size effect and boundary conditions in the brazilian test: Experimental verification. *Materials and Structures*, 32, pp.210-17.
- Rocco, C., Guinea, G.V., Planas, J. & Elices, M., 1999. Size effect and boundary conditions in brazilian test: theoretical analysis. *Materials and Structures*, 32, pp.437-44.
- Rossi, P. & Chanvillard, G., 2000. Fibre Reinforced Concretes. Bagnaux, France. RILEM S.A.R.L.
- SABS 0100, 2000. *Structural use of concrete. Part 1: Design*. 2nd ed. Pretoria: South African Bureau of Standards.
- SANS 5863, 2006. *Concrete tests: Compression strength of hardened concrete*. Pretoria: South African Bureau of Standards.
- SANS 5864, 2006. *Concrete tests: Flexural strength of hardened concrete*. Pretoria: South African Bureau of Standards.
- SANS 6253, 2006. *Concrete tests: Tensile splitting strength of concrete*. Pretoria: South African Bureau of Standards.

- Soranakom, C. & Mobasher, B., 2007. Closed-form solutions for flexural response of fibre-reinforced concrete beams. *Journal for Engineering and Mechanics*, 133(8), pp.933-41.
- Soranakom, C. & Mobasher, B., 2009. Flexural Design of Fibre-Reinforced Concrete. *ACI Materilas Journal*, 106(5).
- Soranakom, C., Yekan-Far, M. & Mobasher, B., 2008. Development of design guidelines for strain softening fibre reinforced concrete. In *7th International Symposium of Fibre Reinforced Concrete: Design and applications..* BEFIB.
- Suwannakarn, S., 2009. *Post cracking characteristics of high perfomance fibre reinforced cementitious composites*. PhD Thesis. University of Michigan.
- Swamy, R.N. & Al-Ta'an, S.A., 1981. Deformation and ultimate strenght in flexure of reinforced concrete beams made with steel fibre concrete. *ACI Journal*, 78(5), pp.395-405.
- Tan, K.H., Paramasivam, P. & Tan, K., 1995. *Cracking characteristics of reinforced steel fibre concrete beams under short- and long - term loadings*. New York: Elsevier.
- Tjiptobroto, P. & Hansen, W., 1993. Tensile strain-hardeneing and multiple cracking in high perfomance cement based composites. *ACI Materials Journal* , 90(1).
- van Zijl, G.P.A.G. & Boshoff, W.P., 2006. *Verification of Materials Design Formulae for the Structural use of Ductile Fibre Reinforced Cement Composites*. (Unpublished manuscript).
- van Zijl, G. & Song, G., 2005. *Developing fibre reinforced cementitious composites of high cement replacement ratio*. University of Stellenbosch.
- van Zijl, G. & Wittman, F., eds., 2011. *Durability of Strain-Hardening Fibre-Reinforced Cement-based Composite (SHCC)*. Springer Publishers, ISBN-13: 978-94-007-0337-7.
- Vandewalle, L., 2003. Test and design methods for steel fibre reinforced concrete: Design with stress-strain method. In *Rilem Proceeding 31, TC 162-TDF Workshop*. Bochum, 2003.
- Vandewalle, L. *et al.*, 2002. Recommendations of RILEM TC162-TDF: Test and Design Methods for Steel Fibre Reinforced Concrete: Bending test(final recommendation). *Materials and Structures*, 35, pp.579-82.
- Vandewalle, L. & Dupont, D., 2003. Test and Design methods for steel fibre reinforced concrete. In *Bending Test and Interpretation*. Bochum, 2003. RILEM Proceeding 31 of TC 162-TDF Workshop.
- Williamson, G.R., 1973. *M-62 Compression characteristics and structural beam design analysis of steel fibre reinforced concrete*. Technical report. Champaign: US Army.

Zeranka, S., 2010. *The impact of rheology on the mechanical properties of fibre reinforced concrete*. Bsc. Thesis. University of Stellenbosch.

A. DERIVATIONS

A.1 Derivation of formulae for the neutral axis, curvature and lever arm based on equivalent stress blocks derived from a bilinear compression model and drop-down tensile model

With reference to Figures 3.8 and 3.9 given in Section 3.3.1, the following formulae are derived for stages 2 and 3:

Stage 2 :(Compression stress before yielding and tensile stress after cracking)

Using equilibrium of forces;

$$\frac{1}{2}\sigma_c bx = \eta_t f_{tk} b \lambda_t (h - x) \quad \text{A.1}$$

Replacing σ_c with $E_c \varepsilon_c$ and f_{tk} with $E_c \varepsilon_{ty}$ and noting that $\beta_t = \eta_t \lambda_t$, the ratio of the neutral axis to overall depth is derived from Equation A.1 as follows:

$$\frac{x}{h} = \frac{2\beta_t \varepsilon_{ty}}{\varepsilon_c + 2\beta_t \varepsilon_{ty}} \quad \text{A.2}$$

Using compressive strain at extreme edge of the beam section, curvature can be expressed as follows:

$$\text{Curvature} = \frac{\varepsilon_c}{x} \quad \text{A.3}$$

Substituting the neutral axis in Equation A.3 by the value of x derived from Equation A.2 gives the following expression for curvature:

$$\text{Curvature} = \frac{\varepsilon_c^2}{2h\beta_t \varepsilon_{ty}} + \frac{\varepsilon_c}{h} \quad \text{A.4}$$

The lever arm can be determined by taking moment about the position where the resultant compression and tension forces act.

Taking moment about the position where the resultant compression force acts;

$$M = \beta_t f_{tk} b(h - x)Z = \beta_t E_c \varepsilon_{ty} b(h - x)Z \quad \text{A.5}$$

Taking moment about the position where the resultant tension force acts;

$$M = \frac{1}{2}\sigma_c bxZ = \frac{1}{2}E_c \varepsilon_c bxZ \quad \text{A.6}$$

Equating Equation A.5 and A.6 and substituting for x as given in Equation A.2 gives the following expression

$$\frac{Z}{h} = 1 + \frac{x}{h} \left(\frac{\lambda_t}{2} - \frac{1}{3} \right) - \frac{\lambda_t}{2} \quad \text{A.7}$$

Stage 3 :(Compression stress after yielding and tensile stress after cracking)

Using equilibrium of forces;

$$\eta_c \lambda_c f_{ck} bx = \eta_t f_{tk} b \lambda_t (h - x) \quad \text{A.8}$$

Replacing f_{ck} with $E_c \varepsilon_{cy}$ and f_{tk} with $E_c \varepsilon_{ty}$ and noting that $\beta_t = \eta_t \lambda_t$ and $\beta_c = \eta_c \lambda_c$, the ratio of the neutral axis to overall depth is derived from Equation A.8 as follows:

$$\frac{x}{h} = \frac{\beta_t \epsilon_{ty}}{\beta_c \epsilon_{cy} + \beta_t \epsilon_{ty}} \quad \text{A.9}$$

Using compressive strain at extreme edge of the beam section, curvature can be expressed as follows:

$$\text{Curvature} = \frac{\epsilon_c}{x} \quad \text{A.10}$$

Substituting the neutral axis in Equation A.10 by the value of x derived from Equation A.9 gives the following expression for the curvature:

$$\text{Curvature} = \frac{\epsilon_c^2}{2h\beta_t \epsilon_{ty}} + \frac{\epsilon_c}{h} \quad \text{A.11}$$

The lever arm can be determined by taking moment about the position where the resultant compression and tension forces act.

Taking moment about the position where the resultant compression force acts;

$$M = \beta_t f_{tk} b(h-x)Z = \beta_t E_c \epsilon_{ty} b(h-x)Z \quad \text{A.12}$$

Taking moment about the position where the resultant tension force acts;

$$M = \beta_c f_{ck} bxZ = \beta_c E_c \epsilon_{cy} bxZ \quad \text{A.13}$$

Equating Equation A.12 and A.13 and substituting for x as given in Equation A.9 gives the following expression

$$\frac{Z}{h} = 1 + \frac{x}{2h} (\lambda_t - \lambda_c) - \frac{\lambda_t}{2} \quad \text{A.14}$$

B. EXPERIMENTAL RESULTS

B.1 Compression test results from preliminary tests (Phase I)

The compressive behaviour for SFRC was determined by using 100mm cube samples. Four categories representing varying steel fibres of 0%, 0.5%, 1.0% and 1.5% were tested and the maximum compression strength and the Young's modulus are given in Tables B.1.1-B.1.4.

Table B.1.1: Compression parameters for concrete without steel fibres (PC0.0%)

Sample No.	Maximum compressive strength (MPa)	Young's modulus (MPa)
1	30.83	29143
2	31.48	32868
3	33.2	36346
Average	31.84	32786
Standard deviation	1.22	3620
CoV	0.039	0.110
Characteristic value	29.52	-

Table B.1.2: Compression parameters for concrete with 0.5% steel fibres (PC0.5%)

Sample No.	Maximum compressive strength (MPa)	Young's modulus (MPa)
1	35.79	36573
2	34.67	42359
3	34.34	30519
Average	34.93	36484
Standard deviation	0.758	5921
CoV	0.022	0.162
Characteristic value	33.50	-

Table B.1.3: Compression parameters for concrete with 1.0% steel fibres (PC1.0%)

Sample No.	Maximum compressive strength (MPa)	Young's modulus (MPa)
1	44.18	33994
2	41.10	41436
3	42.45	46674
Average	42.58	40701
Standard deviation	1.540	6372
CoV	0.036	0.157
Characteristic value	39.67	-

Appendix: Experimental results

Table B.1.4: Compression parameters for concrete with 1.5% steel fibres (PC1.5%)

Sample No.	Maximum compressive strength (MPa)	Young's modulus (MPa)
1	43.29	30593
2	41.06	33856
Average	42.18	32230
Standard deviation	1.577	2307
CoV	0.037	0.072
Characteristic value	39.01	-

B.2 Compression test results from model verification tests (Phase II)

The compressive behaviour for SFRC was determined by using 100mm cube samples. Three categories representing varying steel fibres of 0%, 1.0% and 1.5% were tested and the maximum compression strength, strain at maximum compression strength and the Young's modulus are given in Tables B.2.1-B.2.6.

Table B.2.1: Compression parameters for concrete without steel fibres (MC-A0.0%)

Sample No.	Maximum compressive strength (MPa)	Young's modulus (MPa)
A1	29.96	27138
A2	34.04	34793
A3	30.08	34995
A4	33.41	30823
Average	31.87	31937
Standard deviation	2.16	3732
CoV	0.068	0.117
Characteristic value	27.93	-

Table B.2.2: Compression parameters for SFRC with $V_f = 1.0\%$ (MC-B1.0%)

Sample No.	Maximum compressive strength (MPa)	Young's modulus (MPa)
B1	32.03	33630
B2	35.87	29530
B3	37.31	31670
B4	33.51	31880
Average	34.68	31678
Standard deviation	2.36	1680
CoV	0.068	0.053
Characteristic value	30.36	-

Appendix: Experimental results

Table B.2.3: Compression parameters for SFRC with $V_f = 1.0\%$ (MC-C1.0%)

Sample No.	Maximum compressive strength (MPa)	Young's modulus (MPa)
C1	25.82	45177
C2	24.70	42627
C3	26.28	39804
Average	25.60	42536
Standard deviation	0.814	2688
CoV	0.032	0.068
Characteristic value	24.06	-

Table B.2.4: Compression parameters for SFRC with $V_f = 1.5\%$ (MC-D1.5%)

Sample No.	Maximum compressive strength (MPa)	Young's modulus (MPa)
D1	39.87	32229
D2	40.95	37761
D3	42.06	31662.83
D4	41.97	33187
D5	41.14	33901
Average	41.20	33748
Standard deviation	0.890	2403
CoV	0.022	0.071
Characteristic value	39.60	-

Table B.2.5: Compressive parameters for SFRC with $V_f = 1.5\%$ (MC-E1.5%)

Sample No.	Maximum compressive strength (MPa)	Young's modulus (MPa)
E1	42.39	32726
E2	41.86	34317
E3	41.98	31719
E4	39.85	29586
E5	39.83	31624
E6	41.28	31388
Average	41.20	31893
Standard deviation	1.110	1565
CoV	0.027	0.049
Characteristic value	39.24	-

Appendix: Experimental results

Table B.2.6: Compressive parameters for SFRC without steel fibres (MC-F0.0%)

Sample No.	Maximum compressive strength (MPa)	Young's modulus (MPa)
F1	37.79	29187
F2	39.55	34432
F3	35.42	33166
F4	34.64	38999
F5	35.38	35936
F6	36.87	37329
Average	36.61	34842
Standard deviation	1.836	3453
CoV	0.050	0.0991
Characteristic value	33.35	-

B.3 Splitting test results from preliminary tests (Phase One)

The tensile behaviour for SFRC was determined by using 100mm cube samples. Four categories representing varying steel fibres of 0%, 0.5%, 1.0% and 1.5% were tested and the maximum splitting strength, maximum uniaxial tensile strength derived from both the code definition and elastic approach by Rocco *et al* (2001) and fracture toughness where relevant are given in Tables B3.1-B.3.3.

Table B.3.1: Maximum tensile strength for concrete with 0% and 0.5% steel fibres (PC0.0%, PC0.5%)

Sample No.	Splitting strength (MPa)		Direct tension-N (MPa)		Direct tension-M (MPa)	
	$V_f=0\%$	$V_f=0.5\%$	$V_f=0\%$	$V_f=0.5\%$	$V_f=0\%$	$V_f=0.5\%$
1	3.74	3.57	3.37	3.22	3.61	3.45
2	3.93	3.64	3.54	3.27	3.79	3.51
3	3.72	4.09	3.35	3.68	3.59	3.94
Average	3.80	3.77	3.42	3.39	3.66	3.63
St Dev.	0.115	0.281	0.104	0.253	0.111	0.271
CoV	0.030	0.075	0.030	0.075	0.030	0.075
Charact. value	3.58	3.24	3.22	2.91	3.45	3.12

Table B.3.2: Maximum tensile strength and toughness for concrete with 1% steel fibres (PC1.0%)

Sample No.	f_{tsp} (MPa)	f_{t-N} (MPa)	f_{t-M} (MPa)	G_{sp} (N/mm)	$G-N$ (N/mm)	$G-M$ (N/mm)	Young's modulus (MPa)
1	3.99	3.59	3.85	4.33	3.56	4.18	37510
2	4.20	3.78	4.05	4.68	3.84	4.51	26982
3	4.11	3.70	3.97	4.69	3.87	4.52	39249
Average	4.10	3.69	3.96	4.56	3.76	4.40	34580
Std Dev.	0.103	0.093	0.100	0.204	0.171	0.1963	6638
CoV	0.025	0.025	0.025	0.045	0.046	0.045	0.192
Charact. value	3.91	3.51	3.77	-	-	-	-

Appendix: Experimental results

Table B.3.3: Maximum tensile strength and toughness for concrete with 1.5% steel fibres (PC1.5%)

Sample No.	f_{tsp} (MPa)	f_{t-N} (MPa)	f_{t-M} (MPa)	G_{sp} (N/mm)	$G-N$ (N/mm)	$G-M$ (N/mm)	Young's modulus (MPa)
1	4.82	4.34	4.65	6.20	5.28	5.98	40620
2	5.89	5.30	5.68	6.90	5.85	6.65	28831
3	4.51	4.06	4.35	4.26	3.48	4.11	36008
Average	5.08	4.57	4.90	5.78	4.87	5.58	35153
Std Dev.	0.724	0.651	0.698	1.365	1.233	1.316	5940
CoV	0.143	0.143	0.143	0.236	0.253	0.236	0.169
Charact. value	3.71	3.34	3.58	-	-	-	-

B.4 Splitting test results from model verification tests (Phase Two)

The tensile behaviour for SFRC was determined by using 100mm cube samples. Three categories representing varying steel fibres of 0%, 1.0% and 1.5% were tested and the maximum splitting strength, maximum uniaxial tensile strength derived from both the code definition and elastic approach by Rocco *et al* (2001) and fracture toughness are given in Tables B4.1-B.4.6. Figure B4.1 shows the cross section of some cubes after splitting test.

Table B.4.1: Maximum tensile strength for concrete without steel fibres (MC-A0.0%)

Sample No.	f_{tsp} (MPa)	f_{t-N} (MPa)	f_{t-M} (MPa)
A1	3.82	3.44	3.66
A2	3.26	2.94	3.12
A3	3.94	3.54	3.76
A4	3.85	3.47	3.68
Average	3.72	3.35	3.56
Standard deviation	0.307	0.276	0.294
CoV	0.083	0.083	0.083
Characteristic value	3.16	2.84	3.02

Table B.4.2: Maximum tensile strength and toughness for concrete with 1.0% steel fibres (MC-B1.0%)

Sample No.	f_{tsp} (MPa)	f_{t-N} (MPa)	f_{t-M} (MPa)	G_{sp} N/mm	$G-N$ (N/mm)	$G-M$ (N/mm)	Young's modulus (MPa)
B1	3.81	3.42	3.64	4.13	3.42	3.95	34239
B2	4.94	4.44	4.72	5.61	4.82	5.36	28844
Average	4.37	3.93	4.18	4.87	4.12	4.65	31542
Std. Dev.	0.800	0.720	0.765	1.045	0.988	0.999	3815
CoV	0.183	0.183	0.183	0.215	0.240	0.215	0.121
Charact. value	2.76	2.49	2.64	-	-	-	-

Appendix: Experimental results

Table B.4.3: Maximum tensile strength and toughness for concrete with 1.0% steel fibres (MC-C1.0%)

Sample No.	f_{tsp} (MPa)	f_{t-N} (MPa)	f_{t-M} (MPa)	G_{sp} (N/mm)	$G-N$ (N/mm)	$G-M$ (N/mm)	Young's modulus (MPa)
C1	4.53	4.08	4.33	5.36	4.49	5.12	-
C2	4.33	3.89	4.14	4.34	3.51	4.15	40244
C3	4.30	3.87	4.11	3.94	3.17	3.77	36912
C4	4.08	3.67	3.90	4.43	3.68	4.24	32851
Average	4.31	3.88	4.12	4.52	3.71	4.32	36669
Std. Dev.	0.186	0.167	0.177	0.600	0.560	0.574	3702
CoV	0.043	0.043	0.043	0.133	0.151	0.133	0.101
Charact. value	3.97	3.57	3.80	-	-	-	-

Table B.4.4: Maximum tensile strength and toughness for concrete with 1.5% steel fibres (MC-D1.5%)

Sample No.	f_{tsp} (MPa)	f_{t-N} (MPa)	f_{t-M} (MPa)	G_{sp} (N/mm)	$G-N$ (N/mm)	$G-M$ (N/mm)	Young's modulus (MPa)
D1	5.61	5.05	5.36	6.43	5.51	6.15	39144
D2	5.89	5.30	5.63	6.34	5.38	6.07	31775
D3	5.48	4.93	5.24	5.87	4.94	5.62	36093
Average	5.66	5.09	5.41	6.22	5.28	5.94	35671
Std. Dev.	0.212	0.191	0.202	0.300	0.2990	0.2850	3702
CoV	0.038	0.038	0.037	0.048	0.0567	0.0479	0.104
Charact. value	5.26	4.73	5.03	-	-	-	-

Table B.4.5: Maximum tensile strength and toughness for concrete with 1.5% steel fibres (MC-E1.5%)

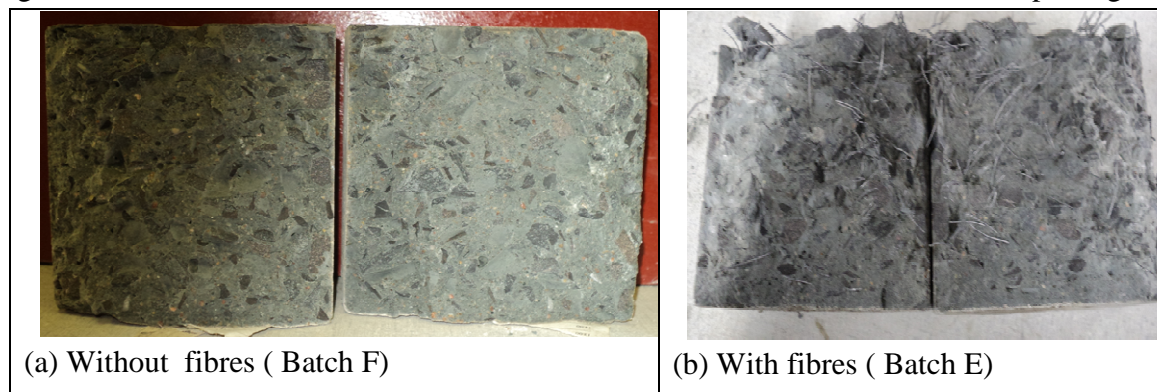
Sample No.	f_{tsp} (MPa)	f_{t-N} (MPa)	f_{t-M} (MPa)	G_{sp} (N/mm)	$G-N$ (N/mm)	$G-M$ (N/mm)	Young's modulus (MPa)
E1	5.61	5.05	5.37	6.15	5.28	5.89	30660
E2	5.95	5.36	5.70	6.03	5.00	5.77	39756
E3	6.06	5.45	5.79	6.24	5.23	5.96	29035
E4	5.75	5.18	5.50	5.63	4.67	5.39	28670
E5	5.54	4.99	5.30	5.93	4.97	5.67	35025
E6	5.54	4.99	5.30	5.70	4.76	5.45	-
Average	5.74	5.17	5.49	0.242	0.244	0.233	32629
Std. Dev.	0.220	0.198	0.211	0.041	0.049	0.041	4717
CoV	0.038	0.038	0.039	6.15	5.28	5.89	0.145
Charact. value	5.35	4.82	5.12	-	-	-	-

Appendix: Experimental results

Table B.4.6: Maximum tensile strength for concrete without steel fibres (MC-F0.0%)

Sample No.	f_{tsp} (MPa)	f_{t-N} (MPa)	f_{t-M} (MPa)
F1	3.41	3.07	3.26
F2	3.81	3.43	3.64
F3	4.31	3.87	4.12
F4	3.51	3.16	3.36
F5	3.93	3.53	3.75
F6	3.86	3.48	3.70
Average	3.80	3.42	3.64
Standard deviation	0.320	0.288	0.306
CoV	0.084	0.084	0.084
Characteristic value	3.23	2.91	3.10

Figure B4.1: Distribution of constituent materials for concrete and SFRC after the splitting test

**B.5 Flexural response for MB2-A0.0% beams**

Three specimens, 150 x 300 x 750 mm with 2Y10 RB-II steel bars but without steel fibres were tested using a four-point bending. Table B5.1 gives flexural results obtained from the experiment while a description of failure mode is given in Table B.5.2 display. Figure B.5.1 illustrates the failure pattern during the experiment.

Table B.5.1: Flexural response for MB2-A0.0% beams






Sample No.	Cracking force, P_{cr} (kN)	Maximum force, P_u (kN)	Cracking moment, M_{cr-exp} (kNm)	Maximum moment, M_{u-exp} (kNm)
A1	79	171.65	6.93	15.06
A2	84	186.91	7.37	16.40
A3	86	170.56	7.55	14.97
Average	83.0	176.4	7.3	15.5
Standard deviation	3.606	9.141	0.319	0.801
CoV	0.043	0.052	0.044	0.052

Appendix: Experimental results

Table B.5.2: Experimental observation and modes of failure for MB2-A.0.0% beams

Sample	Experimental observation and mode of failure
A1	Two flexural cracks initiated at different times during experiment followed by some shear cracks. Final failure by flexural cracks with concrete crushing at compression zone as shown in Figure B.5.1 (a).
A2	Three flexural cracks initiated, small shear cracks observed towards failure. Final failure by flexural cracks with concrete crushing at compression zone as shown in Figure B.5.1(b).
A3	Two flexural cracks initiated followed by shear cracks towards failure. Final failure by flexural cracks with concrete crushing at compression zone as shown in Figure B.5.1(c).

Figure B.5.1: Experimental observations during flexural tests for MB2-A.0.0% beams

Sample No.	Intermediate cracking mode	Final failure state
(a): Beam A1	Not available	
(b): Beam A2		
(c): Beam A3		

Appendix: Experimental results

B.6 Flexural response for MB2-B1.0% beams

Three specimens, 150 x 300 x 750 mm with 2Y10 RB-II steel bars but with 1.0% steel fibres were tested using a four-point bending. Table B5.1 gives flexural results obtained from the experiment while a description of failure mode is given in Table B.6.2 display. Figure B.6.1 illustrates the failure pattern during the experiment.



Table B.6.1: Flexural response for MB2-B1.0% beams

Sample No.	Cracking force, P_{cr} (kN)	Maximum force, P_u (kN)	Cracking moment, M_{cr-exp} (kNm)	Maximum moment, M_{u-exp} (kNm)
B1	139	225.7	12.20	19.81
B2	136	208.6	11.93	18.30
B3	122	199.9	10.71	17.54
Average	132.3	211.4	11.6	18.6
Standard deviation	9.074	13.126	0.794	1.155
CoV	0.069	0.062	0.068	0.062

Table B.6.2: Experimental observation and modes of failure for MB2-B1.0% beams

Sample	Experimental observation and mode of failure
B1	Both flexural and shear cracks are initiated. Final failure is by flexural–shear mechanism as seen in Figure B.6.1 (a). Concrete moderately crushed at compression zone.
B2	Two flexural cracks initiated at different times during experiment followed by some shear cracks. Final failure by flexural cracks with moderate concrete crushing at compression zone as seen in Figure B.6.1 (b). Reinforcing bar ruptured.
B3	One flexural crack initiated during experiment followed by a few shear cracks. Final failure by flexural cracks with moderate concrete crushing at compression zone. All tensile reinforcing bars burst resulting into total collapse of the section (see Figure B.6.1 (c)).

Figure B6.1: Experimental observations during flexural tests for MB2-B1.0% beams

Sample No.	Intermediate cracking mode	(Close to) final failure state
(a): Beam B1		

Appendix: Experimental results

**B.7 Flexural response for MB0-C1.0% beams**

Three specimens, 150 x 300 x 750 mm with 1.0% steel fibres but without reinforcing bars were tested using a four-point bending. Table B7.1 gives flexural results obtained from the experiment while a description of failure mode is given in Table B.7.2 display. Figure B.7.1 illustrates the failure pattern during the experiment.

Table B7.1: Flexural response for MB0-C1.0% beams






Sample No.	Maximum force	Maximum moment
	P_u (kN)	M_{u-exp} (kNm)
C1	69.44	6.09
C2	67.46	5.92
C3	62.69	5.50
Average	66.5	5.8
Standard deviation	3.470	0.304
CoV	0.052	0.052

Table B.7.2: Experimental observation and modes of failure for MB0-C1.0% beams

Sample	Experimental observation and mode of failure
C1	One flexural crack initiated, no shear cracks seen. Final failure by flexural cracks. No concrete crushing at the compression zone of section (see Figure B.7.1(a)).
C2	One flexural crack initiated, no shear cracks seen. Final failure by flexural cracks. No concrete crushing at the compression zone of section (see Figure B.7.1(b)).
C3	One flexural crack initiated, no shear cracks seen. Final failure by flexural cracks. No concrete crushing at the compression zone of section (see Figure B.7.1(c)).

Appendix: Experimental results

Figure B7.1: Experimental observations during flexural tests for MB0-C1.0% beams

Sample No.	Intermediate cracking mode	(Close to) final failure state
(a): Beam C1	Not available	
(b): Beam C2		
(c): Beam C3		

B.8 Flexural response for MB2-D1.5% beams

Three specimens, 150 x 300 x 750 mm with 2Y10 RB-II steel bars but with 1.5% steel fibres were tested using a four-point bending. Table B8.1 gives flexural results obtained from the experiment while a description of failure mode is given in Table B.8.1 display. Figure B.8.1 illustrates the failure pattern during the experiment.

Table B.8.1: Flexural response for MB2-D1.5% beams







Sample No.	Cracking force, P_{cr} (kN)	Maximum force, P_u (kN)	Cracking moment, M_{cr-exp} (kNm)	Maximum moment, M_{u-exp} (kNm)
D1	120	147.8	13.80	17.00
D2	120	148.8	13.80	17.11
D3	140	151.2	16.10	17.39
Average	126.7	149.3	14.6	17.2
Standard deviation	11.547	1.747	1.328	0.201
CoV	0.091	0.012	0.091	0.012

Appendix: Experimental results

Table B.8.2: Experimental observation and modes of failure for MB2-D1.5% beams

Sample	Experimental observation and mode of failure
D1	One flexural crack initiated, no shear cracks seen. Final failure by flexural cracks. Moderate concrete crushing at the compression zone of section (see Figure B.8.1(a)).
D2	One flexural crack initiated, no shear cracks seen. Final failure by flexural cracks. Moderate concrete crushing at the compression zone of section (see Figure B.8.1(b)).
D3	One flexural crack initiated, no shear cracks seen. Final failure by flexural cracks. Moderate concrete crushing at the compression zone of section (see Figure B.8.1(c)).

Figure B.8.1: Experimental observations during flexural tests for MB2-D1.5% beams

Sample No.	Intermediate cracking mode	(Close to) final failure state
(a): Beam D1		
(b): Beam D2		
(c): Beam D3		

Appendix: Experimental results

B.9 Flexural response for MB0-E1.5% beams

Three specimens, 150 x 300 x 750 mm with 1.5% steel fibres but without reinforcing bars were tested using a four-point bending. Table B.9.1 gives flexural results obtained from the experiment while a description of failure mode is given in Table B.9.2 display. Figure B.9.1 illustrates the failure pattern during the experiment.





Table B.9.1 Flexural response for MB0-E1.5% beams

Sample No.	Maximum force	Maximum moment
	P_u (kN)	M_{u-exp} (kNm)
E1	68.12	7.83
E2	67.16	7.72
E3	55.48	6.38
Average	63.6	7.3
Standard deviation	7.037	0.807
CoV	0.111	0.110

Table B.9.2 Experimental observation and modes of failure for MB0-E1.5% beams

Sample	Experimental observation and mode of failure
E1	One flexural crack initiated, no shear cracks seen. Final failure by flexural cracks. No concrete crushing at the compression zone of section (see Figure B.9.1(a)).
E2	One flexural crack initiated, no shear cracks seen. Final failure by flexural cracks. No concrete crushing at the compression zone of section (see Figure B.9.1(b)).
E3	One flexural crack initiated, no shear cracks seen. Final failure by flexural cracks. No concrete crushing at the compression zone of section (see Figure B.9.1(c)).

Figure B.9.1: Experimental observations during flexural tests for MB0-E1.5% beams

Sample No.	Intermediate cracking mode	(Close to) final failure state
(a): Beam E1		
(b): Beam E2		

Appendix: Experimental results

**B.10 Flexural response for MB2-F0.0% beams**

Three specimens, 150 x 300 x 750 mm with 2Y10 RB-II steel bars but without steel fibres were tested using a four-point bending. Table B10.1 gives flexural results obtained from the experiment while a description of failure mode is given in Table B.10.2 display. Figure B.10.1 illustrates the failure pattern during the experiment.

Table B.10.1: Flexural response for MB2-F0.0% beams



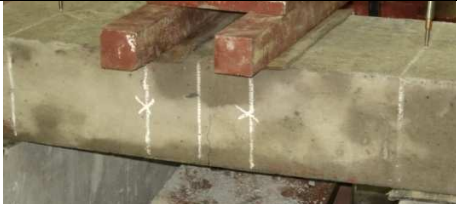



Sample No.	Cracking force, P_{cr} (kN)	Maximum force, P_u (kN)	Cracking moment, M_{cr-exp} (kNm)	Maximum moment, M_{u-exp} (kNm)
F1	74	142.81	8.51	16.42
F2	76	135.88	8.74	15.63
F3	80	138.82	9.20	15.96
Average	76.7	139.2	8.8	16.0
Standard deviation	3.055	3.478	0.351	0.397
CoV	0.040	0.025	0.040	0.025

Table B.10.2: Experimental observation and modes of failure for MB2-F0.0% beams

Sample	Experimental observation and mode of failure
F1	One flexural crack initiated, flexural-shear crack developed in shear-flexural region. Final failure by flexural cracks. Concrete crushing occurred at the compression zone of section (see Figure B.10.1(a)).
F2	One flexural crack initiated, flexural-shear crack developed in shear-flexural region. Final failure by flexural cracks. Concrete crushing occurred at the compression zone of section (see Figure B.10.1(b)).
F3	One flexural crack initiated, flexural-shear crack developed in shear-flexural region. Final failure by flexural cracks. Concrete crushing occurred at the compression zone of section (see Figure B.10.1(c)).

Appendix: Experimental results

Figure B.10.1: Experimental observations during flexural tests for MB2-F0.0% beams

Sample No.	Intermediate cracking mode	(Close to) final failure state
(a): Beam F1		
(b): Beam F2		
(c): Beam F3		

C. ANALYSIS

C.1. Post-cracking tensile parameters

From experimental data, tensile strength and toughness parameters are determined. Toughness parameter at a prescribed plastic displacement (crack width) is determined from both the block shift approach and approach developed by Rocco *et al* (2001). The post-cracking tensile strength which depends on toughness is given here together with the normalised post-cracking tensile strength. The formulae for the determination of these parameters are outlined in Chapter 4. Young's modulus determined from the compression test data is used to determine elastic displacement (δ_e) for each sample group while total displacement is taken at a limiting strain of 0.025. For a gauge length of 80mm used during the splitting test, this translates to a total displacement of 2.0mm from which plastic displacement (\approx average crack width, w_p) is determined. Note that the characteristic value for μ is determined from the ratio of characteristic post-cracking tensile strength to characteristic tensile strength.

$$\delta_e = \frac{f_t}{E_c}, \delta_T = \varepsilon_{tu} L_g \text{ and } w_p = \delta_T - \delta_e$$

C.1.1 Post-cracking tensile parameters derived from code definition

Table C.1.1: Post-cracking tensile parameters for PC1.0%, $E_c = 40.70\text{GPa}$

Sample No.	f_{t-N} (MPa)	G-N (N/mm)	w_p (mm)	f_{teq} (MPa)	μ
1	3.59	3.56	1.993	1.79	0.497
2	3.78	3.84	1.993	1.93	0.510
3	3.70	3.87	1.993	1.94	0.525
Mean	3.69	3.76	1.993	1.89	0.511
Standard deviation	0.093	0.171	0.0002	0.086	0.014
CoV	0.025	0.046	0.0001	0.046	0.027
Characteristic value	3.51	-	-	1.72	0.490

Table C.1.2: Post-cracking tensile parameters for PC1.5%, $E_c = 32.23\text{GPa}$

Sample No.	f_{t-N} (MPa)	G-N (N/mm)	w_p (mm)	f_{teq} (MPa)	μ
1	4.34	5.28	1.989	2.65	0.611
2	5.30	5.85	1.987	2.94	0.555
3	4.06	3.48	1.990	1.75	0.431
Mean	4.57	4.87	1.989	2.45	0.532
Standard deviation	0.651	1.233	0.0016	0.622	0.092
CoV	0.143	0.253	0.0008	0.254	0.173
Characteristic value	3.34	-	-	1.27	0.382

Appendix: Analysis

Table C.1.3: Post-cracking tensile parameters for MC-B1.0%, $E_c = 31.68\text{GPa}$

Sample No.	f_{t-N} (MPa)	G-N (N/mm)	w_p (mm)	f_{teq} (MPa)	μ
B1	3.42	3.42	1.991	1.72	0.502
B2	4.44	4.82	1.989	2.42	0.546
Mean	3.93	4.12	1.990	2.07	0.524
Standard deviation	0.720	0.988	0.0018	0.499	0.0311
CoV	0.183	0.240	0.0009	0.241	0.0595
Characteristic value	2.49	-	-	1.07	0.429

Table C.1.4: Post-cracking tensile parameters for MC-C1.0%, $E_c = 42.54\text{GPa}$

Sample No.	f_{t-N} (MPa)	G-N (N/mm)	w_p (mm)	f_{teq} (MPa)	μ
C1	4.08	4.49	1.992	2.25	0.553
C2	3.89	3.51	1.993	1.76	0.453
C3	3.87	3.17	1.993	1.59	0.411
C4	3.67	3.68	1.993	1.85	0.503
Mean	3.88	3.71	1.993	1.86	0.480
Standard deviation	0.167	0.560	0.0003	0.281	0.061
COV	0.043	0.151	0.00016	0.151	0.128
Characteristic value	3.57	-	-	1.35	0.378

Table C.1.5: Post-cracking tensile parameters for MC-D1.5%, $E_c = 33.75\text{GPa}$

Sample No.	f_{t-N} (MPa)	G-N (N/mm)	w_p (mm)	f_{teq} (MPa)	μ
D1	5.05	5.51	1.987	2.77	0.549
D2	5.30	5.38	1.986	2.71	0.511
D3	4.93	4.94	1.987	2.49	0.504
Mean	5.09	5.28	1.987	2.66	0.521
Standard deviation	0.191	0.299	0.0005	0.151	0.024
CoV	0.038	0.057	0.0003	0.057	0.047
Characteristic value	4.73	-	-	2.37	0.501

Table C.1.6: Post-cracking tensile parameters for MC-E1.5%, $E_c = 31.89\text{GPa}$

Sample No.	f_{t-N} (MPa)	G-N (N/mm)	w_p (mm)	f_{teq} (MPa)	μ
E1	5.05	5.28	1.986	2.66	0.526
E2	5.36	5.00	1.985	2.52	0.469
E3	5.45	5.23	1.985	2.64	0.483
E4	5.18	4.67	1.986	2.35	0.455
E5	4.99	4.97	1.986	2.50	0.502
E6	4.99	4.76	1.986	2.39	0.480
Mean	5.17	4.99	1.986	2.51	0.485
Standard deviation	0.198	0.244	0.0005	0.1231	0.025
CoV	0.038	0.049	0.0003	0.0490	0.052
Characteristic value	4.82	-	-	2.29	0.475

C.1.2 Post-cracking tensile parameters derived from theory of elasticity approach by Rocco et al (2001)

Table C.2.1: Post-cracking tensile parameters for PC1.0%, $E_c = 40.70\text{GPa}$

Sample No.	f_{t-M} (MPa)	G-M (N/mm)	w_p (mm)	f_{teq} (MPa)	μ
1	3.85	4.18	1.992	2.10	0.544
2	4.05	4.51	1.992	2.26	0.559
3	3.97	4.52	1.992	2.27	0.572
Mean	3.96	4.40	1.992	2.21	0.558
Standard deviation	0.099	0.196	0.0002	0.099	0.014
CoV	0.025	0.045	0.0001	0.045	0.025
Characteristic value	3.77	-	-	2.02	0.537

Table C.2.2: Post-cracking tensile parameters for PC1.5%, $E_c = 32.23\text{GPa}$

Sample No.	f_{t-M} (MPa)	G-M (N/mm)	w_p (mm)	f_{teq} (MPa)	μ
1	4.65	5.98	1.988	3.01	0.646
2	5.68	6.65	1.986	3.35	0.589
3	4.35	4.11	1.989	2.07	0.475
Mean	4.90	5.58	1.988	2.81	0.570
Standard deviation	0.698	1.316	0.0017	0.664	0.087
CoV	0.143	0.236	0.0009	0.237	0.153
Characteristic value	3.58	-	-	1.55	0.434

Table C.2.3: Post-cracking tensile parameters for MC-B1.0%, $E_c = 31.68\text{GPa}$

Sample No.	f_{t-M} (MPa)	G-M (N/mm)	w_p (mm)	f_{teq} (MPa)	μ
B1	3.64	3.95	1.991	1.98	0.545
B2	4.72	5.36	1.988	2.70	0.571
Mean	4.18	4.65	1.989	2.34	0.558
Standard deviation	0.765	0.999	0.0019	0.504	0.018
CoV	0.183	0.215	0.0010	0.215	0.033
Characteristic value	2.64	-	-	1.33	0.502

Appendix: Analysis

Table C.2.4: Post-cracking tensile parameters for MC-C1.0%, $E_c = 42.54\text{GPa}$

Sample No.	f_{t-M} (MPa)	G-M (N/mm)	w_p (mm)	f_{teq} (MPa)	μ
C1	4.33	5.12	1.992	2.57	0.594
C2	4.14	4.15	1.992	2.08	0.503
C3	4.11	3.77	1.992	1.89	0.461
C4	3.90	4.24	1.993	2.13	0.545
Mean	4.12	4.32	1.992	2.17	0.526
Standard deviation	0.177	0.574	0.0003	0.288	0.057
COV	0.043	0.133	0.0002	0.133	0.109
Characteristic value	3.79	-	-	1.64	0.433

Table C.2.5: Post-cracking tensile parameters for MC-D1.5%, $E_c = 33.75\text{GPa}$

Sample No.	f_{t-M} (MPa)	G-M (N/mm)	w_p (mm)	f_{teq} (MPa)	μ
D1	5.36	6.15	1.987	3.09	0.577
D2	5.63	6.07	1.987	3.05	0.542
D3	5.24	5.62	1.988	2.83	0.540
Mean	5.41	5.94	1.987	2.99	0.553
Standard deviation	0.202	0.285	0.0005	0.144	0.021
CoV	0.037	0.048	0.0002	0.048	0.038
Characteristic value	5.03	-	-	2.72	0.541

Table C.2.6: Post-cracking tensile parameters for MC-E1.5%, $E_c = 31.89\text{GPa}$

Sample No.	f_{t-M} (MPa)	G-M (N/mm)	w_p (mm)	f_{teq} (MPa)	μ
E1	5.37	5.89	1.987	2.96	0.552
E2	5.70	5.77	1.986	2.91	0.510
E3	5.79	5.96	1.985	3.00	0.519
E4	5.50	5.39	1.986	2.71	0.493
E5	5.30	5.67	1.987	2.85	0.539
E6	5.30	5.45	1.987	2.74	0.518
Mean	5.49	5.69	1.986	2.86	0.522
Standard deviation	0.2112	0.233	0.0005	0.118	0.021
CoV	0.0385	0.041	0.0003	0.041	0.040
Characteristic value	5.12	-	-	2.66	0.519

C.2. Distribution of reaction forces at supports for the model verification beams using finite element analysis

C.2.1 Finite element modelling approach

Plane stress theory is applied in the development of the finite element models used for this research problem. While in some case, more than one crack developed during the experimental execution, only a weak three-element single strip at the middle of the beam is improvised in finite element model to induce cracking. The strength for this single strip represents the material properties determined from the material characterisation process while the surrounding elements have slightly higher properties.

Finite element model schematisation for the four-point bending

The beam element is subjected to two point loads (4-point bending) allowing the middle span of the beam to be subjected to an equal moment so that the weakest part will crack first. In order to induce development of a single crack, a strip of weaker elements is improvised into the finite element model along the mid section, denoted by S3 in Figure C.2.1. Four-noded membrane elements 5mm x 5mm are used to model the standard beam. Points of contact for loading are provided by use of 50mm square metal rod (denoted by S6 and S7 in Figure C.2.1) representing bearings in the actual experimental set up. In order to allow smooth distribution of load at support, membrane elements (denoted by S8 and S9) are provided between the beam and the supports. The supports are modelled as square blocks, with 85mm sides.

Since the experiments are conducted on a simply supported beam, the model is developed to take this into account. Boundary conditions are modelled to reflect to a greater extent the physical behaviour while ensuring development of structurally stable system. In this regard, the beam is allowed to move laterally with minimal shear resistance provided by the membrane element. Furthermore, some nodes provide restraint in vertical translation while others provide restraint in both lateral and vertical translation as indicated in the Figure C.2.2. The connection between bearings and the beam is made such that the material in the beam at the bearing does not experience excessive stresses. This is done by tying degrees of freedom appropriately as shown in the figure. As the beam deflects during loading, a portion of it may start to lift up. The loss of contact during testing is provided through an iterative process where some nodes are released if it is found that they have tensile reaction forces after running the program.

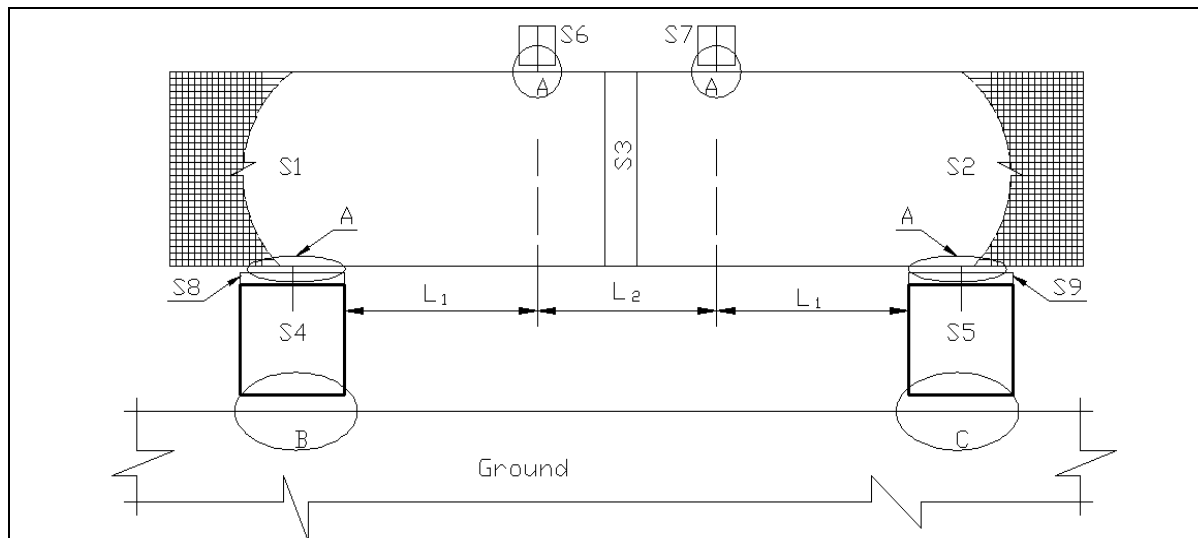


Figure C.2.1: Finite element model showing meshing and layout of the beam

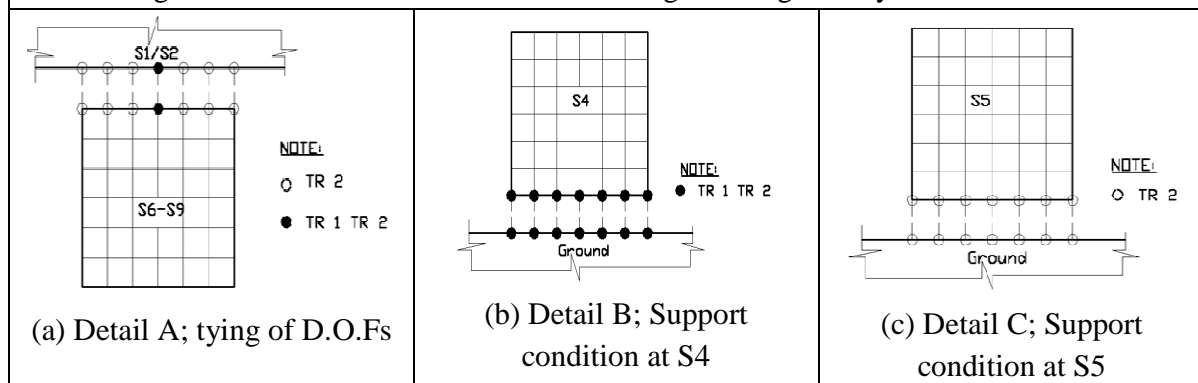
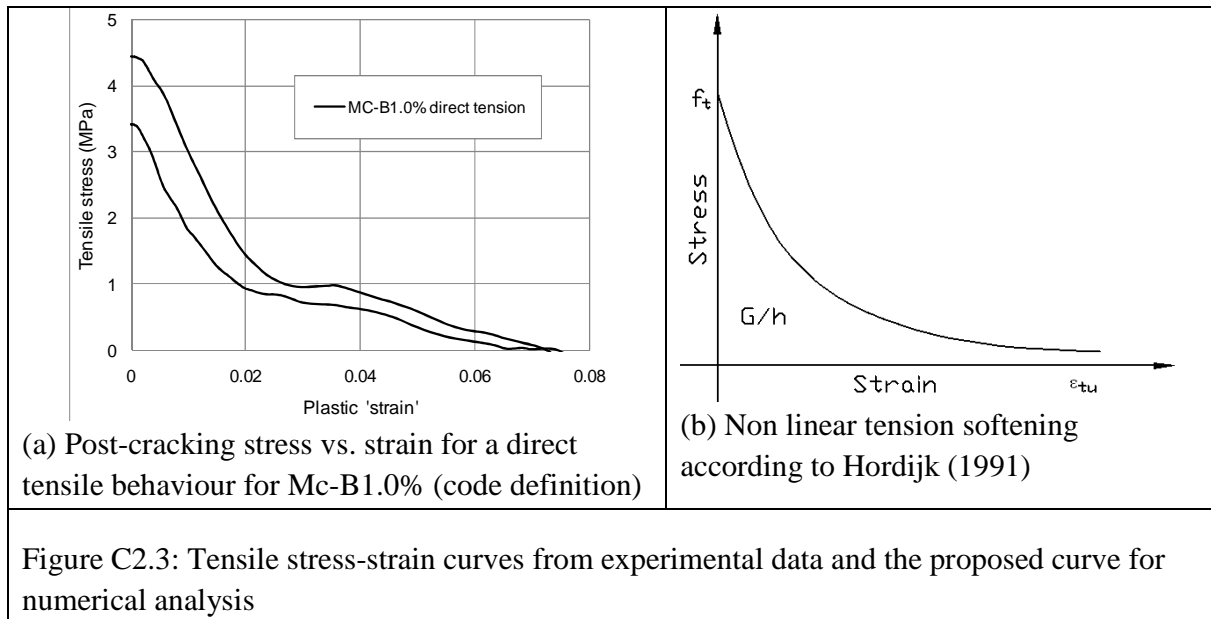


Figure C.2.2: Boundary conditions for the finite element model

Material modelling for Steel fibre reinforced concrete

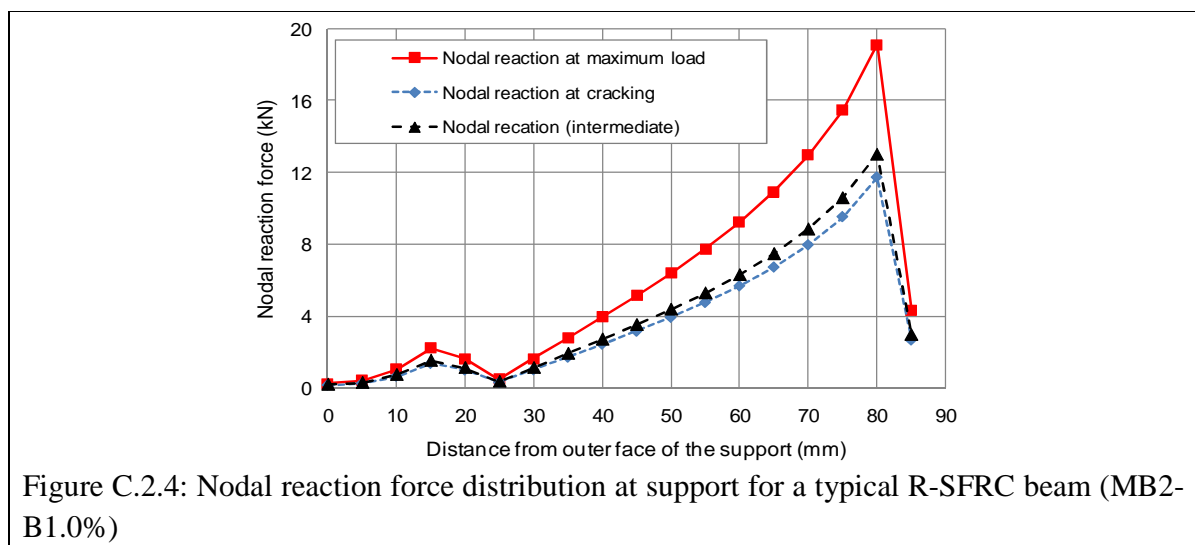
Steel fibre-reinforced concrete is modelled using a total strain model, with elastic-perfect plastic stress-strain law for compression, and Hordijk for tension. Note that for the elastic-perfect plastic compression model, the yield stress was assumed to be equal to the maximum compressive strength. Based on tension softening behaviour obtained from the tension tests carried out during characterisation test (given in Figure C.2.3(a)) it was decided that the tension softening model according to Hordijk (1991) better represented the actual behaviour of the material in tension. The softening model developed by Hordijk requires that the material fracture energy and peak tensile strength be known as indicated in Figure C.2.3 (b).

Appendix: Analysis

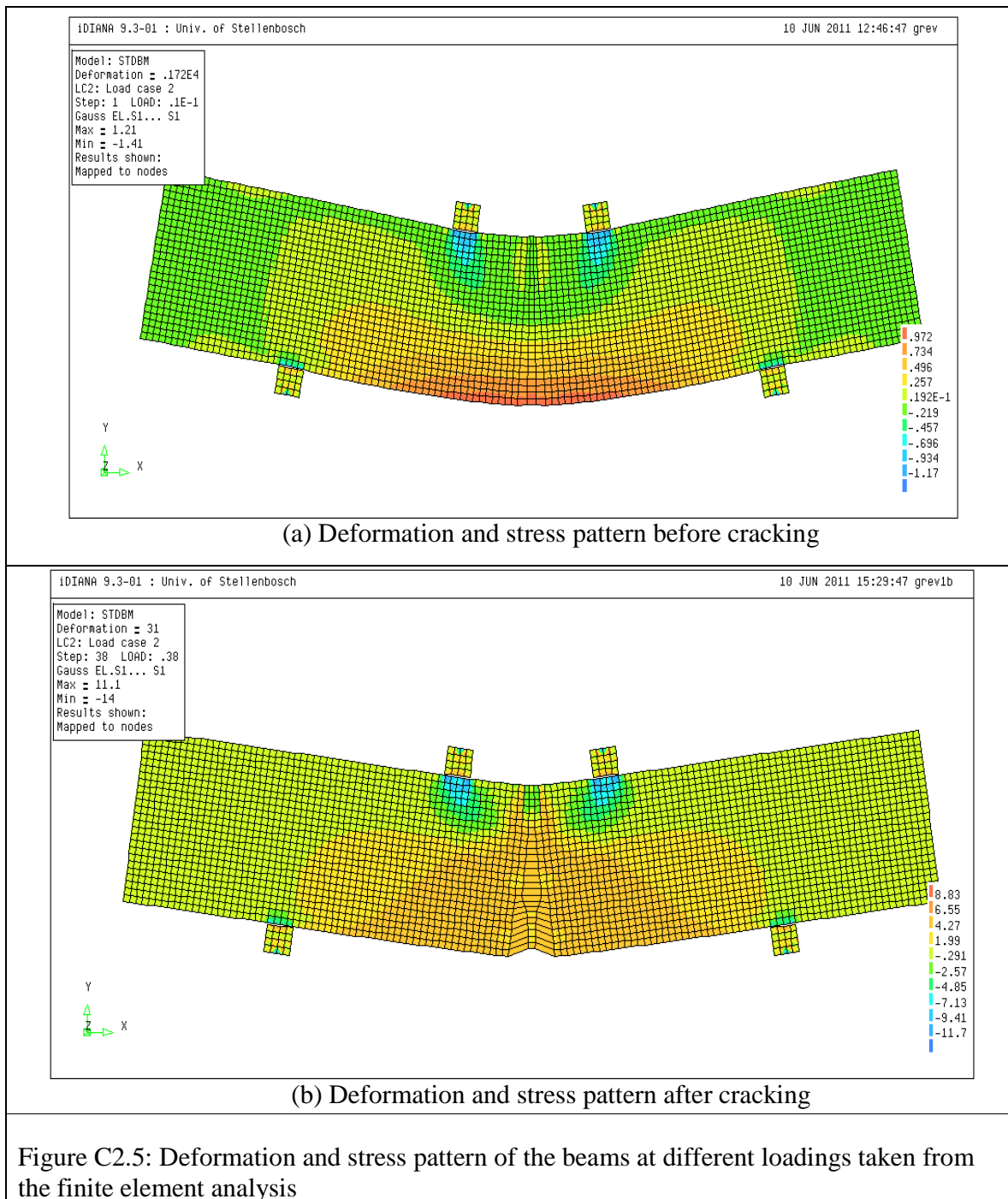


C.2.2 Finite element analysis results and evaluation

Compression and tensile characterisation data obtained from characterisation data from Phase II of the experiments were used for the numerical model, with cube compression strength converted to cylindrical strength by multiplying a factor of 0.8. The distribution of nodal reaction forces for a typical R-SFRC (MB2-B1.0% beams) is shown in Figure C.2.4. Nodal reactions at cracking load, maximum load capacity and a load between cracking and maximum load (intermediate) are all shown in the figure. Figure C2.5 shows the deformation pattern of the beams at different loadings taken from the finite element analysis. Figure C2.6 displays the nodal load distribution for a SFRC beam without steel bars (MB0-C1.0%) at maximum loading. It is clear that the shape/ pattern of nodal reaction distribution is similar in all cases.



Appendix: Analysis



Appendix: Analysis

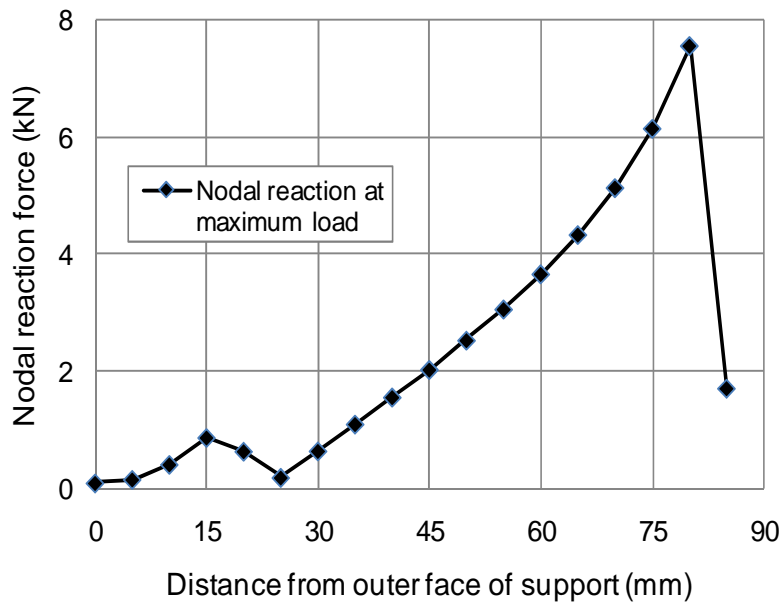


Figure C.2.6: Nodal reaction force distribution at support for a typical SFRC beam without steel bars (MB0-C1.0%)

Table C.2.1 summarises the total nodal reaction forces for a typical R-SFRC beam (MB2-B1.0%) and SFRC beam without reinforcing bars (MB0-C1.0%). The position where the resultant forces act are also given in the table together with a factor, α_b , representing the fraction of the bearing length from the inner face of the support to the position where resultant force acts. The value of α_b may be taken as 0.3 for all loading cases. Note that the bearing length used for the numerical analysis was 85mm

Table C.2.1: Nodal reactions and the values of α_b for different loading configurations

Loading configuration	Total reaction force (kN)	Total moment of the nodal reactions about outer support face (kNmm)	Position of resultant force from inner support face x_R (mm)	$\alpha_b = \frac{x_R}{85}$
R-SFRC-Cracking	72.5	4239	26.5	0.31
R-SFRC-Maximum	105.8	6601	22.6	0.27
SFRC(no rebar)-Maximum	42.4	2645	22.6	0.27
Average value				0.28